

QCD Corrections in Inclusive Rare B Decays

Inauguraldissertation
der Philosophisch-naturwissenschaftlichen Fakultät
der Universität Bern

vorgelegt von

Kay Axel Bieri

von Escholzmatt/LU

Leiter der Arbeit: PD Dr. Ch. Greub
Institut für theoretische Physik
Universität Bern

QCD Corrections in Inclusive Rare B Decays

Inauguraldissertation
der Philosophisch-naturwissenschaftlichen Fakultät
der Universität Bern

vorgelegt von

Kay Axel Bieri

von Escholzmatt/LU

Leiter der Arbeit: PD Dr. Ch. Greub
Institut für theoretische Physik
Universität Bern

Von der Philosophisch-naturwissenschaftlichen Fakultät angenommen.

Der Dekan:



Bern, den 13. Mai 2004

Prof. Dr. G. Jäger

*Science! true daughter of Old Time thou art!
Who alterest all things with thy peering eyes.
Why preyest thou thus upon the poet's heart,
Vulture, whose wings are dull realities?
How should he love thee? or how deem thee wise,
Who wouldst not leave him in his wandering
To seek for treasure in the jewelled skies.
Albeit he soared with an undaunted wing?
Hast thou not dragged Diana from her car?
And driven the Hamadryad from the wood
To seek a shelter in some happier star?
Hast thou not torn the Naiad from her flood,
The Elfin from the green grass, and from me
The summer dream beneath the tamarind tree*

Edgar Allan Poe, Sonnet to Science

ABSTRACT

This PhD thesis is devoted to rare inclusive B decays and perturbative QCD corrections thereof. In particular we focus on the radiative decay $B \rightarrow X_s \gamma$ and the semileptonic decays $B \rightarrow X_s \ell^+ \ell^-$ and $B \rightarrow X_d \ell^+ \ell^-$. Rare B decays play an essential role in today's world of particle physics. In the Standard Model (SM) these decay modes are loop-induced due to absent tree-level flavor-changing neutral currents (FCNC). Various extensions of the SM such as two-Higgs-doublet models or supersymmetric theories provide contributions to rare B decays which are not necessarily suppressed relative to the SM prediction. Thus, being sensitive to new physics (NP) effects, these decays serve as an excellent testbed of the Standard Model. In conjunction with available experimental data, they can set important constraints on parameter spaces of non-SM theories. Even in the absence of new physics, rare B decays provide a rich source of information. They are used for precise determinations of CKM matrix elements such as $|V_{ts}|$ and $|V_{td}|$ or to give insights on the top quark. Among rare B decays, inclusive modes are especially attractive since they deliver theoretically clean observables which are dominated by the underlying quark process due to "Heavy Quark Expansion". In this thesis we calculate missing $\mathcal{O}(\alpha_s)$ corrections to the processes $b \rightarrow s \ell^+ \ell^-$ and $b \rightarrow d \ell^+ \ell^-$. We apply our result to calculate the NP-sensitive *forward-backward asymmetry* for both decays. In the case of $b \rightarrow d \ell^+ \ell^-$, we also calculate the CP asymmetry. For the process $b \rightarrow s \gamma$ we make the first step towards a NNLL result by calculating $\mathcal{O}(a_s^2 n_f)$ matrix elements (n_f is the number of flavors). The need of a full NNLL result is motivated by theoretical uncertainties in the definition of the charm mass. Furthermore, since measurements of the branching ratio $\text{BR}(B \rightarrow X_s \gamma)$ will become much more precise in the near future, it will become mandatory to extend theoretical predictions to NNLL precision.

Contents

Introduction	1
I Fundamentals	7
1 The Standard Model	9
1.1 Overview	10
1.2 Massless fermion fields and G_{SM}	13
1.3 The Higgs mechanism, boson masses	16
1.4 Fermion masses and the CKM matrix	18
2 Theoretical framework for inclusive B meson decays	22
2.1 Operator product expansion, effective Hamiltonians	22
2.2 Heavy quark limit	26
2.2.1 Heavy quark effective theory	27
2.2.2 Heavy quark expansion	28
2.3 Matching procedure	30
2.4 RG improved perturbation theory	35
3 Mellin-Barnes integrals	44
References	52
II Physical Review D 66 (2002) 094013	55
“NNLL calculations to the angular distribution and to the forward-backward asymmetries in $b \rightarrow X_s \ell^+ \ell^-$ ”	
1 Introduction	58

2	Theoretical framework	60
3	Previous results for $\delta\Gamma/d\hat{s}$ and modifications needed for $d\Gamma/(d\hat{s} d \cos \theta)$	62
4	NNLL results for double differential decay width and forward-backward-asymmetries	64
5	Regularization of infrared- and collinear singularities	67
6	Phase space	69
6.1	Fully differential phase space formula for lepton pair at rest	69
6.2	Phase space integrations	71
7	Calculation of virtual- and bremsstrahlung corrections associated with O_7, O_9 and O_{10}	72
7.1	Construction of $f_{99}(\hat{s}, z)$	73
7.2	Construction of $f_{910}(\hat{s})$	74
8	Phenomenological analysis	75
9	Summary	78
A	$\omega_{77}(\hat{s})$, $\omega_{99}(\hat{s})$ and $\omega_{79}(\hat{s})$	81
B	Auxiliary quantities A_i, T_9, U_9 and W_9	81
	References	83
III	Physical Review D 67 (2003) 114019	87
	“Fermionic NNLL corrections to $b \rightarrow s\gamma$”	
1	Introduction	90
2	Virtual corrections to $b \rightarrow s\gamma$ associated with O_1 and O_2	93
2.1	Regularized three-loop corrections to $\langle s\gamma O_2 b \rangle$	93
2.2	Counterterm contributions to $\langle s\gamma O_2 b \rangle$	97

2.3 Renormalized result for $\langle s\gamma O_2 b\rangle$	99
3 Real and virtual corrections to $\langle s\gamma O_7 b\rangle$	100
4 Virtual corrections to $\langle s\gamma O_8 b\rangle$	105
5 Numerical impact of the $\mathcal{O}(\alpha_s^2 n_f)$ corrections	107
6 Conclusions	113
A Building blocks	113
B Regularized three-loop results for $\langle s\gamma O_2 b\rangle$	116
C Correction functions needed for the NLL result	118
D $\mathcal{O}(\alpha_s^2 n_f)$ contributions to various Z factors	120
E Implementing the photon energy cut-off in the $\mathcal{O}(\alpha_s n_f)$ terms	120
References	122
IV HEP 2003 Conference Proceedings, hep-ph/0310214	125
“Review on the inclusive rare decays $B \rightarrow X_s \gamma$ and $B \rightarrow X_d \gamma$ in the Standard Model”	
1 Introduction	128
2 Theoretical framework	129
3 NLL (and partial NNLL) results for $\text{BR}(B \rightarrow X_s \gamma)$	130
4 Partially integrated BR and photon energy spectrum	132
5 $B \rightarrow X_d \gamma$ in the SM	135
References	137

V	Physical Review D 69 (2004) 074007	141
	”Virtual- and bremsstrahlung corrections to $b \rightarrow d \ell^+ \ell^-$ in the Standard Model”	
1	Introduction	144
2	Effective Hamiltonian	146
3	Virtual $\mathcal{O}(\alpha_s)$ corrections to the matrix elements $\langle d \ell^+ \ell^- O_{1,2}^{u,c} b \rangle$	148
3.1	Diagrams 3.1a) and b)	150
3.2	Diagrams 3.1d)	151
3.3	Diagrams 3.1c)	152
3.4	Diagrams 3.1e)	153
3.5	$\mathcal{O}(\alpha_s)$ counterterms to $\langle d \ell^+ \ell^- O_{1,2}^{u,c} b \rangle$	153
3.6	Renormalized form factors of O_1^u and O_2^u	156
4	Virtual corrections to the matrix elements of the operators O_7, O_8, O_9 and O_{10}	158
4.1	Renormalized matrix element of O_7	158
4.2	Renormalized matrix element of the operator O_8	158
4.3	Renormalized matrix element of O_9 and O_{10}	159
5	Corrections to the Decay Width $B \rightarrow X_d \ell^+ \ell^-$	160
6	Phenomenological analysis	161
7	Summary	167
A	Calculation techniques	168
A.1	Reducing tensor integrals with dimension-shifting techniques	168
A.2	Integration by parts	170
B	Calculation of the diagrams 3.1d)	172
C	Solution of the RG equation for the Wilson coefficients	175

D One-loop matrix elements of the four-quark operators	177
E Finite bremsstrahlung corrections	178
References	181
Acknowledgments	185
Curriculum Vitae	187

Introduction

In the summer of 1977 a team of physicists led by Leon M. Lederman discovered the Υ -resonance¹ [1] at Fermilab. The resonance was eventually understood as being a bound state of the bottom quark and its antiquark. A few years prior to this discovery, weak preliminary evidence for a third charged lepton was found with the Mark I detector at SLAC [2]. This led Haim Harrari, based on the lepton-quark-universality, to propose in 1975 a third generation of quarks, whose members he named bottom and top. At that time, the paper written by Kobayashi and Maskawa [3] speculating on six quarks as a source of CP violation was mostly unknown, and the model of a third generation of quarks was not very popular. It was only after the discovery of Υ (and the confirmation of a third charged lepton by the PLUTO detector [4]) that this theory became widely accepted.

Since the discovery of the b -quark, a lot of experiments have been devoted to the field of B -physics. The experimental result by Lederman's group was confirmed at other accelerators and several more $b\bar{b}$ bound states were found [5, 6, 7, 8]. Among these bound states, the $\Upsilon(4S)$ resonance is especially interesting since it is the lightest bound state heavy enough to decay into a B -meson pair [9] (B^+B^- or $B^0\bar{B}^0$). The branching ratio of $\Upsilon(4S)$ decaying into a B -meson pair is above 96%. Thus, this resonance provides a suitable laboratory to study B -meson decays with a rather pure sample. The first detectors to extensively study B -physics at the $\Upsilon(4S)$ resonance were ARGUS at DESY (Deutsches-Elektronen-Synchrotron) in Hamburg and CLEO in Cornell [10, 11, 12, 13]. Throughout the running time of the ARGUS detector (1982 to 1992), the ARGUS collaboration conducted many ground-breaking experiments [14, 15, 16]. Most notably is the first observation of $B^0 - \bar{B}^0$ mixing [17]. ARGUS and CLEO (which is still running, now in its third experimental phase) have long been passed in terms of produced B -meson pairs by the two B -factories BaBar (SLAC, USA) and Belle (KEK, Japan)². They both work with an e^+e^- accelerator, but unlike the experiment in Cornell, the energies of the two beams are asymmetric, yielding a $\Upsilon(4S)$ which is not at rest in the labor system. This setup was proposed in [19] and allows for a better spatial separation of the individual B -decay vertices. Furthermore, it enhances the lifetimes of the B -mesons and thus makes their time evolution more accessible. Both factories have started taking data in 1999 and stand at around 178×10^6 (BaBar) [20] and 207×10^6 (Belle) [21] generated $B\bar{B}$ pairs as of January 2004. One reason for Belle's higher production (the luminosity has now reached levels of above $11 \times 10^{33}/\text{cm}^2/\text{s}$ as opposed to BaBar, whose peak is slightly above $7.1 \times 10^{33}/\text{cm}^2/\text{s}$) lies in the design of the experiment: the crossing angle of the beams in the interaction section is of the order 10 mrad (unlike

¹In 1976 experimental data hinted at a resonance at around 6 GeV. After an "availability search" of the Greek alphabet, the letter Υ (Upsilon) was chosen as its name. Later the resonance turned out to be an "Oops-Leon" (pun intended). The real resonance, discovered in 1977, was then given the name Υ .

²In ten years ARGUS collected 514/pb of luminosity [18]. Since around May 2003, Belle can collect this amount every single day it takes data.

BaBar, which works with head-on collisions). This allows to eliminate parasitic collisions and makes it much easier to manipulate the two beams at the collision point³.

Despite the success which has been achieved at $\Upsilon(4S)$ B -factories, they have some disadvantages. First of all, the $\Upsilon(4S)$ resonance is too light to decay into any B -mesons other than B^\pm and B^0 . Although this can be viewed as an advantage since one gets a very pure sample of these mesons, it limits the type of physics one can experiment with. Another detriment is the low production cross section of b -quarks at e^+e^- machines. Hadron colliders are not tagged by these two problems: The planned B factories at CERN (LHCb) [22] and at Fermilab (BTeV) [23], will be able to produce B_x mesons ($x = u, d, s, c$) as well as b -baryons. Furthermore the production rate of $B\bar{B}$ pairs is expected to be of the order 10^{12} per year, increasing statistics by several orders of magnitude. They are scheduled to acquire data in 2007 (LHCb) and 2009 (BTeV).

The main motivation for building these experiments is to detect discrepancies between measured observables and corresponding calculations from the Standard Model (SM) (see Chapter 1 of Part I in this thesis for an introduction and overview of the Standard Model). These measurements serve as a test of the SM as well as on its various extensions. A very interesting observable to measure is CP violation (CPV) [24, 25]. Within the Standard Model, CPV is generated by a single non-vanishing phase in the Cabibbo-Kobayashi-Maskawa (CKM) matrix. This means that every CP violation effect is linked to the value of this phase. One known discrepancy between the SM and experimental data arising from this fact is baryon number asymmetry: Assuming that the evolution of the universe began from a matter-antimatter symmetric state, CP violation is necessary to explain the observed asymmetry today [26]. The CPV effect due to the phase is orders of magnitudes too weak to cause this effect (in order to be consistent with high-energy experiments). Various “new physics” (NP) models introduce new sources of CPV⁴ and could thus cope with this and maybe further discrepancies between experiments and the Standard Model. CP violation was first experimentally detected in the K^0 system forty years ago [28]. The measured effect was rather small, namely around 0.2%. In 1981, it was pointed out [29, 30] that the CKM framework [3] predicts large CP violation in many decays of B mesons for a certain range of quark mixing parameters. Subsequent measurements of the B -meson lifetime [31] and the discovery of $B^0\bar{B}^0$ mixing [17] indicated that these parameters lie within such a range. In 2001, both BaBar and Belle confirmed these theoretical findings and found CPV in the B^0 system [32, 33]. Their values for the parameter $\sin 2\beta$ ⁵ is in good agreement with the predicted results.

Among B -physics processes, rare B decays take an especially suited role for detection of NP effects. They are by definition induced at the one-loop level. Thus, additional contributions of non-SM particles (e.g. SUSY particles (charginos, gluinos, stops, ...) or particles from

³The geometrical reduction of the luminosity due to a nonzero crossing angle has been found to be negligible.

⁴E.g. the MSSM (Minimal SuperSymmetric Model) contains 44 CP-violating phases [27].

⁵Belle and BaBar have a different notation for the angles of the unitarity triangle. The angle β (BaBar) is called ϕ_1 by the Belle collaboration.

extended Higgs models) to various observables (branching ratios, CP asymmetries, forward-backward asymmetries) are not suppressed by a factor $\alpha/(4\pi)$ relative to SM contributions. This allows to observe these particles indirectly through their influence on rare processes accessible with today's accelerators. Furthermore, rare decays can be used to set stringent constraints on the parameter space of SM extensions such as the MSSM. These constraints can in turn be helpful to tune setups in experiments at future hadron colliders designed to detect new particles directly (i.e. to produce them as real particles instead of virtual ones) by tuning their setup accordingly. Besides being sensitive to new physics, rare B decays can also be used to determine some of the CKM matrix elements (e.g. V_{td} and V_{ts}). For all these undertakings, it is essential to acquire precise theoretical predictions of the observables involved. Inclusive rare B decays are particularly suited for this purpose: unlike exclusive B decays (e.g. $B \rightarrow K^*\ell^+\ell^-$) they are theoretically cleaner since they do not depend on a specific model to describe final hadronic states. Inclusive processes are dominated by contributions that are reliably calculable in perturbation theory. Heavy quark expansion [34, 35] and renormalization group improved perturbative QCD [36] form a solid theoretical framework to describe these decays. Essentially, they are determined by the underlying decays of free b -quarks. On the experimental side, these decays are much more difficult to measure than their exclusive counterparts.

This thesis is devoted to rare inclusive B decays. We focus solely on perturbative corrections and present NNLL results to the three processes $B \rightarrow X_{s,d}\ell^+\ell^-$ and $B \rightarrow X_s\gamma$. The work is split up into the following five parts:

- Part I contains basic knowledge important for understanding the chapters that follow. It gives a short but thorough overview of the Standard Model. This overview is followed by an introduction to the theoretical framework of inclusive rare B decays. The final chapter in this part discusses a method useful for evaluating Feynman diagrams, namely the method of Mellin-Barnes representations.
- In Part II we present NNLL results for the so-called *forward-backward asymmetry* $A_{\text{FB}}(\hat{s})^6$ in the process $b \rightarrow X_s\ell^+\ell^-$. We circumvent theoretical problems arising from long-distance effects by restricting \hat{s} to the interval $0.05 \leq \hat{s} \leq 0.25$. The forward-backward asymmetry is particularly sensitive to new physics in the considered kinematical window [37, 38] and can thus be used, together with experimental data, to perform a model-independent test of the Standard Model.
- Part III is devoted to NNLL calculations in the process $b \rightarrow s\gamma$. In particular, we present the result for all $\mathcal{O}(\alpha_s^2)$ terms proportional to the number of fermion flavors n_f . As the measurements of the branching ratio for this process become much more precise in the near future, it is important to perform a full NNLL calculation. This paper is a first step towards this very challenging goal.

⁶The quantity \hat{s} is the invariant mass squared of the lepton pair, normalized with m_b^2 .

-
- Part [IV](#) reviews for the two processes $B \rightarrow X_s \gamma$ and $B \rightarrow X_d \gamma$ both the theoretical and the experimental status.
 - The full NNLL corrections to the process $b \rightarrow d \ell^+ \ell^-$ are calculated in Part [V](#). The work is an extension of analogous calculations done for the process $b \rightarrow s \ell^+ \ell^-$ [[39](#), [40](#)]. In the latter, the CKM-suppressed Feynman diagrams involving a u -quark were neglected and therefore any CPV effect was eliminated right at the beginning. In the process $b \rightarrow d \ell^+ \ell^-$ this suppression is not present anymore and the corresponding diagrams need to be taken into account. We present the resulting CP asymmetry as well as the branching ratio. Furthermore, we can profit from our own work in Part [II](#) and give the results for the forward-backward asymmetry for this process as well.

References

- [1] W. R. Innes *et al.*, *Phys. Rev. Lett.* **39** (1977) 1240, E:*Phys. Rev. Lett.* **39** (1977) 1640.
- [2] M. L. Perl *et al.*, *Phys. Rev. Lett.* **35** (1975) 1489.
- [3] M. Kobayashi and T. Maskawa, *Prog. Theor. Phys.* **49** (1973) 652.
- [4] J. Burmester *et al.* [PLUTO Collaboration], *Phys. Lett.* **B 68** (1977) 301.
- [5] C. Berger *et al.* [Pluto Collaboration], *Phys. Lett.* **B 76** (1978) 243.
- [6] J. K. Bienlein *et al.*, *Phys. Lett.* **B 78** (1978) 360.
- [7] D. Andrews *et al.*, *Phys. Rev. Lett.* **44** (1980) 1108.
- [8] D. Andrews *et al.*, *Phys. Rev. Lett.* **45** (1980) 219.
- [9] C. Bebek *et al.*, *Phys. Rev. Lett.* **46** (1981) 84.
- [10] R. Fulton *et al.* [CLEO Collaboration], *Phys. Rev. Lett.* **64** (1990) 16.
- [11] S. Henderson *et al.* [CLEO Collaboration], *Phys. Rev.* **D 45** (1992) 2212.
- [12] M. S. Alam *et al.* [CLEO Collaboration], *Phys. Rev. Lett.* **74** (1995) 2885.
- [13] B. Barish *et al.* [CLEO Collaboration], *Phys. Rev. Lett.* **76** (1996) 1570.
- [14] H. Albrecht *et al.* [ARGUS Collaboration], *Phys. Lett.* **B 197** (1987) 452.
- [15] H. Albrecht *et al.* [ARGUS Collaboration], *Phys. Lett.* **B 234** (1990) 409.
- [16] H. Albrecht *et al.* [ARGUS Collaboration], *Phys. Lett.* **B 318** (1993) 397.
- [17] H. Albrecht *et al.* [ARGUS Collaboration], *Phys. Lett.* **B 192** (1987) 245.

-
- [18] D. Wegener, [hep-ex/9802001](#).
- [19] P. Oddone, in *Proceedings of the UCLA Workshop: Linear Collider $B\bar{B}$ Factory Conceptual Design*, edited by D. Stork, World Scientific (1987), p. 243.
- [20] [Latest results for integrated luminosity at BaBar](#).
- [21] [Latest results for integrated luminosity at Belle](#).
- [22] N. Harnew [LHCb Collaboration], *Nucl. Phys.* **120** (*Proc. Suppl.*) (2003) 305.
- [23] R. K. Kutschke [BTeV Collaboration], *Nucl. Phys.* **120** (*Proc. Suppl.*) (2003) 311.
- [24] S. Plaszczynski, [hep-ph/9804330](#).
- [25] K. Rybicki [BELLE Collaboration], *Acta Phys. Polon.* **B30** (1999) 1837.
- [26] A. D. Sakharov, *Pisma Zh. Eksp. Teor. Fiz.* **5** (1967) 32 [*JETP Lett.* **5** (1967) 34, 392-393. 1991 *UFNAA*, 161, 61-64. 1991) 24].
- [27] S. Dimopoulos, S. Raby and F. Wilczek, *Phys. Rev.* **D 24** (1981) 1681.
- [28] J. H. Christenson, J. W. Cronin, V. L. Fitch and R. Turlay, *Phys. Rev. Lett.* **13** (1964) 138.
- [29] I. I. Y. Bigi and A. I. Sanda, *Nucl. Phys.* **B 193** (1981) 85.
- [30] A. B. Carter and A. I. Sanda, *Phys. Rev. Lett.* **45** (1980) 952.
- [31] E. Fernandez *et al.*, *Phys. Rev. Lett.* **51** (1983) 1022.
- [32] K. Abe *et al.* [Belle Collaboration], *Phys. Rev. Lett.* **87** (2001) 091802, [hep-ex/0107061](#); K. Abe *et al.* [Belle Collaboration], *Phys. Rev.* **D 66** (2002) 071102, [hep-ex/0208025](#).
- [33] B. Aubert *et al.* [BABAR Collaboration], *Phys. Rev. Lett.* **87** (2001) 091801, [hep-ex/0107013](#); B. Aubert *et al.* [BABAR Collaboration], *Phys. Rev. Lett.* **89** (2002) 281802, [hep-ex/0207055](#).
- [34] M. A. Shifman and M. B. Voloshin, *Sov. J. Nucl. Phys.* **47** (1988) 511, *E:Yad. Fiz.* **47** (1988) 801.
- [35] N. Isgur and M. B. Wise, *Phys. Lett.* **B 232** (1989) 113; *Phys. Lett.* **B 237** (1990) 527.
- [36] G. Grunberg, *Phys. Lett.* **B 95** (1980) 70, *E:Phys. Lett.* **B 501** (1982) 501.
- [37] A. Ali, P. Ball, L. T. Handoko and G. Hiller, *Phys. Rev.* **D 61** (2000) 074024, [hep-ph/9910221](#).

-
- [38] J-W. Chen, G. Rupak and M. J. Savage, *Phys. Lett. B* **410** (1997) 285.
- [39] H. H. Asatryan, H. M. Asatrian, C. Greub and M. Walker, *Phys. Rev. D* **65** (2002) 074004, [hep-ph/0109140](#).
- [40] H. H. Asatryan, H. M. Asatrian, C. Greub and M. Walker, *Phys. Rev. D* **66** (2002) 034009, [hep-ph/0204341](#).

PART I

Fundamentals

1 The Standard Model

The Standard Model (SM) of electroweak and strong interactions has been an extremely successful model since its dawn in the 1960's [1, 2, 3] and early 1970's [4, 5]. One of the stunning features of the SM was that it predicted a new interaction: the weak neutral current. Experimentally, this current was discovered in the “Gargamelle Neutrino Experiment” in 1973 [6] and yielded the first big success of the theory. The experiment was looking for processes of the form $\nu_\mu/\bar{\nu}_\mu + N \rightarrow \nu_\mu/\bar{\nu}_\mu + \text{hadrons}$ (neutral current) as well as for $\nu_\mu/\bar{\nu}_\mu + N \rightarrow \mu^-/\mu^+ + \text{hadrons}$ (charged current). Together with the data extracted from these low energy processes and similar experiments in the 1970's [7, 8], the Standard Model was able to predict the masses of the mediating vector bosons W^\pm and Z . The first experiments which directly produced the W^- and Z -bosons took place in 1983 at CERN [9, 10]. The measured mass was in good agreement with the predictions of the SM. A couple of years later, experiments at LEP were able to measure the Z -mass much more precisely. These experiments were also able to probe the theory at the one-loop level and found agreement in many observables up to differences of the order of 1%. Another success story concerns the top quark: in the Standard Model, this quark is required as the weak isospin partner of the bottom quark. In 1995, it was directly observed with the CDF (Collider Detector at Fermilab) [11].

Despite its many successes, the SM does have some deficiencies:

- Gravity is not included in the Standard Model.
- Why is the electroweak scale so small (hierarchy problem)?
- There is no explanation why only the electroweak part is chiral. Similarly, the Standard Model incorporates but does not explain electric charge quantization.
- Strong CP violation problem (see e.g. [12]): The parameter θ responsible for strong CP violation has been found experimentally to be below 10^{-9} [13], although a value of the order 1 is perfectly allowed by the QCD gauge invariance. There is no natural reason in the SM which states why θ is zero or why it is so small.
- No explanation for the wide range of quark masses (few MeV to hundred GeV) and the masses of the charged leptons (half an MeV to 1.8 GeV).
- Recent experiments have shown that neutrinos do in fact have a non-zero mass. The Standard Model does not account for massive neutrinos.

Many of these deficiencies can be solved by extending the model (e.g. masses for neutrinos can be introduced into the model with ease). Others might already have been solved (in [14], the authors propose that the strong CP problem is actually a non-problem and can easily be gotten rid of). In spite of all these deficiencies, the SM has been and still is a very successful model. High-precision measurements of observables have continued to show

terrific agreement with theoretical calculations within the Standard Model [15, 16, 17]. Since the model describes our world very precisely at low energies, any superordinate theory must merge into it in the limit of small energies. It is therefore essential to know at least the basic structure of the SM.

In this chapter we give an overview of the principles of the Standard Model. We put our emphasize on the particle content, their interactions and parameters such as masses and couplings and omit certain topics which are of secondary interest to the presented work. Specifically, we leave out the discussion on quantization of non-Abelian gauge fields, which can be found elsewhere (see any decent textbook on the topic, e.g. [18]. For the original paper, see [19]).

1.1 Overview

The Standard Model is a gauge field theory based on the gauge group G_{SM} :

$$G_{\text{SM}} = SU(3)_C \otimes SU(2)_L \otimes U(1)_Y. \quad (1)$$

The groups $SU(3)_C$ and $G_{\text{ew}} = SU(2)_L \otimes U(1)_Y$ correspond to the strong interaction and the electroweak interaction, respectively. The subscripts give information on which parts of the SM the groups act non-trivially: the strong interaction acts on *color-charged* particles (quarks and gluons) and leaves all other particles untouched. The group $SU(2)_L$ (sometimes called “weak isospin”), on the other hand, only acts on left-handed fields. It therefore maximally violates parity. Finally, the group $U(1)_Y$ acts on particles with weak hypercharge. As we see later in Section 1.3, G_{ew} spontaneously breaks down to the group $U(1)_Q$, with Q being the “normal” electric charge. Tables 1.1 and 1.2 summarize the fermionic and bosonic fields of the theory as well as their transformation properties.

In Table 1.1 we see that the quark fields have an additional index, the color index. Every quark flavor q ($q = u, d, s, c, t, b$) occurs in three different versions or colors (*chromos*, greek for color). Quantum chromodynamics (QCD) jumbles these versions. In order to tighten the notation, we collect these three versions in a vector:

$$q = (q^1 \ q^2 \ q^3)^T, \quad \text{for } q = u, d, s, c, t, b. \quad (2)$$

The fundamental constituents of any Dirac-spinor ψ are the Weyl fermions. In the chiral basis, ψ can be written in the following way:

$$\psi = \begin{pmatrix} \phi \\ 0 \end{pmatrix} + \begin{pmatrix} 0 \\ \chi \end{pmatrix}, \quad (3)$$

with ϕ and χ being Weyl spinors (these spinors have two components). Introducing the two chiral projectors L and R ,

$$L = \frac{1 - \gamma_5}{2}, \quad R = \frac{1 + \gamma_5}{2}, \quad (4)$$

Generation			$SU(3)_C$	$SU(2)_L$			$U(1)_Y$	$U(1)_Q$
1	2	3	Rep.	T_2	T_2^3	Rep.	Y	Q
$\begin{pmatrix} u^\alpha \\ d^\alpha \end{pmatrix}_L$	$\begin{pmatrix} c^\alpha \\ s^\alpha \end{pmatrix}_L$	$\begin{pmatrix} t^\alpha \\ b^\alpha \end{pmatrix}_L$	3	1/2 1/2	1/2 -1/2	2	1/6 1/6	2/3 -1/3
u_R^α d_R^α	c_R^α s_R^α	t_R^α b_R^α	3	0 0	0 0	1	2/3 -1/3	2/3 -1/3
$\begin{pmatrix} \nu_e \\ e \end{pmatrix}_L$	$\begin{pmatrix} \nu_\mu \\ \mu \end{pmatrix}_L$	$\begin{pmatrix} \nu_\tau \\ \tau \end{pmatrix}_L$	1	1/2 1/2	1/2 -1/2	2	-1/2 -1/2	0 -1
e_R	μ_R	τ_R	1	0	0	1	-1	-1

Table 1.1: Fermionic content (quarks and leptons) of the Standard Model and its transformation properties. The subscript L (R) corresponds to left-handed (right-handed) fields. The superscript α denotes the color index.

Boson	$SU(3)_C$ Rep.	$SU(2)_L$ Rep.	Y	Q	Function
W_μ	1	3			$SU(2)_L$ gauge bosons
B_μ	1	1			$U(1)_Y$ gauge boson
G_μ^α	8	1	0	0	$SU(3)_C$ gauge bosons
$\phi = \begin{pmatrix} \phi^+ \\ \phi^0 \end{pmatrix}$	1	2	1/2 1/2	1 0	Generation of masses

Table 1.2: Bosonic content (gauge fields, Higgs boson) of the Standard Model and its transformation properties. The superscript α denotes the color index.

we can define left- and right-handed fields ψ_L and ψ_R :

$$\begin{aligned}\psi_L &= L\psi \leftrightarrow \phi, \\ \psi_R &= R\psi \leftrightarrow \chi.\end{aligned}\tag{5}$$

The Standard Model contains 45 Weyl fermions, 12 gauge bosons and one Higgs doublet¹. The number of independent parameters in the model is 18, viz.:

- 6 fermion masses: $m_u, m_d, m_c, m_s, m_t, m_b$;
- 3 lepton masses: m_e, m_μ, m_τ ;
- 1 gauge boson mass: m_Z (the mass of the electrically charged bosons W^\pm is connected to m_Z via the couplings);
- 1 Higgs boson mass;
- 3 couplings: g, g', g_s ;
- 4 CKM matrix parameters;

In the following, primed fermion fields denote weak eigenstates whereas unprimed fields are mass eigenstates.

¹As has been said before, we do not discuss the various ghost fields present in the theory.

1.2 Massless fermion fields and G_{SM}

We write down the Lagrangian for the fermion fields of the first generation. We consider at first a free and massless theory. For reasons that become clear in a moment, we group some of the terms in a special way:

$$\begin{aligned} \mathcal{L}_{1,\text{free}} = & i (\bar{\nu}'_e \ \bar{e}')_L \not{\partial} \begin{pmatrix} \nu'_e \\ e' \end{pmatrix}_L + i (\bar{u}' \ \bar{d}')_L \not{\partial} \begin{pmatrix} u' \\ d' \end{pmatrix}_L \\ & + i \bar{e}'_R \not{\partial} e_R + i \bar{u}'_R \not{\partial} u'_R + i \bar{d}'_R \not{\partial} d'_R. \end{aligned} \quad (6)$$

This Lagrangian is invariant under global G_{SM} transformations, which act in the following way on the fermion fields:

$$\begin{aligned} \begin{pmatrix} \nu'_e \\ e' \end{pmatrix}_L & \xrightarrow{G_{\text{SM}}} e^{i g T_2^a \theta^a} e^{i g' y_L^l \phi} \begin{pmatrix} \nu'_e \\ e' \end{pmatrix}_L, \\ \begin{pmatrix} u' \\ d' \end{pmatrix}_L & \xrightarrow{G_{\text{SM}}} e^{i g T_2^a \theta^a} e^{i g' y_L^q \phi} \begin{pmatrix} e^{i g_s T_3^b \chi^b} u' \\ e^{i g_s T_3^b \chi^b} d' \end{pmatrix}_L, \\ e'_R & \xrightarrow{G_{\text{SM}}} e^{i g' y_R^l \phi} e'_R, \\ u'_R & \xrightarrow{G_{\text{SM}}} e^{i g' y_R^u \phi} e^{i g_s T_3^b \chi^b} u'_R, \\ d'_R & \xrightarrow{G_{\text{SM}}} e^{i g' y_R^d \phi} e^{i g_s T_3^b \chi^b} d'_R. \end{aligned} \quad (7)$$

There are a lot of parameters and variables given in Eq. (7): the quantities θ^a , χ^b and ϕ are the “rotation angles” of the transformation; T_2^a and T_3^b are the generators of $SU(2)$ and $SU(3)$, respectively; the quantities $y_L^{l,q}$ are the weak hypercharge of the left-handed leptons and quarks, respectively, whereas $y_R^{l,u,d}$ denote the same quantities for the right-handed fields. Note here that in order for the two groups $SU(2)_L$ and $U(1)_Y$ to commute, the weak isospin partners must have the same Y quantum number. Since the right-handed fields are left untouched by $SU(2)_L$, they can have a different weak hypercharge. Indeed, as one can see in Table 1.1, y_R^u and y_R^d are not equal. Finally, the quantities g , g' and g_s are the couplings of the electroweak and strong interaction.

We would now like to elevate the transformation to a local one:

$$\theta^a, \chi^b, \phi \rightarrow \theta^a(x), \chi^b(x), \phi(x).$$

Under such a transformation, the Lagrangian in Eq. (6) is not invariant anymore. We fix this by replacing the partial derivatives with covariant ones. With the notation²

$$\begin{aligned} \psi_1 &= (\nu'_{e,L} \ e'_L \ e'_R \ u'_L \ d'_L \ u'_R \ d'_R)^T, \\ \mathbf{Y} &= \text{Block} [y_L^l, y_L^l, y_R^l, y_L^q, y_L^q, y_R^u, y_R^d], \\ \tilde{\mathbf{T}}_2^a &= \text{Block} [T_2^a, 0, T_2^a, 0, 0], \\ \tilde{\mathbf{T}}_3^b &= \text{Block} [0, 0, 0, T_3^b, T_3^b, T_3^b, T_3^b] \end{aligned} \quad (8)$$

²The function $\text{Block}[\dots]$ denotes a block matrix.

at hand, we make the following ansatz for the covariant derivative:

$$\mathbf{D}_\mu = \partial_\mu + i g \tilde{\mathbf{T}}_2^a W_\mu^a + i g' \mathbf{Y} B_\mu + i g_s \tilde{\mathbf{T}}_3^b G_\mu^b. \quad (9)$$

Gauge invariance requires that the newly introduced gauge fields W_μ^a , B_μ and G_μ^b transform under G_{SM} according to

$$\begin{aligned} T_2^a W_\mu^a(x) &\xrightarrow{G_{\text{SM}}} e^{i g T_2^a \theta^a(x)} \left(T_2^a W_\mu^a(x) - \frac{i}{g} \partial_\mu \right) e^{-i g T_2^a \theta^a(x)}, \\ B_\mu(x) &\xrightarrow{G_{\text{SM}}} B_\mu(x) - \partial_\mu \phi(x), \\ T_3^b G_\mu^b(x) &\xrightarrow{G_{\text{SM}}} e^{i g_s T_3^b \chi^b(x)} \left(T_3^b G_\mu^b(x) - \frac{i}{g_s} \partial_\mu \right) e^{-i g_s T_3^b \chi^b(x)}. \end{aligned} \quad (10)$$

It is now easy to check that the Lagrangian

$$\mathcal{L}_1 = i \bar{\psi}_1 \mathbf{D}_\mu \gamma^\mu \psi_1 \quad (11)$$

is invariant under local G_{SM} transformations. In order to arrive at \mathcal{L}_1 we needed to add to the theory one gauge boson for each of the twelve generators of G_{SM} .

Still missing is a kinetic term for the gauge bosons. This term must be chosen such that it does not break gauge invariance of the Lagrangian. In analogy to QED, we define field strength tensors as follows:

$$\begin{aligned} i g W_{\mu\nu}^a T_2^a &\doteq [\partial_\mu + i g T_2^b W_\mu^b, \partial_\nu + i g T_2^c W_\nu^c], \\ i g' B_{\mu\nu} &\doteq [\partial_\mu + i g' B_\mu, \partial_\nu + i g' B_\nu], \\ i g_s G_{\mu\nu}^a T_3^a &\doteq [\partial_\mu + i g_s T_3^b G_\mu^b, \partial_\nu + i g_s T_3^c G_\nu^c]. \end{aligned} \quad (12)$$

Their explicit form is given by

$$\begin{aligned} W_{\mu\nu}^a(x) &= \partial_\mu W_\nu^a(x) - \partial_\nu W_\mu^a(x) - g \epsilon^{abc} W_\mu^b(x) W_\nu^c(x), \\ B_{\mu\nu}(x) &= \partial_\mu B_\nu(x) - \partial_\nu B_\mu(x), \\ G_{\mu\nu}^a(x) &= \partial_\mu G_\nu^a(x) - \partial_\nu G_\mu^a(x) - g_s f^{abc} G_\mu^b(x) G_\nu^c(x). \end{aligned} \quad (13)$$

The quantities ϵ^{abc} and f^{abc} are the structure constants of $SU(2)$ and $SU(3)$, respectively.

We are now ready to write down the missing piece of the Lagrangian:

$$\mathcal{L}_{\text{YM}} = -\frac{1}{4} W_{\mu\nu}^A W^{\mu\nu,A} - \frac{1}{4} B_{\mu\nu} B^{\mu\nu} - \frac{1}{4} G_{\mu\nu}^B G^{\mu\nu,B}. \quad (14)$$

Unlike QED, the Lagrangian in Eq. (14) contains interaction terms between the gauge bosons of QCD (G^a) as well as interaction terms between the W^a -bosons. This is a feature of any non-Abelian gauge theory: The interaction terms arise due to the nonlinear terms in the definition of $W_{\mu\nu}^A$ and $G_{\mu\nu}^A$. The boson B belongs to an Abelian group and therefore the corresponding field strength tensor does not contain nonlinear terms.

Let us now focus on the electroweak gauge bosons and their interaction with matter. The physical particles mediating the electroweak interaction are the charged W -bosons W^\pm , the neutral Z -boson and the well-known photon field A_μ . The charged bosons are given through

$$\begin{aligned} W_\mu^+ &= \frac{1}{\sqrt{2}} (W_\mu^1 - i W_\mu^2) , \\ W_\mu^- &= \frac{1}{\sqrt{2}} (W_\mu^1 + i W_\mu^2) . \end{aligned} \quad (15)$$

The Z -boson and the photon are linear combinations of the B_μ - and the W_μ^3 -fields. The combinations can be written with the weak mixing angle θ_W (also known as Weinberg angle):

$$\begin{pmatrix} Z_\mu \\ A_\mu \end{pmatrix} = \begin{pmatrix} \cos \theta_W & -\sin \theta_W \\ \sin \theta_W & \cos \theta_W \end{pmatrix} \begin{pmatrix} W_\mu^3 \\ B_\mu \end{pmatrix}. \quad (16)$$

From experiment we know that the photon does not couple to the neutrino since it has a vanishing electric charge. By choosing

$$\begin{aligned} \sin \theta_W &= \frac{g'}{\sqrt{g^2 + g'^2}} , \\ \cos \theta_W &= \frac{g}{\sqrt{g^2 + g'^2}} , \end{aligned} \quad (17)$$

and defining the coupling constant e as

$$e = \frac{g g'}{\sqrt{g^2 + g'^2}} , \quad (18)$$

we can write the interaction terms of the leptons with the gauge bosons as follows:

$$\begin{aligned} \mathcal{L}_{\text{int}} &= -\frac{g}{\sqrt{2}} (\bar{\nu}'_{e,L} \gamma^\mu e'_L W_\mu^+ + \bar{e}'_L \gamma^\mu \nu'_{e,L} W_\mu^-) - e A_\mu j_{\text{em}}^\mu - \frac{g}{\cos \theta_W} Z_\mu j_{\text{NC}}^\mu \\ &\quad - \frac{g}{\sqrt{2}} (\bar{u}'_L \gamma^\mu d'_L W_\mu^+ + \bar{d}'_L \gamma^\mu u'_L W_\mu^-) - e A_\mu j_{\text{em},q}^\mu - \frac{g}{\cos \theta_W} Z_\mu j_{\text{NC},q}^\mu , \\ j_{\text{em}}^\mu &= -\bar{e}' \gamma^\mu e' , \\ j_{\text{NC}}^\mu &= \frac{1}{2} \bar{\nu}'_{e,L} \gamma^\mu \nu'_{e,L} - \frac{1}{2} \bar{e}'_L \gamma^\mu e'_L - \sin^2 \theta_W j_{\text{em}}^\mu , \\ j_{\text{em},q}^\mu &= \frac{2}{3} \bar{u}' \gamma^\mu u' - \frac{1}{3} \bar{d}' \gamma^\mu d' , \\ j_{\text{NC},q}^\mu &= \frac{1}{2} \bar{u}'_L \gamma^\mu u'_L - \frac{1}{2} \bar{d}'_L \gamma^\mu d'_L - \sin^2 \theta_W j_{\text{em},q}^\mu . \end{aligned} \quad (19)$$

Here, we set the weak hypercharges of the fermions as given in Table 1.1 in order to get the electric charges right. We can already see a relation between the three quantum numbers T_2^3 , Y and Q :

$$Q = T_2^3 + Y. \quad (20)$$

In Section 1.3 we see the reason for this.

We can now extend our discussion to all three families. The complete Lagrangian is

$$\mathcal{L} = i\bar{\psi}_1 \not{D} \psi_1 + i\bar{\psi}_2 \not{D} \psi_2 + i\bar{\psi}_3 \not{D} \psi_3 + \mathcal{L}_{\text{YM}}. \quad (21)$$

The two vectors ψ_2 and ψ_3 are defined in a similar way as ψ_1 : they collect all fermions of the 2nd and 3rd generation, respectively.

1.3 The Higgs mechanism, boson masses

In Section 1.2 we constructed a massless theory which is invariant under a local G_{SM} transformation. From experimental data we know that most of the presented particles do in fact have a mass. Unlike QED, we cannot simply write down an explicit mass term for e.g. the electron:

$$\begin{aligned} \mathcal{L}_{e\text{-mass}}^{\text{QED}} &= -m_e \bar{e} e \\ &= -m_e \bar{e}_L e_R - m_e \bar{e}_R e_L. \end{aligned} \quad (22)$$

A term like this mixes left- and right-handed fields. Since they transform differently under $SU(2)_L$, this term would explicitly break gauge invariance³. Weinberg [3] and Salam proposed a way to introduce masses via spontaneous symmetry breaking. They introduced a scalar Higgs field,

$$\Phi = \begin{pmatrix} \phi^+ \\ \phi^0 \end{pmatrix}, \quad (23)$$

which transforms as a doublet under $SU(2)_L$ (the superscripts correspond with the electric charge). The most general free and renormalizable Lagrangian involving only the Higgs doublet takes the following form:

$$\begin{aligned} \mathcal{L}_{\text{free}}^{\text{Higgs}} &= (\partial_\mu \Phi^\dagger) (\partial^\mu \Phi) - V(\Phi), \\ V(\Phi) &= \kappa \Phi^\dagger \Phi + \lambda (\Phi^\dagger \Phi)^2. \end{aligned} \quad (24)$$

For a Lagrangian which is invariant under local G_{SM} transformations, the partial derivative must be replaced with a covariant one:

$$D_\mu = \partial_\mu + i g T_2^a W_\mu^a + i g' y_H B_\mu. \quad (25)$$

In order for spontaneous symmetry breaking to occur, κ must be negative. We therefore replace κ by $-\mu^2$ with $\mu \in \mathbb{R}$. The field configuration that minimizes the potential $V(\phi)$

³The Lagrangian given in Eq. (22) is also not invariant under $U(1)_Y$.

is degenerated. It can be written as

$$\begin{aligned}\Phi_{\tilde{\theta}} &= e^{iT_2^a \theta^a} \begin{pmatrix} 0 \\ \rho_0 \end{pmatrix}, \\ \rho_0 &= \sqrt{\frac{\mu^2}{\lambda}}.\end{aligned}\tag{26}$$

We now work in unitary gauge and take our ground state to be $\Phi_{\tilde{\theta}}$. The Lagrangian given in Eq. (24) is invariant under $SU(2)_L$, the ground state, however, is not. The generator Q of $U(1)_Q$, which is given by $T_2^3 + Y$, annihilates the ground state (for a value of the weak hypercharge of the Higgs field as given in Table 1.2) and therefore implies that the vacuum is invariant under the corresponding group. Through the process of spontaneous symmetry breaking, the group $SU(2)_L \otimes U(1)_Y$ breaks down to $U(1)_Q$. The gauge bosons of the broken symmetries (W_μ^\pm and Z_μ) acquire now a mass which is associated with ρ_0 : in the unitary gauge, the Higgs doublet can be written as

$$\Phi = \frac{1}{\sqrt{2}} \begin{pmatrix} 0 \\ \tilde{\rho}(x) \end{pmatrix} = \frac{1}{\sqrt{2}} \begin{pmatrix} 0 \\ \rho_0 + \rho(x) \end{pmatrix},\tag{27}$$

with $\rho(x)$ being the physical Higgs field. It has a vacuum expectation value of zero. We replace the Higgs doublet in the Lagrangian with the expression given in Eq. (27) and rewrite the gauge bosons with Eq. (15) and (16). This procedure yields interaction terms of the physical Higgs field with the gauge bosons of the broken symmetries as well as terms which can be interpreted as mass terms for W^\pm and Z . The masses can be read off of these terms:

$$\begin{aligned}m_Z^2 &= \frac{e^2 \rho_0^2}{4 \sin^2 \theta_W \cos^2 \theta_W}, \\ m_W^2 &= \frac{e^2 \rho_0^2}{4 \sin^2 \theta_W}.\end{aligned}\tag{28}$$

We see that the masses of the Z - and the W -boson are related through the Weinberg angle:

$$\frac{m_W}{m_Z} = \cos \theta_W.\tag{29}$$

There is no mass term for the photon field: the photon is a gauge boson of an unbroken symmetry group, namely $U(1)_Q$, and therefore remains massless [20, 21]. Because of that, there is also no interaction term of the photon with the Higgs field. All of this is consistent with phenomenology.⁴

The mass m_H of the Higgs field itself is contained in the potential term and is proportional to ρ_0 as well:

$$m_H^2 = 2 \lambda \rho_0^2.\tag{30}$$

⁴The couplings of the W - and Z -bosons to the Higgs field are proportional to their respective masses squared. The upper experimental limit for a photon mass is currently of the order 10^{-16} eV [13]. One would therefore have a hard time finding such a coupling experimentally.

1.4 Fermion masses and the CKM matrix

The masses of the gauge bosons W^\pm and Z were generated through spontaneous symmetry breaking of the gauge group $SU(2)_L \otimes U(1)_Y$. How can we obtain the still missing fermion masses? We need to find terms which couple the fermions to the Higgs doublet. They must be renormalizable as well as gauge invariant. Furthermore, they must be Lorentz scalars. The most general possibility for such a term is the Yukawa-Lagrangian. For the charged leptons of the first generation, the Lagrangian takes the following form:⁵

$$\mathcal{L}_{1,\text{Yukawa}}^{\text{Leptons}} = -c_e \bar{e}'_R \Phi^\dagger \begin{pmatrix} \nu'_e \\ e' \end{pmatrix}_L + \text{h.c.} \quad (31)$$

A value for the weak hypercharge of the Higgs field of $1/2$ guarantees that this Lagrangian is gauge invariant. The generalization to three generations is readily available:

$$\mathcal{L}_{\text{Yukawa}}^{\text{Leptons}} = -(\bar{e}'_R \quad \bar{\mu}'_R \quad \bar{\tau}'_R) \mathbf{C}_l \begin{pmatrix} \Phi^\dagger \begin{pmatrix} \nu'_e \\ e' \end{pmatrix}_L \\ \Phi^\dagger \begin{pmatrix} \nu'_\mu \\ \mu' \end{pmatrix}_L \\ \Phi^\dagger \begin{pmatrix} \nu'_\tau \\ \tau' \end{pmatrix}_L \end{pmatrix} + \text{h.c.} \quad (32)$$

Replacing Φ according to Eq. (27) splits $\mathcal{L}_{\text{Yukawa}}^{\text{Leptons}}$ up into two parts: one part characterizes the interaction between the leptons and the physical Higgs field; the other part is given by

$$\mathcal{L}_{\text{Mass}}^{\text{Leptons}} = -(\bar{e}'_R \quad \bar{\mu}'_R \quad \bar{\tau}'_R) \mathbf{M}_l \begin{pmatrix} e' \\ \mu' \\ \tau' \end{pmatrix}_L + \text{h.c.}, \quad (33)$$

$$\mathbf{M}_l = \frac{\rho_0}{\sqrt{2}} \mathbf{C}_l.$$

The label already hints at the function this part of the Lagrangian is going to provide. In principle, the matrix \mathbf{M}_l is an arbitrary complex 3×3 matrix and cannot be identified with a mass matrix. However, it is always possible to transform the charged lepton fields in such a way that \mathbf{M}_l is diagonal and its elements are positive real numbers (or zero). Applying this transformation to all terms in the Lagrangian yields the latter expressed in mass eigenstates of the charged leptons. This newly found Lagrangian contains flavor-mixing terms in the charged current. A suitable transformation of the (left-handed) neutrino fields eliminates these terms and leaves the rest of the Lagrangian unchanged (except that it is now expressed in these new neutrino fields).⁶ Thus, we arrive at a Lagrangian whose

⁵Instead of Φ , one can actually choose any scalar $SU(2)_L$ doublet with the correct weak hypercharge.

⁶Such a transformation exists only because the neutrinos are massless: when transforming the neutrino fields, we do not have to be considerate of a possible neutrino mass matrix.

electroweak interaction terms are completely equivalent to the ones in Eq. (21) (e.g. there is still no current that connects leptons of different generations with one another). All occurring lepton fields are mass eigenstates and we can therefore drop the prime in the notation.

We now turn to the masses of the quarks. For the down-type quarks (d , s and b) we introduce a Yukawa-Lagrangian similar to the one in Eq. (32). We denote the corresponding (still arbitrary complex) Yukawa matrix with \mathbf{C}_q^d . The up-type quarks are a little trickier. Instead of Φ we use $i\sigma_2\Phi^*$ as the $SU(2)_L$ doublet, with σ_2 being the second Pauli matrix:

$$\mathcal{L}_{\text{Yukawa}}^{\text{u-quarks}} = -(\bar{u}'_R \ \bar{c}'_R \ \bar{t}'_R) \mathbf{C}_q^u \begin{pmatrix} i\sigma_2\Phi^* \begin{pmatrix} u' \\ d' \end{pmatrix}_L \\ i\sigma_2\Phi^* \begin{pmatrix} c' \\ s' \end{pmatrix}_L \\ i\sigma_2\Phi^* \begin{pmatrix} t' \\ b' \end{pmatrix}_L \end{pmatrix} + \text{h.c.} \quad (34)$$

As before with the charged leptons, both Yukawa matrices can be diagonalized by unitary transformations of the quark fields. We give them here explicitly:

$$\begin{pmatrix} u' \\ c' \\ t' \end{pmatrix}_L = \mathbf{V}_u \begin{pmatrix} u \\ c \\ t \end{pmatrix}_L, \quad \begin{pmatrix} u' \\ c' \\ t' \end{pmatrix}_R = \mathbf{U}_u \begin{pmatrix} u \\ c \\ t \end{pmatrix}_R,$$

$$\begin{pmatrix} d' \\ s' \\ b' \end{pmatrix}_L = \mathbf{V}_d \begin{pmatrix} d \\ s \\ b \end{pmatrix}_L, \quad \begin{pmatrix} d' \\ s' \\ b' \end{pmatrix}_R = \mathbf{U}_d \begin{pmatrix} d \\ s \\ b \end{pmatrix}_R,$$

with $\mathbf{V}_u, \mathbf{U}_u, \mathbf{V}_d, \mathbf{U}_d \in U(3)$. Unlike in the lepton sector, there exists only one set of these matrices (apart from unphysical phase transformations) that diagonalizes the Yukawa coupling matrices. Because of that, the form of the Lagrangian for the mass eigenstates is different than for the weak eigenstates. Explicitly, we have a charged current which mixes quark generations with one another. Defining the Cabibbo-Kobayashi-Maskawa matrix (CKM matrix) as

$$\mathbf{V}_{\text{CKM}} = \mathbf{V}_u^\dagger \mathbf{V}_d, \quad (35)$$

we can write the coupling term of the quarks with the W^\pm -bosons as follows:

$$\mathcal{L}_{\text{CC}}^{\text{Quarks}} = -\frac{1}{2} \frac{e}{\sin\theta_W} (W_\mu^+ J^{\mu,-} + W_\mu^- J^{\mu,+}),$$

$$J^{\mu,-} = (\bar{u} \ \bar{c} \ \bar{t})_L \mathbf{V}_{\text{CKM}} \begin{pmatrix} d \\ s \\ b \end{pmatrix}_L, \quad (36)$$

The Lagrangian written in terms of mass eigenstates mixes quarks of different generations and different electric charge with one another. The neutral currents, however, stay diagonal: flavor-changing neutral currents (FCNC) are induced at the one-loop level and are therefore suppressed.

The CKM matrix operates by definition on the down-type quark. Its elements are conveniently labeled as

$$\begin{aligned} \begin{pmatrix} d' \\ s' \\ b' \end{pmatrix} &= \mathbf{V}_{\text{CKM}} \begin{pmatrix} d \\ s \\ b \end{pmatrix}, \\ \mathbf{V}_{\text{CKM}} &= \begin{pmatrix} V_{ud} & V_{us} & V_{ub} \\ V_{cd} & V_{cs} & V_{cb} \\ V_{td} & V_{ts} & V_{tb} \end{pmatrix}, \end{aligned} \quad (37)$$

hinting at which element is responsible for the mixing of two specific quark flavors. Note here that the weak eigenstates on the lhs of Eq. (37) are not the same weak eigenstates as in Eq. (6). They are, however, connected by unitary transformations. For reasons of readability we choose not to introduce another symbol.

The matrix \mathbf{V}_{CKM} is a product of unitary matrices and is therefore unitary itself. Such a matrix has in principle 9 real parameters. However, only four of them (three angles and one phase) are physical. The other five parameters can be gotten rid of by suitable transformations which leave the remaining terms in the Lagrangian invariant. The one phase still present is the only source of CP-violation in the SM⁷.

The standard parameterization of \mathbf{V}_{CKM} was proposed in [22]. It is obtained by the product of three complex rotation matrices, where the rotations are characterized by the Euler angles θ_{12} , θ_{13} and θ_{23} and an overall phase δ :

$$\mathbf{V}_{\text{CKM}} = \begin{pmatrix} c_{12} c_{13} & s_{12} c_{13} & s_{13} e^{-i\delta} \\ -s_{12} c_{23} - c_{12} s_{23} s_{13} e^{i\delta} & c_{12} c_{23} - s_{12} s_{23} s_{13} e^{i\delta} & s_{23} c_{13} \\ s_{12} s_{23} - c_{12} c_{23} s_{13} e^{i\delta} & -c_{12} s_{23} - c_{12} s_{23} s_{13} e^{i\delta} & c_{23} c_{13} \end{pmatrix}, \quad (38)$$

where $c_{ij} = \cos \theta_{ij}$ and $s_{ij} = \sin \theta_{ij}$. This parameterization has the advantage that the rotation angles are defined and labeled in a way which relates to the mixing of two specific generations. If one of these angles vanishes, the mixing between those two generations vanishes as well.

Another parameterization which accounts for the hierarchy between the different matrix elements was introduced by Wolfenstein [23]. It is an approximate parameterization in which each matrix element is expanded in the small parameter $\lambda = |V_{us}| \approx 0.22$. From phenomenology we know that c_{13} and c_{23} are very close to unity (e.g. c_{13} deviates from

⁷Neglecting the parameter θ connected with strong CP violation, mentioned in the introduction of this chapter.

one only in the sixth decimal place [13]). Thus, we can set $c_{13} = c_{23} = 1$ to an excellent approximation. With the further identifications

$$\begin{aligned}s_{23} &= A \lambda^2, \\ s_{13} e^{-i\delta} &= A \lambda^3 (\rho - i\eta),\end{aligned}$$

the Wolfenstein parameterization is given by

$$\mathbf{V}_{\text{CKM}} = \begin{pmatrix} 1 - \frac{\lambda^2}{2} & \lambda & A \lambda^3 (\rho - i\eta) \\ -\lambda & 1 - \frac{\lambda^2}{2} & A \lambda^2 \\ A \lambda^3 (1 - \rho - i\eta) & -A \lambda^2 & 1 \end{pmatrix} + \mathcal{O}(\lambda^4). \quad (39)$$

This parameterization turns out to be very useful in the study of rare B decays.

2 Theoretical framework for inclusive B meson decays

In this chapter we elaborate on the theoretical framework for inclusive B meson decays. The first section gives an overview on the effective Hamiltonian which is used throughout this thesis. This Hamiltonian is constructed by integration out the heavy degrees of freedom from the Standard Model followed by an operator product expansion. The following section discusses methods to approximate decays of physical particles with the underlying quark transition in case of heavy particles. In Section 2.3 we look at the matching procedure which is needed to connect the full Standard Model theory to the effective Hamiltonian presented in Section 2.1. We conclude this chapter with a discussion of the renormalization group equation and the anomalous dimension matrix.

2.1 Operator product expansion, effective Hamiltonians¹

The decay of a b -quark usually has two distinct parts. These parts are separated from each other conceptually and practically by physics at very different energy scales. Let us illustrate this point with the transition $b \rightarrow c d \bar{u}$. In the left frame of Fig. 2.1, we see the dominant Standard Model Feynman diagram corresponding to this process. The amplitude is given as

$$A = \left(\frac{-i g}{\sqrt{2}} \right)^2 V_{cb} V_{ud}^* (\bar{d} \gamma_\mu L u) \frac{1}{i} \frac{g^{\mu\nu} - \frac{k^\mu k^\nu}{m_W^2}}{k^2 - m_W^2} (\bar{c} \gamma_\nu L b), \quad (40)$$

where k denotes the four-momentum flowing through the W propagator. The two scales involved are m_W (≈ 80 GeV) and k , which is of the order of the mass m_b (≈ 4.8 GeV) of the decaying b -quark. Since the ratio of these two scales is small we can attempt to expand the amplitude in k :

$$A = \frac{g^2}{2i} V_{cb} V_{ud}^* \left[\frac{1}{m_W^2} \underbrace{(\bar{d} \gamma_\mu L u) (\bar{c} \gamma^\mu L b)}_{\text{dim 6 operator}} + \frac{1}{m_W^4} (\text{dim 8 operator}) + \dots \right]. \quad (41)$$

¹Some people seem to dislike the expression 'effective', claiming that the meaning of this word (successful, efficient, powerful) somehow promises more than the corresponding theory can deliver. The same, however, can be said about 'super'symmetric theories. We understand the expression *effective theory* or *effective Hamiltonian* to describe a theory which is active or operative in a given energy range or a given situation. E.g. Newton's theory of motion describes our everyday world (far away from accelerators) to an excellent degree. There is no need to relativistically add the velocities of a train and a passenger walking around in this train. This would only complicate the calculation with hardly any benefit at all. Newton's theory is in this sense in operation or effective in the given situation. The same can be said about the effective theory we are about to present in this chapter. It is a means of describing decays of B -mesons accurately (enough) while trying to simplify the involved calculations as much as possible.

The former nonlocal interaction is replaced by an infinite sum of local operators of ascending dimension. These operators only contain the light fields; the physics of the high scale is incorporated in the couplings of the individual operators. Higher-order operators are suppressed by inverse powers of the W mass. Because of this strong suppression, truncating the series after the first term is still an excellent approximation of the amplitude. We can thus write down an effective Hamiltonian which describes this process:

$$\begin{aligned}\mathcal{H}_{\text{eff}} &= \frac{4G_F}{\sqrt{2}} V_{cb} V_{ud}^* C (\bar{d} \gamma_\mu L u) (\bar{c} \gamma^\mu L b) , \\ G_F &= \frac{g^2}{4\sqrt{2} m_W^2} ,\end{aligned}\tag{42}$$

with G_F being the well known Fermi constant. The quantity C is the so-called Wilson

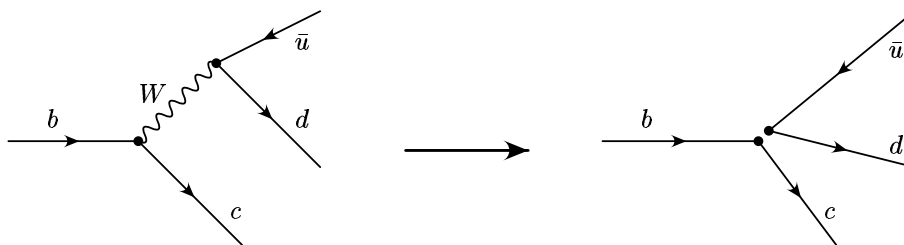


Figure 2.1: The process $b \rightarrow c d \bar{u}$ from a high-energy (left) and low-energy (right) point of view.

coefficient corresponding to the given local operator and is in this simple case, namely in the tree approximation of the amplitude, equal to +1. When considering QCD corrections, the effective Hamiltonian given in Eq. (42) changes:

$$\begin{aligned}\mathcal{H}_{\text{eff}} &= \frac{4G_F}{\sqrt{2}} V_{cb} V_{ud}^* (C_1(\mu) O_1 + C_2(\mu) O_2) , \\ O_1 &= (\bar{d}_\alpha \gamma_\mu L u_\beta) (\bar{c}_\beta \gamma^\mu L b_\alpha) , \\ O_2 &= (\bar{d}_\alpha \gamma_\mu L u_\alpha) (\bar{c}_\beta \gamma^\mu L b_\beta) ,\end{aligned}\tag{43}$$

with α and β being color indices. QCD effects summoned a new operator, viz O_1 . It differs from the already existing operator O_2 in its color structure. Along with the new operator comes a new Wilson coefficient. Consistent with the effective Hamiltonian in Eq. (42), it is zero in the limit $\alpha_s \rightarrow 0$: the operator O_1 starts contributing to the amplitude only at order α_s . The Wilson coefficients $C_1(\mu)$ and $C_2(\mu)$ are functions of the W mass, the strong coupling α_s and the renormalization scale μ . The latter can be viewed as a separation scale: all physics above μ is contained in the Wilson coefficients whereas long distance contributions (below μ) are incorporated in matrix elements involving the operators O_1 and O_2 .

In the literature, the method just described is known under “operator product expansion” (OPE) and was first introduced by Wilson in 1969 [24] (hence the name for the coefficients). OPE is a crucial tool for the theory of weak decays, not only in the case of B mesons, but also for kaons, mesons with charm content, light or heavy baryons and weakly decaying hadrons in general. The most important property of OPE is the factorization of long- and short-distance contributions as described above. The short-distance part is in general independent of any external states; Furthermore, since the strong coupling α_s is small at high energies (due to the asymptotic freedom of QCD), the Wilson coefficients can be systematically calculated in fixed order perturbation theory when using a high renormalization scale. The problem to evaluate matrix elements involving local operators and external states, however, remains. Generally, this task requires nonperturbative techniques such as QCD sum rules or lattice QCD. In decays of heavy hadrons, the fact that the mass of the underlying heavy quark is still large in comparison with the QCD scale Λ_{QCD} can be exploited. This can be achieved e.g. by using the heavy quark effective theory (HQET) or by using the heavy quark expansion (HQE). Both of these approaches are described in some detail in Section 2.2.

As has been mentioned in the introduction, this thesis focuses on the three inclusive processes $B \rightarrow X_{s,d} \ell^+ \ell^-$ and $B \rightarrow X_s \gamma$. We now look at the relevant portions of the effective Hamiltonian for each of these processes. For transitions of the form $b \rightarrow s Y$, where Y denotes e.g. a lepton-pair, a photon, or a gluon, the relevant Hamiltonian is given by

$$\mathcal{H}_{\text{eff}}^{b \rightarrow s} = \frac{4 G_F}{\sqrt{2}} \left[\sum_{i=1}^2 C_i(\mu) (\lambda_c O_{i,s}^c + \lambda_u O_{i,s}^u) - \lambda_t \sum_{i=3}^{10} C_i(\mu) O_{i,s} \right], \quad (44)$$

where the quantities $\lambda_q = V_{qb} V_{qs}^*$ collect the dependence of the CKM matrix elements. The contributions containing the operators $O_{1,s}^u$ and $O_{2,s}^u$ are strongly suppressed due to $|\lambda_u| \ll |\lambda_c|, |\lambda_t|$. The approximation $\lambda_u = 0$ can therefore be used² and the Hamiltonian simplifies due to unitarity properties of the CKM matrix:

$$\mathcal{H}_{\text{eff}}^{b \rightarrow s} = -\frac{4 G_F}{\sqrt{2}} \lambda_t \sum_{i=1}^{10} C_i(\mu) O_{i,s}, \quad (45)$$

with $O_{1,s} = O_{1,s}^c$ and $O_{2,s} = O_{2,s}^c$. One has some freedom in the choice of the operator basis $\{O_{i,s}\}$. We follow [25] and define the operators as follows:

$$\begin{aligned} O_{1,s} &= (\bar{s}_L \gamma_\mu T^a c_L) (\bar{c}_L \gamma^\mu T^a b_L), & O_{2,s} &= (\bar{s}_L \gamma_\mu c_L) (\bar{c}_L \gamma^\mu b_L), \\ O_{3,s} &= (\bar{s}_L \gamma_\mu b_L) \sum_q (\bar{q} \gamma^\mu q), & O_{4,s} &= (\bar{s}_L \gamma_\mu T^a b_L) \sum_q (\bar{q} \gamma^\mu T^a q), \\ O_{5,s} &= (\bar{s}_L \gamma_\mu \gamma_\nu \gamma_\rho b_L) \sum_q (\bar{q} \gamma^\mu \gamma^\nu \gamma^\rho q), & O_{6,s} &= (\bar{s}_L \gamma_\mu \gamma_\nu \gamma_\rho T^a b_L) \sum_q (\bar{q} \gamma^\mu \gamma^\nu \gamma^\rho T^a q), \\ O_{7,s} &= \frac{e}{g_s^2} \bar{m}_b(\mu) (\bar{s}_L \sigma^{\mu\nu} b_R) F_{\mu\nu}, & O_{8,s} &= \frac{1}{g_s} \bar{m}_b(\mu) (\bar{s}_L \sigma^{\mu\nu} T^a b_R) G_{\mu\nu}^a, \\ O_{9,s} &= \frac{e^2}{g_s^2} (\bar{s}_L \gamma_\mu b_L) \sum_\ell (\bar{\ell} \gamma^\mu \ell), & O_{10,s} &= \frac{e^2}{g_s^2} (\bar{s}_L \gamma_\mu b_L) \sum_\ell (\bar{\ell} \gamma^\mu \gamma_5 \ell), \end{aligned} \quad (46)$$

²Note that this simplification removes any CP violating effect from the Hamiltonian. Thus, if one is interested in CP asymmetries, this approximation cannot be employed.

where $F_{\mu\nu}$ and $G_{\mu\nu}^a$ denote the field strength tensors of the electromagnetic and the strong field, respectively and T^a ($a=1, \dots, 8$) are $SU(3)_c$ generators. The quantity $\overline{m}_b(\mu)$ is the running b -quark mass in the modified minimal subtraction scheme ($\overline{\text{MS}}$) at the renormalization scale μ (see Section 2.4). To first order in α_s it is related to the pole mass m_b by

$$\overline{m}_b(\mu) = m_b \left[1 - \frac{4}{3} \frac{\alpha_s(\mu)}{\pi} + \frac{\alpha_s(\mu)}{\pi} \ln \left(\frac{m_b^2}{\mu^2} \right) \right].$$

The operators $O_{1,s} - O_{6,s}$ are defined such that problems connected with the treatment of γ_5 in an arbitrary dimension d do not arise [26]. The factors $1/g_s^2$ in the definition of the operators $O_{7,s}$, $O_{9,s}$ and $O_{10,s}$ as well as the factor $1/g_s$ present in $O_{8,s}$ are artificial. They were chosen by Misiak [27] in order to simplify the organization of the calculation: With these definitions, the one-loop anomalous dimensions (needed for a leading logarithmic (LL) calculation) of the operators $O_{i,s}$ are all proportional to g_s^2 , while two-loop anomalous dimensions (needed for a next-to-leading logarithmic (NLL) calculation) are proportional to g_s^4 , etc. We comment further on this issue in Section 2.4 when we look at the anomalous dimension matrix itself.

We turn to transitions of the form $b \rightarrow dY$, where Y is again understood to be either a lepton-pair, a photon or a gluon. The relevant part of the effective Hamiltonian for these processes is similar to Eq. (44). It reads

$$\mathcal{H}_{\text{eff}}^{b \rightarrow d} = \frac{4G_F}{\sqrt{2}} \left[\sum_{i=1}^2 C_i(\mu) (\xi_c O_{i,d}^c + \xi_u O_{i,d}^u) - \xi_t \sum_{i=3}^{10} C_i(\mu) O_{i,d} \right]. \quad (47)$$

The CKM dependence is contained in $\xi_q = V_{qb}V_{qd}^*$, $q \in \{u, c, t\}$. These three quantities are all of the order λ^3 , where λ is the expansion parameter in the Wolfenstein representation of the CKM matrix (see Eq. (39)). Thus, one cannot neglect contributions arising from the operators $O_{1,d}^u$ and $O_{2,d}^u$ and therefore the dependence of the CKM matrix elements does not globally factorize. Because of this it can be expected that CP asymmetry effects for $b \rightarrow dY$ transitions are much larger than for corresponding decays with an s -quark. The operators present in Eq. (47) are given as

$$\begin{aligned} O_{1,d}^c &= (\bar{d}_L \gamma_\mu T^a c_L) (\bar{c}_L \gamma^\mu T^a b_L), & O_{2,d}^c &= (\bar{d}_L \gamma_\mu c_L) (\bar{c}_L \gamma^\mu b_L), \\ O_{1,d}^u &= (\bar{d}_L \gamma_\mu T^a u_L) (\bar{u}_L \gamma^\mu T^a b_L), & O_{2,d}^u &= (\bar{d}_L \gamma_\mu u_L) (\bar{u}_L \gamma^\mu b_L), \\ O_{3,d} &= (\bar{d}_L \gamma_\mu b_L) \sum_q (\bar{q} \gamma^\mu q), & O_{4,d} &= (\bar{d}_L \gamma_\mu T^a b_L) \sum_q (\bar{q} \gamma^\mu T^a q), \\ O_{5,d} &= (\bar{d}_L \gamma_\mu \gamma_\nu \gamma_\rho b_L) \sum_q (\bar{q} \gamma^\mu \gamma^\nu \gamma^\rho q), & O_{6,d} &= (\bar{d}_L \gamma_\mu \gamma_\nu \gamma_\rho T^a b_L) \sum_q (\bar{q} \gamma^\mu \gamma^\nu \gamma^\rho T^a q), \\ O_{7,d} &= \frac{e}{g_s^2} \overline{m}_b(\mu) (\bar{d}_L \sigma^{\mu\nu} b_R) F_{\mu\nu}, & O_{8,d} &= \frac{1}{g_s} \overline{m}_b(\mu) (\bar{d}_L \sigma^{\mu\nu} T^a b_R) G_{\mu\nu}^a, \\ O_{9,d} &= \frac{e^2}{g_s^2} (\bar{d}_L \gamma_\mu b_L) \sum_\ell (\bar{\ell} \gamma^\mu \ell), & O_{10,d} &= \frac{e^2}{g_s^2} (\bar{d}_L \gamma_\mu b_L) \sum_\ell (\bar{\ell} \gamma^\mu \gamma_5 \ell). \end{aligned} \quad (48)$$

Once the effective Hamiltonian is constructed the steps necessary to calculate physical observables in inclusive B decays are threefold:

- **Matching calculation:** The full Standard Model theory must be matched onto the effective theory in order to determine the Wilson coefficients C_i . This calculation is performed at the high scale $\mu_W \sim m_W, m_t$ where the coefficients can be worked out in fixed order perturbation theory:

$$C_i(\mu_W) = C_i^{(0)}(\mu_W) + \frac{g_s^2}{16\pi^2} C_i^{(1)}(\mu_W) + \frac{g_s^4}{(16\pi^2)^2} C_i^{(2)}(\mu_W) + \mathcal{O}(g_s^6). \quad (49)$$

Since the Wilson coefficients comprise only physics of the high scale, they do not depend on external momenta and small masses. The matching procedure can thus be done in a momentum configuration which simplifies the calculations as much as possible. When choosing a special set-up, however, one loses the explicit check that the coefficients only depend on high scales. We look at a sample matching procedure in Section 2.3.

- **Renormalization group equation:** The renormalization group equation (RGE) must be solved in order to evolve the Wilson coefficients from the high scale μ_W to the low scale $\mu_b \sim m_b$. This step requires the knowledge of the anomalous dimension matrix γ as well as the function β which governs the scale dependence of α_s . In Section 2.4 we show how to systematically calculate γ .
- **Determination of the matrix elements:** The last missing ingredients are the hadronic matrix elements calculated at the low scale $\mu = \mu_b \approx m_b$. At μ_b , the strong running coupling constant $\alpha_s(\mu)$ is still small enough ($\alpha_s(\mu_b) \approx 0.21$) to allow for an expansion. In the case of inclusive decays, heavy quark expansion justifies an approximation of the true hadronic matrix elements with the underlying quark level transition. For further details on how to calculate these matrix elements we refer to Section 3 of this part and to Parts II, III and V. In the aforementioned Section 3 we look at a handy tool to help tackle the problem of evaluating complicated Feynman diagrams, namely the method of Mellin-Barnes representations.

2.2 Heavy quark limit

QCD confinement implies that free quarks are not asymptotic states of the theory. Instead, nonperturbative QCD effects dress the quark level transitions to hadronic transitions. E.g. the quark decaying process $b \rightarrow s \ell^+ \ell^-$ can be realized in nature within the hadronic transition $B \rightarrow K \ell^+ \ell^-$. In this section we present two methods to deal with the problem of hadronic matrix elements. Both methods are based on the heavy quark limit. In Section 2.1 we removed the degrees of freedom of the heavy particles (the W and Z bosons and the top quark) completely from the low-energy part. Here, we try to find a method to describe the properties and decays of hadrons *containing* a heavy particle, namely the b -quark. Since it does not just appear as an intermediate particle we cannot proceed in the same manner as in Section 2.1.

2.2.1 Heavy quark effective theory

HQET describes the static approximation for a heavy quark, formulated in a covariant way as an effective theory. It allows for a systematic inclusion of power corrections (i.e. corrections in inverse powers of the mass m_Q of the heavy quark). We follow [28] and sketch the derivation of its Lagrangian. Our starting point is the usual QCD Lagrangian for one heavy quark field ψ (see also Eq. (9)):

$$\begin{aligned}\mathcal{L}(x) &= i \bar{\psi}(x) \not{D}(x) \psi(x) - m_Q \bar{\psi}(x) \psi(x), \\ D_\mu(x) &= \partial_\mu + i g_s T^a G_\mu^a(x).\end{aligned}\tag{50}$$

The momentum of the heavy quark can be decomposed in a part that scales with the mass m_Q and a residual part k :

$$p = m_Q v + k,$$

where v is the four-velocity of the heavy hadron. The momentum k is determined by soft QCD bound state interactions and is thus of order Λ_{QCD} . Next, we decompose the quark field ψ :

$$\begin{aligned}h_v(x) &= e^{i m_Q v \cdot x} P_{+v} \psi(x), \\ H_v(x) &= e^{i m_Q v \cdot x} P_{-v} \psi(x), \\ P_{\pm v} &= \frac{1 \pm \not{v}}{2}.\end{aligned}\tag{51}$$

The symbols $P_{\pm v}$ are projection operators. Their action represents the covariant generalization of decomposing ψ into upper and lower components. Using the standard representation for the γ -matrices, this is evident in the rest frame where $\not{v} = \gamma^0$. Using Eq. (51) we see that

$$\psi(x) = e^{-i m_Q v \cdot x} (h_v(x) + H_v(x)).\tag{52}$$

The exponential factor $e^{i m_Q v \cdot x}$ present in the definition of $h_v(x)$ and $H_v(x)$ removes the large-frequency part of the x -dependence in ψ resulting from the large momentum $m v$. Therefore, the x -dependence of $h_v(x)$ and $H_v(x)$ is dominated by the small residual momentum k . Multiplying the equation of motion $(i \not{D} - m_Q) \psi = 0$ with the projectors $P_{\pm v}$ and using Eqs. (51) and (52), we arrive at a coupled system of equations, representing the equation of motion for the two fields $h_v(x)$ and $H_v(x)$:

$$\begin{aligned}i v \cdot D h_v &= -i \not{D}_\perp H_v, \\ (i v \cdot D + 2 m_Q) H_v &= i \not{D}_\perp h_v,\end{aligned}\tag{53}$$

with

$$D_\perp^\mu \doteq D^\mu - v^\mu v \cdot D.$$

The second equation in (53) implies, together with the fact that derivatives acting on h_v scale like Λ_{QCD} , that H_v is suppressed with respect to h_v by a factor of order Λ_{QCD}/m_Q .

Thus, h_v contains the large components of the quark field and H_v the small components. The HQET Lagrangian is now obtained by expressing Eq. (50) in terms of h_v and H_v and eliminating the latter with help of Eq. (53). We find

$$\begin{aligned}\mathcal{L}_{\text{eff}} &= i\bar{h}_v v \cdot D h_v + i\bar{h}_v \not{D}_\perp \frac{1}{i v \cdot D + 2m_Q} i \not{D}_\perp h_v \\ &= \mathcal{L}_{\text{HQET}} + \frac{1}{2m_Q} \sum_{l=0}^{\infty} i\bar{h}_v \not{D}_\perp \left(-\frac{i v \cdot D}{2m_Q} \right)^l i \not{D}_\perp h_v, \\ \mathcal{L}_{\text{HQET}} &\doteq i\bar{h}_v v \cdot D h_v.\end{aligned}\tag{54}$$

In the second line of Eq. (54) we have employed an OPE to express the nonlocal operator $(i v \cdot D + 2m_Q)^{-1}$ as an infinite sum of local operators with ascending dimension. The operators of higher dimension are suppressed by inverse powers of the mass of the heavy quark. The term $\mathcal{L}_{\text{HQET}}$ corresponds with the infinite mass limit. It has two new symmetries not present in full QCD: the first one is an invariance under rotation in flavor space. Consider a theory with two heavy quarks c and b moving with the same velocity v . The corresponding Lagrangian in the heavy quark limit reads

$$\mathcal{L}_{b,c} = i\bar{c}_v v \cdot D c_v + i\bar{b}_v v \cdot D b_v.\tag{55}$$

This Lagrangian is invariant under an $SU(2)$ transformation:

$$\begin{pmatrix} b_v \\ c_v \end{pmatrix} \rightarrow \begin{pmatrix} b'_v \\ c'_v \end{pmatrix} = U_v \begin{pmatrix} b_v \\ c_v \end{pmatrix}.$$

The reason for this symmetry is that the two heavy quarks are not distinguishable. The only parameter that made them unique, namely their masses, is not present anymore. The discussion can be extended to N_h heavy quarks moving with the same velocity v . The symmetry group is then $SU(N_h)$. The second symmetry is connected with the decoupling of the spin of a heavy quark with the gluon field. This makes the heavy quark spin operator the generator of another $SU(2)$ symmetry. These two symmetries are known as the spin-flavor symmetries of HQET [29]. They lead to relations between different heavy-hadron form factors.

The heavy quark effective theory has many applications in the field of B physics. It has e.g. been used to calculate the form factors for $B \rightarrow D l \bar{\nu}_l$ and $B \rightarrow D^* l \bar{\nu}_l$ at zero recoil of the D or D^* meson [30]. Further, it has been employed to extract CKM matrix elements such as $|V_{cb}|$ or $|V_{ub}|$ [31]. Worth mentioning is also their predictive power in the field of B meson spectroscopy. In the field of inclusive decays, however, HQET cannot be applied directly [32]. The method used there is described in Section 2.2.2.

2.2.2 Heavy quark expansion

The technique employed to calculate observables within inclusive B decays goes by the name of heavy quark expansion (HQE). It is based on the optical theorem for inclusive

decays and an operator product expansion in Λ_{QCD}/m_b of the transition operator. Let H be a heavy hadron containing a b -quark. Further, X denotes an inclusive final state.³ With help of the optical theorem, the decay width $\Gamma(H \rightarrow X)$ can be written as

$$\Gamma(H \rightarrow X) = \frac{1}{2m_H} \langle H | \mathcal{T} | H \rangle, \quad (56)$$

$$\mathcal{T} = \text{Im} \left[i \int d^4x T \{ \mathcal{H}_{\text{eff}}(x) \mathcal{H}_{\text{eff}}(0) \} \right], \quad (57)$$

where T denotes the time-ordering operator. \mathcal{H}_{eff} is the effective Hamiltonian of the theory. In our context, it corresponds with any of the Hamiltonians (45) and (47) from Section 2.1, depending on the nature of the inclusive final state X . In order to compute $\Gamma(H \rightarrow X)$ we apply an operator product expansion to the transition operator \mathcal{T} . The resulting series has the following form [28]:

$$\mathcal{T} = \Gamma_b \bar{b} b + \frac{z_G}{m_b^2} \bar{b} g_s \sigma_{\mu\nu} G^{\mu\nu} b + \sum \frac{z_{qi}}{m_b^3} \bar{b} \Gamma_i q \bar{q} \Gamma_i b + \dots \quad (58)$$

With use of HQET described in the preceding section, we can write the matrix element $\langle H | \bar{b} b | H \rangle$ as an expansion in inverse powers of the b -quark mass:

$$\langle H | \bar{b} b | H \rangle = 1 + \frac{1}{2m_b^2} \langle H | \bar{h} (iD)^2 h | H \rangle + \frac{1}{4m_b^2} \langle H | \bar{h} g_s \sigma_{\mu\nu} G^{\mu\nu} h | H \rangle + \mathcal{O}\left(\frac{1}{m_b^3}\right). \quad (59)$$

Plugging all this into the starting equation (56) we arrive at the following result:

$$\Gamma(H \rightarrow X) = \Gamma_b \left[1 + \sum_{n=2}^{\infty} z_n \left(\frac{\Lambda_{\text{QCD}}}{m_b} \right)^n \right]. \quad (60)$$

This equation is of fundamental importance to the phenomenology of inclusive B decays. It states that the inclusive decay width $\Gamma(H \rightarrow X)$ is, up to corrections that start at $\mathcal{O}(m_b^{-2})$, nothing but the decay width of the underlying heavy quark decay. The corrections can be interpreted as follows:

- There are two distinct corrections of order m_b^{-2} . The first one has its origin in the expansion of $\langle H | \bar{b} b | H \rangle$ using HQET. Physically, it corresponds to the movement of the b -quark inside the hadron (Fermi motion). The second corrective term describes the interaction of the gluon field with the spin of the heavy quark. It arises from the OPE of the transition operator \mathcal{T} (through the parameter z_G) as well as from the expansion of $\langle H | \bar{b} b | H \rangle$.
- Spectator effects are first seen at order m_b^{-3} . They account for the direct participation of the spectator quark in the weak interaction. Spectator are mainly responsible for lifetime differences among the B mesons [33]. Their contributions are enhanced by

³E.g. $X = Y_s \gamma$, where Y_s denotes any hadronic final state containing an s -quark.

a phase space factor of $16\pi^2$ due to the change in the kinematics of the process. Thus, compared with the leading corrections, spectator effects are not necessarily suppressed [34]. It has been shown experimentally, however, that their contributions in the decay rates of B^\pm and B^0 are on the percent level [35].

In this thesis, we concentrate on rare inclusive B decays and perturbative QCD corrections thereof. Of particular interest are (differential) decay widths and related observables such as forward-backward asymmetries and CP violating effects. The use of HQE allows us to approximate these quantities through the underlying b -quark decay while keeping nonperturbative effects well under control. The heavy quark expansion has also been applied to nonperturbative effects arising from resonant $\bar{c}c$ states in the process $B \rightarrow X_s\gamma$ [36] as well as $B \rightarrow X_s e^+e^-$ [37]. The corrections are of the order $\Lambda_{\text{QCD}}^2/m_c^2$ and were found to be at the percent level for e.g. the decay rate of $B \rightarrow X_s\gamma$. These nonperturbative effects are not terribly relevant for this thesis since we work in a region far away from resonant states. However, as opposed to former work [38, 39], it nicely illustrates a model-independent treatment of such long-distance effects.

2.3 Matching procedure

In this section we pick up on the Hamiltonian for the process $b \rightarrow cd\bar{u}$ introduced in Section 2.1 and illustrate with it the matching procedure. It has been used for the same purpose before in one form or another (see e.g. [40] or [41]) since it provides a simple setting to illuminate most aspects present in a matching calculation.

From the discussion in Section 2.1 we know that

$$\begin{aligned} C_1(\mu) &= C_1^{(0)}(\mu) + \frac{\alpha_s}{4\pi} C_1^{(1)}(\mu) + \mathcal{O}(\alpha_s^2), \\ C_2(\mu) &= C_2^{(0)}(\mu) + \frac{\alpha_s}{4\pi} C_2^{(1)}(\mu) + \mathcal{O}(\alpha_s^2), \end{aligned} \tag{61}$$

with

$$C_1^{(0)}(\mu) = 0, \quad C_2^{(0)}(\mu) = 1.$$

We now present the procedure to extract $C_1^{(1)}(\mu)$ and $C_2^{(1)}(\mu)$. The steps involved are: i) Calculation of the amplitude in the full Standard Model, ii) Calculation of the amplitude in the effective theory and iii) Extraction of the Wilson coefficients through comparison of the two results. Since the Wilson coefficients incorporate only physics at a scale $\gg m_b$, we can simplify the calculations by putting all small masses to zero.⁴ In principle, we can also set all external momenta to zero. However, in order to avoid collinear and infrared singularities, we keep them as regulators and choose all of them to be equal to p with $p^2 < 0$.

⁴This is not possible in a matching calculation including e.g. the operator $O_{7,s}$ from Eq. (46): since its definition already includes a small mass, setting them to zero would yield a vanishing amplitude.

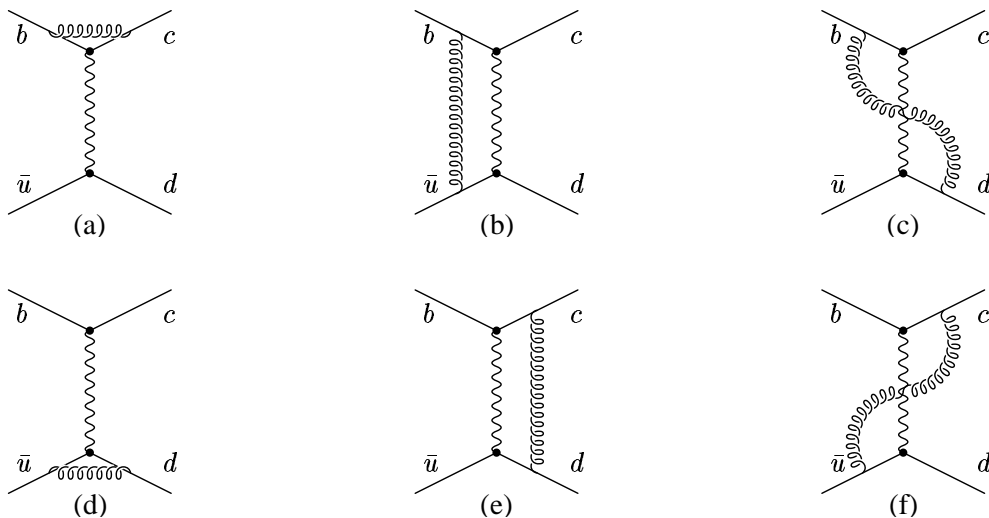


Figure 2.2: $\mathcal{O}(\alpha_s)$ diagrams for $b \rightarrow cd\bar{u}$ in the full theory. The curly lines represent virtual gluons whereas the wiggly lines denote a virtual W boson. Corrections on external lines and counterterm diagrams are not shown.

In Fig. 2.2 we see the set of $\mathcal{O}(\alpha_s)$ diagrams contributing to the amplitude for $b \rightarrow cd\bar{u}$. Since their calculation is straightforward, we merely present the result:

$$\begin{aligned}
 A^{\text{SM}} = & -\frac{4iG_F}{\sqrt{2}}V_{bc}V_{ud}^* \left[S_2 + \frac{\alpha_s}{4\pi} \left\{ 2C_F \ln\left(\frac{\mu^2}{-p^2}\right) + \frac{3}{N_c} \ln\left(\frac{m_W^2}{-p^2}\right) + \frac{5+16\ln 2}{6N_c} \right\} S_2 \right. \\
 & \left. - 3\frac{\alpha_s}{4\pi} \left\{ \ln\left(\frac{m_W^2}{-p^2}\right) + \frac{5+16\ln 2}{18} \right\} S_1 \right], \tag{62}
 \end{aligned}$$

where S_i , $i = 1, 2$ denotes the tree-level matrix element of the operator O_i . The constants N_c and C_F stand for the number of colors and for the eigenvalue of the quadratic Casimir operator, respectively. C_F can be expressed solely with N_c :

$$\sum_a T^a T^a = C_F \mathbf{1}, \quad C_F = \frac{N_c^2 - 1}{2N_c}.$$

For $N_c = 3$ we have $C_F = 4/3$.

A few words are in order to describe Eq. (62). First of all, we omitted all terms which vanish in the limit $p^2 \rightarrow 0$ because we only need the regulating property of p . Further, A^{SM} does not contain contributions from self-energy and counterterm graphs (however, we renormalized the quark fields in order to compensate for the divergences arising from Figs. 2.2(a) and (d)). They appear in the same way in the effective calculation and thus do not contribute to C_1 and C_2 . Finally, we added the tree-level transition amplitude to the result so that A^{SM} incorporates the complete amplitude up to terms of order α_s^2 .

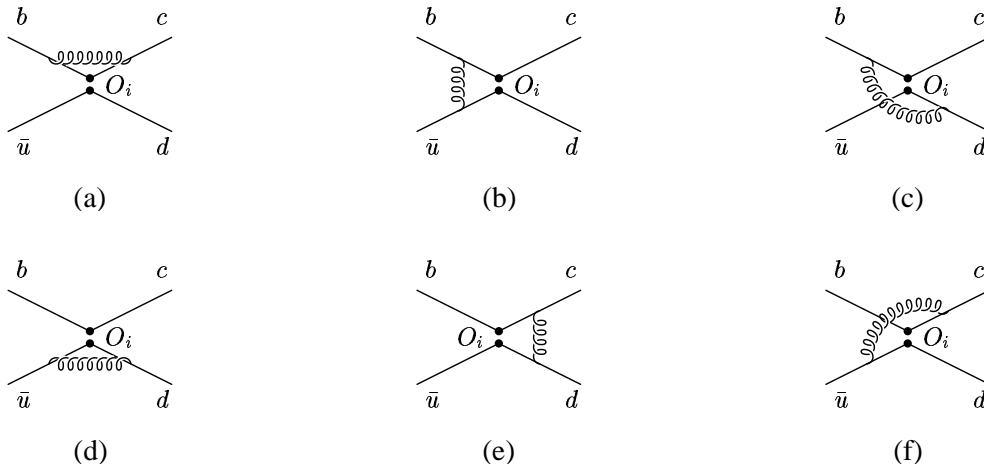


Figure 2.3: $\mathcal{O}(\alpha_s)$ diagrams for $b \rightarrow cd\bar{u}$ in the effective theory. Virtual gluons are represented by wiggly lines. The operator O_i stands for either O_1 or O_2 . Corrections on external lines and counterterm diagrams are not shown.

We now turn to the calculation of A^{eff} , the amplitude in the effective theory. The relevant $\mathcal{O}(\alpha_s)$ diagrams are depicted in Fig. 2.3. When analyzing these graphs, we see a difference in their divergent structure compared with the corresponding SM graphs. In the full theory, only two diagrams (the vertex corrections Fig. 2.2(a) and (d)) are ultraviolet divergent; the other four graphs are UV finite.⁵ In the effective theory, the missing W propagators imply that the other four diagrams are divergent as well. This fact has some consequences to be discussed later in this section. Denoting the sum of all diagrams in Fig. 2.3 involving O_i (and adding the tree level matrix element of O_i) with $\langle O_i \rangle$, we find after a short calculation:

$$\begin{aligned}
 \langle O_1 \rangle &= S_1 + \frac{\alpha_s}{4\pi} \left[2C_F \ln\left(\frac{\mu^2}{-p^2}\right) + \frac{3}{N_c} \frac{1}{\epsilon} + \frac{3}{N_c} \ln\left(\frac{\mu^2}{-p^2}\right) + \frac{19 + 8 \ln 2}{9} \right] S_1 \\
 &\quad - 3 \frac{\alpha_s}{4\pi} \left[\frac{1}{\epsilon} + \ln\left(\frac{\mu^2}{-p^2}\right) + \frac{19 + 8 \ln 2}{3} \right] S_2 + 2C_F \frac{\alpha_s}{4\pi} \frac{1}{\epsilon} S_1, \\
 \langle O_2 \rangle &= S_2 + \frac{\alpha_s}{4\pi} \left[2C_F \ln\left(\frac{\mu^2}{-p^2}\right) + \frac{3}{N_c} \frac{1}{\epsilon} + \frac{3}{N_c} \ln\left(\frac{\mu^2}{-p^2}\right) + \frac{19 + 8 \ln 2}{9} \right] S_2 \\
 &\quad - 3 \frac{\alpha_s}{4\pi} \left[\frac{1}{\epsilon} + \ln\left(\frac{\mu^2}{-p^2}\right) + \frac{19 + 8 \ln 2}{3} \right] S_1 + 2C_F \frac{\alpha_s}{4\pi} \frac{1}{\epsilon} S_2.
 \end{aligned} \tag{63}$$

We have again neglected terms which vanish in the limit $p^2 \rightarrow 0$. Further, since the quantities $\langle O_i \rangle$ only collect the matrix elements, the prefactors from Eq. (43) are omitted. We must now try to get rid of the UV divergences. By applying the quark field renormalization (i.e. $q_{\text{bare}} \rightarrow q_{\text{ren}}$)⁶ we notice that the last term on the rhs of both equations of

⁵For large loop momenta ℓ their integrands scale like $|\ell|^{-6}$.

⁶We denote operators which are built out of renormalized quark fields with a subscript r .

(42) vanishes; the other poles, however, remain present. This is a direct consequence of the missing W -boson propagators: the OPE replaced the nonlocal interaction in full theory with local operators. These operators are singular themselves⁷ and must therefore be renormalized. As can be seen from Eq. (63), it is not enough to simply introduce factors Z_i (see Section 2.4 for a treatise of the renormalization of QCD) for each operator and define renormalized operators through $O_{i,r} = Z_i O_{i,r}^{\text{ren}}$. With such a procedure it is not possible to arrive at UV finite quantities $\langle O_{i,r}^{\text{ren}} \rangle$. The operators $O_{1,r}$ and $O_{2,r}$ mix under renormalization and thus a mixing matrix Z^{op} is needed. With the help of Eq. (63) this matrix can be easily determined:

$$\begin{aligned} \begin{pmatrix} O_{1,r} \\ O_{2,r} \end{pmatrix} &= Z^{\text{op}} \begin{pmatrix} O_{1,r}^{\text{ren}} \\ O_{2,r}^{\text{ren}} \end{pmatrix}, \\ Z^{\text{op}} &= 1 + \frac{\alpha_s}{4\pi\epsilon} \begin{pmatrix} \frac{3}{N_c} & -3 \\ -3 & \frac{3}{N_c} \end{pmatrix} + \mathcal{O}(\alpha_s^2). \end{aligned} \quad (64)$$

The quantities $\langle O_{i,r}^{\text{ren}} \rangle$ amount to

$$\begin{aligned} \langle O_{1,r}^{\text{ren}} \rangle &= S_1 + \frac{\alpha_s}{4\pi} \left[2C_F \ln \left(\frac{\mu^2}{-p^2} \right) + \frac{3}{N_c} \ln \left(\frac{\mu^2}{-p^2} \right) + \frac{19 + 8 \ln 2}{9} \right] S_1 \\ &\quad - 3 \frac{\alpha_s}{4\pi} \left[\ln \left(\frac{\mu^2}{-p^2} \right) + \frac{19 + 8 \ln 2}{3} \right] S_2, \\ \langle O_{2,r}^{\text{ren}} \rangle &= S_2 + \frac{\alpha_s}{4\pi} \left[2C_F \ln \left(\frac{\mu^2}{-p^2} \right) + \frac{3}{N_c} \ln \left(\frac{\mu^2}{-p^2} \right) + \frac{19 + 8 \ln 2}{9} \right] S_2 \\ &\quad - 3 \frac{\alpha_s}{4\pi} \left[\ln \left(\frac{\mu^2}{-p^2} \right) + \frac{19 + 8 \ln 2}{3} \right] S_1, \end{aligned} \quad (65)$$

and the effective amplitude A^{eff} is given by

$$A^{\text{eff}} = -\frac{4iG_F}{\sqrt{2}} V_{bc} V_{ud}^* \left[C_1(\mu) \langle O_{1,r}^{\text{ren}} \rangle + C_2(\mu) \langle O_{2,r}^{\text{ren}} \rangle \right]. \quad (66)$$

We are now in the position to extract the Wilson coefficients. By comparing the prefactors of S_1 and S_2 in (62) to the ones from (66) we find:

$$\begin{aligned} C_1(\mu) &= -3 \frac{\alpha_s}{4\pi} \ln \left(\frac{m_W^2}{\mu^2} \right) + \frac{\alpha_s}{4\pi} \frac{11}{2} + \mathcal{O}(\alpha_s^2), \\ C_2(\mu) &= 1 + 3 \frac{\alpha_s}{4\pi} \ln \left(\frac{m_W^2}{\mu^2} \right) - \frac{\alpha_s}{4\pi} \frac{11}{6} + \mathcal{O}(\alpha_s^2). \end{aligned} \quad (67)$$

We saw that the effective theory introduces additional divergences not present in the full theory. We got rid of these divergences by renormalizing the operators $O_{1,r}$ and $O_{2,r}$. In Section 2.4 we show another way to deal with them, namely by renormalizing the Wilson

⁷They must cope for the divergences introduced by their stashing away of the W propagators.

coefficients themselves. The additional divergences also have another effect: they forced us to calculate all diagrams in the effective theory in an arbitrary dimension d . In $d = 4$ dimensions we can make use of the following exact identities:

$$\begin{aligned}
 \gamma_\alpha \gamma_\beta \gamma_\mu L \gamma^\beta \gamma^\alpha \otimes \gamma^\mu L &= 4 \gamma_\mu L \otimes \gamma^\mu L, \\
 \gamma_\mu L \gamma_\alpha \gamma_\beta \otimes \gamma^\mu L \gamma^\alpha \gamma^\beta &= 16 \gamma_\mu L \otimes \gamma^\mu L, \\
 \gamma_\mu L \gamma_\alpha \gamma_\beta \otimes \gamma^\beta \gamma^\alpha \gamma^\mu L &= 4 \gamma_\mu L \otimes \gamma^\mu L.
 \end{aligned}
 \tag{68}$$

These relations can easily be proven by use of the ‘‘Greek method’’ [42]⁸: One makes an ansatz of the form $A \gamma_\mu L \otimes \gamma^\mu L$, chooses a suitable Dirac structure for \otimes and contracts Lorentz indices to solve for the unknown constant A . In $d = 4 - 2\epsilon$ dimensions these equations are valid only up to terms of order ϵ^1 . We can try to calculate ϵ -dependent corrections using the Greek method with $A \rightarrow A(\epsilon)$, yielding

$$\gamma_\alpha \gamma_\beta \gamma_\mu L \gamma^\beta \gamma^\alpha \otimes \gamma^\mu L = 4(1 - \epsilon)^2 \gamma_\mu L \otimes \gamma^\mu L, \tag{69}$$

$$\gamma_\mu L \gamma_\alpha \gamma_\beta \otimes \gamma^\mu L \gamma^\alpha \gamma^\beta = 4(4 - \epsilon - \epsilon^2) \gamma_\mu L \otimes \gamma^\mu L, \tag{70}$$

$$\gamma_\mu L \gamma_\alpha \gamma_\beta \otimes \gamma^\beta \gamma^\alpha \gamma^\mu L = 4(1 - \epsilon)^2 \gamma_\mu L \otimes \gamma^\mu L. \tag{71}$$

We used Eq. (69) up to $\mathcal{O}(\epsilon^1)$ in all SM and effective diagrams where the virtual gluon does not switch fermion lines. Eqs. (70) and (71) were used to the same order in ϵ to evaluate Figs. (2.3)(b) and (e) and Figs. (2.3)(c) and (f), respectively. The remaining four diagrams do not suffer from UV divergences and are evaluated in $d = 4$ dimensions. As has been shown in [43], the procedure just described eventually leads to incorrect two-loop anomalous dimensions. One must supplement the Greek method by introducing evanescent operators (i.e. operators that vanish as $\epsilon \rightarrow 0$) on the rhs of Eqs. (70) and (71). In view of the calculation presented in this section, evanescent operators influence the constant $\mathcal{O}(\alpha_s)$ terms arising from the four rightmost diagrams depicted in Eq. (2.3). All other diagrams can either be evaluated in $d = 4$ dimensions or only make use of Eq. (69). The latter is not tainted by evanescent operators since the contraction of Lorentz indices happens on the same fermion line. For further discussions about evanescent operators we refer to [44] and [45]. We would only like to mention that one has some freedom in the choice of these operators. By using the Greek method to determine the $\mathcal{O}(\epsilon^1)$ terms in Eqs. (70) and (71) we picked the same definition as Ref. [43].

Eq. (67) gives us the Wilson coefficients as an expansion in the strong coupling $\alpha_s = \alpha_s(\mu)$ up to terms of order α_s^2 . As can be seen the coefficients have a logarithmic dependence on μ of the form $\ln(m_W^2/\mu^2)$. At an arbitrary order α_s^n , this dependence has the following

⁸The method was named after the nationality of the authors which proposed it in [42].

structure⁹:

$$\begin{aligned}
 C_{i,n}(\mu) = & c_{n0} \left[\alpha_s(\mu) \ln \left(\frac{m_W^2}{\mu^2} \right) \right]^n + c_{n1} \alpha_s(\mu) \left[\alpha_s(\mu) \ln \left(\frac{m_W^2}{\mu^2} \right) \right]^{n-1} \\
 & + c_{n2} \alpha_s(\mu)^2 \left[\alpha_s(\mu) \ln \left(\frac{m_W^2}{\mu^2} \right) \right]^{n-2} + \dots + c_{nn} \alpha_s(\mu)^n.
 \end{aligned} \tag{72}$$

Contingent on which scale μ the matching procedure is performed, these logarithms pick up large values. For $\mu = \mu_b \approx m_b$ the logarithms are bigger than 5, with the effect that they spoil the expansion in $\alpha_s(\mu_b)$.¹⁰ Terms of the form $[\alpha_s(\mu_b) \ln(m_W^2/\mu_b^2)]^n$ (the so-called “leading logarithms”) are not suppressed anymore and must all be taken into account even at leading order. At next-to-leading order, we must resum all terms of the form $\alpha_s(\mu_b) [\alpha_s(\mu_b) \ln(m_W^2/\mu_b^2)]^{n-1}$ and so on. So why do we actually need the Wilson coefficients at a scale μ_b ? When working at $\mu_W \approx m_W$ the logarithms are $\ll 1$ and the fixed order expansion works perfectly well. We must remember, however, that the physics also sits in the matrix elements. These matrix elements have a logarithmic dependence on μ similar to the one given in Eq. (72). Since the largest mass in them is m_b , we would have to deal with large logarithms in the matrix elements when choosing μ close to m_W . One way or another, these terms creep into our calculation and must be taken care of. In Section 2.4 we show the usual procedure to do this.

2.4 RG improved perturbation theory

When calculating transition amplitudes to tree-level approximation, we do not have to deal with ultraviolet divergences; they appear, however, when we start to consider loop contributions. In order to give sense to the divergent integrals arising from loop diagrams, we use dimensional regularization [46]: integrals are calculated in an arbitrary dimension $d = 4 - 2\epsilon$. Divergences show up as poles in ϵ . We get rid of these divergences by expressing the bare (and divergent) variables present in the Lagrangian with renormalized quantities:

$$\begin{aligned}
 G_\mu^{A, \text{bare}} &= \sqrt{Z_3} G_\mu^A, & q^{\text{bare}} &= \sqrt{Z_q} q, \\
 g_s^{\text{bare}} &= \mu^\epsilon Z_g g_s, & m^{\text{bare}} &= Z_m m,
 \end{aligned} \tag{73}$$

where q denotes a quark field. The scale μ has been introduced to ensure that the coupling constant g_s remains dimensionless in an arbitrary dimension d . One has some freedom in the choice of the renormalization scheme. The simplest one is the minimal subtraction scheme MS [47] in which only the divergent parts are subtracted. In this thesis we work

⁹At higher orders in α_s the Wilson coefficients depend on other heavy masses such as m_t . However, the logarithmic dependence on μ can always be cast into the form given in Eq. (72).

¹⁰Another circumstance which doesn't actually spoil the expansion but at least degrades its convergence is the asymptotic freedom property of QCD: the strong coupling is larger at smaller energies and thus $\alpha_s(\mu_b) > \alpha_s(m_W)$.

solely in the modified MS scheme ($\overline{\text{MS}}$ scheme) in which also the artifacts $(\ln(4\pi) - \gamma_E)$ are removed.¹¹

The factors Z are the renormalization constants. They are chosen such that all divergences vanish once the Greens functions have been expressed solely in terms of renormalized quantities. In the $\overline{\text{MS}}$ scheme, they are given by

$$\begin{aligned} Z_3 &= 1 - \frac{1}{\epsilon} \frac{\alpha_s}{4\pi} \left(\frac{2}{3} N_f - \frac{5}{3} N_c \right) + \mathcal{O}(\alpha_s^2), & Z_q &= 1 - \frac{1}{\epsilon} \frac{\alpha_s}{4\pi} C_F + \mathcal{O}(\alpha_s^2), \\ Z_g &= 1 - \frac{1}{\epsilon} \frac{\alpha_s}{4\pi} \left(\frac{11}{6} N_f - \frac{1}{3} N_c \right) + \mathcal{O}(\alpha_s^2), & Z_m &= 1 - \frac{1}{\epsilon} \frac{\alpha_s}{4\pi} 3C_F + \mathcal{O}(\alpha_s^2), \end{aligned}$$

where N_c and N_f denote the number of colors and the number of effective flavors, respectively. The word *effective* in this context means all quark flavors still present in the theory. By going from higher to lower scales μ one systematically integrates out flavors with masses higher than μ . There is some freedom at which scale a given flavor is integrated out. For our specific purposes, N_f is almost always 5 since we are interested in the energy range m_b to m_t .

By using dimensional regularization we introduced an arbitrary scale μ into the theory. We could also have used an entirely different regularization scheme to make sense of the divergent integrals. Our personal choice of the renormalization scale μ or the regularization scheme itself can, of course, in no way influence physical observables such as decay rates or CP asymmetries. In order to have a good theoretical framework, we must take this circumstance into account. In our case, this leads to the requirement that the bare quantities must not be dependent on μ . This further implies, through Eq. (73), that the renormalized quantities have to be μ -dependent. In case of the coupling constant g_s this provides us with the following differential equation, the so-called “renormalization group equation” (RGE) for g_s :

$$\mu \frac{d}{d\mu} g_s(\mu) = -\epsilon g_s(\mu) + \beta(g_s), \quad (74)$$

where we have used the notation

$$\begin{aligned} \beta(g_s) &= g_s^2 \frac{\partial}{\partial g_s} Z_{g,1}(g_s), \\ Z_g &= 1 + \sum_{k=1}^{\infty} \frac{1}{\epsilon^k} Z_{g,k}(g_s). \end{aligned} \quad (75)$$

It is important to note that Z_g (and actually all Z factors) are not directly dependent on the scale μ in the $\overline{\text{MS}}$ scheme. Rather, they pick up their dependence indirectly through

¹¹These annoying terms arise from dimensional regularization: $\ln(4\pi)$ originates from an additional factor $(2\pi)^{2\epsilon}$ present in the measure of loop integrals whereas γ_E gets produced when derivatives of Euler Γ -functions with ϵ -dependent arguments are taken.

$g_s = g_s(\mu)$.

The function $\beta(g_s)$ is the so-called renormalization group function associated with g_s . It can be written as a power series in g_s :

$$\beta(g_s) = -\frac{g_s^3}{16\pi^2} \sum_{k=0}^{\infty} \beta_k \left(\frac{g_s^2}{16\pi^2} \right)^k. \quad (76)$$

The individual β_i 's are solely determined by the $1/\epsilon$ poles of the renormalization factor Z_g at order α_s^i . The first two constants are given by

$$\beta_0 = \frac{1}{3} (11 N_c - 2 N_f), \quad \beta_1 = \frac{1}{3} (34 N_c - 10 N_c N_f - 6 C_F N_f). \quad (77)$$

We can rewrite Eq. (74) for g_s in terms of $\alpha_s = g_s^2/(4\pi)$. Setting $\epsilon = 0$ and solving the resulting equation to lowest order, we derive the solution

$$\alpha_s(\mu) = \frac{\alpha_s(\mu_0)}{1 + \frac{\beta_0}{2\pi} \alpha_s(\mu_0) \ln\left(\frac{\mu}{\mu_0}\right)}. \quad (78)$$

Once $\alpha_s(\mu)$ is known at some value μ_0 , we can calculate the strong coupling at an arbitrary scale μ .¹² Ref. [48] gives a current status report of different measurements of $\alpha_s(\mu)$ at the mass of the Z boson. The world average amounts to $\alpha_s(m_Z) = 0.118 \pm 0.003$.

We deduced this result to illustrate two important points:

- For $\beta_0 > 0$ the following equation always holds:

$$\alpha_s(\mu_2) > \alpha_s(\mu_1) \quad \text{for } \mu_1 > \mu_2.$$

This is nothing but the asymptotic freedom of QCD: the strong coupling is smaller at shorter distances (or equivalently at higher energies). For μ going to infinity, the coupling vanishes.

- By expanding the lowest order result for $\alpha_s(\mu)$ (see Eq. (78)) in $\alpha_s(\mu_0)$ we get

$$\alpha_s(\mu) = \alpha_s(\mu_0) \left(1 + \sum_{n=1}^{\infty} \left[\beta_0 \frac{\alpha_s(\mu_0)}{4\pi} \ln\left(\frac{\mu_0^2}{\mu^2}\right) \right]^n \right). \quad (79)$$

Comparing this with Eq. (72) we see that the solution to the RGE for $\alpha_s(\mu)$ automatically sums up the leading logarithms. Similarly, when including β_1 in the differential equation, the result sums up the next-to-leading logarithms as well. The problem with large logarithms can thus be dealt with by means of renormalization group methods.

¹²Since $\alpha_s(\mu)$ depends on the effective number of quark flavors N_f , Eq. (74) is actually a system of equations with boundary conditions $\alpha_s^{N_f=5}(m_t) = \alpha_s^{N_f=6}(m_t)$, $\alpha_s^{N_f=4}(m_b) = \alpha_s^{N_f=5}(m_b)$ etc.

For the running mass $m(\mu)$ we get the following RGE:

$$\mu \frac{d}{d\mu} m(\mu) = -\gamma_m(g_s) m(\mu), \quad (80)$$

with

$$\begin{aligned} \gamma_m(g_s) &= -g_s \frac{\partial}{\partial g_s} Z_{m,1}, \\ Z_m &= 1 + \sum_{k=1}^{\infty} \frac{1}{\epsilon^k} Z_{m,k}(g_s). \end{aligned} \quad (81)$$

At lowest order in both β and γ_m , the solution to this equation is given by

$$m(\mu) = m(\mu_0) \left[\frac{\alpha_s(\mu)}{\alpha_s(\mu_0)} \right]^{\frac{\gamma_m^{(0)}}{2\beta_0}}. \quad (82)$$

We now turn to the renormalization group treatment of the Wilson coefficients. In Section 2.3 we stated that the effective (local) operators O_i are singular objects. In order to get rid of associated divergences, we introduced renormalized operators and corresponding Z factors similar to Eq. (73). We generalize the discussion to a Lagrangian containing n operators O_i and Wilson coefficients C_i . The connection between the Lagrangians expressed in bare and in renormalized operators is as follows:

$$\mathcal{L} = \sum_{k=1}^n C_k(\mu) O_k^{\text{bare}} = \sum_{k=1}^n C_k(\mu) \sum_{i=1}^n Z_{ki}^{\text{op}} O_{i,r}^{\text{ren}}. \quad (83)$$

Equivalently, one might look at the Wilson coefficients as bare quantities which need to be renormalized and the operators remain unchanged. In this picture we have

$$\vec{C}^{\text{bare}} = Z^c \vec{C}^{\text{ren}}, \quad (84)$$

where the vector \vec{C}^{bare} (\vec{C}^{ren}) collects all bare (renormalized) Wilson coefficients and Z^c denotes the mixing matrix, now for the coefficients instead of the operators. Eq. (83) then changes to

$$\mathcal{L} = \sum_{k=1}^n C_k^{\text{bare}}(\mu) O_k = \sum_{k=1}^n \sum_{i=1}^n Z_{ik}^c C_k^{\text{ren}}(\mu) O_{i,r}. \quad (85)$$

The relation between Z^{op} and Z^c can be found by comparing Eqs. (83) and (85):

$$(Z^c)^T = (Z^{\text{op}})^{-1}. \quad (86)$$

Our aim is to find a way to systematically deal with the problem of large logarithms as stated in Section 2.3. We follow the solution method for the coupling constant α_s

presented in this chapter and start with the renormalization group equation for the Wilson coefficients:

$$\mu \frac{d}{d\mu} \vec{C}(\mu) = \gamma^T(g_s) \vec{C}(\mu), \quad (87)$$

where we have dropped the label “ren” to simplify the notation. The anomalous dimension matrix γ is given through

$$\gamma(g_s) \doteq (Z^{\text{op}})^{-1} \mu \frac{d}{d\mu} Z^{\text{op}}. \quad (88)$$

Similarly, it can be expressed through Z^c using Eq. (86). As before with β and γ_m , only the $1/\epsilon$ poles of Z^{op} are needed to find the matrix γ :

$$\begin{aligned} \gamma(g_s) &= -g_s \frac{\partial}{\partial g_s} Z_1^{\text{op}}(g_s), \\ Z^{\text{op}}(g_s) &= 1 + \sum_{k=1}^{\infty} \frac{1}{\epsilon^k} Z_k^{\text{op}}(g_s). \end{aligned} \quad (89)$$

The anomalous dimension matrix can further be written as a Taylor series in α_s :

$$\gamma(\alpha_s) = \gamma^{(0)} \frac{\alpha_s}{4\pi} + \gamma^{(1)} \left(\frac{\alpha_s}{4\pi} \right)^2 + \gamma^{(2)} \left(\frac{\alpha_s}{4\pi} \right)^3 + \dots \quad (90)$$

In the $\overline{\text{MS}}$ scheme the matrices $\gamma^{(i)}$ are constants with respect to the scale μ since γ is again only dependent on μ indirectly through the strong coupling.

The general solution to the RGE of the Wilson coefficients is conveniently written with the evolution matrix $U(\mu, \mu_0)$:

$$\begin{aligned} \vec{C}(\mu) &= U(\mu, \mu_0) \vec{C}(\mu_0), \\ U(\mu_0, \mu_0) &= 1. \end{aligned} \quad (91)$$

The evolution matrix fulfills the same differential equation as the Wilson coefficients themselves. The exact solution can be written down at once:

$$U(\mu, \mu_0) = T_g \exp \left[\int_{g_s(\mu_0)}^{g_s(\mu)} dg' \frac{\gamma^T(g')}{\beta(g')} \right], \quad (92)$$

where T_g is the g -ordering operator (see e.g. [40]). This operator is needed since the anomalous dimension matrix evaluated at different values of $g_s(\mu)$ does in general not commute.¹³

¹³In a theory without operator mixing, all matrices $\gamma^{(i)}$ are diagonal and thus commute with one another, implying that $\gamma(g_{s,1})$ and $\gamma(g_{s,2})$ commute as well for arbitrary values of $g_{s,1}$ and $g_{s,2}$.

Since Eq. (92) is not very useful to work with, we elaborate on a method to derive an expedient expression for $U(\mu, \mu_0)$. We start by noticing that $\gamma^{(0)}$ can be diagonalized with a suitable matrix V . We introduce new quantities in the following way:

$$\begin{aligned}\vec{C}(\mu) &= V \vec{\tilde{C}}(\mu) \\ \gamma^{(i)} &= V \tilde{\gamma}^{(i)} V^{-1}, \quad i = 0, 1, 2, \dots, \\ U(\mu, \mu_0) &= V \tilde{U}(\mu, \mu_0) V^{-1}.\end{aligned}\tag{93}$$

The variables equipped with a tilde satisfy equations similar to (87) and (91):

$$\begin{aligned}\frac{d}{d \ln \mu} \vec{\tilde{C}}(\mu) &= \tilde{\gamma}^T(\alpha_s) \vec{\tilde{C}}(\mu), \\ \vec{\tilde{C}}(\mu) &= \tilde{U}(\mu, \mu_0) \vec{\tilde{C}}(\mu_0), \\ \frac{d}{d \ln \mu} \tilde{U}(\mu, \mu_0) &= \tilde{\gamma}^T(\alpha_s) \tilde{U}(\mu, \mu_0), \\ \tilde{U}(\mu_0, \mu_0) &= 1.\end{aligned}\tag{94}$$

To leading logarithmic approximation, the solution $\tilde{U}^{(0)}(\mu, \mu_0)$ to the renormalization group equation for $\tilde{U}(\mu, \mu_0)$ is readily found: since $\tilde{\gamma}^{(0)}$ is diagonal, the problem reduces to a set of independent differential equations, yielding

$$\tilde{U}^{(0)}(\mu, \mu_0) = \left(\left(\frac{\alpha_s(\mu_0)}{\alpha_s(\mu)} \right)^{\frac{\tilde{\gamma}^{(0)}}{2\beta_0}} \right)_D,$$

where $\tilde{\gamma}^{(0)}$ collects the diagonal elements of the matrix $\tilde{\gamma}^{(0)}$. The result is completely analogous to the solution found for the running mass $m(\mu)$ given in Eq. (82). In order to attain subleading terms, we follow Appendix C of Part V and make the following ansatz for $\tilde{U}(\mu, \mu_0)$:

$$\tilde{U}(\mu, \mu_0) = \left(1 + \sum_{i=1}^{\infty} \left(\frac{\alpha_s(\mu)}{4\pi} \right)^i \tilde{J}_i \right) \tilde{U}^{(0)}(\mu, \mu_0) \tilde{K}.\tag{95}$$

The matrix \tilde{K} is independent of μ and must be chosen such that the boundary condition $\tilde{U}(\mu_0, \mu_0) = 1$ is satisfied. By use of Eq. (95) and the explicit expression for $\tilde{U}^{(0)}(\mu, \mu_0)$ we can write the lhs and rhs of the RGE for $\tilde{U}(\mu, \mu_0)$ as

$$\begin{aligned}\text{lhs} &= \sum_{j=1}^{\infty} \left(\frac{\alpha_s(\mu)}{4\pi} \right)^j L_j \tilde{U}^{(0)}(\mu, \mu_0) \tilde{K}, \\ \text{rhs} &= \sum_{j=1}^{\infty} \left(\frac{\alpha_s(\mu)}{4\pi} \right)^j R_j \tilde{U}^{(0)}(\mu, \mu_0) \tilde{K}.\end{aligned}$$

The unknown matrices \tilde{J}_i can be constructed order by order in α_s through the relations $L_j = R_j$. As an illustration, we give the explicit solutions to \tilde{J}_1 and \tilde{J}_2 :

$$\begin{aligned}\tilde{J}_{1,ij} &= \delta_{ij} \tilde{\gamma}_i^{(0)} \frac{\beta_1}{2\beta_0^2} - \frac{\tilde{\gamma}_{ij}^{(1)\text{T}}}{2\beta_0 + \tilde{\gamma}_i^{(0)} - \tilde{\gamma}_j^{(0)}} , \\ \tilde{J}_{2,ij} &= \delta_{ij} \tilde{\gamma}_i^{(0)} \frac{\beta_2}{4\beta_0^2} - \frac{\tilde{\gamma}_{ij}^{(2)\text{T}} + \left(2\beta_1 - \frac{\beta_1}{\beta_0} \tilde{\gamma}_j^{(0)}\right) \tilde{J}_{1,ij} + \left(\tilde{\gamma}^{(1)\text{T}} \tilde{J}_1\right)_{ij}}{4\beta_0 + \tilde{\gamma}_i^{(0)} - \tilde{\gamma}_j^{(0)}} .\end{aligned}\tag{96}$$

The matrix \tilde{K} can be expressed with \tilde{J}_1 and \tilde{J}_2 and is found to be

$$\tilde{K} = 1 - \frac{\alpha_s(\mu_0)}{4\pi} \tilde{J}_1 - \left(\frac{\alpha_s(\mu_0)}{4\pi}\right)^2 \left(\tilde{J}_2 - \tilde{J}_1^2\right) + \mathcal{O}(\alpha_s^3).\tag{97}$$

We now have all ingredients at hand to give the solution to the initial problem, namely to the renormalization group equation of the Wilson coefficients:

$$\begin{aligned}\vec{C}(\mu) &= U(\mu, \mu_0) \vec{C}(\mu_0) , \\ U(\mu, \mu_0) &= V \left(1 + \frac{\alpha_s(\mu)}{4\pi} \tilde{J}_1 + \left(\frac{\alpha_s(\mu)}{4\pi}\right)^2 \tilde{J}_2\right) \tilde{U}^{(0)}(\mu, \mu_0) \tilde{K} V^{-1} + \mathcal{O}(\alpha_s^3).\end{aligned}\tag{98}$$

This solution allows us to solve the problem presented in Section 2.3: we can accomplish the matching calculation for the Wilson coefficients at the high scale μ_W where large logarithms are absent. The result then serves as a set of initial values to be fed into the renormalization group equation (87). By use of Eq. (98), the coefficients can be evolved from μ_W down to μ_b . Finally, we can compute matrix elements involving the local operators O_i at the scale μ_b , where large logarithms are again absent.

After having introduced the anomalous dimension matrix γ we can go back to Section 2.1 and look at the operator basis (46) again.¹⁴ We have mentioned that the prefactors of the operators $O_{i,s}$ $i = 7, 8, 9, 10$ were chosen to simplify the book-keeping of operator mixing. These factors are artificial in the sense that they do not arise from actual couplings present in the operators. Let us look at what happens if these unnatural factors were not present. We define new operators (and accordingly also new Wilson coefficients) as follows:

$$\begin{aligned}\tilde{O}_{i,s} &= \frac{\alpha_s}{4\pi} O_{i,s} , \\ \tilde{C}_{i,s} &= \frac{4\pi}{\alpha_s} C_{i,s} , \\ \tilde{C}_{i,s} \tilde{O}_{i,s} &= C_{i,s} O_{i,s} ,\end{aligned}\tag{99}$$

where $i = 7, 8, 9, 10$. In the process $b \rightarrow s \ell^+ \ell^-$ operator mixing starts at $\mathcal{O}(\alpha_s^0)$: The four-Fermi operators $\tilde{O}_{1,s}, \dots, \tilde{O}_{6,s}$ mix into the operator $\tilde{O}_{9,s}$ despite missing virtual gluons

¹⁴The comments we are about to make also hold for the corresponding operators from the basis (48).

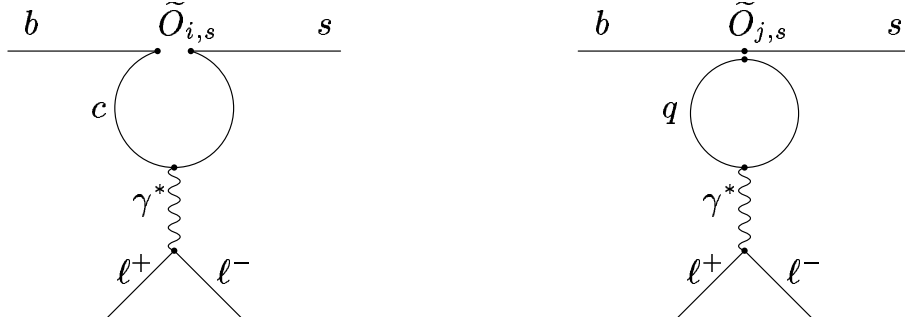


Figure 2.4: The depicted diagrams are responsible for $\mathcal{O}(\alpha_s^0)$ mixing of the four-quark operators $\tilde{O}_1, \dots, \tilde{O}_6$ into \tilde{O}_9 . The subscript i takes the values 1 and 2 whereas $j \in \{3, 4, 5, 6\}$. respectively.

through the Feynman diagrams depicted in Fig. 2.4. This yields $1/\epsilon$ poles in the mixing matrix Z^{op} which are proportional to α_s^0 and the anomalous dimension matrix γ could not be written according to Eq. (90) anymore: the one-loop anomalous dimensions would have terms proportional to α_s^1 as well as terms proportional to α_s^0 . Analogous entries would be found in subsequent anomalous dimensions. This is not the case for the operator basis given in Eq. (46): the additional factors $1/g_s^2$ in the operators $O_{7,s}$ to $O_{10,s}$ ¹⁵ make sure that, for any $n \in \mathbb{N}$, the n -loop anomalous dimensions are proportional to α_s^n . In case of the transition $b \rightarrow s \gamma$ operator mixing starts first at $\mathcal{O}(\alpha_s)$ and these additional factors are not needed. Therefore in this case, we often work in a basis where the operators in the Hamiltonian from Eq. (44) are replaced with the following basis:

$$\begin{aligned}
 O_1 &= (\bar{s}_L \gamma_\mu T^a c_L)(\bar{c}_L \gamma^\mu T^a b_L), & O_2 &= (\bar{s}_L \gamma_\mu c_L)(\bar{c}_L \gamma^\mu b_L), \\
 O_3 &= (\bar{s}_L \gamma_\mu b_L) \sum_q (\bar{q} \gamma^\mu q), & O_4 &= (\bar{s}_L \gamma_\mu T^a b_L) \sum_q (\bar{q} \gamma^\mu T^a q), \\
 O_5 &= (\bar{s}_L \gamma_\mu \gamma_\nu \gamma_\rho b_L) \sum_q (\bar{q} \gamma^\mu \gamma^\nu \gamma^\rho q), & O_6 &= (\bar{s}_L \gamma_\mu \gamma_\nu \gamma_\rho T^a b_L) \sum_q (\bar{q} \gamma^\mu \gamma^\nu \gamma^\rho T^a q), \\
 O_7 &= \frac{e}{16\pi^2} \bar{m}_b(\mu) (\bar{s}_L \sigma^{\mu\nu} b_R) F_{\mu\nu}, & O_8 &= \frac{g_s}{16\pi^2} \bar{m}_b(\mu) (\bar{s}_L \sigma^{\mu\nu} T^a b_R) G_{\mu\nu}^a.
 \end{aligned} \tag{100}$$

For $i < 7$ we have $O_i = O_{1,s}$. For $i = 7, 8$ the operator O_i (and the corresponding Wilson coefficient) coincides with $\tilde{O}_{i,s}$ defined in Eq. (99). Note that we dropped the operators $O_{9,s}$ and $O_{10,s}$ since they are of no importance for the process $b \rightarrow s \gamma$ (when neglecting electromagnetic corrections).

We conclude this section with a short discussion of what is actually needed to calculate a physical observable to a given approximation. Let us look at the process $B \rightarrow X_s \gamma$ and the relevant operator basis (100). The heavy quark expansion discussed in Subsection 2.2.2

¹⁵Although the operators $O_{1,s}$, to $O_{6,s}$ only mix into $O_{9,s}$ without QCD corrections, the factor $1/g_s^2$ must also be present in the operators $O_{7,s}$, $O_{8,s}$ and $O_{10,s}$: since these operators themselves only start to mix into $O_{9,s}$ at $\mathcal{O}(\alpha_s^1)$, the relative power of g_s between them and $O_{9,s}$ must not be changed.

allows us to approximate this transition with the quark-level process up to correctional terms of order m_b^{-2} . For a leading logarithmic accuracy, it suffices to perform the matching procedure without considering QCD corrections. Since the process $b \rightarrow s \gamma$ is absent at tree level in the Standard Model, this step requires the evaluation of one-loop diagrams in both the full and effective theory. Next, the anomalous dimension matrix must be known to order α_s , involving two-loop calculations. The matrix elements $\langle s \gamma | O_i | b \rangle$ are needed again without QCD corrections. At this order in α_s , only the operators $O_3 - O_7$ are of relevance. The four-Fermi operators $O_3 - O_6$ contribute via one-loop diagrams whereas O_7 contributes through a tree-level matrix element. At NLL approximation, all three steps need to be improved by one order in α_s : $\mathcal{O}(\alpha_s)$ QCD corrections must be included in the matching procedure, resulting in a two-loop calculation; three-loop diagrams must be considered to find the next-to-leading term $\gamma^{(1)}$ in the expansion of γ and two-loop contributions must be evaluated to gain the necessary $\mathcal{O}(\alpha_s)$ matrix elements. Furthermore, in order to get rid of infrared divergences, we must also include corresponding bremsstrahlung diagrams.

it indeed reproduces the correct result. Afterwards we make a couple of general remarks about how and when to implement MB representations. Further, we point out a couple of pitfalls to avoid. More advanced real-life calculations can be found in Parts III and V.

The example integral under consideration is given by

$$I_\epsilon = \int_0^1 \frac{dx}{(1-x)^{1-\epsilon}}, \quad (102)$$

where ϵ is real positive and close to zero. The solution to this integral can easily be found by integrating over x and is $I_\epsilon = 1/\epsilon$. We try to confirm this result using Eq. (101). Note that this equation is truly an identity and the Mellin-Barnes approach must therefore reproduce the exact result and not just an expanded approximation. With the identifications $\lambda \leftrightarrow 1-\epsilon$ and $z = x$, we find

$$I_\epsilon = \frac{1}{2\pi i} \frac{1}{\Gamma(1-\epsilon)} \int_0^1 dx \int_\gamma ds \Gamma(-s) \Gamma(1-\epsilon+s) (-x)^s. \quad (103)$$

The path γ has two constraints. First, it must be chosen such that it separates the two poles series present in Eq. (103). Second the integral over x must be defined on the entire path. Both constraints are fulfilled for a path γ chosen parallel and arbitrarily close to the imaginary axis, intersecting the real axis at a negative value. We boldly exchange the order of integration and resolve the integral over x , yielding:

$$I_\epsilon = \frac{1}{2\pi i} \frac{1}{\Gamma(1-\epsilon)} \int_\gamma ds f(s), \quad (104)$$

$$f(s) = \frac{(-1)^s}{1+s} \Gamma(-s) \Gamma(1-\epsilon+s).$$

The integral over s can be carried out by closing the path γ in the right halfplane of the complex s plane and by using the residue theorem. The only poles we need to consider are located at $s_p = 0, 1, 2, \dots$. The corresponding residues are easily found:

$$\text{Res}[f(s_p)] = -\frac{\Gamma(1+s_p-\epsilon)}{\Gamma(2+s_p)}, \quad s_p = 0, 1, 2, \dots \quad (105)$$

The sum over all residues can be performed and gives:

$$\sum_{s_p=0}^{\infty} \text{Res}[f(s_p)] = \Gamma(-\epsilon). \quad (106)$$

The residue theorem yields an additional factor $2\pi i$ and a minus sign (since the path is clockwise oriented). Plugging all this into the first equation of (104), we conclude that

$$I_\epsilon = -\frac{\Gamma(-\epsilon)}{\Gamma(1-\epsilon)} = \frac{1}{\epsilon}. \quad (107)$$

In this derivation we implicitly assumed that the integral along the path γ' added to close the contour is zero. We make up for this inattentiveness and sketch a way to prove this. First, we deform the path γ to run parallel and slightly to the right of the imaginary s -axis. Close to the real axis it is dented to the left such that the pole series arising from the two Γ -functions are separated from each other. This distortion is valid since $f(s)$ is analytic in the concerned region. We parametrize the path γ' to close the contour as follows:

$$\gamma' : s(t) = R e^{it}, \quad -\frac{\pi}{2} < t < \frac{\pi}{2}, \quad (108)$$

where the radius R is meant to go to infinity. Note that the absolute value of t is explicitly less than $\pi/2$, allowing us to disregard possible problems on the imaginary axis. Before we can examine the function $f(s)$ for large values of $|s|$ we need to give sense to the factor $(-1)^s$. By equipping the variable x in Eq. (102) with a small negative imaginary part, we can rewrite it as follows:

$$\begin{aligned} x \rightarrow x - i\delta &\Rightarrow (-1)^s \rightarrow (-1 + i\delta)^s, \\ (-1 + i\delta)^s &= e^{i\pi s} + \mathcal{O}(\delta), \end{aligned} \quad (109)$$

where we have used the identity

$$(-a \pm i\delta)^\beta = (a \mp i\delta)^\beta e^{\pm i\pi\beta}. \quad (110)$$

The term of order δ in Eq. (109) is not needed anymore and can be dropped. We further rewrite $f(s)$ to put it into a more suitable form. The factor $\Gamma(-s)$ can be expressed as follows:

$$\begin{aligned} \Gamma(-s) &= -\frac{\pi}{\Gamma(1+s) \sin(\pi s)}, \\ \sin(\pi s) &= \frac{e^{i\pi s} - e^{-i\pi s}}{2i}. \end{aligned}$$

We multiply numerator and denominator of the resulting expression with $\exp(-i\pi s)$ and arrive at

$$f(s) = \frac{-2\pi i}{1+s} \frac{1}{1 - e^{-2i\pi s}} \frac{\Gamma(1+s-\epsilon)}{\Gamma(1+s)}. \quad (111)$$

For s with large values of $|s|$, the function $\Gamma(s)$ can be approximated with Stirling's formula:

$$\Gamma(s) = \sqrt{2\pi} s^{s-1/2} e^{-s} + \mathcal{O}(s^{-1}). \quad (112)$$

Eq. (112) is valid for $|s| \rightarrow \infty$ and $|\arg(s)| < \pi$. Since the real part of $1+s-\epsilon$ is always positive we can employ it for both Γ -functions in Eq. (111)²:

$$\frac{\Gamma(1+s-\epsilon)}{\Gamma(1+s)} \approx \frac{\sqrt{2\pi} (1+s-\epsilon)^{1+s-\epsilon-1/2} e^{-s-1+\epsilon}}{\sqrt{2\pi} (1+s)^{1+s-1/2} e^{-s-1}} \approx e^\epsilon s^{-\epsilon}. \quad (113)$$

²For ϵ larger than 1 we must deform γ further to the right, Luckily this is always possible since $f(s)$ is holomorphic away from the real axis.

Thus, we can approximate $f(s)$ on the path γ' as follows:

$$f(s) \approx \frac{-2i\pi e^\epsilon}{1+s} \frac{s^{-\epsilon}}{1-e^{-2i\pi s}}. \quad (114)$$

We divide γ' into three parts and look at the individual contributions to the integral separately:

$$\begin{aligned} \gamma'_1 &: \frac{\delta t}{2} < t < \frac{\pi}{2}, \\ \gamma'_2 &: -\frac{\pi}{2} < t < -\frac{\delta t}{2}, \\ \gamma'_3 &: -\frac{\delta t}{2} \leq t \leq \frac{\delta t}{2}, \end{aligned} \quad (115)$$

where δt is chosen close to zero. On γ'_1 the imaginary part of s is always positive. Hence, $f(s)$ goes exponentially fast to zero as R approaches infinity because of the exp-function in the denominator. We can therefore conclude that the integral over γ'_1 is zero. The contribution from the path γ'_2 is proportional to the following expression for large values of R :

$$\int_{\gamma'_2} dt f(s) \propto \frac{R^{1-\epsilon}}{1+R}. \quad (116)$$

In the limit $R \rightarrow \infty$ this contribution vanishes as well. Here, one can explicitly see the importance of ϵ . Setting ϵ to zero would have the following effects:

- The integral in Eq. (102) is not defined anymore.
- The integral along the path γ'_2 yields a nonzero value.
- The sum of all residues arising from $\Gamma(-s)$ diverges. The same holds true for the pole sequence arising from $\Gamma(1-\epsilon+s)$.
- The integral along the path γ diverges. This can be seen by explicit calculation.

We are left with the contribution of the path γ'_3 . At first, this part seems to be a little trickier because of the infinite pole series present on the real axis. However, as we are about to see, this causes no problem whatsoever. We define the following sequence:

$$f_n = f\left(n + \frac{1}{2}\right), \quad n = 1, 2, \dots \quad (117)$$

This series is strictly monotonic decreasing and goes to zero as n approaches infinity. With use of a theorem from complex analysis we can approximate the contribution of the path γ'_3 by

$$\begin{aligned} \left| \int_{\gamma'_3} dt f(s) \right| &\leq \left| K \lim_{n \rightarrow \infty} \tilde{n} f_n \right| \\ &\leq \left| K' \lim_{n \rightarrow \infty} \frac{\tilde{n}^{1-\epsilon}}{1+\tilde{n}} \right|, \end{aligned} \quad (118)$$

where $\tilde{n} = n + 1/2$ and K and K' are constants with respect to n . We see that for the integral over γ'_3 to be zero it is again crucial that ϵ is nonzero and positive, which is the case here. There is a more intuitive way to show that the poles on the real axis cannot be of any relevance for the integral over γ'_3 . The residue theorem only holds for a path which is free of any poles. In the process of $R \rightarrow \infty$ we must therefore make sure that for any R the path γ'_3 does not cross the real axis at an integer value. We can define a new path γ'_4 as follows:

$$\begin{aligned} \gamma'_4 &= \gamma'_3 \text{ for } R \notin \mathbb{N}, \\ \gamma'_4 &= R e^{it} + \frac{1}{2} \left(1 - \frac{|t|}{\delta t} \right) \text{ for } R \in \mathbb{N}. \end{aligned} \quad (119)$$

The integral over γ'_4 in the limit $R \rightarrow \infty$ is easily viable and gives again zero. When using Mellin-Barnes representations in conjunction with the residue theorem, one always faces the problem of a path similar to γ'_3 : the two Gamma-functions $\Gamma(-s)$ and $\Gamma(s + \lambda)$ are always present and hence there are pole series stretching to infinity in both halfplanes of the complex s plane.

What would have happened if we chose to equip x with a positive imaginary part (see Eq. (109))? For the calculation of the residues of the right-sided poles this choice is completely irrelevant (we even introduced this imaginary part after evaluating the residues). The function $f(s)$ as presented in Eq. (114) would feel two changes: i) The overall sign is flipped and ii) The sign of the argument of the exp-function is positive. The first change is again irrelevant. The second one would simply interchange the roles of γ'_1 and γ'_2 : the integral along the path γ' is still zero. All this is in agreement with the fact that the initial problem does not know about an imaginary part of x .

What if we choose to close the path γ on the left-hand side? The corresponding residues are readily calculated:

$$\text{Res}[f(\epsilon - k)] = e^{i\pi\epsilon} \frac{\Gamma(k - 1 - \epsilon)}{\Gamma(k)}, \quad k = 1, 2, 3, \dots \quad (120)$$

The sum over all residues vanishes³ and we infer that the integral over the path γ'' needed to close the contour on the left-hand side must yield a finite result equal to $-1/\epsilon$. In most cases, it is too difficult to actually calculate contributions from such paths. Rather, one tries to close the contour such that the integral over the added path vanishes.

The presented example shows how the integral I_ϵ can be evaluated by Mellin-Barnes techniques. However, since the straightforward way of integrating over x is much easier, it does not reflect the power of this method. In real-life calculations one often faces multi-dimensional Feynman parameter integrals which are much more complicated than I_ϵ (see e.g. Eq. (69) of Part V). In many cases it is hardly possible to evaluate them analytically and one looks for a result expanded in a suitable parameter. This is where the Mellin-Barnes approach shines. In Feynman diagram applications MB representation are mostly

³The residue for the pole located at $s = \epsilon - 1$ is equal to minus the sum of all other residues.

used to substitute “propagator like” expressions of the form $(K^2 - M^2)^{-\lambda}$. We rephrase Eq. (101) to allow for a more direct implementation:

$$\frac{1}{(K^2 - M^2)^\lambda} = \frac{1}{(K^2)^\lambda} \frac{1}{\Gamma(\lambda)} \frac{1}{2\pi i} \int_\gamma ds \left(-\frac{M^2}{K^2}\right)^s \Gamma(-s)\Gamma(\lambda + s). \quad (121)$$

Note that in most cases the quantity $K^2 - M^2$ is equipped with a positive or negative imaginary part $\pm i\delta$. This allows us by use of Eq. (110) to flip the sign in the term $(-M^2/K^2)^s$ if necessary. An expansion is now naturally given when K^2 and M^2 are chosen appropriately. Consider for this the following example:

$$F(m_1, m_2, \epsilon) = \int_0^1 dy \int_0^1 dx \frac{m_2^{2\epsilon} x^{1+2\epsilon} (1-x)^{-1-2\epsilon} y^{2\epsilon}}{[m_1^2 - x(1-y)m_2^2 - i\delta]^{1+2\epsilon}}, \quad (122)$$

where $m_1 \gg m_2$. Further, $F(m_1, m_2, \epsilon)$ is only of interest in the limit $\epsilon \rightarrow 0$. An exact result for the integral in terms of the two masses is hardly attainable. However, due to the hierarchy of m_1 and m_2 , a result expanded in the ratio $r = m_2^2/m_1^2$ might be good enough depending on the application. We rewrite Eq. (122) in terms of r and apply a Mellin-Barnes representation⁴ with the identifications

$$K^2 = 1, \quad M^2 = x(1-y)r + i\frac{\delta}{m_1^2}, \quad \lambda = 1 + 2\epsilon, \quad (123)$$

and arrive at

$$F(m_1, m_2, \epsilon) = \frac{m_1^{-2}}{\Gamma(1+2\epsilon)} \frac{r^\epsilon}{2\pi i} \int_\gamma ds e^{-i\pi s} \Gamma(-s)\Gamma(1+s+2\epsilon) r^s \int_0^1 dy \int_0^1 dx x^{1+s+2\epsilon} (1-x)^{-1-2\epsilon} y^{2\epsilon} (1-y)^s. \quad (124)$$

The path γ can be chosen parallel to the imaginary s -axis intersecting the real axis somewhere between $-1-2\epsilon$ ⁵ and 0. The integration over the two Feynman parameters is readily resolved and yields simple Euler β -functions. By closing the contour on the right-hand side and using the residue theorem the expansion in r comes out naturally with the factor r^s . We skip all intermediate steps and present the result for $F(m_1, m_2, \epsilon)$ up to terms of order r^4 :

$$F(m_1, m_2, \epsilon) = \frac{-1}{24m_1^2} \left[(12 + 6r + 4r^2 + 3r^3) \left(\frac{1}{\epsilon} + \ln(r) \right) + 12r + 12r^2 + 11r^3 \right]. \quad (125)$$

⁴Note that we tuned the example such that a direct expansion in neither r nor ϵ is possible.

⁵The integrals over the Feynman parameters demand that γ crosses the real axis at a value of $s > -1-2\epsilon$ and $s > -1$. Since ϵ must be negative in order to regulate the x -integral, it follows that $s > -1-2\epsilon$ is the stronger constraint.

It turns out that in this simple example the infinite residue sum can be performed and an analytically exact result in r can be attained:

$$F(m_1, m_2, \epsilon) = \frac{1}{2m_2^2} \left[\frac{\ln(1-r)}{\epsilon} - \ln(1-r)^2 + \ln(1-r) \ln(r) \right]. \quad (126)$$

We conclude this section with a list of general remarks about the Mellin-Barnes approach:

- The two presented examples may lead to the impression that pole sequences in the complex plane of the Mellin-Barnes parameter s only arise from the s -dependent Γ -functions in Eq. (121). This is certainly not true. We usually introduce Mellin-Barnes representations to be in a position to calculate existing integrals over Feynman parameters. These integrations can produce further pole sequences, single poles or even compensate existing ones. If one chooses to use the residue theorem to evaluate the integral over s , one must make sure to take all enclosed poles into account. When an integral introduces new poles, it may also have an effect on the path γ : we already mentioned that the integral over s must be defined on γ . New poles indicate that the corresponding integral does only exist for certain values of s and therefore impose additional constraints on γ . It may even happen that a suitable contour γ cannot be found. In these cases, a MB representation with the chosen K^2 , M^2 and λ does not exist.
- It can pay off to try different ways to replace a certain expression with a MB integral. We had a case where we needed to evaluate a three-dimensional integral over Feynman parameters x , y and u . We wanted to put Eq. (121) to use for the factor $(1-uy)^{-\lambda}$ appearing in the integrand. The most obvious identifications ($K^2 \leftrightarrow 1$ and $M^2 \leftrightarrow uy$ or vice-versa) were incompatible with the residue theorem (the contour needed to close the path γ in the right-half plane as well as the corresponding one in the left-half plane gave divergent contributions). However, by rewriting the initial expression to $(1-u+(1-y)u)^{-\lambda}$ and relating $K^2 \leftrightarrow 1-u$ and $M^2 \leftrightarrow (1-y)u$ we were able to tackle the problem.
- We can employ several Mellin-Barnes representations within the same Feynman diagram if necessary. E.g. H. M. Asatrian has analytically checked our result for diagram 3.1d) depicted on page 148 using three Mellin-Barnes integrals. In [53] a sextuple MB representation has been incorporated to attack one specific Feynman diagram. The result is expressed through finite double and triple MB integrals and generalized polylogarithms which allows for further numerical evaluation. Multiple MB representations introduce new challenging problems: First of all, one might face the task of evaluating coupled poles, i.e. poles in one complex plane which depend on the value of another Mellin-Barnes parameter. Further, finding out where to put the paths γ_i so that all given constraints are fulfilled is a nontrivial problem. Once these contours are determined, closing them and identifying all poles lying in the enclosed region can be far from concise. Finally, we saw in the evaluation of the integral in

Eq. (102) how complicated it is to prove that a given path γ'_i , which was added in order to use the residue theorem, does not give a contribution. With multiple such paths (which can depend on various Mellin-Barnes parameters and also on quantities such as masses and the dimensional regularization parameter ϵ), an analytic proof is mostly unattainable and one must fall back on numerical methods.

- In some cases it is necessary to calculate an integral up to order ϵ^1 or to even higher orders in ϵ . When a single Mellin-Barnes representation suffices to tackle a given integral, these terms are almost always trivially obtained: since we have to keep ϵ fixed when evaluating the residues, an expansion in ϵ is only possible after the integral over the MB parameter s is resolved. But at that point, the expansion in ϵ is pretty much the last thing we need to accomplish.

An equation worth mentioning in the context of this section is Barnes' lemma: For a contour γ which separates the increasing and decreasing sequences of poles, the following identity holds:

$$\frac{1}{2\pi i} \int_{\gamma} ds \Gamma(u+s) \Gamma(v+s) \Gamma(w-s) \Gamma(x-s) = \frac{\Gamma(u+w) \Gamma(u+x) \Gamma(v+w) \Gamma(v+x)}{\Gamma(u+v+w+x)}, \quad (127)$$

where u, v, w and x are constants with respect to s . The path γ is meant to start at $-i\infty$ and go to $i\infty$ as in Eq. (101). Although the structure of the integral looks quite special, it is sometimes possible to cast an integrand into this form. Consider the integral

$$B_{\epsilon} = \int_0^1 dx \int_0^1 dy \frac{(1-x)^{1-\epsilon} (1-y)^{\epsilon-1}}{(x+(1-x)y)^{1+\epsilon}},$$

where ϵ is positive and close to zero. We write an MB representation with $K^2 \leftrightarrow x$ and $M^2 \leftrightarrow -(1-x)y$ and arrive indeed at an integral of the desired form. Using Eq. (127) we find

$$B_{\epsilon} = \frac{\pi \Gamma(2-\epsilon)}{\Gamma(3-2\epsilon) \Gamma(1+\epsilon) \sin(\pi\epsilon)}.$$

There is a second lemma by Barnes which involves Γ -functions in the numerator as well as in the denominator of the integrand. For this and similar identities we refer to [54].

References

- [1] S. L. Glashow, *Nucl. Phys.* **22** (1961) 579.
- [2] M. Gell-Mann, *Phys. Rev.* **125** (1962) 1067.
- [3] S. Weinberg, *Phys. Rev. Lett.* **19** (1967) 1264.
- [4] H. Fritzsch, M. Gell-Mann and H. Leutwyler, *Phys. Lett.* **B 47** (1973) 365.
- [5] G. 't Hooft, *Nucl. Phys.* **B 33** (1971) 173; G. 't Hooft, *Nucl. Phys.* **B 35** (1971) 167.
- [6] F. J. Hasert *et al.* [Gargamelle Neutrino Collaboration], *Phys. Lett.* **B 46** (1973) 138.
- [7] A. C. Benvenuti *et al.*, *Phys. Rev. Lett.* **32** (1974) 125.
- [8] S. J. Barish *et al.*, *Phys. Rev. Lett.* **33** (1974) 448.
- [9] G. Arnison *et al.* [UA1 Collaboration], *Phys. Lett.* **B 126** (1983) 398.
- [10] P. Bagnaia *et al.* [UA2 Collaboration], *Phys. Lett.* **B 129** (1983) 130.
- [11] F. Abe *et al.* [CDF Collaboration], *Phys. Rev. Lett.* **74** (1995) 2626, [hep-ex/9503002](#).
- [12] J. R. Ellis and M. K. Gaillard, *Nucl. Phys.* **B 150** (1979) 141.
- [13] K. Hagiwara *et al.* [Particle Data Group Collaboration], *Phys. Rev.* **D 66** (2002) 010001.
- [14] H. Banerjee *et al.*, *Phys. Lett.* **B 573** (2003) 109, [hep-ph/0012284](#).
- [15] U. Amaldi *et al.*, *Phys. Rev.* **D 36** (1987) 1385.
- [16] G. Costa, J. R. Ellis, G. L. Fogli, D. V. Nanopoulos and F. Zwirner, *Nucl. Phys.* **B 297** (1988) 244.
- [17] R. Assmann *et al.*, *Eur. Phys. J.* **C 6** (1999) 187.
- [18] S. Weinberg, “The Quantum Theory of Fields, Volume II”, Cambridge University Press, 1996.
- [19] V. N. Popov and L. D. Faddeev, FERMILAB-PUB-72-057-T, [SPIRES entry](#).
- [20] T. W. B. Kibble, *Phys. Rev.* **155** (1967) 1554.
- [21] S. Weinberg, *Phys. Rev. Lett.* **18** (1967) 507.
- [22] L. L. Chau and W. Y. Keung, *Phys. Rev. Lett.* **53** (1984) 1802.
- [23] L. Wolfenstein, *Phys. Rev. Lett.* **51** (1983) 1945.

-
- [24] K. G. Wilson, *Phys. Rev.* **179** (1969) 1499.
- [25] C. Bobeth, M. Misiak and J. Urban, *Nucl. Phys.* **B 574** (2000) 291, [hep-ph/9910220](#).
- [26] K. G. Chetyrkin, M. Misiak and M. Munz, *Nucl. Phys.* **B 520** (1998) 279, [hep-ph/9711280](#).
- [27] M. Misiak, *Nucl. Phys.* **B 393** (1993) 23, E:*Nucl. Phys.* **B 439** (1995) 461.
- [28] G. Buchalla, [hep-ph/0202092](#).
- [29] N. Isgur and M. B. Wise, *Phys. Lett.* **B 232** (1989) 113; *Phys. Lett.* **B 237** (1990) 527.
- [30] J. N. Simone, S. Hashimoto, A. S. Kronfeld, P. B. Mackenzie and S. M. Ryan, *Prepared for 31st International Conference on High Energy Physics (ICHEP 2002), Amsterdam, The Netherlands, 24-31 Jul 2002*.
- [31] M. B. Wise, *Nucl. Instrum. Meth.* **408** (1998) 1, [hep-ph/9803247](#).
- [32] A. F. Falk, [hep-ph/9812217](#).
- [33] I. I. Y. Bigi, [hep-ph/9508408](#).
- [34] M. Neubert and C. T. Sachrajda, *Nucl. Phys.* **B 483** (1997) 339, [hep-ph/9603202](#).
- [35] I. J. Kroll, [hep-ex/9602005](#).
- [36] M. B. Voloshin, *Phys. Lett.* **B 397** (1997) 275, [hep-ph/9612483](#).
- [37] G. Buchalla, G. Isidori and S. J. Rey, *Nucl. Phys.* **B 511** (1998) 594, [hep-ph/9705253](#).
- [38] M. R. Ahmady, *Phys. Rev.* **D 53** (1996) 2843, [hep-ph/9508213](#).
- [39] A. Ali, G. Hiller, L. T. Handoko and T. Morozumi, *Phys. Rev.* **D 55** (1997) 4105, [hep-ph/9609449](#).
- [40] A. J. Buras, [hep-ph/9806471](#).
- [41] M. Walker, *Ph.D. thesis* (2002) 29.
- [42] N. Tracas and N. Vlachos, *Phys. Lett.* **B 115** (1982) 419.
- [43] A. J. Buras and P. H. Weisz, *Nucl. Phys.* **B 333** (1990) 66.
- [44] M. J. Dugan and B. Grinstein, *Phys. Lett.* **B 256** (1991) 239.
- [45] S. Herrlich and U. Nierste, *Nucl. Phys.* **B 455** (1995) 39, [hep-ph/9412375](#).
- [46] C. G. Bollini and J. J. Giambiagi, *Nuovo Cim.* **B 12** (1972) 20.

- [47] G. 't Hooft, *Nucl. Phys.* **B 61** (1973) 455.
- [48] M. Schmelling, [hep-ex/9701002](#).
- [49] O. V. Tarasov, *Phys. Rev.* **D 54** (1996) 6479, [hep-th/9606018](#).
- [50] S. Actis, A. Ferroglia, G. Passarino, M. Passera and S. Uccirati, [hep-ph/0402132](#).
- [51] V. A. Smirnov, *Renormalization and Asymptotic Expansions* (Birkhäuser, Basel, 1991); *Applied Asymptotic Expansions in Momenta and Masses* (Springer-Verlag, Heidelberg, 2001); *Mod. Phys. Lett.* **A 10** (1995) 1485, [hep-th/9412063](#).
- [52] E. E. Boos and A. I. Davydychev, *Theor. Math. Phys.* **89** (1991) 1052, *Teor. Mat. Fiz.* **89** (1991) 56.
- [53] V. A. Smirnov, *Phys. Lett.* **B 500** (2001) 330, [hep-ph/0011056](#).
- [54] W. N. Bailey, *Generalized Hypergeometric Series* (Cambridge University Press, London, 1935; reprinted by Stechert-Hafner, New York, 1964).

PART II

NNLL calculations to the angular
distribution and to the
forward-backward
asymmetries in $b \rightarrow X_s \ell^+ \ell^-$

published in

Physical Review D 66 (2002) 094013

NNLL corrections to the angular distribution and to the forward-backward asymmetries in $b \rightarrow X_s \ell^+ \ell^-$

H.M. Asatrian^a, K. Bieri^b, C. Greub^b and A. Hovhannisyan^a

^a *Yerevan Physics Institute, 2 Alikhanyan Br., 375036 Yerevan, Armenia;*

^b *Institut für Theoretische Physik, Universität Bern,
CH-3012 Bern, Switzerland.*

ABSTRACT

We present next-to-next-to leading logarithmic (NNLL) results for the double differential decay width $d\Gamma(b \rightarrow X_s \ell^+ \ell^-)/(d\hat{s} d \cos(\theta))$, where $s = \hat{s} m_b^2$ is the invariant mass squared of the lepton pair and θ is the angle between the momenta of the b -quark and the ℓ^+ , measured in the rest-frame of the lepton pair. From these results we also derive NNLL results for the lepton forward-backward asymmetries, as these quantities are known to be very sensitive to new physics. While the principal steps in the calculation of the double differential decay width are the same as for $d\Gamma(b \rightarrow X_s \ell^+ \ell^-)/d\hat{s}$, which is already known to NNLL precision, genuinely new calculations for the combined virtual- and gluon bremsstrahlung corrections associated with the operators O_7 , O_9 and O_{10} are necessary. In this paper, we neglected certain other bremsstrahlung contributions, which are known to have only a small impact on $d\Gamma(b \rightarrow X_s \ell^+ \ell^-)/d\hat{s}$. We find that the NNLL corrections drastically reduce the renormalization scale (μ) dependence of the forward-backward asymmetries. In particular, \hat{s}_0 , the position at which the forward-backward asymmetries vanish, is essentially free of uncertainties due to the renormalization scale at NNLL precision. We find $\hat{s}_0^{\text{NNLL}} = 0.162 \pm 0.005$, where the error is dominated by the uncertainty in m_c/m_b . This is to be compared with $\hat{s}_0^{\text{NLL}} = 0.144 \pm 0.020$, where the error is dominated by uncertainties due to the choice of μ .

1 Introduction

Rare B -meson decays are known to be important sources for informations on the standard model (SM) of electroweak and strong interactions and its extensions. Being very sensitive to the actual physics at the scales of several hundred GeV, they can be used to distinguish between different models of fundamental physics and, in particular, to find significant deviations from the SM predictions. Even restricting the consideration to the SM case, these decays can be used to retrieve important information on the properties of the top quark, e.g. to determine the elements V_{ts} and V_{td} of the Cabibbo-Kobayashi-Maskawa (CKM) matrix.

The first measured rare B -meson decay was the exclusive channel $B \rightarrow K^*\gamma$, observed by the CLEO collaboration in 1992 [1]. It was followed by the observation of the corresponding inclusive mode $B \rightarrow X_s\gamma$ [2]. The measured decay rate [2, 3, 4, 5] and the photon energy spectrum [6] for the latter are in good agreement with the predictions of the SM [7, 8, 9, 10, 11, 12, 13]. Thus, these observables are well suited for constraining the SM extensions, such as two-Higgs doublet models [14, 9, 15], left-right symmetric models [16], supersymmetric models [17, 18, 19, 20, 21, 22], etc.

Among the other rare transitions, the inclusive decay $B \rightarrow X_s\ell^+\ell^-$ plays a remarkable role. The measurement of various kinematical distributions of the decay products will tighten the constraints on the extensions of the SM or perhaps even reveal some deviations, in particular when combined with improved data on $B \rightarrow X_s\gamma$ [23].

Recently, the BELLE collaboration has reported the observation of the exclusive transition $B \rightarrow K\mu^+\mu^-$ [24], with a rate consistent with the SM predictions. This measurement was confirmed by the BABAR collaboration [25]. Very recently, also a measurement of the branching ratio for the inclusive decay $B \rightarrow X_s\ell^+\ell^-$ was published by the BELLE collaboration [26].

The interest towards *inclusive* rare decays is motivated by the fact that they can be well approximated in suitably chosen kinematical ranges by the underlying b -quark decay. The corrections to this simple partonic picture, which can be systematically calculated in the framework of Heavy Quark Expansion (HQE), manifest themselves as power corrections in $1/m_b$ [27, 28, 29].

The main problem of the theoretical description of $B \rightarrow X_s\ell^+\ell^-$ is due to the long-distance contributions from $\bar{c}c$ resonant states. When the invariant mass \sqrt{s} of the lepton pair is close to the mass of a resonance, only model-dependent predictions for such long distance contributions are available today. It is therefore unclear whether the theoretical uncertainty can be reduced to less than $\pm 20\%$ when integrating over these domains [30].

However, when restricting \sqrt{s} to a region below the resonances, the long distance effects are under control. The left-over effects of the resonances can again be analyzed within the framework HQE and manifest themselves as $1/m_c$ power corrections. All available studies indicate that for the region $0.05 < \hat{s} = s/m_b^2 < 0.25$ these non-perturbative effects are below

10% [28, 31, 32, 33, 34, 35]. Consequently, the differential decay rate for $B \rightarrow X_s \ell^+ \ell^-$ can be precisely predicted in this region, using renormalization group improved perturbation theory. It was pointed out in the literature that the invariant mass distribution of the lepton pair and the forward-backward asymmetries are particularly sensitive to new physics in this kinematical window [31, 36, 37, 38, 15].

Although the consideration of inclusive decays allows to avoid the most difficult issues of hadronic physics, the *perturbative* QCD corrections play a very important role for all rare B -decays. Calculations of the next-to-leading logarithmic (NLL) QCD corrections to the invariant mass distribution of the lepton pair ($d\Gamma(b \rightarrow X_s \ell^+ \ell^-)/d\hat{s}$) were performed in Refs. [39] and [40]. It turned out that the NLL result suffers from a relatively large ($\pm 16\%$) dependence on the matching scale μ_W . To reduce it, next-to-next-to leading logarithmic (NNLL) corrections to the Wilson coefficients were calculated by Bobeth et al. [41]. This required a two-loop matching calculation of the full SM theory onto the effective theory, followed by a renormalization group evolution of the Wilson coefficients, using up to three-loop anomalous dimensions [41, 10]. Including these NNLL corrections to the Wilson coefficients, the matching scale dependence is indeed removed to a large extent.

As has been pointed out in Ref. [41], this partial NNLL result suffers from a relatively large ($\sim \pm 13\%$) renormalization scale (μ_b) dependence ($\mu_b \sim \mathcal{O}(m_b)$). In order to further improve the theoretical prediction, we recently calculated the virtual two-loop corrections to the matrix elements $\langle s \ell^+ \ell^- | O_i | b \rangle$ ($i = 1, 2$) as well as the virtual (α_s) one-loop corrections to O_7, \dots, O_{10} and the corresponding bremsstrahlung corrections [42, 43, 44]. This improvement reduced the renormalization scale dependence of $d\Gamma(b \rightarrow X_s \ell^+ \ell^-)/d\hat{s}$ by a factor of 2.

In the present paper, we present a calculation of the double differential decay width $d\Gamma/(d\hat{s} d\cos(\theta))$ and the forward-backward asymmetries for the decay $b \rightarrow X_s \ell^+ \ell^-$ at NNLL precision. θ denotes the angle between the momenta of the positively charged lepton (ℓ^+) and the b -quark, measured in the rest-frame of the lepton pair. It is well-known that the measurement of the forward-backward asymmetries along with detailed experimental information on the invariant mass distribution of the lepton pair can be used, in combination with the measurement of the radiative decay $B \rightarrow X_s \gamma$, to perform “a model-independent test” of the SM [45, 46, 23]. In particular, for some extensions of the SM the branching ratio for the process $B \rightarrow X_s \gamma$ is the same as in the SM, but the Wilson coefficient C_7 has opposite sign [23, 47, 48, 21]. As shown in Refs. [45, 46, 23], the measurement of the shape of the forward-backward asymmetries as a function of \hat{s} in the process $B \rightarrow X_s \ell^+ \ell^-$ would allow to determine whether the SM sign or the opposite sign of C_7 is realized in nature. Needless to say, the measurement of the forward-backward asymmetries also yields additional (and complementary) information for determining the Wilson coefficients C_9 and C_{10} .

Being a crucial observable in the search for new physics in rare B decays, the forward-backward asymmetries should be calculated in the SM as precisely as possible. As the available NLL results suffer from a large dependence on the renormalization scale, we per-

form a NNLL calculation of these asymmetries in the present paper. Note that the NNLL corrections to the forward-backward asymmetries cannot be straightforwardly derived from our previous results for $d\Gamma(b \rightarrow X_s \ell^+ \ell^-)/d\hat{s}$, i.e., a partial recalculation is required. In particular, this concerns the bremsstrahlung contributions associated with the operators O_7 , O_9 and O_{10} , which are needed for the cancellation of the infrared- and collinear singularities in the virtual corrections.

The paper is organized as follows: In Section 2 we recall the theoretical framework. Section 3 is devoted to the previous results on $d\Gamma(b \rightarrow X_s \ell^+ \ell^-)/d\hat{s}$ and explains why modifications are needed for the derivation of the double differential decay width. In Section 4 the analytical results for the double differential decay width and for the forward-backward asymmetries are presented. In Sections 5, 6 and 7 the technical issues needed for the derivation of the double differential decay width are explained. In Section 8 a detailed phenomenological analysis for the forward-backward asymmetries is presented; the angular distributions are also shortly discussed. Finally, in Section 9 we briefly summarize our paper. In this section we also compare our results on the forward-backward asymmetries with those reported in Ref. [49], which appeared when we were working out the double differential decay width.

2 Theoretical framework

As mentioned above, the QCD corrections give significant (sometimes even dominant) contributions to the decay rates of rare processes. The most efficient tool for analyzing these corrections in a systematic way is the effective Hamiltonian technique. The effective Hamiltonian for a particular decay channel of a b -quark is obtained by integrating out the heavy degrees of freedom which are (in the context of the SM) the top quark, the W^\pm and Z^0 bosons. The effective Hamiltonian for the decay $b \rightarrow X_s \ell^+ \ell^-$ reads

$$\mathcal{H}_{\text{eff}} = -\frac{4G_F}{\sqrt{2}} V_{ts}^* V_{tb} \sum_{i=1}^{10} C_i O_i, \quad (1)$$

where we have omitted the contributions which are weighed by the small CKM factor $V_{ub} V_{us}^*$. The dimension six effective operators can be chosen as [41]

$$\begin{aligned} O_1 &= (\bar{s}_L \gamma_\mu T^a c_L)(\bar{c}_L \gamma^\mu T^a b_L), & O_2 &= (\bar{s}_L \gamma_\mu c_L)(\bar{c}_L \gamma^\mu b_L), \\ O_3 &= (\bar{s}_L \gamma_\mu b_L) \sum_q (\bar{q} \gamma^\mu q), & O_4 &= (\bar{s}_L \gamma_\mu T^a b_L) \sum_q (\bar{q} \gamma^\mu T^a q), \\ O_5 &= \bar{s}_L \gamma_\mu \gamma_\nu \gamma_\rho b_L \sum_q \bar{q} \gamma^\mu \gamma^\nu \gamma^\rho q, & O_6 &= \bar{s}_L \gamma_\mu \gamma_\nu \gamma_\rho T^a b_L \sum_q \bar{q} \gamma^\mu \gamma^\nu \gamma^\rho T^a q, \\ O_7 &= \frac{e}{g_s^2} m_b (\bar{s}_L \sigma^{\mu\nu} b_R) F_{\mu\nu}, & O_8 &= \frac{1}{g_s} m_b (\bar{s}_L \sigma^{\mu\nu} T^a b_R) G_{\mu\nu}^a, \\ O_9 &= \frac{e^2}{g_s^2} (\bar{s}_L \gamma_\mu b_L)(\bar{\ell} \gamma^\mu \ell), & O_{10} &= \frac{e^2}{g_s^2} (\bar{s}_L \gamma_\mu b_L)(\bar{\ell} \gamma^\mu \gamma_5 \ell). \end{aligned} \quad (2)$$

The subscripts L and R refer to left- and right-handed fermion fields. The factors $1/g_s^2$ in the definition of the operators O_7 , O_9 and O_{10} , as well as the factor $1/g_s$ present in O_8 have been chosen by Misiak [39] in order to simplify the organization of the calculation: With these definitions, the one-loop anomalous dimensions (needed for a leading logarithmic (LL) calculation) of the operators O_i are all proportional to g_s^2 , while two-loop anomalous dimensions (needed for a next-to-leading logarithmic (NLL) calculation) are proportional to g_s^4 , etc.

In this setup, the principal steps which lead to a (formally) LL, NLL, NNLL prediction for the decay amplitude for $b \rightarrow X_s \ell^+ \ell^-$ are the following:

1. A matching calculation between the full SM theory and the effective theory has to be performed in order to determine the Wilson coefficients C_i at the high scale $\mu_W \sim m_W, m_t$. At this scale, the coefficients can be worked out in fixed order perturbation theory, i.e. they can be expanded in g_s^2 :

$$C_i(\mu_W) = C_i^{(0)}(\mu_W) + \frac{g_s^2}{16\pi^2} C_i^{(1)}(\mu_W) + \frac{g_s^4}{(16\pi^2)^2} C_i^{(2)}(\mu_W) + O(g_s^6). \quad (3)$$

At LL order, only $C_i^{(0)}$ is needed, at NLL order also $C_i^{(1)}$, etc. While the coefficient $C_7^{(2)}$, which is needed for a NNLL analysis, is known for quite some time [8], $C_9^{(2)}$ and $C_{10}^{(2)}$ have been calculated only recently [41] (see also [50]).

2. The renormalization group equation (RGE) has to be solved in order to get the Wilson coefficients at the low scale $\mu_b \sim m_b$. For this RGE step the anomalous dimension matrix to the relevant order in g_s is required, as described above. After these two steps one can decompose the Wilson coefficients $C_i(\mu_b)$ into a LL, NLL and NNLL part according to

$$C_i(\mu_b) = C_i^{(0)}(\mu_b) + \frac{g_s^2(\mu_b)}{16\pi^2} C_i^{(1)}(\mu_b) + \frac{g_s^4(\mu_b)}{(16\pi^2)^2} C_i^{(2)}(\mu_b) + O(g_s^6). \quad (4)$$

3. In order to get the decay amplitude, the matrix elements $\langle s \ell^+ \ell^- | O_i(\mu_b) | b \rangle$ have to be calculated. At LL precision, only the operator O_9 contributes, as this operator is the only one which at the same time has a Wilson coefficient starting at lowest order and an explicit $1/g_s^2$ factor in the definition. Hence, in the NLL precision QCD corrections (virtual and bremsstrahlung) to the matrix element of O_9 are needed. They have been calculated a few years ago [39, 40]. At NLL precision, also the other operators start contributing, viz. $O_7(\mu_b)$ and $O_{10}(\mu_b)$ contribute at tree-level and the four-quark operators O_1, \dots, O_6 at one-loop level. Accordingly, QCD corrections to the latter matrix elements are needed for a NNLL prediction of the decay amplitude.

As known for a long time [51], the formally leading term $\sim (1/g_s^2) C_9^{(0)}(\mu_b)$ to the amplitude for $b \rightarrow s \ell^+ \ell^-$ is smaller than the NLL term $\sim (1/g_s^2) [g_s^2/(16\pi^2)] C_9^{(1)}(\mu_b)$. As in our earlier

papers on the NNLL prediction for $\text{BR}(b \rightarrow X_s \ell^+ \ell^-)$ [42, 43, 44], we adapt our systematics to the numerical situation and treat the sum of these two terms as a NLL contribution. This is, admittedly, some abuse of language, because the decay amplitude then starts with a term which is called NLL. Using this adapted counting, no QCD corrections to the matrix elements $\langle s \ell^+ \ell^- | O_i(\mu_b) | b \rangle$ ($i = 1, \dots, 10$) are needed when working at NLL precision, while one-gluon (virtual- and bremsstrahlung) corrections are necessary at NNLL precision.

When working out in the following the QCD corrections to the matrix elements, we often also use the related operators $\tilde{O}_{7,\dots}, \tilde{O}_{10}$, defined according to

$$\tilde{O}_j = \frac{\alpha_s}{4\pi} O_j, \quad (j = 7, \dots, 10), \quad (5)$$

with the corresponding Wilson coefficients

$$\tilde{C}_j = \frac{4\pi}{\alpha_s} C_j, \quad (j = 7, \dots, 10). \quad (6)$$

3 Previous results for $d\Gamma/d\hat{s}$ and modifications needed for $d\Gamma/(d\hat{s} d \cos \theta)$

To obtain the NNLL approximation for $d\Gamma(b \rightarrow X_s \ell^+ \ell^-)/d\hat{s}$, using the modified counting discussed above, virtual- and gluon bremsstrahlung corrections were calculated in Refs. [42, 43, 44] and combined with the Wilson coefficients evaluated to the corresponding precision. For completeness, we briefly repeat these results, and put them into a slightly different form than presented in Refs. [42, 43, 44]. The distribution of the invariant mass squared of the lepton pair can be written as

$$\begin{aligned} \frac{d\Gamma(b \rightarrow X_s \ell^+ \ell^-)}{d\hat{s}} &= \left(\frac{\alpha_{\text{em}}}{4\pi} \right)^2 \frac{G_F^2 m_{b,\text{pole}}^5 |V_{ts}^* V_{tb}|^2}{48 \pi^3} (1 - \hat{s})^2 \\ &\left\{ (1 + 2\hat{s}) \left(|\tilde{C}_9^{\text{eff}}|^2 + |\tilde{C}_{10}^{\text{eff}}|^2 \right) \left[1 + \frac{2\alpha_s}{\pi} \omega_{99}(\hat{s}) \right] + 4 \left(1 + \frac{2}{\hat{s}} \right) |\tilde{C}_7^{\text{eff}}|^2 \left[1 + \frac{2\alpha_s}{\pi} \omega_{77}(\hat{s}) \right] \right. \\ &\left. + 12 \text{Re} \left(\tilde{C}_7^{\text{eff}} \tilde{C}_9^{\text{eff}*} \right) \left[1 + \frac{2\alpha_s}{\pi} \omega_{79}(\hat{s}) \right] \right\} + \frac{d\Gamma^{\text{Brems,A}}}{d\hat{s}} + \frac{d\Gamma^{\text{Brems,B}}}{d\hat{s}}. \quad (7) \end{aligned}$$

$\frac{d\Gamma^{\text{Brems,A}}}{d\hat{s}}$ and $\frac{d\Gamma^{\text{Brems,B}}}{d\hat{s}}$ are the finite bremsstrahlung corrections discussed in detail in Ref. [44] (see Eqs. (13) and (22) in this reference). The other bremsstrahlung corrections, associated with the operators \tilde{O}_7 , \tilde{O}_9 and \tilde{O}_{10} suffer from infrared- and collinear singularities. They are contained, combined with the corresponding virtual corrections, in the quantities $\omega_{99}(\hat{s})$, $\omega_{77}(\hat{s})$ and $\omega_{79}(\hat{s})$. As they will be needed in the construction of the double differential decay width, we repeat their explicit form in Appendix A. The virtual corrections to the matrix elements of O_1 , O_2 and O_8 , on the other hand, are infrared finite. They can be written as multiples of tree-level matrix elements of the operators \tilde{O}_7 , \tilde{O}_9 and \tilde{O}_{10} , and

are usually absorbed (through the functions $F_i^{(j)}$ ($i = 1, 2, 8; j = 7, 9$)) into the effective Wilson coefficients \tilde{C}_7^{eff} , \tilde{C}_9^{eff} and $\tilde{C}_{10}^{\text{eff}}$, which read

$$\tilde{C}_7^{\text{eff}} = A_7 - \frac{\alpha_s(\mu)}{4\pi} \left(C_1^{(0)} F_1^{(7)}(\hat{s}) + C_2^{(0)} F_2^{(7)}(\hat{s}) + A_8^{(0)} F_8^{(7)}(\hat{s}) \right), \quad (8)$$

$$\begin{aligned} \tilde{C}_9^{\text{eff}} = & A_9 + T_9 h(\hat{m}_c^2, \hat{s}) + U_9 h(1, \hat{s}) + W_9 h(0, \hat{s}) \\ & - \frac{\alpha_s(\mu)}{4\pi} \left(C_1^{(0)} F_1^{(9)}(\hat{s}) + C_2^{(0)} F_2^{(9)}(\hat{s}) + A_8^{(0)} F_8^{(9)}(\hat{s}) \right), \end{aligned} \quad (9)$$

$$\tilde{C}_{10}^{\text{eff}} = A_{10}. \quad (10)$$

The quantities $C_1^{(0)}$, $C_2^{(0)}$, A_7 , $A_8^{(0)}$, A_9 , A_{10} , T_9 , U_9 and W_9 are Wilson coefficients or linear combinations thereof. Their analytical expressions and numerical values are given in Appendix B. The one-loop function $h(\hat{m}_c^2, \hat{s})$ is also given there, while the two-loop functions $F_{1,2}^{(7),(9)}$, and the one-loop functions $F_8^{(7),(9)}$ are given in Ref. [43]. We remind the reader that in the above results the QCD corrections to the matrix elements of the operators $O_3 - O_6$ were not taken into account *systematically*, as they are weighted by small Wilson coefficients.

It may appear as a surprise that a NNLL calculation for $d\Gamma(b \rightarrow X_s \ell^+ \ell^-)/d\hat{s}$ is available, while the corresponding result for $d^2\Gamma(b \rightarrow X_s \ell^+ \ell^-)/(d\hat{s} d\cos(\theta))$ is still missing. The reason is a technical one. When aiming only at $d\Gamma(b \rightarrow X_s \ell^+ \ell^-)/d\hat{s}$, it is convenient to integrate in a first step over the lepton momenta after multiplying the well-known expression for the fully differential decay width by a factor 1 in the form (note that $\hat{s} = q^2/m_b^2$)

$$1 = \int \delta^d(q - l_1 - l_2) d^d q. \quad (11)$$

This is precisely what we did in our previous works [42, 43, 44]. It is evident that after this step the angular correlation between hadronic and leptonic variables is lost. For this reason, the phase space integrations have to be done in another way when aiming at a calculation of the double differential decay width. While these modifications connected to phase space are straightforward for the lowest order and the virtual corrections, where only three particles are in the final state, a genuinely new calculation is needed for the gluon bremsstrahlung process with four particles in the final state.

We decide to postpone the discussion of these technical issues to Sections 5–7, as we prefer to first present the final results for the double differential decay width and for the forward-backward asymmetries.

4 NNLL results for the double differential decay width and the forward-backward asymmetries

We write the double differential decay width $d^2\Gamma(b \rightarrow X_s \ell^+ \ell^-)/(d\hat{s} dz)$ ($z = \cos(\theta)$) in a form which is analogous to the expression for $d\Gamma(b \rightarrow X_s \ell^+ \ell^-)/d\hat{s}$ in Eq. (7). We obtain

$$\begin{aligned}
\frac{d^2\Gamma(b \rightarrow X_s \ell^+ \ell^-)}{d\hat{s} dz} &= \left(\frac{\alpha_{\text{em}}}{4\pi}\right)^2 \frac{G_F^2 m_{b,\text{pole}}^5 |V_{ts}^* V_{tb}|^2}{48\pi^3} (1 - \hat{s})^2 \\
&\left\{ \frac{3}{4} [(1 - z^2) + \hat{s}(1 + z^2)] \left(|\tilde{C}_9^{\text{eff}}|^2 + |\tilde{C}_{10}^{\text{eff}}|^2 \right) \left(1 + \frac{2\alpha_s}{\pi} f_{99}(\hat{s}, z) \right) \right. \\
&+ \frac{3}{\hat{s}} [(1 + z^2) + \hat{s}(1 - z^2)] |\tilde{C}_7^{\text{eff}}|^2 \left(1 + \frac{2\alpha_s}{\pi} f_{77}(\hat{s}, z) \right) \\
&- 3\hat{s}z \text{Re}(\tilde{C}_9^{\text{eff}} \tilde{C}_{10}^{\text{eff}*}) \left(1 + \frac{2\alpha_s}{\pi} f_{910}(\hat{s}) \right) \\
&+ 6 \text{Re}(\tilde{C}_7^{\text{eff}} \tilde{C}_9^{\text{eff}*}) \left(1 + \frac{2\alpha_s}{\pi} f_{79}(\hat{s}, z) \right) \\
&\left. - 6z \text{Re}(\tilde{C}_7^{\text{eff}} \tilde{C}_{10}^{\text{eff}*}) \left(1 + \frac{2\alpha_s}{\pi} f_{710}(\hat{s}) \right) \right\}. \tag{12}
\end{aligned}$$

The effective Wilson coefficients are the same as those used for $d\Gamma/d\hat{s}$; they are given in Eqs. (8)-(10). In particular, they contain the virtual corrections to the matrix elements of the operators O_1 , O_2 and O_8 . The sum of virtual- and bremsstrahlung corrections to the matrix elements of O_7 , O_9 and O_{10} is incorporated in the functions $f_{99}(\hat{s}, z)$, $f_{77}(\hat{s}, z)$, $f_{910}(\hat{s})$, $f_{79}(\hat{s}, z)$ and $f_{710}(\hat{s})$. These functions are the analogues of $\omega_{99}(\hat{s})$, $\omega_{77}(\hat{s})$ and $\omega_{79}(\hat{s})$ which enter Eq. (7). As indicated in the notation, the functions f_{710} and f_{910} only depend on \hat{s} , while f_{99} , f_{77} and f_{79} depend also on z . In Eq. (12) we do not include the purely finite bremsstrahlung corrections, which in the case for $d\Gamma/d\hat{s}$ were encoded in Eq. (7) in the last two terms. This omission is motivated by the fact that these corrections have a negligible impact on $d\Gamma/d\hat{s}$.

We now turn to the forward-backward asymmetries. We will investigate both, the so-called normalized- and the unnormalized forward-backward asymmetry. The normalized version, $\overline{A}_{\text{FB}}(\hat{s})$, is defined as

$$\overline{A}_{\text{FB}}(\hat{s}) = \frac{\int_{-1}^1 \frac{d^2\Gamma(b \rightarrow X_s \ell^+ \ell^-)}{d\hat{s} dz} \text{sgn}(z) dz}{\int_{-1}^1 \frac{d^2\Gamma(b \rightarrow X_s \ell^+ \ell^-)}{d\hat{s} dz} dz}, \tag{13}$$

while the definition of the unnormalized forward-backward asymmetry $A_{\text{FB}}(\hat{s})$ reads

$$A_{\text{FB}}(\hat{s}) = \frac{\int_{-1}^1 \frac{d^2\Gamma(b \rightarrow X_s \ell^+ \ell^-)}{d\hat{s} dz} \text{sgn}(z) dz}{\Gamma(B \rightarrow X_c e \nu_e)} \text{BR}_{\text{sl}}. \tag{14}$$

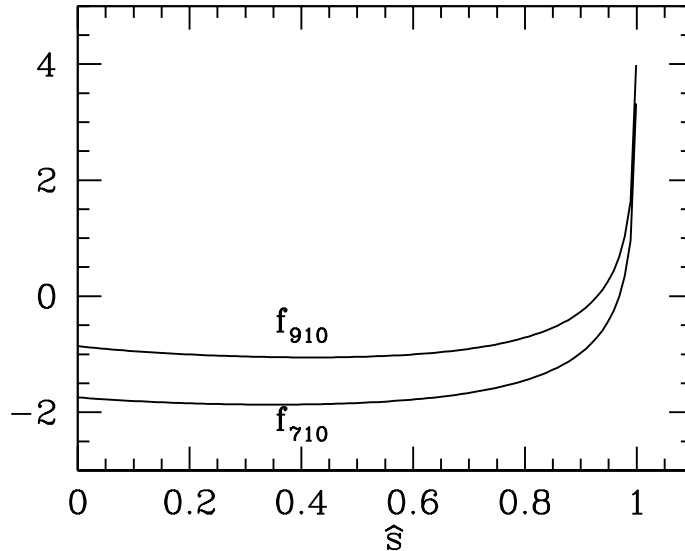


Figure 4.1: Functions $f_{710}(\hat{s})$ and $f_{910}(\hat{s})$ which in the forward-backward asymmetries incorporate virtual- and bremsstrahlung corrections to the (O_7, O_{10}) and (O_9, O_{10}) interference terms. $\mu/m_b=1$.

The denominator in Eq. (14) is the semileptonic decay width, which is usually put into the definition of the unnormalized forward-backward asymmetry in order to cancel the fifth power of m_b present in the numerator. The expression for $\Gamma(b \rightarrow X_c e \bar{\nu}_e)$ is well-known, including $O(\alpha_s)$ QCD corrections [52], and can be taken e.g. from Ref. [43]. The factor BR_{sl} in Eq. (14) denotes the measured semileptonic branching ratio of the B -meson.

In the numerator, both asymmetries involve the same forward-backward integral over the double differential decay width. For this integral one obtains

$$\int_{-1}^1 \frac{d^2\Gamma(b \rightarrow X_s \ell^+ \ell^-)}{d\hat{s} dz} \text{sgn}(z) dz = \left(\frac{\alpha_{\text{em}}}{4\pi}\right)^2 \frac{G_F^2 m_{b,\text{pole}}^5 |V_{ts}^* V_{tb}|^2}{48\pi^3} (1-\hat{s})^2 \left[-3\hat{s} \text{Re}(\tilde{C}_9^{\text{eff}} \tilde{C}_{10}^{\text{eff}*}) \left(1 + \frac{2\alpha_s}{\pi} f_{910}(\hat{s})\right) - 6 \text{Re}(\tilde{C}_7^{\text{eff}} \tilde{C}_{10}^{\text{eff}*}) \left(1 + \frac{2\alpha_s}{\pi} f_{710}(\hat{s})\right) \right]. \quad (15)$$

This result shows that only the interference terms (O_9, O_{10}) and (O_7, O_{10}) contribute to the asymmetries. The two functions $f_{710}(\hat{s})$ and $f_{910}(\hat{s})$ in Eq. (15), which incorporate the sum of virtual- and bremsstrahlung corrections to the matrix elements of O_7 , O_9 and O_{10} , are plotted in Fig. 4.1.

The main new result of this paper is encoded in the functions $f_{99}(\hat{s}, z)$, $f_{77}(\hat{s}, z)$, $f_{910}(\hat{s})$, $f_{79}(\hat{s}, z)$, and $f_{710}(\hat{s})$, which we managed to calculate analytically. We obtain (μ denotes

the renormalization scale)

$$f_{710} = -\frac{1}{18\hat{s}(1-\hat{s})^2} \left(6\hat{s}(3+9\hat{s}-2\hat{s}^2)\text{Li}_2(\hat{s}) - 12\hat{s}(1+13\hat{s}-4\hat{s}^2)\text{Li}_2(\sqrt{\hat{s}}) \right. \\ \left. + 3(1-23\hat{s}+23\hat{s}^2-\hat{s}^3)\ln(1-\hat{s}) + 6\hat{s}(13-16\hat{s}+3\hat{s}^2)\ln(1-\sqrt{\hat{s}}) \right. \\ \left. + \hat{s}(5\pi^2(1+\hat{s}) - 3(5-20\sqrt{\hat{s}}+\hat{s})(1-\sqrt{\hat{s}})^2) + 24\hat{s}(1-\hat{s})^2\ln(\mu/m_b) \right),$$

$$f_{910} = -\frac{1}{9\hat{s}(1-\hat{s})^2} \left(6\hat{s}(1+3\hat{s}-\hat{s}^2)\text{Li}_2(\hat{s}) - 12\hat{s}^2(5-2\hat{s})\text{Li}_2(\sqrt{\hat{s}}) \right. \\ \left. + 3(1-10\hat{s}+11\hat{s}^2-2\hat{s}^3)\ln(1-\hat{s}) + 6\hat{s}(5-7\hat{s}+2\hat{s}^2)\ln(1-\sqrt{\hat{s}}) \right. \\ \left. + \hat{s}(3(4\sqrt{\hat{s}}-3)(1-\sqrt{\hat{s}})^2 + \pi^2(2+\hat{s})) \right),$$

$$f_{79} = -\frac{1}{36\hat{s}(1-\hat{s})^2} \left(3\hat{s}(1+\sqrt{\hat{s}})^2 \left(3(5+z^2) - 3\sqrt{\hat{s}}(11-z^2) + 16\hat{s} \right) \text{Li}_2(\hat{s}) \right. \\ \left. + 12\hat{s}\sqrt{\hat{s}}(3+\hat{s})(1-3z^2)\text{Li}_2(\sqrt{\hat{s}}) + 3(1-\hat{s})^2(3-z^2+\hat{s}(9+z^2))\ln(1-\hat{s}) \right. \\ \left. + 3\hat{s}^2(13-15z^2-\hat{s}(5+z^2))\ln(\hat{s}) + 3\hat{s}(7+3z^2+8\hat{s}-\sqrt{\hat{s}}(17-3z^2)) \right. \\ \left. (1+\sqrt{\hat{s}})^2\ln(1-\hat{s})\ln(\hat{s}) + 6\hat{s}\sqrt{\hat{s}}(3+\hat{s})(1-3z^2)\ln(1-\sqrt{\hat{s}})\ln(\hat{s}) \right. \\ \left. - 6\hat{s}(1-\hat{s})(5z^2-\hat{s}(4-3z^2)) + \hat{s}\pi^2(7+3z^2+8\hat{s}^2-\hat{s}(19-9z^2)) \right. \\ \left. + 48\hat{s}(1-\hat{s})^2\ln(\mu/m_b) \right),$$

$$f_{77} = -\frac{1}{18(1-\hat{s})^2(1+z^2+\hat{s}(1-z^2))} \left(12\sqrt{\hat{s}}(3+6\hat{s}-\hat{s}^2)(1-3z^2)\text{Li}_2(\sqrt{\hat{s}}) \right. \\ \left. + 3(1+\sqrt{\hat{s}})^2 \left(8(1+z^2) - \sqrt{\hat{s}} \left(19-14\sqrt{\hat{s}}+15\hat{s}-8\hat{s}\sqrt{\hat{s}} \right. \right. \right. \\ \left. \left. + \left(7-\sqrt{\hat{s}}(2-\sqrt{\hat{s}})(3+8\sqrt{\hat{s}}) \right) z^2 \right) \right) \text{Li}_2(\hat{s}) + 6(1-\hat{s})^2(5+z^2+\hat{s}(1-z^2)) \\ \ln(1-\hat{s}) + 6\hat{s}(5-7z^2+\hat{s}(1-11z^2)-2\hat{s}^2(1-z^2))\ln(\hat{s}) + 3(1+\sqrt{\hat{s}})^2 \\ \left(4(1+z^2) - \sqrt{\hat{s}} \left(11-z^2 - \sqrt{\hat{s}} \left(6-7\sqrt{\hat{s}}+4\hat{s}+(2-\sqrt{\hat{s}})(3+4\sqrt{\hat{s}})z^2 \right) \right) \right) \\ \ln(1-\hat{s})\ln(\hat{s}) + 6\sqrt{\hat{s}}(3+6\hat{s}-\hat{s}^2)(1-3z^2)\ln(1-\sqrt{\hat{s}})\ln(\hat{s}) \\ \left. + 2(2\pi^2(1+z^2-3\hat{s}(1-z^2)-\hat{s}^2(1-3z^2)+\hat{s}^3(1-z^2)) + (1-\hat{s})(\hat{s}(19-68z^2) \right. \\ \left. + 4(1+z^2)-\hat{s}^2(11-16z^2))) + 48(1-\hat{s})^2(1+z^2+\hat{s}(1-z^2))\ln(\mu/m_b) \right),$$

$$\begin{aligned}
 f_{99} = & \frac{1}{18(1-\hat{s})^2(1+\hat{s}-z^2(1-\hat{s}))} \left(12\sqrt{\hat{s}}(5+12\hat{s}-\hat{s}^2)(1-3z^2)\text{Li}_2(\sqrt{\hat{s}}) - 3(1+\sqrt{\hat{s}})^2 \right. \\
 & \left. \left(8-11\sqrt{\hat{s}}+20\hat{s}-17\hat{s}\sqrt{\hat{s}}+8\hat{s}^2 - (1+\sqrt{\hat{s}}) \left(8-\sqrt{\hat{s}} \left(9-\sqrt{\hat{s}}(21-8\sqrt{\hat{s}}) \right) \right) z^2 \right) \right. \\
 & \text{Li}_2(\hat{s}) + 6\hat{s} \left(3-13z^2 + \hat{s}(9-23z^2) + 2\hat{s}^2(1+z^2) \right) \ln(\hat{s}) - 12(1-\hat{s})^2 \\
 & \left(2-z^2 + \hat{s}(1+z^2) \right) \ln(1-\hat{s}) - 3(1+\sqrt{\hat{s}})^2 \left(4-4z^2 - \sqrt{\hat{s}}(3+7z^2) + 12\hat{s}(1-z^2) \right. \\
 & \left. - \hat{s}\sqrt{\hat{s}}(9+5z^2) + 4\hat{s}^2(1+z^2) \right) \ln(1-\hat{s}) \ln(\hat{s}) + 6\sqrt{\hat{s}}(5+12\hat{s}-\hat{s}^2)(1-3z^2) \ln(\hat{s}) \\
 & \ln(1-\sqrt{\hat{s}}) + 3(1-\hat{s}) \left(5-5z^2 + \hat{s}(28-66z^2) - \hat{s}^2(5-3z^2) \right) \\
 & \left. - 2\pi^2 \left(2-2z^2 + 5\hat{s}(1-3z^2) - \hat{s}^2(1+9z^2) + 2\hat{s}^3(1+z^2) \right) \right).
 \end{aligned}$$

In the following three sections, we discuss the technical issues needed to derive the functions $f_{99}(\hat{s}, z)$, $f_{77}(\hat{s}, z)$, $f_{910}(\hat{s})$, $f_{79}(\hat{s}, z)$ and $f_{710}(\hat{s})$. In Section 5 we discuss the regularization of infrared- and collinear singularities at the level of the matrix elements (or matrix elements squared). In Section 6 we first derive a formula for the fully differential decay width in the rest frame of the lepton pair, which for us was crucial in order to derive *analytical results* for the functions f . Using this formula, we derive the phase space expressions for the double differential decay width. Finally, in Section 7 we present some tricks, which allow us to drastically simplify the calculation of the gluon bremsstrahlung process. These tricks are based on the *universal structure of infrared- and collinear singularities*.

5 Regularization of infrared- and collinear singularities

As mentioned above, the virtual corrections to the matrix elements of the operators O_7 , O_9 and O_{10} , shown in Figs. 5.1b) and 5.2b), suffer from infrared- and collinear singularities. According to the KNL theorem, these singularities cancel when taking into account the corresponding bremsstrahlung corrections shown in Figs. 5.1c) and 5.2c). As these cancellations only happen at the level of the decay rate, both virtual- and bremsstrahlung corrections have to be regularized. As in our previous works on $d\Gamma/d\hat{s}$, we use for the derivation of the double differential decay width a non-vanishing strange quark mass as a regulator of the collinear singularities and dimensional regularization ($d = 4 - 2\epsilon$) for the infrared singularities. In the usual derivation of the decay width $d\Gamma/d\hat{s}$ one integrates out the lepton variables in the first step, after inserting a factor 1 in the form of Eq. (11). It turns out that in the Dirac trace of the lepton tensor $L_{\mu\nu}$ the terms with an odd number of γ_5 matrices become zero after this integration. Furthermore, as the integrated lepton tensor is symmetric in μ and ν , it follows that also in the hadron tensor (which is contracted with the lepton tensor over the indices μ and ν) only traces with an even number of γ_5 matrices survive. Therefore, the γ_5 problems which usually appear in d -dimensions,

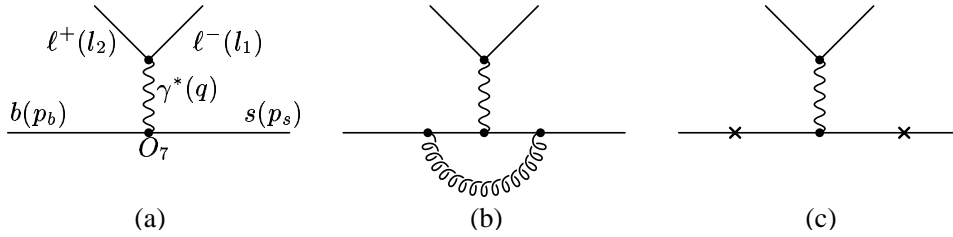


Figure 5.1: Feynman diagrams associated with the operator O_7 . (a) shows the lowest order diagram, (b) and (c) show virtual- and bremsstrahlung corrections, respectively. The cross denotes the possible emission of the gluon.

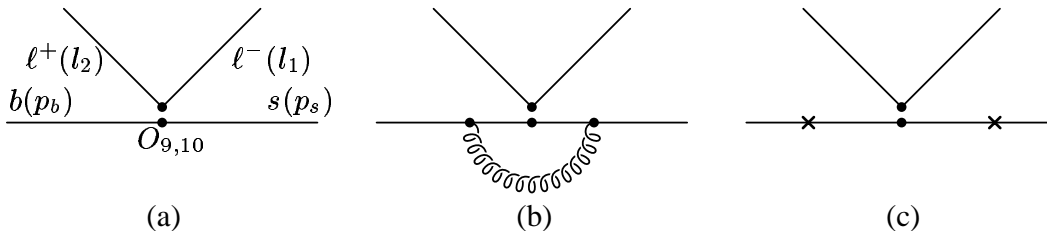


Figure 5.2: Feynman diagrams associated with the operators O_9 and O_{10} . (a) shows the lowest order diagrams, (b) and (c) show virtual- and bremsstrahlung corrections, respectively.

can be avoided when calculating $d\Gamma/d\hat{s}$. These statements are no longer true if one aims to calculate the double differential decay width, which means that traces with an odd number of γ_5 matrices are unavoidable.

In our derivation of the virtual corrections to the double differential decays width, we calculated the loop corrections to the matrix elements as in our previous papers [42, 43], viz. using anticommuting γ_5 and letting propagate all d polarizations of the virtual gluon in the loop. Using $(d - 1)$ -dimensional rotation invariance, the momenta of the external particles can be assumed to lie in four dimensions. Therefore, to proceed from the regulated matrix elements to the double differential decay width, we do the remaining Dirac algebra in $d = 4$ dimensions. The subsequent phase space integrals are, however, treated in d dimensions.

We now turn to the bremsstrahlung corrections. When calculating the squares of the matrix elements associated with O_7 , O_9 , O_{10} (and interference terms) some care has to be taken in order to do the infrared regularization consistently. As in the virtual corrections all d gluon polarizations were allowed to propagate, we have to emit all $d - 2$ transverse polarizations in the bremsstrahlung process. As shown in Refs. [53, 54], this can be implemented by doing the Dirac algebra in $d = 4$ by summing the contributions from the emission

of a gluon with the 2 possible transverse directions in four dimensions (characterized by normal 4-dimensional polarization vectors), and from the emission of the $(d-4)$ transverse polarizations showing in the $d-4$ extra dimensions. Each of the latter couples to the quarks (which remain in four dimensions) with a γ_5 . The subsequent phase space integrations are again worked out in d -dimensions.

6 Phase space

6.1 Fully differential phase space formula for lepton pair at rest

Starting from the well-known expression for the differential decay width for the process $b \rightarrow s\ell^+\ell^-$ and inserting a unit factor according to Eq. (11), one obtains

$$d\Gamma^{\text{b-rest}}(b \rightarrow s\ell^+\ell^-) = \frac{|\overline{M}|^2}{2m_b} D\Phi^{\text{b-rest}}, \quad (16)$$

where $|\overline{M}|^2$ is the squared matrix element, summed and averaged over spins and colors of the particles in the final- and initial state, respectively. Note that in our application $|\overline{M}|^2$ depends only on scalar products of four-vectors. $D\Phi^{\text{b-rest}}$ is the phase space factor which can be written as

$$\begin{aligned} D\Phi^{\text{b-rest}} &= D\Phi_1^{\text{b-rest}} D\Phi_2^{\text{b-rest}} ds, \\ D\Phi_1^{\text{b-rest}} &= (2\pi)^d \frac{d^{d-1}q}{2q^0} \frac{d^{d-1}p_s}{(2\pi)^{d-1}2p_s^0} \delta^d(p_b - p_s - q), \\ D\Phi_2^{\text{b-rest}} &= \frac{d^{d-1}l_1}{(2\pi)^{d-1}2l_1^0} \frac{d^{d-1}l_2}{(2\pi)^{d-1}2l_2^0} \delta^d(q - l_1 - l_2). \end{aligned} \quad (17)$$

p_b, p_s, l_1, l_2 denote the four-momenta of the b -quark, the s -quark, the negatively and positively charged leptons, respectively, while $q = (l_1 + l_2)$, $q^0 = \sqrt{\vec{q}^2 + s}$ and $s = q^2$. Note that Eqs. (16) and (17) generate the correct distributions of the decay products for a b -quark decay at rest or with fixed velocity.

Our main goal is to calculate the double differential decay width $\frac{d^2\Gamma(b \rightarrow X_s \ell^+ \ell^-)}{d\hat{s}dz}$, where $\hat{s} = s/m_b^2$ and $z = \cos\theta$ with θ being the angle between the momenta of the b -quark and the ℓ^+ , measured in the rest frame of the $(\ell^+\ell^-)$ -pair. For this purpose it is convenient to first derive a fully differential phase space formula in the rest frame of the lepton pair. In the following, unprimed momenta refer to the rest frame of the b -quark and primed ones to the corresponding momenta in the rest frame of the lepton pair. While in the rest frame of the b -quark the value of the vector $\vec{q} = \vec{l}_1 + \vec{l}_2$ varies from event to event, it is \vec{p}'_b which varies from event to event in the rest frame of the lepton pair. The relation between \vec{q} and \vec{p}'_b can be found from the equation

$$p'_b = \Lambda_q p_b; \quad p_b = (m_b, \vec{0}), \quad (18)$$

where Λ_q is the Lorentz boost, which transforms the vector \vec{q} to rest. We obtain

$$\vec{p}'_b = -\frac{m_b}{\sqrt{s}}\vec{q} \quad (\text{and } p'_b{}^0 = \frac{m_b}{\sqrt{s}}q^0). \quad (19)$$

In the expression for the decay width this relation is most easily implemented by multiplying Eq. (16) with a factor 1 in the form

$$1 = \int d^{d-1}p'_b \delta^{d-1}\left(\vec{p}'_b + \frac{m_b}{\sqrt{s}}\vec{q}\right). \quad (20)$$

We anticipate that the integration over the variable \vec{q} will finally perform the variable transformation $\vec{q} \leftrightarrow \vec{p}'_b$. However, before doing this step we express all the unprimed momenta in the matrix element squared and in the delta functions with their primed counterparts, e.g. $l_2 = \Lambda_q^{-1}l'_2$, etc. Note that due to Lorentz invariance of $|\overline{M}|^2$, this quantity is independent of Λ_q^{-1} , and therefore independent of \vec{q} . The same is also true for the measure factors of the final state particles and for the d -dimensional δ -functions in Eq. (17). The only remaining \vec{q} dependence is contained in the term

$$\frac{d^{d-1}q}{2q^0} \delta^{d-1}\left(\vec{p}'_b + \frac{m_b}{\sqrt{s}}\vec{q}\right).$$

Integrating this Eq. over \vec{q} , one obtains

$$\int \frac{d^{d-1}q}{2q^0} \delta^{d-1}\left(\vec{p}'_b + \frac{m_b}{\sqrt{s}}\vec{q}\right) = \left(\frac{\sqrt{s}}{m_b}\right)^{d-2} \frac{1}{2p'_b{}^0}.$$

To summarize: The expression for the fully differential decay width $d\Gamma(b \rightarrow s\ell^+\ell^-)$ in the *rest frame of the lepton pair* can be written as

$$d\Gamma(b \rightarrow s\ell^+\ell^-) = \frac{|\overline{M}|^2}{2m_b} D\Phi, \quad (21)$$

with

$$\begin{aligned} D\Phi &= D\Phi_1 D\Phi_2 ds, \\ D\Phi_1 &= (2\pi)^d \left(\frac{\sqrt{s}}{m_b}\right)^{d-2} \frac{d^{d-1}p_b}{2p_b^0} \frac{d^{d-1}p_s}{(2\pi)^{d-1}2p_s^0} \delta^d(p_b - p_s - q), \\ D\Phi_2 &= \frac{d^{d-1}l_1}{(2\pi)^{d-1}2l_1^0} \frac{d^{d-1}l_2}{(2\pi)^{d-1}2l_2^0} \delta^d(q - l_1 - l_2). \end{aligned} \quad (22)$$

As all momenta refer to the rest frame of the lepton pair, we omitted the primes in Eqs. (21) and (22).

For the case of real gluon emission, $b \rightarrow sg\ell^+\ell^-$, the expression for the fully differential decay width in the rest frame of the $(\ell^+\ell^-)$ -pair can be derived in an analogous way. We

obtain

$$d\Gamma(b \rightarrow sg\ell^+\ell^-) = \frac{|\overline{M}|^2}{2m_b} D\Phi^{\text{brems}},$$

$$D\Phi^{\text{brems}} = D\Phi_1^{\text{brems}} D\Phi_2 ds, \quad (23)$$

$$D\Phi_1^{\text{brems}} = (2\pi)^d \left(\frac{\sqrt{s}}{m_b} \right)^{d-2} \frac{d^{d-1}p_b}{2p_b^0} \frac{d^{d-1}p_s}{(2\pi)^{d-1}2p_s^0} \frac{d^{d-1}r}{(2\pi)^{d-1}2r^0} \delta^d(p_b - r - p_s - q). \quad (24)$$

$D\Phi_2$ is the same as in Eq. (22) and r is the four-momentum of the gluon.

6.2 Phase space integrations

In this subsection we present the results for the phase space formulas for the double differential decay width where we integrate over the variables constrained by the δ -functions and over the variables on which $|\overline{M}|^2$ does not depend.

To get the desired expression for the bremsstrahlung process, we start from Eq. (23) and integrate over \vec{l}_1 and \vec{p}_s by making use of the spacial parts of the two d -dimensional δ -functions. Using then rotation invariance in $(d-1)$ dimensions, we can assume that in $|\overline{M}|^2$ the ‘‘three-momenta’’ of the remaining particles have the form

$$\begin{aligned} \vec{p}_b &= (|\vec{p}_b|, 0, 0; \dots), \\ \vec{l}_2 &= (E_2 \cos \theta, E_2 \sin \theta, 0; \dots), \\ \vec{r} &= (E_r \cos \theta_1, E_r \sin \theta_1 \cos \theta_2, E_r \sin \theta_1 \sin \theta_2; \dots), \end{aligned} \quad (25)$$

where the dots symbolize the components of extra space dimensions, which are all zero. E_2 and E_r are the energies of the massless positively charged lepton and the gluon, respectively. Making use of the remaining two one-dimensional δ -functions, we can express E_2 and θ_1 in terms of the other variables as

$$E_2 = \frac{\sqrt{s}}{2} \quad ; \quad \cos \theta_1 = \frac{2E_b\sqrt{s} - 2E_r\sqrt{s} + 2E_rE_b - s - m_b^2 + m_s^2}{2E_r|\vec{p}_b|}. \quad (26)$$

E_b is the energy of the b -quark and \sqrt{s} is the invariant mass of the lepton pair. After integration over the additional polar angles of \vec{p}_b , \vec{l}_2 and \vec{r} , on which $|\overline{M}|^2$ does not depend, we obtain (using $z = \cos \theta$, $z_2 = \cos \theta_2$, $\hat{s} = s/m_b^2 = q^2/m_b^2$, $d = 4 - 2\epsilon$)

$$\begin{aligned} \frac{d^2\Gamma(b \rightarrow sg\ell^+\ell^-)}{d\hat{s} dz} &= \left(\frac{\mu^2 e^\gamma}{4\pi} \right)^{3\epsilon} \frac{m_b^{1-2\epsilon} \hat{s}^{1-2\epsilon}}{(2\pi)^{3d-4} 2^{7-4\epsilon}} \Omega_{d-1} \Omega_{d-2} \Omega_{d-3} \times \\ &\int |\overline{M}|^2 W^{-\epsilon} (1-z^2)^{-\epsilon} (1-z_2^2)^{-1/2-\epsilon} dz_2 dE_r dE_b, \end{aligned} \quad (27)$$

where W reads

$$W = 4(E_r - E_r^{\min})(E_r^{\max} - E_r)(m_b^2 - 2\sqrt{s}E_b + s).$$

The three factors Ω stem from the integration over the polar angles on which $|\overline{M}|^2$ does not depend (explicitly, $\Omega_d = 2\pi^{d/2}/\Gamma(d/2)$). The boundaries of the integration variables are

$$\begin{aligned} E_r^{\min} = \frac{m_b^2 + s - 2E_b\sqrt{s} - m_s^2}{2(E_b + |\vec{p}_b| - \sqrt{s})} \leq E_r \leq \frac{m_b^2 + s - 2E_b\sqrt{s} - m_s^2}{2(E_b - |\vec{p}_b| - \sqrt{s})} = E_r^{\max}, \\ m_b \leq E_b \leq \frac{m_b^2 + s - m_s^2}{2\sqrt{s}}, \\ -1 \leq z_2 \leq 1. \end{aligned} \quad (28)$$

To get the corresponding expression for the double differential decay width for the process $b \rightarrow s\ell^+\ell^-$, we start from Eq. (21) and integrate over \vec{l}_1 and \vec{p}_s by making use of the spacial parts of the two d -dimensional δ -functions. Using rotation invariance, the three momenta of the remaining particles (b -quark and ℓ^+) can be assumed to have the form as in Eq. (25). The remaining two one-dimensional δ -functions can be used to express the energy E_b of the b -quark and the energy E_2 of ℓ^+ in terms of s . Explicitly, we obtain

$$E_b = \frac{m_b^2 + s - m_s^2}{2\sqrt{s}} \quad ; \quad E_2 = \frac{\sqrt{s}}{2}.$$

After integration over the angles of \vec{p}_b and \vec{l}_2 , on which $|\overline{M}|^2$ does not depend, we obtain

$$\frac{d^2\Gamma(b \rightarrow s\ell^+\ell^-)}{d\hat{s}dz} = \left(\frac{\mu^2 e^\gamma}{4\pi}\right)^{2\epsilon} \frac{m_b^{-2\epsilon} \hat{s}^{1/2-2\epsilon}}{(2\pi)^{2d-3} 2^{6-2\epsilon}} \Omega_{d-1} \Omega_{d-2} |\overline{M}|^2 (1-z^2)^{-\epsilon} |\vec{p}_b|^{d-3}. \quad (29)$$

7 Calculation of the sum of virtual- and bremsstrahlung corrections associated with O_7 , O_9 and O_{10}

In this section, we explain in some detail the tricks which allow to construct the functions f_{99} and f_{910} in Eq. (12) in a simplified manner. The other functions f_{77} , f_{79} and f_{710} can be obtained in an analogous way. We use the notations

$$\Gamma_{ij}(\hat{s}, z) = \frac{d^2\Gamma_{ij}}{d\hat{s}dz} \quad \text{and} \quad \Gamma_{ij}(\hat{s}) = \frac{d\Gamma_{ij}}{d\hat{s}} \quad (i \leq j)$$

for the contributions of the pair $(\tilde{O}_i, \tilde{O}_j)$ to the double differential decay width and to the invariant mass distribution, respectively. To make explicit the lowest order piece $(^0)$, the virtual- (v) and bremsstrahlung (b) corrections, we write

$$\begin{aligned} \Gamma_{ij}(\hat{s}, z) &= \Gamma_{ij}^0(\hat{s}, z) + \Gamma_{ij}^v(\hat{s}, z) + \Gamma_{ij}^b(\hat{s}, z), \\ \Gamma_{ij}(\hat{s}) &= \Gamma_{ij}^0(\hat{s}) + \Gamma_{ij}^v(\hat{s}) + \Gamma_{ij}^b(\hat{s}). \end{aligned} \quad (30)$$

As mentioned in Section 3, the virtual corrections to the matrix element were written in our earlier papers as multiples of tree-level matrix elements, explicitly

$$\begin{aligned}
 \langle sl^+ \ell^- | \tilde{O}_7 | b \rangle_{\text{virt}} &= -\frac{\alpha_s}{4\pi} F_7^{(7)} \langle \tilde{O}_7 \rangle_{\text{tree}} - \frac{\alpha_s}{4\pi} F_7^{(9)} \langle \tilde{O}_9 \rangle_{\text{tree}}, \\
 \langle sl^+ \ell^- | \tilde{O}_9 | b \rangle_{\text{virt}} &= -\frac{\alpha_s}{4\pi} F_9^{(7)} \langle \tilde{O}_7 \rangle_{\text{tree}} - \frac{\alpha_s}{4\pi} F_9^{(9)} \langle \tilde{O}_9 \rangle_{\text{tree}}, \\
 \langle sl^+ \ell^- | \tilde{O}_{10} | b \rangle_{\text{virt}} &= -\frac{\alpha_s}{4\pi} F_9^{(7)} \langle \tilde{O}_{7,5} \rangle_{\text{tree}} - \frac{\alpha_s}{4\pi} F_9^{(9)} \langle \tilde{O}_{10} \rangle_{\text{tree}}.
 \end{aligned} \tag{31}$$

Note that $\langle \tilde{O}_{7,5} \rangle_{\text{tree}}$ is obtained from $\langle \tilde{O}_7 \rangle_{\text{tree}}$ by replacing the lepton vector current by the corresponding axial vector current. As the explicit form of the (infrared singular) functions $F_9^{(9)}$ and $F_7^{(7)}$ is not needed in the following construction, we only list $F_9^{(7)}$ and $F_7^{(9)}$:

$$F_9^{(7)}(\hat{s}) = \frac{2}{3} \ln(1 - \hat{s}); \quad F_7^{(9)}(\hat{s}) = \frac{16}{3\hat{s}} \ln(1 - \hat{s}). \tag{32}$$

7.1 Construction of $f_{99}(\hat{s}, z)$

The virtual corrections to the double- or single differential decay width are now readily obtained. For $\Gamma_{99}^v(\hat{s}, z)$ and $\Gamma_{99}^v(\hat{s})$ we get

$$\begin{aligned}
 \Gamma_{99}^v(\hat{s}, z) &= -\frac{2\alpha_s}{4\pi} F_9^{(9)}(\hat{s}) \Gamma_{99}^0(\hat{s}, z) - \frac{\alpha_s}{4\pi} F_9^{(7)}(\hat{s}) \Gamma_{79}^0(\hat{s}, z), \\
 \Gamma_{99}^v(\hat{s}) &= -\frac{2\alpha_s}{4\pi} F_9^{(9)}(\hat{s}) \Gamma_{99}^0(\hat{s}) - \frac{\alpha_s}{4\pi} F_9^{(7)}(\hat{s}) \Gamma_{79}^0(\hat{s}).
 \end{aligned} \tag{33}$$

We note that $\Gamma_{99}^0(\hat{s}, z)$ and $\Gamma_{99}^0(\hat{s})$ are understood to be evaluated in d -dimensions as described in Sections 5 and 6, because the function $F_9^{(9)}$ is infrared singular.

We now turn to the crucial point of our construction, which drastically simplifies the calculation of the bremsstrahlung corrections. We form the combination

$$\hat{\Gamma}_{99}^v(\hat{s}, z) = \Gamma_{99}^v(\hat{s}, z) - \frac{\Gamma_{99}^0(\hat{s}, z)}{\Gamma_{99}^0(\hat{s})} \Gamma_{99}^v(\hat{s}), \tag{34}$$

in which the contributions proportional to the singular function $F_9^{(9)}$ drop out completely. $\hat{\Gamma}_{99}^v(\hat{s}, z)$ is therefore finite. Explicitly, we get

$$\hat{\Gamma}_{99}^v(\hat{s}, z) = \frac{\alpha_s}{4\pi} F_9^{(7)}(\hat{s}) \frac{m_b^5 \alpha_{\text{em}}^2 G_F^2 |V_{tb} V_{ts}^*|^2 \tilde{C}_9^2 (1 - \hat{s})^3 (1 - 3z^2)}{256\pi^5 (1 + 2\hat{s})}. \tag{35}$$

We now form the analogous combination for the bremsstrahlung corrections, viz.

$$\hat{\Gamma}_{99}^b(\hat{s}, z) = \Gamma_{99}^b(\hat{s}, z) - \frac{\Gamma_{99}^0(\hat{s}, z)}{\Gamma_{99}^0(\hat{s})} \Gamma_{99}^b(\hat{s}). \tag{36}$$

It follows from the Kinoshita-Lee-Neuenberg (KLN) theorem that $\hat{\Gamma}_{99}^b(\hat{s}, z)$ must also be finite. Using Eqs. (34) and (36), one can write the sum of the virtual- and bremsstrahlung corrections to the double differential decay width in the form

$$\Gamma_{99}^v(\hat{s}, z) + \Gamma_{99}^b(\hat{s}, z) = \hat{\Gamma}_{99}^v(\hat{s}, z) + \hat{\Gamma}_{99}^b(\hat{s}, z) + \frac{\Gamma_{99}^0(\hat{s}, z)}{\Gamma_{99}^0(\hat{s})} (\Gamma_{99}^v(\hat{s}) + \Gamma_{99}^b(\hat{s})) . \quad (37)$$

$\hat{\Gamma}_{99}^v(\hat{s}, z)$ on the r.h.s of Eq. (37) is given in Eq. (35). $(\Gamma_{99}^v(\hat{s}) + \Gamma_{99}^b(\hat{s}))$ is also known, viz.

$$\Gamma_{99}^v(\hat{s}) + \Gamma_{99}^b(\hat{s}) = \Gamma_{99}^0(\hat{s}) \left(1 + \frac{2\alpha_s}{\pi} \omega_{99}(\hat{s}) \right) , \quad (38)$$

where $\omega_{99}(\hat{s})$ is given in Refs. [42, 43] (see also Eq. (48)). $\Gamma_{99}^0(\hat{s}, z)$ which in Eq. (37) is only needed in $d = 4$ dimensions, reads

$$\Gamma_{99}^0(\hat{s}, z) = \frac{m_b^5 \alpha_{\text{em}}^2 G_F^2 |V_{tb} V_{ts}^*|^2 \tilde{C}_9^2}{1024\pi^5} (1 - \hat{s})^2 [(1 - z^2) + \hat{s}(1 + z^2)] . \quad (39)$$

This implies that the sum of virtual- and bremsstrahlung corrections to the double differential decay width, and hence the function $f_{99}(\hat{s}, z)$ in Eq. (7), is easily obtained once the finite combination $\hat{\Gamma}_{99}^b(\hat{s}, z)$ in Eq. (36) is known.

7.2 Construction of $f_{910}(\hat{s})$

As $\Gamma_{910}^0(\hat{s})$ turns out to be zero, one cannot take the combination analogous to Eq. (34). Instead, we use the combination

$$\hat{\Gamma}_{910}^v(\hat{s}, z) = \Gamma_{910}^v(\hat{s}, z) - \frac{\Gamma_{910}^0(\hat{s}, z)}{\Gamma_{99}^0(\hat{s})} \Gamma_{99}^v(\hat{s}) . \quad (40)$$

Again, the part proportional to the singular function $F_9^{(9)}$ drops out and $\hat{\Gamma}_{910}^v(\hat{s}, z)$ is finite. Explicitly, we find

$$\hat{\Gamma}_{910}^v(\hat{s}, z) = \frac{2\alpha_s}{4\pi} F_9^{(7)}(\hat{s}) \frac{m_b^5 \alpha_{\text{em}}^2 G_F^2 |V_{tb} V_{ts}^*|^2 \tilde{C}_9 \tilde{C}_{10} (1 - \hat{s})^3 z}{128\pi^5 (1 + 2\hat{s})} . \quad (41)$$

The analogous combination for the bremsstrahlung corrections, viz.

$$\hat{\Gamma}_{910}^b(\hat{s}, z) = \Gamma_{910}^b(\hat{s}, z) - \frac{\Gamma_{910}^0(\hat{s}, z)}{\Gamma_{99}^0(\hat{s})} \Gamma_{99}^b(\hat{s}) \quad (42)$$

is also finite. From Eqs. (40) and (42) one gets

$$\Gamma_{910}^v(\hat{s}, z) + \Gamma_{910}^b(\hat{s}, z) = \hat{\Gamma}_{910}^v(\hat{s}, z) + \hat{\Gamma}_{910}^b(\hat{s}, z) + \frac{\Gamma_{910}^0(\hat{s}, z)}{\Gamma_{99}^0(\hat{s})} (\Gamma_{99}^v(\hat{s}) + \Gamma_{99}^b(\hat{s})) . \quad (43)$$

$\hat{\Gamma}_{910}^v(\hat{s}, z)$ and $(\Gamma_{99}^v(\hat{s}) + \Gamma_{99}^b(\hat{s}))$ are given in Eqs. (41) and (38), respectively. $\Gamma_{910}^0(\hat{s}, z)$ which is only needed in $d = 4$ dimensions in Eq. (43), reads

$$\Gamma_{910}^0(\hat{s}, z) = -\frac{m_b^5 \alpha_{\text{em}}^2 G_F^2 |V_{tb} V_{ts}^*|^2 \tilde{C}_9 \tilde{C}_{10}}{256\pi^5} (1 - \hat{s})^2 \hat{s} z. \quad (44)$$

This implies that the function $f_{910}(\hat{s})$ is easily obtained, once the finite combination $\hat{\Gamma}_{910}^b(\hat{s}, z)$ defined in Eq. (42) is known.

To obtain the functions $f_{77}(\hat{s}, z)$, $f_{79}(\hat{s}, z)$ and $f_{710}(\hat{s})$, one can proceed in a similar way. Forming suitable combinations, the hardest part of the calculation of these functions boils down to the evaluation of a finite combination of bremsstrahlung terms.

A remark concerning to the evaluation of the finite bremsstrahlung combinations is in order: We carefully investigated all five combinations (needed to construct the five f -functions) in $d = 4 - 2\epsilon$ dimensions, as in principle terms of order ϵ^1 from the phase space factors could multiply divergent integrals and in this way generate finite terms. We found, however, that this case does not occur in our actual calculations: Expanding all combinations up to order ϵ (or even ϵ^2) before doing the phase space integrations over the variables E_r and E_b (see Section 6), we found that all the occurring integrals are finite. This means, that it is correct to evaluate the finite combinations in $d = 4$ dimensions.

8 Phenomenological analysis

In this section, we mainly investigate the impact of the NNLL QCD corrections on the forward-backward asymmetries defined in Eqs. (13) and (14) in the standard model. We restrict ourselves to the range of $\hat{s} = s/m_b^2$ below 0.25, i.e., to the region below the J/ψ threshold. As our main emphasis is to investigate the improvements in the perturbative part, in particular the reduction of the renormalization scale dependence, we do not include non-perturbative corrections, although in this \hat{s} -region they are known to a large extent [28, 31, 32, 33, 34, 35]. In our analysis, we use the following fixed values for the input parameters: $m_b^{\text{pole}} = 4.8$ GeV, $\alpha_{\text{em}} = 1/133$, $\text{BR}_{\text{sl}} = 0.104$, $m_t^{\text{pole}} = 174$ GeV, $\alpha_s(m_Z) = 0.119$ and $|V_{tb} V_{ts}^*|/|V_{cb}| = 0.976$. The values of m_c/m_b and of the renormalization scale μ are specified in the captions of the individual figures.

In Figs. 8.1 we illustrate the reduction of the renormalization scale dependence of the forward-backward asymmetries when taking into account NNLL QCD corrections. As usual, the renormalization scale is varied between 2.5 GeV and 10.0 GeV. For definiteness, we should mention that in the unnormalized forward-backward asymmetry $A_{\text{FB}}(\hat{s})$, we evaluated the denominator $\Gamma(B \rightarrow X_c e \bar{\nu}_e)$ in Eq. (14) always at $\mu = 5$ GeV¹. The results are remarkable: While the NLL asymmetries (shown by dashed lines for $\mu=2.5, 5.0$ and 10 GeV) suffered from a relatively large renormalization scale dependence, the theoretical

¹We checked that the results only marginally change when varying the scale also in the semileptonic decay width.

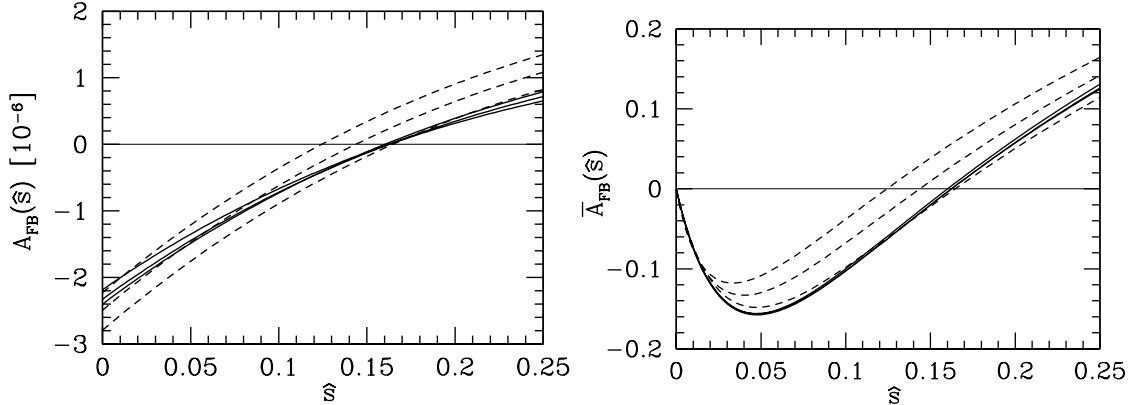


Figure 8.1: Left frame: Unnormalized forward-backward asymmetry $A_{\text{FB}}(\hat{s})$. The three solid lines show the NNLL prediction for $\mu = 2.5, 5.0, 10.0$ GeV, respectively. The corresponding curves in NLL approximation are shown by dashed lines. Right frame: Normalized forward-backward asymmetry $\bar{A}_{\text{FB}}(\hat{s})$. The lines have the same meaning as in the left frame. $m_c/m_b = 0.29$.

uncertainty related to the choice of the renormalization scale is significantly reduced at the NNLL level. For example, at $\hat{s} = 0$ we find

$$A_{\text{FB}}^{\text{NLL}}(0) = -(2.51 \pm 0.28) \times 10^{-6}; \quad A_{\text{FB}}^{\text{NNLL}}(0) = -(2.30 \pm 0.10) \times 10^{-6}. \quad (45)$$

This corresponds to a reduction of the μ -dependence from $\pm 11\%$ to $\pm 4.5\%$, which is similar to the situation found for the differential branching ratio in Ref. [43]. When looking at the position \hat{s}_0 , where the forward-backward asymmetries are zero, the reduction of the μ -dependence at NNLL is even stronger. We find (when only taking into account the error due to the μ -dependence)

$$\hat{s}_0^{\text{NLL}} = 0.144 \pm 0.020; \quad \hat{s}_0^{\text{NNLL}} = 0.162 \pm 0.002. \quad (46)$$

The parts of the NNLL corrections to the forward-backward asymmetries which are contained in the effective Wilson coefficients \tilde{C}_7^{eff} , \tilde{C}_9^{eff} and $\tilde{C}_{10}^{\text{eff}}$ (see Eqs. (9)-(10)), i.e., the virtual corrections to the matrix elements of the operators O_1 , O_2 and O_8 and the NNLL contributions to the Wilson coefficients, are known for quite some time. In Figs. 8.2 we illustrate the importance of the new contributions related to virtual- and bremsstrahlung corrections to O_7 , O_9 and O_{10} , which are encoded through the functions $f_{710}(\hat{s})$ and $f_{910}(\hat{s})$. The solid lines show the full NNLL results, while the dashed ones are obtained by switching off the functions $f_{710}(\hat{s})$ and $f_{910}(\hat{s})$ (in the case of the normalized forward-backward

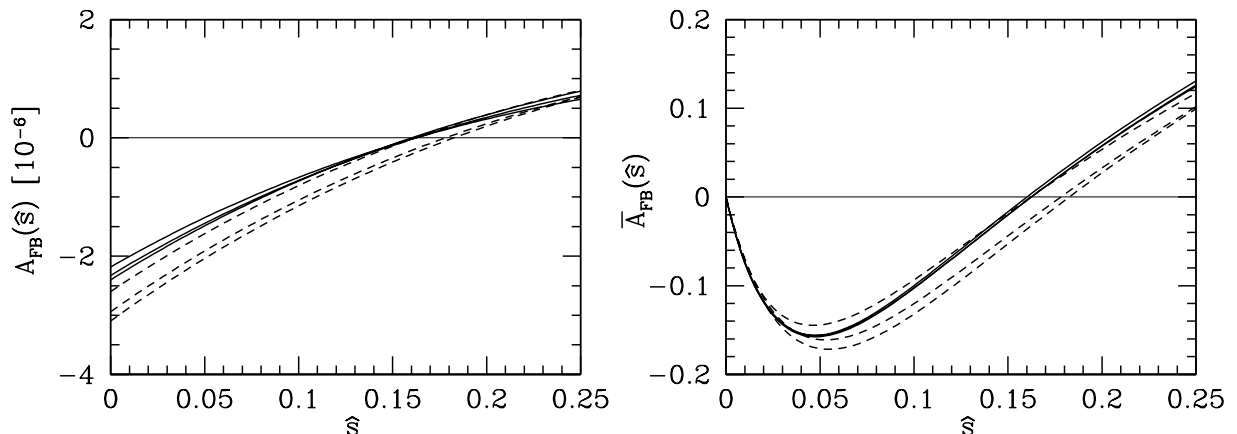


Figure 8.2: Left frame: Unnormalized forward-backward asymmetry $A_{\text{FB}}(\hat{s})$. The three solid lines show the NNLL prediction for $\mu = 2.5, 5.0, 10.0$ GeV, respectively. The dashed lines show the corresponding results when switching off the functions $f_{710}(\hat{s})$ and $f_{910}(\hat{s})$. Right frame: Normalized forward-backward asymmetry $\bar{A}_{\text{FB}}(\hat{s})$. The three solid lines show the NNLL prediction for $\mu = 2.5, 5.0, 10.0$ GeV, respectively. The dashed lines show the corresponding results when switching off the functions $f_{710}(\hat{s})$, $f_{910}(\hat{s})$, $\omega_{77}(\hat{s})$, $\omega_{99}(\hat{s})$, and $\omega_{79}(\hat{s})$. $m_c/m_b = 0.29$.

asymmetry also the functions $\omega_{99}(\hat{s})$, $\omega_{77}(\hat{s})$ and $\omega_{79}(\hat{s})$ are switched off). We find that the new contributions are crucial, in particular for the reduction of the renormalization scale dependence.

As found in Refs. [43, 44], the error on the decay width $d\Gamma(b \rightarrow X_s \ell^+ \ell^-)/d\hat{s}$ due to uncertainties in the input parameters is by far dominated by the uncertainty of the charm quark mass m_c . In principle, there are two sources for this uncertainty. First, it is unclear whether m_c in the virtual- and bremsstrahlung corrections should be interpreted as the pole mass or the $\overline{\text{MS}}$ mass (at an appropriate scale). Second, the question arises what the numerical value of m_c is, once a choice concerning the definition of m_c has been made. These issues were investigated in detail in Ref. [44] and led to the conclusion that the error due to uncertainties in the parameter m_c/m_b is conservatively estimated when using for this quantity $m_c^{\text{pole}}/m_b^{\text{pole}} = 0.29 \pm 0.04$. For a discussion of the corresponding questions for the process $B \rightarrow X_s \gamma$, we refer to [13]. Motivated by these studies, we illustrate in Figs. 8.3 the dependence of the forward-backward asymmetries on $m_c^{\text{pole}}/m_b^{\text{pole}}$. The three lines show the asymmetries for the values $m_c^{\text{pole}}/m_b^{\text{pole}} = 0.25, 0.29$ and 0.33 . We find that for most values of \hat{s} the charm quark mass dependence of the normalized forward-backward asymmetry $\bar{A}_{\text{FB}}(\hat{s})$ is smaller than the one of the unnormalized counterpart $A_{\text{FB}}(\hat{s})$. This is related to the fact that a relatively large charm quark mass dependence enters the observable $A_{\text{FB}}(\hat{s})$

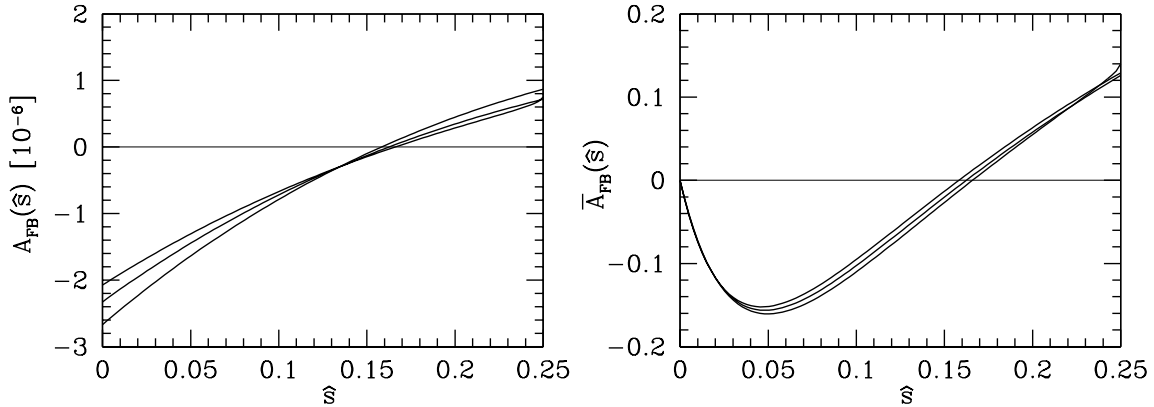


Figure 8.3: Left frame: Unnormalized forward-backward asymmetry $A_{\text{FB}}(\hat{s})$. The three lines show the NNLL prediction for $m_c^{\text{pole}}/m_b^{\text{pole}} = 0.25, 0.29, 0.33$, respectively. The renormalization scale is $\mu = 5$ GeV. Right frame: The same for the normalized forward-backward asymmetry $\bar{A}_{\text{FB}}(\hat{s})$.

through the semileptonic decay width present in the defining Eq. (14); this is not the case for the normalized version (see Eq. (13)). For \hat{s}_0 , the position where the forward-backward asymmetries vanish, we find (when taking into account only the error due to m_c/m_b)

$$\hat{s}_0^{\text{NNLL}} = 0.162 \pm 0.005. \quad (47)$$

We expect that in the future also the angular distribution in θ will become measurable. In the left frame in Fig. 8.4 we show the branching ratio differential in the variable $z = \cos \theta$ for four bins in \hat{s} , using $\mu = 5$ GeV for the renormalization scale and putting $m_c^{\text{pole}}/m_b^{\text{pole}} = 0.29$. In the right frame we show this branching ratio after integrating \hat{s} over the interval $0.05 \leq \hat{s} \leq 0.25$ for three values of the renormalization scale and putting $m_c^{\text{pole}}/m_b^{\text{pole}} = 0.29$.

9 Summary

In this paper we presented NNLL results for the double differential decay width $d\Gamma(b \rightarrow X_s \ell^+ \ell^-)/(d\hat{s} dz)$. The variable z denotes $\cos(\theta)$, where θ is the angle between the momenta of the b -quark and the ℓ^+ , measured in the rest-frame of the lepton pair. To obtain these results, genuinely new calculations were necessary for the combined virtual- and gluon bremsstrahlung corrections associated with the operators O_7 , O_9 and O_{10} . These corrections are encoded in the functions $f_{99}(\hat{s}, z)$, $f_{77}(\hat{s}, z)$, $f_{79}(\hat{s}, z)$, $f_{910}(\hat{s})$ and $f_{710}(\hat{s})$ in the general expression (12) for the double differential decay width. To obtain a NNLL

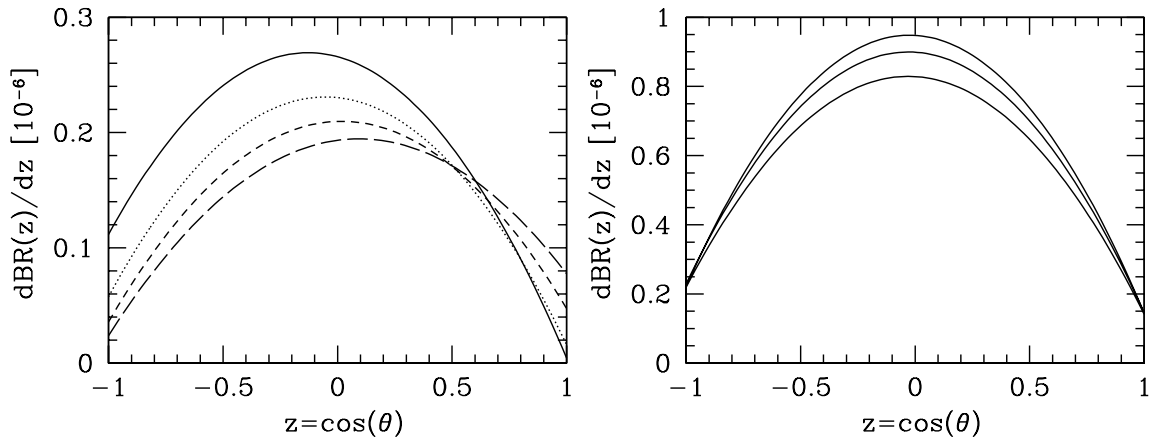


Figure 8.4: Left frame: NNLL branching ratio differential in $z = \cos \theta$ for four bins in \hat{s} . Bin 1: $0.05 \leq \hat{s} \leq 0.10$ (solid); bin 2: $0.10 \leq \hat{s} \leq 0.15$ (dotted); bin 3: $0.15 \leq \hat{s} \leq 0.20$ (short-dashed); bin 4: $0.20 \leq \hat{s} \leq 0.25$ (long-dashed). $m_c^{\text{pole}}/m_b^{\text{pole}} = 0.29$ and $\mu = 5$ GeV. Right frame: NNLL branching ratio differential in $z = \cos \theta$. \hat{s} is integrated in the interval $0.05 \leq \hat{s} \leq 0.25$. The curves correspond to $\mu = 2.5$ GeV (lowest), $\mu = 5.0$ GeV (middle) and $\mu = 10.0$ GeV (uppermost). $m_c^{\text{pole}}/m_b^{\text{pole}} = 0.29$.

prediction for this quantity, we combined these new ingredients with existing results on the NNLL Wilson coefficients and on the virtual corrections to the matrix elements of the operators O_1 , O_2 and O_8 . As the virtual QCD corrections to the matrix elements of O_1 and O_2 are only known for values of $\hat{s} \leq 0.25$, this implies that NNLL corrections to the double differential decay width are available only for values of \sqrt{s} below the J/ψ resonance. In this paper, we neglected certain bremsstrahlung contributions, which in principle contribute at NNLL precision. This omission is well motivated by the fact that the corresponding corrections have a very small impact on $d\Gamma(b \rightarrow X_s \ell^+ \ell^-)/d\hat{s}$.

From our results on the double differential decay width we derived NNLL results for the lepton forward-backward asymmetries, as these quantities are known to be very sensitive to new physics. We found that the NNLL corrections drastically reduce the renormalization scale (μ) dependence of the forward-backward asymmetries. In particular, \hat{s}_0 , the position at which the forward-backward asymmetries vanish, is essentially free of uncertainties due to the renormalization scale at NNLL precision. At NNLL precision, we found $\hat{s}_0^{\text{NNLL}} = 0.162 \pm 0.005$, where the error is dominated the uncertainty in m_c/m_b . This is to be compared with the NLL result, $\hat{s}_0^{\text{NLL}} = 0.144 \pm 0.020$, where the error is dominated by uncertainties due to the choice of μ .

When we were working out the double differential decay width, a paper on the NNLL predictions for the forward-backward asymmetries was submitted to the hep-archive [49]. As these authors used a different regularization scheme for infrared- and collinear singular-

ities and another procedure for the evaluation of the phase space integrals, the two papers provide independent calculations of the forward-backward asymmetries. Our results are in full agreement with those presented in their final version [49].

Acknowledgments: We thank Haik Asatrian and Manuel Walker for useful discussions.

A $\omega_{77}(\hat{s})$, $\omega_{99}(\hat{s})$ and $\omega_{79}(\hat{s})$

In this appendix we repeat the explicit expressions for the functions $\omega_{77}(\hat{s})$, $\omega_{99}(\hat{s})$ and $\omega_{79}(\hat{s})$ which contain the virtual- and bremsstrahlung corrections to the matrix elements associated with the operators \tilde{O}_7 , \tilde{O}_9 and \tilde{O}_{10} . For their derivation, we refer to [42, 43]. The functions read ($\text{Li}_2(x) = -\int_0^x dt/t \ln(1-t)$)

$$\begin{aligned} \omega_{77}(\hat{s}) = & -\frac{8}{3} \ln\left(\frac{\mu}{m_b}\right) - \frac{4}{3} \text{Li}_2(\hat{s}) - \frac{2}{9} \pi^2 - \frac{2}{3} \ln(\hat{s}) \ln(1-\hat{s}) \\ & - \frac{1}{3} \frac{8+\hat{s}}{2+\hat{s}} \ln(1-\hat{s}) - \frac{2}{3} \frac{\hat{s}(2-2\hat{s}-\hat{s}^2)}{(1-\hat{s})^2(2+\hat{s})} \ln(\hat{s}) - \frac{1}{18} \frac{16-11\hat{s}-17\hat{s}^2}{(2+\hat{s})(1-\hat{s})}, \end{aligned} \quad (48)$$

$$\begin{aligned} \omega_{99}(\hat{s}) = & -\frac{4}{3} \text{Li}_2(\hat{s}) - \frac{2}{3} \ln(1-\hat{s}) \ln(\hat{s}) - \frac{2}{9} \pi^2 - \frac{5+4\hat{s}}{3(1+2\hat{s})} \ln(1-\hat{s}) \\ & - \frac{2\hat{s}(1+\hat{s})(1-2\hat{s})}{3(1-\hat{s})^2(1+2\hat{s})} \ln(\hat{s}) + \frac{5+9\hat{s}-6\hat{s}^2}{6(1-\hat{s})(1+2\hat{s})}, \end{aligned} \quad (49)$$

$$\begin{aligned} \omega_{79}(\hat{s}) = & -\frac{4}{3} \ln\left(\frac{\mu}{m_b}\right) - \frac{4}{3} \text{Li}_2(\hat{s}) - \frac{2}{9} \pi^2 - \frac{2}{3} \ln(\hat{s}) \ln(1-\hat{s}) \\ & - \frac{1}{9} \frac{2+7\hat{s}}{\hat{s}} \ln(1-\hat{s}) - \frac{2}{9} \frac{\hat{s}(3-2\hat{s})}{(1-\hat{s})^2} \ln(\hat{s}) + \frac{1}{18} \frac{5-9\hat{s}}{1-\hat{s}}. \end{aligned} \quad (50)$$

B Auxiliary quantities A_i , T_9 , U_9 and W_9

The auxiliary quantities A_i , T_9 , U_9 and W_9 appearing in the effective Wilson coefficients in Eqs. (8)–(10) are the following linear combinations of the Wilson coefficients $C_i(\mu)$ [41, 23]:

$$\begin{aligned} A_7 &= \frac{4\pi}{\alpha_s(\mu)} C_7(\mu) - \frac{1}{3} C_3(\mu) - \frac{4}{9} C_4(\mu) - \frac{20}{3} C_5(\mu) - \frac{80}{9} C_6(\mu), \\ A_8 &= \frac{4\pi}{\alpha_s(\mu)} C_8(\mu) + C_3(\mu) - \frac{1}{6} C_4(\mu) + 20 C_5(\mu) - \frac{10}{3} C_6(\mu), \\ A_9 &= \frac{4\pi}{\alpha_s(\mu)} C_9(\mu) + \sum_{i=1}^6 C_i(\mu) \gamma_{i9}^{(0)} \ln\left(\frac{m_b}{\mu}\right) + \frac{4}{3} C_3(\mu) + \frac{64}{9} C_5(\mu) + \frac{64}{27} C_6(\mu), \\ A_{10} &= \frac{4\pi}{\alpha_s(\mu)} C_{10}(\mu), \\ T_9 &= \frac{4}{3} C_1(\mu) + C_2(\mu) + 6 C_3(\mu) + 60 C_5(\mu), \\ U_9 &= -\frac{7}{2} C_3(\mu) - \frac{2}{3} C_4(\mu) - 38 C_5(\mu) - \frac{32}{3} C_6(\mu), \\ W_9 &= -\frac{1}{2} C_3(\mu) - \frac{2}{3} C_4(\mu) - 8 C_5(\mu) - \frac{32}{3} C_6(\mu). \end{aligned} \quad (51)$$

The entries $\gamma_{i9}^{(0)}$ of the anomalous dimension matrix read for $i = 1, \dots, 6$: $(-32/27, -8/9, -16/9, 32/27, -112/9, 512/27)$. In the contributions which explicitly involve virtual- or brems-strahlung correction only the leading order coefficients $A_i^{(0)}$, $T_9^{(0)}$, $U_9^{(0)}$ and $W_9^{(0)}$ enter. They are given by

$$\begin{aligned}
 A_7^{(0)} &= C_7^{(1)} - \frac{1}{3} C_3^{(0)} - \frac{4}{9} C_4^{(0)} - \frac{20}{3} C_5^{(0)} - \frac{80}{9} C_6^{(0)}, \\
 A_8^{(0)} &= C_8^{(1)} + C_3^{(0)} - \frac{1}{6} C_4^{(0)} + 20 C_5^{(0)} - \frac{10}{3} C_6^{(0)}, \\
 A_9^{(0)} &= \frac{4\pi}{\alpha_s} \left(C_9^{(0)} + \frac{\alpha_s}{4\pi} C_9^{(1)} \right) + \sum_{i=1}^6 C_i^{(0)} \gamma_{i9}^{(0)} \ln\left(\frac{m_b}{\mu}\right) + \frac{4}{3} C_3^{(0)} + \frac{64}{9} C_5^{(0)} + \frac{64}{27} C_6^{(0)}, \\
 A_{10}^{(0)} &= C_{10}^{(1)}, \\
 T_9^{(0)} &= \frac{4}{3} C_1^{(0)} + C_2^{(0)} + 6 C_3^{(0)} + 60 C_5^{(0)}, \\
 U_9^{(0)} &= -\frac{7}{2} C_3^{(0)} - \frac{2}{3} C_4^{(0)} - 38 C_5^{(0)} - \frac{32}{3} C_6^{(0)}, \\
 W_9^{(0)} &= -\frac{1}{2} C_3^{(0)} - \frac{2}{3} C_4^{(0)} - 8 C_5^{(0)} - \frac{32}{3} C_6^{(0)}.
 \end{aligned} \tag{52}$$

We list the leading and next-to-leading order contributions to the quantities A_i , T_9 , U_9 and W_9 in Tab. B.1.

μ	2.5 GeV	5 GeV	10 GeV
α_s	0.267	0.215	0.180
$C_1^{(0)}$	-0.697	-0.487	-0.326
$C_2^{(0)}$	1.046	1.024	1.011
$(A_7^{(0)}, A_7^{(1)})$	(-0.360, 0.031)	(-0.321, 0.019)	(-0.287, 0.008)
$A_8^{(0)}$	-0.164	-0.148	-0.134
$(A_9^{(0)}, A_9^{(1)})$	(4.241, -0.170)	(4.129, 0.013)	(4.131, 0.155)
$(T_9^{(0)}, T_9^{(1)})$	(0.115, 0.278)	(0.374, 0.251)	(0.576, 0.231)
$(U_9^{(0)}, U_9^{(1)})$	(0.045, 0.023)	(0.032, 0.016)	(0.022, 0.011)
$(W_9^{(0)}, W_9^{(1)})$	(0.044, 0.016)	(0.032, 0.012)	(0.022, 0.009)
$(A_{10}^{(0)}, A_{10}^{(1)})$	(-4.372, 0.135)	(-4.372, 0.135)	(-4.372, 0.135)

Table B.1: Coefficients appearing in Eqs. (8)–(10) for $\mu = 2.5$ GeV, $\mu = 5$ GeV and $\mu = 10$ GeV. For $\alpha_s(\mu)$ (in the $\overline{\text{MS}}$ scheme) we used the two-loop expression with five flavors and $\alpha_s(m_Z) = 0.119$. The entries correspond to the pole top quark mass $m_t = 174$ GeV. The superscript (0) refers to lowest order quantities while the superscript (1) denotes the correction terms of order α_s , i.e. $X = X^{(0)} + X^{(1)}$ with $X = C, A, T, U, W$.

Finally, we give the function $h(z, \hat{s})$ which appears in the effective Wilson coefficients in

Eqs. (8)–(10):

$$h(z, \hat{s}) = -\frac{4}{9} \ln(z) + \frac{8}{27} + \frac{16}{9} \frac{z}{\hat{s}} - \frac{2}{9} \left(2 + \frac{4z}{\hat{s}}\right) \sqrt{\left|\frac{4z - \hat{s}}{\hat{s}}\right|} \cdot \begin{cases} 2 \arctan \sqrt{\frac{\hat{s}}{4z - \hat{s}}}, & \hat{s} < 4z \\ \ln \left(\frac{\sqrt{\hat{s}} + \sqrt{\hat{s} - 4z}}{\sqrt{\hat{s}} - \sqrt{\hat{s} - 4z}} \right) - i\pi, & \hat{s} > 4z \end{cases}. \quad (53)$$

References

- [1] R. Ammar et al. [CLEO Collaboration], *Phys. Rev. Lett.* **71** (1993) 674.
- [2] M. S. Alam et al. [CLEO Collaboration], *Phys. Rev. Lett.* **74** (1995) 2885.
- [3] R. Barate et al. [ALEPH Collaboration], *Phys. Lett. B* **429** (1998) 169.
- [4] K. Abe et al. [BELLE Collaboration], *Phys. Lett. B* **511** (2001) 151, [hep-ex/0103042](#).
- [5] B. Aubert et al. [BABAR Collaboration], [hep-ex/0207074](#), [hep-ex/0207076](#).
- [6] S. Chen et al. [CLEO Collaboration], *Phys. Rev. Lett.* **87** (2001) 251807, [hep-ex/0108032](#).
- [7] A. Ali and C. Greub, *Z. Physik C* **49** (1991) 431; *Phys. Lett. B* **259** (1991) 182; *Phys. Lett. B* **361** (1995) 146.
A.L. Kagan and M. Neubert, *Eur. Phys. J. C* **7** (1999) 5.
- [8] K. Adel and Y. P. Yao, *Phys. Rev. D* **49** (1994) 4945;
C. Greub and T. Hurth, *Phys. Rev. D* **56** (1997) 2934;
A. J. Buras, A. Kwiatkowski and N. Pott, *Nucl. Phys. B* **517** (1998) 353.
- [9] M. Ciuchini, G. Degrossi, P. Gambino and G. F. Giudice, *Nucl. Phys. B* **527** (1998) 21.
- [10] K. Chetyrkin, M. Misiak and M. Münz, *Phys. Lett. B* **400** (1997) 206; *Nucl. Phys. B* **518** (1998) 473; *Nucl. Phys. B* **520** (1998) 279.
- [11] C. Greub, T. Hurth and D. Wyler, *Phys. Rev. D* **54** (1996) 3350.
- [12] A. J. Buras, A. Czarnecki, M. Misiak, J. Urban, *Nucl. Phys. B* **611** (2001) 488, [hep-ph/0105160](#).
- [13] P. Gambino and M. Misiak, *Nucl. Phys. B* **611** (2001) 338, [hep-ph/0104034](#).

- [14] F. Borzumati and C. Greub, *Phys. Rev. D* **58** (1998) 074004; *Phys. Rev. D* **59** (1999) 057501.
- [15] H.H. Asatryan, H.M. Asatrian, G.K. Yeghiyan and G.K. Savvidy, *Int. J. Mod. Phys. A* **16** (2001) 3805.
- [16] G.M. Asatryan and A.N. Ioannisyian, *Sov. J. Nucl. Phys.* **51** (1990) 858; *Mod. Phys. Lett. A* **5** (1990) 1089.
- [17] S. Bertolini, F. Borzumati, A. Masiero and G. Ridolfi, *Nucl. Phys. B* **353** (1991) 591.
- [18] M. Ciuchini, G. Degrassi, P. Gambino and G.F. Giudice, *Nucl. Phys. B* **534** (1998) 3.
- [19] C. Bobeth, M. Misiak and J. Urban, *Nucl. Phys. B* **567** (2000) 153.
- [20] F. Borzumati, C. Greub, T. Hurth and D. Wyler, *Phys. Rev. D* **62** (2000) 075005.
- [21] H. H. Asatrian and H. M. Asatrian, *Phys. Lett. B* **460** (1999) 148.
- [22] T. Besmer, C. Greub and T. Hurth, *Nucl. Phys. B* **609** (2001) 359.
- [23] A. Ali, E. Lunghi, C. Greub, G. Hiller, *Phys. Rev. D* **66** (2002) 034002, [hep-ph/0112300](#).
- [24] K. Abe et al. [BELLE Collaboration], *Phys. Rev. Lett.* **88** (2002) 021801, [hep-ex/0109026](#).
- [25] B. Aubert et al. [BABAR Collaboration], [hep-ex/0207082](#).
- [26] J. Kaneko, [BELLE Collaboration], [hep-ex/0208029](#).
- [27] I. Bigi et al., *Phys. Rev. Lett.* **71** (1993) 496;
A. Manohar and M.B. Wise, *Phys. Rev. D* **49** (1994) 1310;
B. Blok et al., *Phys. Rev. D* **49** (1994) 3356;
T. Mannel, *Nucl. Phys. B* **413** (1994) 396.
- [28] A. F. Falk, M. Luke and M. J. Savage, *Phys. Rev. D* **49** (1994) 3367.
- [29] I. Bigi et al., *Phys. Lett. B* **293** (1992) 430, E:*Phys. Lett. B* **297** (1993) 477.
- [30] Z. Ligeti and M. B. Wise, *Phys. Rev. D* **53** (1996) 4937.
- [31] A. Ali, G. Hiller, L. T. Handoko and T. Morozumi, *Phys. Rev. D* **55** (1997) 4105.
- [32] J-W. Chen, G. Rupak and M. J. Savage, *Phys. Lett. B* **410** (1997) 285.
- [33] G. Buchalla, G. Isidori and S. J. Rey, *Nucl. Phys. B* **511** (1998) 594.

-
- [34] G. Buchalla and G. Isidori, *Nucl. Phys. B* **525** (1998) 333.
- [35] F. Krüger and L.M. Sehgal, *Phys. Lett. B* **380** (1996) 199.
- [36] A. Ali, P. Ball, L.T. Handoko, G. Hiller, *Phys. Rev. D* **61** (2000) 074024.
- [37] E. Lunghi and I. Scimemi, *Nucl. Phys. B* **574** (2000) 43.
- [38] E. Lunghi, A. Masiero, I. Scimemi and L. Silvestrini, *Nucl. Phys. B* **568** (2000) 120.
- [39] M. Misiak, *Nucl. Phys. B* **393** (1993) 23, *E:Nucl. Phys. B* **439** (1995) 461.
- [40] A. J. Buras and M. Münz, *Phys. Rev. D* **52** (1995) 186.
- [41] C. Bobeth, M. Misiak and J. Urban, *Nucl. Phys. B* **574** (2000) 291.
- [42] H. H. Asatrian, H. M. Asatrian, C. Greub and M. Walker, *Phys. Lett. B* **507** (2001) 162.
- [43] H. H. Asatrian, H. M. Asatrian, C. Greub and M. Walker, *Phys. Rev. D* **65** (2002) 074004.
- [44] H. H. Asatrian, H. M. Asatrian, C. Greub and M. Walker, *Phys. Rev. D* **66** (2002) 034009.
- [45] T. Goto et al., *Phys. Rev. D* **55** (1997) 4273; T. Goto et al., *Phys. Rev. D* **58** (1998) 094006.
- [46] A. Ali, G. Giudice and T. Mannel, *Z. Physik C* **67** (1995) 417.
- [47] H. M. Asatrian and A. N. Ioannissian, *Phys. Rev. D* **54** (1996) 5642.
- [48] H. M. Asatrian, G. K. Yeghiyan and A. N. Ioannissian, *Phys. Lett. B* **399** (1997) 303.
- [49] A. Ghinculov, T. Hurth, G. Isidori and Y.-P. Yao, [hep-ph/0208088](#).
- [50] G. Buchalla and A. J. Buras, *Nucl. Phys. B* **548** (1999) 309.
- [51] B. Grinstein, M. J. Savage and M. B. Wise, *Nucl. Phys. B* **319** (1989) 271.
- [52] Y. Nir, *Phys. Lett. B* **221** (1989) 184.
- [53] C. Greub, *Helv. Phys. Acta* **64** (1991) 61.
- [54] C. Greub, J. M. Bettens and P. Minkowski, *Helv. Phys. Acta* **64** (1991) 1277.

PART III

Fermionic NNLL corrections to $b \rightarrow s\gamma$

published in

Physical Review D 67 (2003) 114019

Fermionic NNLL corrections to $b \rightarrow s\gamma$

K. Bieri^a, C. Greub^a and M. Steinhauser^b

^a *Institut für Theoretische Physik, Universität Bern, CH-3012 Bern, Switzerland.*

^b *Institut für Theoretische Physik, Universität Hamburg, D-22761 Hamburg, Germany*

ABSTRACT

In this paper we take the first step towards a complete next-to-next-to-leading logarithmic (NNLL) calculation of the inclusive decay rate for $B \rightarrow X_s\gamma$. We consider the virtual corrections of order $\alpha_s^2 n_f$ to the matrix elements of the operators O_1 , O_2 and O_8 and evaluate the real and virtual contributions to O_7 . These corrections are expected to be numerically important. We observe a strong cancelation between the contributions from the current-current operators and O_7 and obtain, after applying naive non-abelianization, a reduction of the branching ratio of 3.9% (for $\mu = 3.0$ GeV) and an increase of 3.4% (for $\mu = 9.6$ GeV).

1 Introduction

Currently, measurements of the inclusive branching ratio $\text{BR}(B \rightarrow X_s \gamma)$ are provided by CLEO [1] (Cornell), by the B factory Belle [2] (KEK), by ALEPH [3] (CERN) and by the preliminary BABAR [4, 5] (SLAC) results, leading to a world average of [6]

$$\text{BR}(B \rightarrow X_s \gamma)_{\text{exp}} = (3.34 \pm 0.38) \times 10^{-4}. \quad (1)$$

This experimental average is in good agreement with the theoretical prediction based on the Standard Model (SM) including next-to-leading logarithmic (NLL) QCD corrections supplemented by certain classes of leading order electroweak terms [7, 8, 9, 10]. For a recent status report on inclusive rare B decays and a complete list of references on NLL calculations of $\text{BR}(B \rightarrow X_s \gamma)$ the reader is referred to [11]. In earlier analyses [12, 8, 13, 14, 15], the ratio m_c/m_b , which enters the calculation of the decay width $\Gamma(B \rightarrow X_s \gamma)$ for the first time at the NLL level, was tacitly interpreted to be the ratio of the pole quark masses. Using $m_c/m_b = 0.29 \pm 0.02$, one obtains $\text{BR}(B \rightarrow X_s \gamma)_{\text{SM}} = (3.35 \pm 0.30) \times 10^{-4}$, where the errors due to the uncertainties in the various input parameters and the estimated uncertainties due to the left-over renormalization scale dependence were added in quadrature. More recently, Gambino and Misiak [16] pointed out that the branching ratio rises to $\text{BR}(B \rightarrow X_s \gamma)_{\text{SM}} = (3.73 \pm 0.30) \times 10^{-4}$ [16] (see also [17]), if one interprets m_c/m_b to be $\bar{m}_c(\mu)/m_b = 0.22 \pm 0.04$, where $\bar{m}_c(\mu)$ is the charm quark mass in the $\overline{\text{MS}}$ -scheme, evaluated at a scale μ in the range $m_c < \mu < m_b$, and m_b is the bottom quark $1S$ mass.

Despite the current theoretical dispersion on the branching ratio, the agreement between the present experimental results and the SM is quite impressive and this has been used to derive model independent bounds on the Wilson coefficients $C_7(m_W)$ and $C_8(m_W)$ (see, for example, Ref. [18]).

Formally, the approximately 11% discrepancy in the branching ratio, stemming from the two different schemes for m_c/m_b , is a NNLL effect. As the measurements of $\text{BR}(B \rightarrow X_s \gamma)$ will become much more precise in the near future, it will become mandatory to systematically extend the theoretical predictions to NNLL precision, in order to fully exploit this process in the search for new physics.

To illustrate the complexity of such a calculation, we briefly explain the theoretical framework. Usually, one works in the effective field theory formalism of the SM, where the W boson and heavier degrees of freedom are integrated out. This results in an effective Hamiltonian in which operators up to dimension six are retained. Adopting the operator definition of [12], the relevant Hamiltonian to describe the processes $b \rightarrow s\gamma$, $b \rightarrow sg$ and $b \rightarrow s\gamma g$ reads

$$H_{\text{eff}} = -\frac{4G_F}{\sqrt{2}} \lambda_t \sum_{i=1}^8 C_i(\mu) O_i(\mu), \quad (2)$$

where G_F is the Fermi coupling constant, $\lambda_t = V_{ts}^* V_{tb}$ (with V_{ij} being elements of the Cabibbo-Kobayashi-Maskawa matrix) and $C_i(\mu)$ are the Wilson coefficient functions evaluated at the scale μ . For practical reasons it is more convenient to use instead of the original functions $C_i(\mu)$ certain linear combinations, the so-called ‘‘effective Wilson coefficients’’ $C_i^{\text{eff}}(\mu)$ introduced in [19, 12]:

$$\begin{aligned} C_i^{\text{eff}}(\mu) &= C_i(\mu), \quad (i = 1, \dots, 6), \\ C_7^{\text{eff}}(\mu) &= C_7(\mu) + \sum_{i=1}^6 y_i C_i(\mu), \\ C_8^{\text{eff}}(\mu) &= C_8(\mu) + \sum_{i=1}^6 z_i C_i(\mu), \end{aligned} \quad (3)$$

where y_i and z_i are defined in such a way that the leading order matrix elements $\langle s\gamma|O_i|b\rangle$ and $\langle sg|O_i|b\rangle$ ($i = 1, \dots, 6$) are absorbed in the leading order terms of $C_7^{\text{eff}}(\mu)$ and $C_8^{\text{eff}}(\mu)$. The explicit values of $\{y_i\}$ and $\{z_i\}$, $y = (0, 0, -\frac{1}{3}, -\frac{4}{9}, -\frac{20}{3}, -\frac{80}{9})$, $z = (0, 0, 1, -\frac{1}{6}, 20, -\frac{10}{3})$ were obtained in Ref. [12] in the $\overline{\text{MS}}$ scheme using fully anticommuting γ_5 which is also adopted in the present paper.

The operators relevant for our calculation read

$$\begin{aligned} O_1 &= (\bar{s}_L \gamma_\mu T^a c_L) (\bar{c}_L \gamma^\mu T^a b_L), \\ O_2 &= (\bar{s}_L \gamma_\mu c_L) (\bar{c}_L \gamma^\mu b_L), \\ O_4 &= (\bar{s}_L \gamma_\mu T^a b_L) \sum_q (\bar{q} \gamma^\mu T^a q), \\ O_7 &= \frac{e}{16\pi^2} \bar{m}_b(\mu) (\bar{s}_L \sigma^{\mu\nu} b_R) F_{\mu\nu}, \\ O_8 &= \frac{g_s}{16\pi^2} \bar{m}_b(\mu) (\bar{s}_L \sigma^{\mu\nu} T^a b_R) G_{\mu\nu}^a. \end{aligned} \quad (4)$$

Here $e = \sqrt{4\pi\alpha_{\text{em}}}$ and $g_s = \sqrt{4\pi\alpha_s}$ denote the electromagnetic and strong coupling constants, respectively. Furthermore, $F_{\mu\nu}$ and $G_{\mu\nu}^a$ are the corresponding field strength tensors and $L = (1 - \gamma_5)/2$ and $R = (1 + \gamma_5)/2$ stand for left- and right-handed projection operators. The factor $\bar{m}_b(\mu)$ in the definition of O_7 and O_8 denotes the bottom mass in the $\overline{\text{MS}}$ scheme.

For a complete NNLL calculation in this framework, the evaluation of three parts is necessary: (1) the computation of the matching coefficients to order α_s^2 which requires a three-loop calculation; (2) the evaluation of the anomalous dimension matrix to order α_s^3 where four-loop diagrams are involved; and (3) the calculation of the order α_s^2 QCD corrections to the matrix elements $\langle s\gamma|O_i(\mu)|b\rangle$ (μ is of order m_b) which, depending on the operator, is either a two- or three-loop calculation.

The relatively large dependence of the NLL prediction for $\text{BR}(B \rightarrow X_s \gamma)_{\text{SM}}$ on the scheme for m_c/m_b illustrates that NNLL effects, in particular those related to step (3), can be rather large.

At this point we should stress, that the issue related to the definition of m_c/m_b serves us as a motivation to initiate a NNLL calculation for $\text{BR}(B \rightarrow X_s \gamma)$. In the present paper we are working out a class of NNLL corrections (to be specified below) to step (3), which is not related to the m_c/m_b issue. However, in many other processes it is known that the kind of terms considered in this paper are the source of very important higher order corrections.

In this paper we consider those corrections of order α_s^2 to the matrix elements for $B \rightarrow X_s \gamma$ associated with the operators O_1 , O_2 , O_7 and O_8 which involve a closed fermion loop. It is needless to say, that at the same time also the matching coefficients and the anomalous dimension matrix should be improved accordingly. Motivated by the fact that the NLL corrections to the matrix elements were numerically more important than the improvements in the Wilson coefficients, we assume for the time being that this could also be the case at the NNLL level. Therefore, we only concentrate on NNLL corrections to the matrix elements. In principle also the contributions from the operators O_i ($i = 3, \dots, 6$) should be considered. However, as the corresponding Wilson coefficients are small, we neglect these contributions. Furthermore, we also neglect the NNLL bremsstrahlung corrections to the interferences (O_1, O_1) , (O_1, O_2) , (O_2, O_2) , (O_1, O_7) , (O_1, O_8) , (O_2, O_7) , (O_2, O_8) , (O_7, O_8) and (O_8, O_8) , since these terms are infrared finite for vanishing gluon energy and numerically relatively small at the NLL level [20].

The fermionic corrections we are interested in are essentially generated by inserting a one-loop fermion bubble into the gluon propagator of the lower order Feynman diagrams. For the numerical evaluation we will assume that $n_f = 5$ massless fermions are present in the fermion loop.

Once the corrections of $\mathcal{O}(\alpha_s^2 n_f)$ are available, it is suggestive to use the hypothesis of naive non-abelianization (NNA) [21] in order to estimate the complete corrections of order α_s^2 . This is based on the observation that the lowest coefficient of the QCD β function, $\beta_0 = 11 - 2n_f/3$, is quite large and thus it is expected that the replacement of n_f by $-3\beta_0/2$ may lead to a good approximation of the full order α_s^2 corrections. There are many physical observables, where NNA provides an excellent approximation to the full two-loop corrections [22, 23] like the inclusive cross section $e^+e^- \rightarrow \text{hadrons}$, the hadronic τ decay or the two-loop relation between the $\overline{\text{MS}}$ and pole quark mass. In particular, we want to mention the semileptonic decay $\Gamma(b \rightarrow c l \nu_l)$ where the deviation of the $\alpha_s^2 \beta_0$ terms from the complete α_s^2 result [24] is less than 20%. We also note that the $\mathcal{O}(\alpha_s^2 \beta_0)$ corrections to the photon energy spectrum in $B \rightarrow X_s \gamma$ (away from the endpoint) were calculated in Ref. [25].

Our presentation is organized as follows: in Section 2 we discuss the virtual corrections associated with $O_{1,2}$ and compute in Section 3 both the real and virtual corrections to O_7 . The virtual corrections to O_8 are considered in Section 4. In Section 5 we combine our findings with the existing NLL results and perform a numerical analysis showing the importance of our new terms. Finally, Section 6 contains our conclusions. In the appendix supplementary material is provided: Appendix A contains the building blocks which are useful for the practical calculations and in Appendix B detailed analytical results are

presented for the corrections to the matrix element $\langle s\gamma|O_2|b\rangle$. For completeness the results of the order α_s corrections are listed in Appendix C and intermediate results needed for the matrix element $\langle s\gamma|O_7|b\rangle$ are given in Appendix D. In Appendix E the results are provided which are necessary to discuss the branching ratio $\text{BR}(b \rightarrow X_s\gamma)_{E_\gamma \geq E_{\text{cut}}}$ where E_{cut} represents a cut-off on the photon energy.

2 Virtual corrections to $b \rightarrow s\gamma$ associated with O_1 and O_2

In this section we derive the (renormalized) order α_s^2 corrections to the matrix elements $\langle s\gamma|O_1|b\rangle$ and $\langle s\gamma|O_2|b\rangle$. Thereby only the contributions proportional to the number of fermion flavors, n_f , are taken into account. We show at the end of this section that the result for $\langle s\gamma|O_1|b\rangle$ can easily be obtained from the one for $\langle s\gamma|O_2|b\rangle$. Therefore, we concentrate in the following on the calculation of the renormalized matrix element M_2 ,

$$M_2 = \langle s\gamma|O_2|b\rangle, \quad (5)$$

which is conveniently written in the form

$$M_2 = M_2^{(0)} + M_2^{(1)} + M_2^{(2)}. \quad (6)$$

The superscript counts the factors of α_s . The leading term vanishes, i.e. $M_2^{(0)} = 0$ and the $\mathcal{O}(\alpha_s)$ calculation has been performed in [20]. In the following, we discuss the $\mathcal{O}(\alpha_s^2 n_f)$ term, $M_2^{(2)}$. In Subsection A we present the calculation and results of the dimensionally regularized three-loop diagrams, while Subsection B is devoted to the calculation of the counterterms. In Subsection C we combine the results of the three-loop results with the counterterms and derive the renormalized expression $M_2^{(2)}$.

2.1 Regularized three-loop corrections to $\langle s\gamma|O_2|b\rangle$

The three-loop diagrams contributing to $M_2^{(2)}$ can be divided into four non-vanishing classes as shown in Figs. 2.1 and 2.2¹. The sum of the diagrams in each class is gauge invariant. The contributions to the matrix element $M_2^{(2)}$ of the individual classes are denoted by $M_{2,\text{bare}}^{(2)}(1)$, $M_{2,\text{bare}}^{(2)}(2)$, $M_{2,\text{bare}}^{(2)}(3)$ and $M_{2,\text{bare}}^{(2)}(4)$, where, e.g., $M_{2,\text{bare}}^{(2)}(1)$ is

$$M_{2,\text{bare}}^{(2)}(1) = M_{2,\text{bare}}^{(2)}(1a) + M_{2,\text{bare}}^{(2)}(1b) + M_{2,\text{bare}}^{(2)}(1c). \quad (7)$$

¹In principle there are also diagrams in which the photon is emitted from the quark-loop insertion in the gluon propagator. However, these contributions vanish due to Furry's theorem.

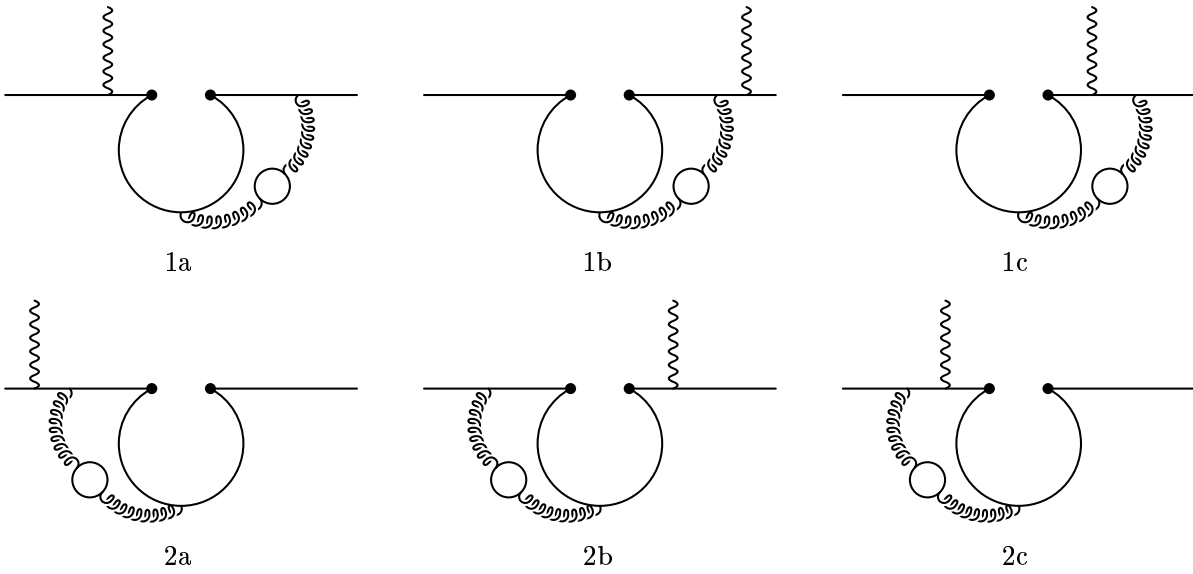


Figure 2.1: Diagrams 1a–c and 2a–c associated with the operator O_2 . The photon is represented by a wavy line and is emitted from a down-type quark in all the diagrams. The virtual gluons are represented by curly lines. The sum of the first three graphs is denoted with $M_{2,\text{bare}}^{(2)}(1)$, whereas the sum of the second three diagrams is called $M_{2,\text{bare}}^{(2)}(2)$.

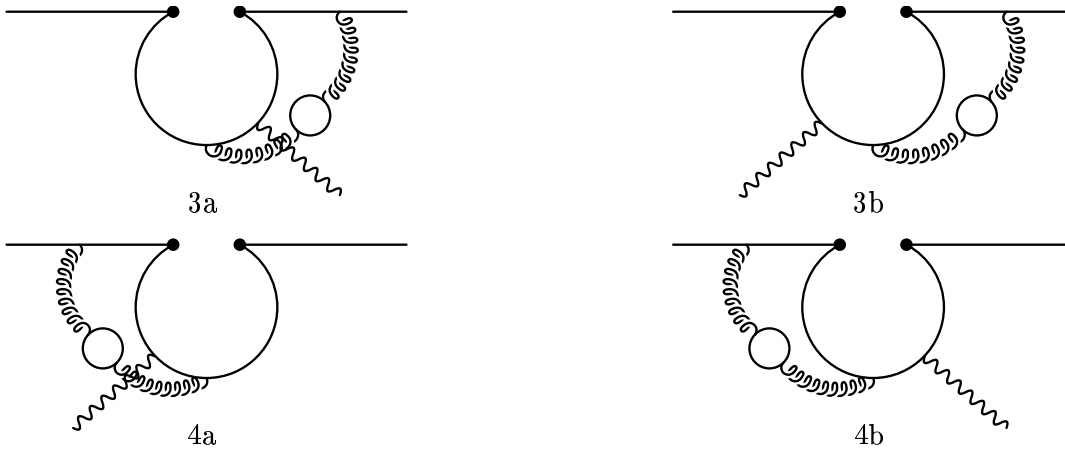


Figure 2.2: Diagrams 3a–b and 4a–b associated with the operator O_2 . The photon is represented by a wavy line and is emitted from an up-type quark in all the diagrams. The virtual gluons are represented by curly lines. The sum of the first two graphs is denoted with $M_{2,\text{bare}}^{(2)}(3)$, whereas the sum of the second two diagrams is called $M_{2,\text{bare}}^{(2)}(4)$.

For the practical calculation we essentially follow the techniques developed in [20]. To make the paper self-contained, we nevertheless present as an example the calculation of the diagram 2c in some detail.

The amplitude $M_{2,\text{bare}}^{(2)}(2c)$ is constructed with the help of the building blocks I_β and $K_{\beta\beta'}^f$,

shown in Fig. A.1 in Appendix A. The analytic expression for I_β is given in Eq. (70), while $K_{\beta\beta'}^f$ is given in Eq. (71) for an arbitrary mass m_f of the quark in the loop. This mass is retained in $K_{\beta\beta'}^f$, because it will be used as a regulator of infrared singularities in the calculation of $\langle s\gamma|O_7|b\rangle$. As $\langle s\gamma|O_2|b\rangle$ is free of infrared singularities, we can put in this section $m_f = 0$. Thus the parameter integral in Eq. (71) can be expressed in terms of Euler Γ functions. Furthermore, only the $g_{\beta\beta'}$ term has to be kept as the other building block I_β is transversal. The diagram 2c can be written as

$$\begin{aligned}
 M_{2,\text{bare}}^{(2)}(2c) &= -\frac{2i}{(4\pi)^\epsilon} \left(\frac{\alpha_s}{\pi}\right)^2 eQ_d C_F T n_f \frac{\Gamma^2(\epsilon)\Gamma^2(2-\epsilon)(1-\epsilon)}{\Gamma(4-2\epsilon)} \\
 &\quad e^{2i\pi\epsilon+3\gamma_E\epsilon} \mu^{6\epsilon} \int \frac{d^d r}{(2\pi)^d} \bar{u}(p') (r_\beta \not{r}' - r^2 \gamma_\beta) \\
 &\quad L \frac{\not{p}' + \not{r}' + m_b}{(p' + r)^2 - m_b^2 + i\delta} \not{\epsilon} \frac{\not{p} + \not{r} + m_b}{(p + r)^2 - m_b^2 + i\delta} \gamma^\beta u(p) \frac{1}{(r^2 + i\delta)^{1+\epsilon}} \\
 &\quad \int_0^1 dx x^{1-\epsilon} (1-x)^{1-\epsilon} \left(r^2 - \frac{m_c^2}{x(1-x)} + i\delta \right)^{-\epsilon}, \tag{8}
 \end{aligned}$$

where $u(p)$ and $u(p')$ are the Dirac spinors of the b and s quark, respectively, while ϵ denotes the polarization vector of the photon. C_F and T are the eigenvalue of the quadratic Casimir operator and the index of the fundamental representation of the color gauge group, respectively, with the numerical values $C_F = 4/3$ and $T = 1/2$. The Euler constant γ_E appears in Eq. (8), because we write the square of the renormalization scale in the form $\mu^2 \exp(\gamma_E)/(4\pi)$. The parameter δ (with $\delta > 0$) in the denominators of the various propagators symbolizes the “ ϵ -prescription”.

In a next step we denote the four different denominators with

$$\begin{aligned}
 D_1 &= (p' + r)^2 - m_b^2 + i\delta, \\
 D_2 &= (p + r)^2 - m_b^2 + i\delta, \\
 D_3 &= r^2 - \frac{m_c^2}{x(1-x)} + i\delta, \\
 D_4 &= r^2 + i\delta,
 \end{aligned}$$

and introduce a Feynman parametrization as follows:

$$\frac{1}{D_1 D_2 D_3^\epsilon D_4^{1+\epsilon}} = \frac{\Gamma(3+2\epsilon)}{\Gamma(\epsilon)\Gamma(1+\epsilon)} \int \frac{du dv dy w^\epsilon y^{\epsilon-1}}{(D_1 u + D_2 v + D_3 y + D_4 w)^{3+2\epsilon}}, \tag{9}$$

with $w = 1 - u - v - y$. The integration variables (u , v and y) run in the simplex S defined through $u, v, y \geq 0$ and $u + v + y \leq 1$. After the integration over r one simplifies the remaining integrals with the help of the substitutions

$$u \rightarrow (1 - u') \left(1 - \frac{1 - v'}{u'} \right), \quad v \rightarrow \frac{1 - u'}{u'} (1 - v'), \quad y \rightarrow u' y'. \tag{10}$$

The integration variable v' varies in the interval $[1-u', 1]$ whereas the other three variables x , y' and u' all vary in the interval $[0, 1]$. We tighten the notation by omitting the primes and arrive at

$$\begin{aligned}
 M_{2,\text{bare}}^{(2)}(2c) &= \frac{1}{8\pi^2} \left(\frac{\alpha_s}{\pi}\right)^2 e Q_d C_F T n_f \frac{\Gamma(\epsilon)\Gamma^2(2-\epsilon)(1-\epsilon)}{\Gamma(4-2\epsilon)} \\
 & e^{3\gamma_E\epsilon} \mu^{6\epsilon} \int_0^1 dx \int_0^1 dy \int_0^1 du \int_{1-u}^1 dv x^{1-\epsilon}(1-x)^{1-\epsilon} y^{\epsilon-1} \\
 & (1-y)^\epsilon u^{2\epsilon-1} \bar{u}(p') \left(\frac{P_1}{\hat{C}^{1+3\epsilon}} + \frac{P_2}{\hat{C}^{3\epsilon}} + \frac{P_3 \hat{C}}{\hat{C}^{3\epsilon}} \right) u(p), \quad (11)
 \end{aligned}$$

where the Dirac matrices P_1 , P_2 and P_3 are polynoms in the Feynman parameters and the expression \hat{C} is given by

$$\hat{C} = m_b^2(1-u)v + \frac{uy}{x(1-x)} m_c^2 - i\delta. \quad (12)$$

We should mention at this point that the expression in Eq. (11) is infrared finite and is therefore regularized for $\epsilon > 0$.

We use the same approach as in [20, 26, 27] and introduce Mellin-Barnes representations for the denominators $\hat{C}^{1+3\epsilon}$ and $\hat{C}^{3\epsilon}$. In general the Mellin-Barnes representation of an expression of the form $(K^2 - M^2)^{-\lambda}$ (with $\lambda > 0$) reads

$$\frac{1}{(K^2 - M^2)^\lambda} = \frac{1}{(K^2)^\lambda} \frac{1}{\Gamma(\lambda)} \frac{1}{2\pi i} \int_\gamma ds \left(-\frac{M^2}{K^2}\right)^s \Gamma(-s)\Gamma(\lambda+s), \quad (13)$$

where the integration path γ runs parallel to the imaginary axis. It intersects the real axis somewhere between $-\lambda$ and 0. The Mellin-Barnes representation for \hat{C}^λ , ($\lambda \in \{3\epsilon, 1+3\epsilon\}$) is implemented by identifying K^2 and M^2 as

$$\begin{aligned}
 K^2 &\leftrightarrow m_b^2(1-u)v, \\
 M^2 &\leftrightarrow -\frac{uy}{x(1-x)} m_c^2 + i\delta. \quad (14)
 \end{aligned}$$

The integration path γ has to be chosen such that the parameter integrals exist for all values of $s \in \gamma$. This means in our case that γ has to intersect the real s -axis between -3ϵ and 0. After interchanging the order of integration, the four Feynman parameter integrals can easily be expressed in terms of products of Euler Γ -functions. What remains to be done is the integration over γ in the complex s -plane. We close the integration path in the right half-plane and use the residue theorem to perform this integral. The residues are located at the following positions:

$$\begin{aligned}
 s &= 0, 1, 2, \dots, \\
 s &= 1-\epsilon, 2-\epsilon, 3-\epsilon, \dots, \\
 s &= 1-2\epsilon, 2-2\epsilon, 3-2\epsilon, \dots, \\
 s &= 1-3\epsilon, 2-3\epsilon, 3-3\epsilon, \dots, \\
 s &= \frac{1}{2}-3\epsilon, \frac{3}{2}-3\epsilon, \frac{5}{2}-3\epsilon, \dots. \quad (15)
 \end{aligned}$$

The sum over the residues naturally leads to an expansion in the small parameter $z = m_c^2/m_b^2$ through the factor $(m_c^2/m_b^2)^s$ in Eq. (13) (see also Eq. (14)). This expansion, however, is not a Taylor series because it also involves logarithms of z , which are generated by the expansion in ϵ . The final result for $M_{2,\text{bare}}^{(2)}(2c)$ can thus be written as

$$M_{2,\text{bare}}^{(2)}(2c) = \sum_{k,l} f_{k,l} z^k \ln^l(z), \quad (16)$$

where the coefficients $f_{k,l}$ are independent of z . The power k is an (non-negative) integer multiple of $\frac{1}{2}$ and $l \in \{0, 1, 2, 3, 4\}$. For a detailed explanation of the range of l we refer to [20].

In a similar way all other diagrams can be treated. The final result for the sum of the three-loop diagrams is given by

$$M_{2,\text{bare}}^{(2)} = M_{2,\text{bare}}^{(2)}(1) + M_{2,\text{bare}}^{(2)}(2) + M_{2,\text{bare}}^{(2)}(3) + M_{2,\text{bare}}^{(2)}(4), \quad (17)$$

where the analytical results for the individual terms of the r.h.s. are listed in Appendix B. We decided to include corrections up to $\mathcal{O}(z^3)$ as the higher order terms lead to a negligible contribution for the physical value $z \approx 0.1$.

2.2 Counterterm contributions to $\langle s\gamma|O_2|b \rangle$

In this section we work out the various counterterms of order $\alpha_s^2 n_f$ which are needed to derive the renormalized result $M_2^{(2)}$. There are counterterm contributions due to the renormalization of the strong coupling constant and due to the mixing of O_2 into other operators.

We first discuss the counterterms related to the renormalization of α_s . As the leading term $M_{2,\text{bare}}^{(0)}$ is zero, only the renormalization of g_s in the two-loop result $M_{2,\text{bare}}^{(1)}$ generates a counterterm which can be written as

$$\begin{aligned} M_{2,g_s}^{(2)} &= 2\delta Z_{g_s}^{(1),n_f} M_{2,\text{bare}}^{(1)}, \\ \delta Z_{g_s}^{(1),n_f} &= \frac{\alpha_s n_f T}{\pi 6\epsilon}. \end{aligned} \quad (18)$$

$M_{2,\text{bare}}^{(1)}$ is the sum of the two-loop diagrams which has to be known including terms of $\mathcal{O}(\epsilon)$. For this reason we extended the calculation of Ref. [20] to order ϵ^1 .

We now turn to the counterterms induced through the mixing of O_2 with other operators. First, we consider the counterterms connected with the mixing of O_2 into four-fermion operators. At order α_s there are non-vanishing mixings into O_1 , O_4 and into the evanescent operator P_{11} , defined in Appendix A of Ref. [12]. As only O_4 has a non-vanishing matrix

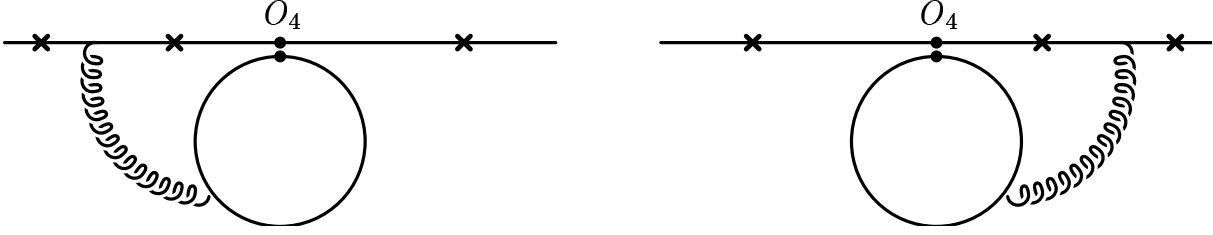


Figure 2.3: Counterterm diagrams to O_2 involving the operator O_4 . The crosses denote the possible places for photon emission. Note that the diagrams where the photon is emitted from the fermion-loop are zero due to Furry's theorem.

element for $b \rightarrow s\gamma$ proportional to $\alpha_s n_f$, the only counterterm of this type is

$$\begin{aligned}
 M_{24,a}^{(2)} &= \delta Z_{24}^{(1)} M_4^{(1)}, \\
 \delta Z_{24}^{(1)} &= \frac{\alpha_s}{\pi} \frac{1}{6\epsilon}, \\
 M_4^{(1)} &= \frac{1}{81} \left(-\frac{72}{\epsilon} + 78 + 288 \ln \left(\frac{m_b}{\mu} \right) + 36i\pi + 1159\epsilon - 150\pi^2\epsilon \right. \\
 &\quad \left. - 312 \ln \left(\frac{m_b}{\mu} \right) \epsilon - 576 \ln^2 \left(\frac{m_b}{\mu} \right) \epsilon + 258i\pi\epsilon - 144i\pi \ln \left(\frac{m_b}{\mu} \right) \epsilon \right. \\
 &\quad \left. + \mathcal{O}(\epsilon^2) \right) \frac{\alpha_s}{4\pi} C_F T n_f Q_d \langle s\gamma | O_7 | b \rangle_{\text{tree}}, \tag{19}
 \end{aligned}$$

where $\delta Z_{24}^{(1)}$ can be found in [12]. The Feynman diagrams contributing to $M_4^{(1)}$, i.e. to the corrections of $\mathcal{O}(\alpha_s n_f)$ to $\langle s\gamma | O_4 | b \rangle_{\text{tree}}$, are depicted in Fig. 2.3. They were computed following the strategy outlined in Section 2.1.

At order $\alpha_s^2 n_f$, there are mixings of O_2 into O_1 , O_4 and P_{11} and again only O_4 has a matrix element of $\mathcal{O}(\alpha_s^0)$. Thus the only counterterm of this type reads

$$\begin{aligned}
 M_{24,b}^{(2)} &= \delta Z_{24}^{(2),n_f} M_4^{(0)}, \\
 \delta Z_{24}^{(2),n_f} &= \left(\frac{\alpha_s}{\pi} \right)^2 \frac{n_f T}{18\epsilon^2}, \\
 M_4^{(0)} &= \left(1 - 2 \ln \left(\frac{m_b}{\mu} \right) \right) \epsilon + \frac{\pi^2 \epsilon^2}{12} + 2 \ln^2 \left(\frac{m_b}{\mu} \right) \epsilon^2 + \mathcal{O}(\epsilon^3) \\
 &\quad C_F Q_d \langle s\gamma | O_7 | b \rangle_{\text{tree}}. \tag{20}
 \end{aligned}$$

In a second step we consider the counterterms connected with the mixing of O_2 into the dipole operators O_7 and O_8 . One can easily see that only one counterterm of this type generates a contribution of $\mathcal{O}(\alpha_s^2 n_f)$: O_2 mixes at three-loop order into O_7 ; in turn, from O_7 the tree-level matrix element for $b \rightarrow s\gamma$ is taken. The resulting counterterm therefore

reads [12, 28]

$$\begin{aligned} M_{27}^{(2)} &= \delta Z_{27}^{(2),n_f} \langle s\gamma | O_7 | b \rangle_{\text{tree}}, \\ \delta Z_{27}^{(2),n_f} &= \left(\frac{\alpha_s}{\pi} \right)^2 C_F T n_f \left[\frac{1}{\epsilon^2} \left(\frac{Q_u}{24} - \frac{Q_d}{81} \right) - \frac{1}{\epsilon} \left(\frac{Q_u}{144} + \frac{2Q_d}{243} \right) \right], \end{aligned} \quad (21)$$

where $Q_u = 2/3$ and $Q_d = -1/3$ are the charge factors of up- and down-type quarks, respectively.

2.3 Renormalized result for $\langle s\gamma | O_2 | b \rangle$

Combining the three-loop result $M_{2,\text{bare}}^{(2)}$, calculated in Subsection A, with the various counterterm contributions discussed in Subsection B (see Eqs. (18), (19), (20), and (21)), we get an ultraviolet finite result. As mentioned earlier, the result is also free of infrared singularities. Inserting the numerical values for the color factors ($C_F = 4/3$, $T = 1/2$) and the electric charge factors ($Q_u = 2/3$, $Q_d = -1/3$), we get the following renormalized result

$$\begin{aligned} M_2^{(2)} &= M_{2,\text{bare}}^{(2)} + M_{2,gs}^{(2)} + M_{24,a}^{(2)} + M_{24,b}^{(2)} + M_{27}^{(2)} \\ &= \left(\frac{\alpha_s}{4\pi} \right)^2 n_f \langle s\gamma | O_7 | b \rangle_{\text{tree}} \left(t_2^{(2)} \ln^2 \left(\frac{m_b}{\mu} \right) + l_2^{(2)} \ln \left(\frac{m_b}{\mu} \right) + r_2^{(2)} \right), \end{aligned} \quad (22)$$

with

$$t_2^{(2)} = \frac{800}{243}, \quad (23)$$

$$\begin{aligned} \text{Re} \left(r_2^{(2)} \right) &= \frac{67454}{6561} - \frac{124\pi^2}{729} - \frac{4}{1215} (11280 - 1520\pi^2 - 171\pi^4 - 5760\zeta(3) \\ &\quad + 6840L - 1440\pi^2 L - 2520\zeta(3)L + 120L^2 + 100L^3 - 30L^4) z \\ &\quad - \frac{64\pi^2}{243} (43 - 12 \ln(2) - 3L) z^{3/2} - \frac{2}{1215} (11475 - 380\pi^2 + 96\pi^4 \\ &\quad + 7200\zeta(3) - 1110L - 1560\pi^2 L + 1440\zeta(3)L + 990L^2 + 260L^3 \\ &\quad - 60L^4) z^2 + \frac{2240\pi^2}{243} z^{5/2} - \frac{2}{2187} (62471 - 2424\pi^2 - 33264\zeta(3) \\ &\quad - 19494L - 504\pi^2 L - 5184L^2 + 2160L^3) z^3 + \mathcal{O}(z^{7/2}), \end{aligned} \quad (24)$$

$$\begin{aligned} \text{Im} \left(r_2^{(2)} \right) &= \frac{4\pi}{729} (495 - 12 (375 - 19\pi^2 + 36\zeta(3) + 84L + 48L^2 - 6L^3) z \\ &\quad + 6 (207 + 38\pi^2 - 72\zeta(3) - 126L - 78L^2 + 12L^3) z^2 \\ &\quad + 8 (67 - 12\pi^2 - 48L) z^3) + \mathcal{O}(z^4), \end{aligned} \quad (25)$$

$$\begin{aligned} \operatorname{Re} \left(l_2^{(2)} \right) &= \frac{16}{243} \left(-145 + (288 - 30\pi^2 - 216\zeta(3) + 216L - 54\pi^2L + 18L^2 \right. \\ &\quad \left. + 6L^3) z + 24\pi^2 z^{3/2} + 6(18 + 2\pi^2 + 12L - 6\pi^2L + L^3) z^2 \right. \\ &\quad \left. - (9 + 14\pi^2 - 182L + 126L^2) z^3 \right) + \mathcal{O}(z^4), \end{aligned} \quad (26)$$

$$\begin{aligned} \operatorname{Im} \left(l_2^{(2)} \right) &= \frac{16\pi}{243} \left(-22 + (180 - 12\pi^2 + 36L + 36L^2) z \right. \\ &\quad \left. - (12\pi^2 - 36L^2) z^2 + (112 - 48L) z^3 \right) + \mathcal{O}(z^4), \end{aligned} \quad (27)$$

where $L = \ln z$. We note that in the derivation of this $\mathcal{O}(\alpha_s^2 n_f)$ result, there was no need to renormalize the parameter m_b in the corresponding $\mathcal{O}(\alpha_s^1)$ expression. Therefore, the symbol $\langle s\gamma | O_7 | b \rangle_{\text{tree}}$ can be interpreted to be (in $M_2^{(1)}$ and $M_2^{(2)}$)

$$\langle s\gamma | O_7 | b \rangle_{\text{tree}} = m_b \frac{e}{8\pi^2} \bar{u}(p') \not{\epsilon} \not{p} u(p), \quad (28)$$

where m_b denotes the pole mass of the b quark. Concerning this point, the reader is also referred to Section 3.

We now turn to the renormalized matrix element $M_1^{(2)}$, associated with the operator O_1 . O_1 , defined in Eq. (4), can be written as

$$O_1 = \frac{1}{2} \tilde{O}_1 - \frac{1}{6} O_2, \quad (29)$$

with

$$\tilde{O}_1 = (\bar{s}_L^\alpha \gamma_\mu c_L^\beta) (\bar{c}_L^\beta \gamma^\mu b_L^\alpha), \quad (30)$$

where α and β are color indices. It is easy to see that \tilde{O}_1 has a vanishing matrix element for $b \rightarrow s\gamma$. Therefore, one obtains

$$M_1^{(2)} = -\frac{1}{6} M_2^{(2)}. \quad (31)$$

3 Real and virtual corrections to $\langle s\gamma | O_7 | b \rangle$

In this section we describe in some detail the steps needed for the calculation of the $\mathcal{O}(\alpha_s^2 n_f)$ corrections to the matrix element $\langle s\gamma | O_7 | b \rangle$. Due to the presence of infrared singularities, the practical calculation proceeds in a slightly different way than for O_2 . As these singularities only get canceled at the level of the decay width when combining the virtual corrections shown in Fig. 3.1(a) with the gluon bremsstrahlung (Fig. 3.1(b)) and the quark-pair emission process (Fig. 3.1(c)), we first derive expressions for the $\mathcal{O}(\alpha_s^2 n_f)$ corrections to these three contributions to the decay width. The corresponding expressions necessary to evaluate $\text{BR}(B \rightarrow X_s \gamma)_{E_\gamma \geq E_{\text{cut}}}$ are discussed in Appendix E.

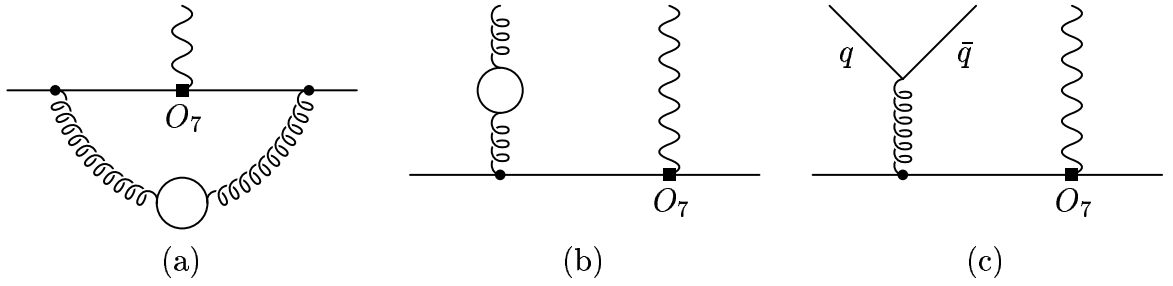


Figure 3.1: Virtual (a), gluon-bremsstrahlung (b) and quark-pair radiation (c) graphs to the operator O_7 . In (b) and (c), the diagrams where the gluon is emitted from the s -quark are not shown.

To fix the notation, we write the contribution from O_7 to the decay width $\Gamma(b \rightarrow X_s\gamma)$ as

$$\Gamma_{77} = \Gamma_{77}^0 \left[1 + \hat{\Gamma}_{77}^{(1)} + \hat{\Gamma}_{77}^{(2),n_f} \right], \quad \Gamma_{77}^0 = \frac{m_b^5 \alpha_{\text{em}}}{32\pi^4} |G_F \lambda_t C_7^{\text{eff}}|^2. \quad (32)$$

The $\mathcal{O}(\alpha_s)$ correction, $\hat{\Gamma}_{77}^{(1)}$, can be extracted from Ref. [20], reading

$$\hat{\Gamma}_{77}^{(1)} = \frac{\alpha_s}{4\pi} \left(-\frac{32}{9} - \frac{16\pi^2}{9} + \frac{64}{3} \ln \left(\frac{m_b}{\mu} \right) \right). \quad (33)$$

We further split $\hat{\Gamma}_{77}^{(2),n_f}$ in Eq. (32) as

$$\hat{\Gamma}_{77}^{(2),n_f} = \hat{\Gamma}_{77}^{(2),(a)} + \hat{\Gamma}_{77}^{(2),(b)} + \hat{\Gamma}_{77}^{(2),(c)}, \quad (34)$$

with obvious notation (Fig. 3.1).

For the calculation of the three parts contributing to $\hat{\Gamma}_{77}^{(2),n_f}$ we could in principle put $m_f = m_s = 0$ at the beginning of the calculation and use dimensional regularization for both infrared and ultraviolet singularities. We found it easier, however, to use the strange quark mass, m_s , and the mass of the quark in the fermion bubble, m_f , as infrared regulators. For formulating the results, it is convenient to introduce the dimensionless quantities

$$r = \frac{m_s^2}{m_b^2}, \quad f = \frac{m_f^2}{m_b^2}. \quad (35)$$

We now turn to the calculations of $\hat{\Gamma}_{77}^{(2),(c)}$, $\hat{\Gamma}_{77}^{(2),(b)}$ and $\hat{\Gamma}_{77}^{(2),(a)}$ (in this order).

Inspecting the explicit expressions for the quark-pair radiation process (cf. Fig. 3.1(c)), one finds that it can be worked out in our “massive” regularization scheme in $d = 4$ dimensions. Furthermore, one realizes that one can also put $m_s = 0$, provided m_f is kept at a (small) fixed value. As a consequence, the quark-pair radiation process is completely regularized by the mass m_f . The evaluation of this process is quite standard: in a first

step the subprocess $b \rightarrow s\gamma g^*$ is considered where g^* represents a virtual gluon. Subsequently the other subprocess, describing the decay of g^* into two fermions, is added. It is straightforward to perform the occurring phase space integrations where only the one over the gluon virtuality is non-trivial. However, in the limit $m_f \rightarrow 0$ also this one can be performed analytically. One arrives at the following result for the quark-pair emission process:

$$\hat{\Gamma}_{77}^{(2),(c)} = \left(\frac{\alpha_s}{4\pi}\right)^2 \frac{n_f}{243} [-12662 + 24\pi^2 + 2592\zeta(3) + (144\pi^2 - 5916)\ln(f) - 900\ln^2(f) - 72\ln^3(f)] . \quad (36)$$

Due to the Kinoshita-Lee-Nauenberg theorem, it follows that the sum of the virtual and the gluon bremsstrahlung corrections also must be finite for $d \rightarrow 4$ and $m_s \rightarrow 0$ for fixed m_f .

We now turn to the gluon bremsstrahlung process. The diagram in Fig. 3.1(b) (combined with the one where the gluon is emitted from the s -quark) can be written as

$$M_{7,\text{bare}}^{(2),(b)} = \frac{\delta Z_3^{(1),n_f}}{2} M_7^{(1),(b)} , \quad (37)$$

where $M_7^{(1),(b)}$ denotes the lowest order matrix element for $b \rightarrow s\gamma g$ and $\delta Z_3^{(1),n_f}$ reads

$$\delta Z_3^{(1),n_f} = -\frac{\alpha_s n_f T}{\pi 36} \left(\frac{12}{\epsilon} - 24 \ln\left(\frac{m_f}{\mu}\right) + \pi^2 \epsilon + 24 \ln^2\left(\frac{m_f}{\mu}\right) \epsilon + \mathcal{O}(\epsilon^2) \right) . \quad (38)$$

Note that the $1/\epsilon$ pole is of ultraviolet origin; the infrared singularity is regulated by m_f in this expression. In addition, there is a counterterm contribution due to the $\overline{\text{MS}}$ renormalization of the strong coupling constant of the form

$$M_{7,\text{ct}}^{(2),(b)} = \delta Z_{g_s}^{(1),n_f} M_7^{(1),(b)} , \quad (39)$$

with

$$\delta Z_{g_s}^{(1),n_f} = \frac{\alpha_s n_f T}{\pi 6\epsilon} . \quad (40)$$

Combining $M_{7,\text{bare}}^{(2),(b)}$ with $M_{7,\text{ct}}^{(2),(b)}$, one obtains the renormalized matrix element $M_7^{(2),(b)}$

$$M_7^{(2),(b)} = \left(\delta Z_{g_s}^{(1),n_f} + \frac{\delta Z_3^{(1),n_f}}{2} \right) M_7^{(1),(b)} , \quad (41)$$

from which the $\mathcal{O}(\alpha_s^2 n_f)$ contribution to the decay width is obtained in a straightforward

way. One gets

$$\begin{aligned}
 \hat{\Gamma}_{77}^{(2),(b)} &= 2 \left(\delta Z_{g_s}^{(1),n_f} + \frac{\delta Z_3^{(1),n_f}}{2} \right) \hat{\Gamma}_{77}^{(1),(b)} \\
 &= \left(\frac{\alpha_s}{4\pi} \right)^2 \frac{C_F T n_f}{18} \left[\frac{48}{\epsilon} \left(2 \ln(f) + 4 \ln \left(\frac{m_b}{\mu} \right) + \ln(f) \ln(r) \right. \right. \\
 &\quad \left. \left. + 2 \ln \left(\frac{m_b}{\mu} \right) \ln(r) \right) - 8\pi^2 + 416 \ln(f) - 32\pi^2 \ln(f) \right. \\
 &\quad \left. - 48 \ln^2(f) + 832 \ln \left(\frac{m_b}{\mu} \right) - 64\pi^2 \ln \left(\frac{m_b}{\mu} \right) - 960 \ln^2 \left(\frac{m_b}{\mu} \right) \right. \\
 &\quad \left. - 576 \ln(f) \ln \left(\frac{m_b}{\mu} \right) - 4 \ln(r) \left(\pi^2 - 18 \ln(f) + 6 \ln^2(f) \right. \right. \\
 &\quad \left. \left. - 36 \ln \left(\frac{m_b}{\mu} \right) + 120 \ln^2 \left(\frac{m_b}{\mu} \right) + 72 \ln(f) \ln \left(\frac{m_b}{\mu} \right) \right) \right. \\
 &\quad \left. - 24 \ln^2(r) \left(\ln(f) + 2 \ln \left(\frac{m_b}{\mu} \right) \right) \right], \tag{42}
 \end{aligned}$$

where $\hat{\Gamma}_{77}^{(1),(b)}$ is the corresponding (normalized) decay width for $b \rightarrow s\gamma g$ in the $\mathcal{O}(\alpha_s)$ approximation. As in our regularization scheme the sum $\delta Z_{g_s}^{(1),n_f} + \delta Z_3^{(1),n_f}/2$ is finite (in ϵ), $\hat{\Gamma}_{77}^{(1),(b)}$ is only needed up to terms of order ϵ^0 , which simplified the calculation.

We now turn to the evaluation of the virtual corrections shown in Fig. 3.1(a) and also discuss the various counterterm contributions. For the diagram shown in this figure, we obtain

$$\begin{aligned}
 M_{7,\text{bare}}^{(2),(a)} &= \frac{1}{81} \left[\frac{54}{\epsilon^2} (2 \ln(r) - 1) + \frac{18}{\epsilon} \left(2 + 12 \ln(r) - 6 \ln(r) \ln(f) \right. \right. \\
 &\quad \left. \left. - 24 \ln(r) \ln \left(\frac{m_b}{\mu} \right) - 3 \ln^2(r) + 6 \ln(f) + 12 \ln \left(\frac{m_b}{\mu} \right) \right) \right. \\
 &\quad \left. + 1718 + 123\pi^2 + 840 \ln(f) + 36\pi^2 \ln(f) + 90 \ln^2(f) \right. \\
 &\quad \left. + 18 \ln^3(f) - 144 \ln \left(\frac{m_b}{\mu} \right) - 432 \ln^2 \left(\frac{m_b}{\mu} \right) - 432 \ln(f) \ln \left(\frac{m_b}{\mu} \right) \right. \\
 &\quad \left. + 18 \ln(r) \left(24 + \pi^2 - 12 \ln(f) + 3 \ln^2(f) - 48 \ln \left(\frac{m_b}{\mu} \right) + 48 \ln^2 \left(\frac{m_b}{\mu} \right) \right. \right. \\
 &\quad \left. \left. + 24 \ln(f) \ln \left(\frac{m_b}{\mu} \right) \right) - 54 \ln^2(r) \left(2 - \ln(f) - 4 \ln \left(\frac{m_b}{\mu} \right) \right) + 18 \ln^3(r) \right] \\
 &\quad \left(\frac{\alpha_s}{4\pi} \right)^2 C_F T n_f \langle s\gamma|O_7|b\rangle_{\text{tree}}. \tag{43}
 \end{aligned}$$

We stress that this expression is derived in such a way that m_s is understood to be sent to zero prior to m_f . This procedure is justified by the fact that for fixed m_f the sum of the virtual- and gluon bremsstrahlung contributions must be finite in the limit $m_s \rightarrow 0$, as discussed above.

The counterterm contribution $M_{7,\text{ct}}^{(2),(a)}$ at $\mathcal{O}(\alpha_s^2 n_f)$ has various sources. There is a contribution $M_{7,\text{ct}_1}^{(2),(a)}$ due to the renormalization of g_s in the $\mathcal{O}(\alpha_s)$ vertex diagram (i.e. like the one in Fig. 3.1(a), but without the fermion bubble), yielding

$$\begin{aligned}
 M_{7,\text{ct}_1}^{(2),(a)} &= \frac{1}{9} \left[-\frac{12}{\epsilon^2} \ln(r) - \frac{6}{\epsilon} \ln(r) \left(4 - \ln(r) - 4 \ln \left(\frac{m_b}{\mu} \right) \right) \right. \\
 &\quad + 12 - \ln(r) \left(48 + \pi^2 - 48 \ln \left(\frac{m_b}{\mu} \right) + 24 \ln^2 \left(\frac{m_b}{\mu} \right) \right) \\
 &\quad \left. + 12 \ln^2(r) \left(1 - \ln \left(\frac{m_b}{\mu} \right) \right) - 2 \ln^3(r) \right] \\
 &\quad \left(\frac{\alpha_s}{4\pi} \right)^2 C_F T n_f \langle s\gamma | O_7 | b \rangle_{\text{tree}} .
 \end{aligned} \tag{44}$$

Then, there is a counterterm contribution $M_{7,\text{ct}_2}^{(2),(a)}$ of the form

$$M_{7,\text{ct}_2}^{(2),(a)} = \left(\frac{\delta Z_{2,b}^{(2),n_f}}{2} + \frac{\delta Z_{2,s}^{(2),n_f}}{2} + \delta Z_{77}^{(2),n_f} + \delta Z_{m_b}^{\text{on},(2),n_f} \right) \langle s\gamma | O_7 | b \rangle_{\text{tree}} . \tag{45}$$

Here, $\delta Z_{2,b}^{(2),n_f}$ and $\delta Z_{2,s}^{(2),n_f}$ are the $\mathcal{O}(\alpha_s^2 n_f)$ pieces of the on-shell wave function renormalization constants for the b and s quark, respectively, while the operator renormalization factor $\delta Z_{77}^{(2),n_f}$ refers to the $\overline{\text{MS}}$ scheme. Note that the presence of the *on-shell* renormalization factor $\delta Z_{m_b}^{\text{on},(2),n_f}$ in Eq. (45) implies that in the lower order contributions the symbol $\langle s\gamma | O_7 | b \rangle_{\text{tree}}$ is understood to be the tree-level matrix element of O_7 in which the running b -quark mass is replaced by the corresponding pole mass. The explicit form of the various δZ factors occurring in Eq. (45) can be seen in Appendix D.

After combining Eqs. (43), (44) and (45) into the renormalized matrix element, the calculation of $\hat{\Gamma}_{77}^{(2),(a)}$ is straightforward. We obtain

$$\begin{aligned}
 \hat{\Gamma}_{77}^{(2),(a)} &= \left(\frac{\alpha_s}{4\pi} \right)^2 \frac{C_F T n_f}{81} \left[\frac{-216}{\epsilon} \left(2 \ln(f) + 4 \ln \left(\frac{m_b}{\mu} \right) + \ln(f) \ln(r) \right) \right. \\
 &\quad \left. + 2 \ln \left(\frac{m_b}{\mu} \right) \ln(r) \right] + 7495 + 624\pi^2 + 1086 \ln(f) + 72\pi^2 \ln(f) \\
 &\quad + 666 \ln^2(f) + 36 \ln^3(f) - 6336 \ln \left(\frac{m_b}{\mu} \right) + 6048 \ln^2 \left(\frac{m_b}{\mu} \right)
 \end{aligned} \tag{46}$$

$$\begin{aligned}
 &+2592 \ln(f) \ln\left(\frac{m_b}{\mu}\right) + 18 \ln(r) \left(\pi^2 - 18 \ln(f) + 6 \ln^2(f)\right) \\
 &-36 \ln\left(\frac{m_b}{\mu}\right) + 120 \ln^2\left(\frac{m_b}{\mu}\right) + 72 \ln(f) \ln\left(\frac{m_b}{\mu}\right) \\
 &+108 \ln^2(r) \left(\ln(f) + 2 \ln\left(\frac{m_b}{\mu}\right)\right) \Big].
 \end{aligned}$$

We now combine virtual and gluon bremsstrahlung corrections given in Eqs. (46) and (42), respectively. We obtain (after putting $T = 1/2$ and $C_F = 4/3$)

$$\begin{aligned}
 \hat{\Gamma}_{77}^{(2),(a)+(b)} &= \left(\frac{\alpha_s}{4\pi}\right)^2 \frac{n_f}{243} \left[14990 + 1176\pi^2 + (5916 - 144\pi^2) \ln(f) + 900 \ln^2(f) \right. \\
 &\quad \left. + 72 \ln^3(f) - 576(9 + \pi^2) \ln\left(\frac{m_b}{\mu}\right) + 3456 \ln^2\left(\frac{m_b}{\mu}\right) \right], \quad (47)
 \end{aligned}$$

where the $1/\epsilon$ poles and the mass singularities associated with m_s are canceled.

When combining this result with the quark-pair emission process in Eq. (36), we obtain the final result

$$\hat{\Gamma}_{77}^{(2),n_f} = \left(\frac{\alpha_s}{4\pi}\right)^2 n_f \left(2t_7^{(2)} \ln^2\left(\frac{m_b}{\mu}\right) + 2l_7^{(2)} \ln\left(\frac{m_b}{\mu}\right) + 2r_7^{(2)} \right), \quad (48)$$

with

$$\begin{aligned}
 t_7^{(2)} &= \frac{64}{9}, \\
 l_7^{(2)} &= -\frac{32}{27} (9 + \pi^2), \\
 r_7^{(2)} &= \frac{4}{81} (97 + 50\pi^2 + 108\zeta(3)). \quad (49)
 \end{aligned}$$

The cancelation of the $\ln(f)$ terms is a strong check for the correctness of the individual pieces of the calculation.

For later convenience we formally introduce an amplitude M_7 in such a way that its square reproduces the result of Eq. (48). Adopting the notation of Eq. (6) one gets

$$M_7^{(2)} = \left(\frac{\alpha_s}{4\pi}\right)^2 n_f \langle s\gamma|O_7|b\rangle_{\text{tree}} \left(t_7^{(2)} \ln^2\left(\frac{m_b}{\mu}\right) + l_7^{(2)} \ln\left(\frac{m_b}{\mu}\right) + r_7^{(2)} \right). \quad (50)$$

4 Virtual corrections to $\langle s\gamma|O_8|b\rangle$

We first discuss the two-loop diagrams depicted in Fig. 4.1, which contain the building block $K_{\beta\beta'}^f$ (see Eq. (71)). As these diagrams are free of infrared singularities, we put the

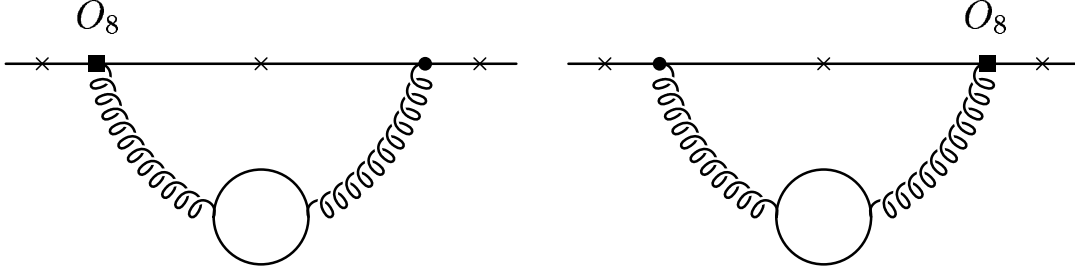


Figure 4.1: Graphs associated with virtual corrections to the operator O_8 . The crosses denote the possible places where the photon can be emitted.

masses m_f of the quarks in the fermion loop as well as the strange quark mass m_s to zero from the beginning. The calculation can be performed along the same lines as described in Section 2.1. However, due to the absence of m_c , the actual evaluation of the diagrams turns out to be much simpler. The result can be cast into the form

$$M_{8,\text{bare}}^{(2)} = \left(\frac{\alpha_s}{4\pi}\right)^2 C_F T n_f Q_d \langle s\gamma | O_7 | b \rangle_{\text{tree}} \frac{4}{27} \left[530 - 28\pi^2 - 180\zeta(3) + 93i\pi + \left(\frac{18}{\epsilon^2} + \frac{1}{\epsilon} (120 - 6\pi^2 + 18i\pi)\right) \left(\frac{m_b}{\mu}\right)^{-4\epsilon} \right]. \quad (51)$$

The counterterm contribution of $\mathcal{O}(\alpha_s^2 n_f)$, denoted by $M_{8,\text{ct}}^{(2)}$, stems from the renormalization of g_s and from the mixing of O_8 into the operator O_7 . We obtain

$$M_{8,\text{ct}}^{(2)} = \delta Z_{87}^{(2),n_f} \langle s\gamma | O_7 | b \rangle_{\text{tree}} + 2\delta Z_{g_s}^{(1),n_f} M_8^{(1)}, \quad (52)$$

with

$$\begin{aligned} \delta Z_{87}^{(2),n_f} &= \left(\frac{\alpha_s}{\pi}\right)^2 C_F T n_f \frac{Q_d}{36\epsilon} \left(\frac{6}{\epsilon} - 7\right), \\ \delta Z_{g_s}^{(1),n_f} &= \frac{\alpha_s n_f T}{\pi 6\epsilon}, \\ M_8^{(1)} &= -\frac{\alpha_s}{4\pi} \frac{1}{3} Q_d C_F \langle s\gamma | O_7 | b \rangle_{\text{tree}} \left[\frac{12}{\epsilon} + 33 - 2\pi^2 - 24 \ln\left(\frac{m_b}{\mu}\right) + 6i\pi + \epsilon \left(72 - 4\pi^2 - 36\zeta(3) - 66 \ln\left(\frac{m_b}{\mu}\right) + 4\pi^2 \ln\left(\frac{m_b}{\mu}\right) + 24 \ln^2\left(\frac{m_b}{\mu}\right) + 12i\pi - 12i\pi \ln\left(\frac{m_b}{\mu}\right) \right) + \mathcal{O}(\epsilon^2) \right]. \end{aligned} \quad (53)$$

$\delta Z_{87}^{(2),n_f}$ is obtained from [12, 28]. The sum of $M_{8,\text{bare}}^{(2)}$ and $M_{8,\text{ct}}^{(2)}$ leads to the renormalized result (using $T = 1/2$, $C_F = 4/3$ and $Q_d = -1/3$)

$$M_8^{(2)} = \left(\frac{\alpha_s}{4\pi}\right)^2 n_f \langle s\gamma | O_7 | b \rangle_{\text{tree}} \left[t_8^{(2)} \ln^2\left(\frac{m_b}{\mu}\right) + l_8^{(2)} \ln\left(\frac{m_b}{\mu}\right) + r_8^{(2)} \right], \quad (54)$$

with

$$\begin{aligned}
 t_8^{(2)} &= -\frac{64}{27}, \\
 l_8^{(2)} &= \frac{16}{81} (47 - 2\pi^2 + 6i\pi), \\
 r_8^{(2)} &= \frac{8}{243} (-314 + 16\pi^2 + 72\zeta(3) - 57i\pi).
 \end{aligned} \tag{55}$$

5 Numerical impact of the $\mathcal{O}(\alpha_s^2 n_f)$ corrections

It is well-known that the inclusive decay rate for $B \rightarrow X_s \gamma$ is given by the corresponding b -quark decay rate $\Gamma(b \rightarrow X_s \gamma)$, up to power corrections of the form $(\Lambda_{\text{QCD}}/m_b)^2$ [29] and $(\Lambda_{\text{QCD}}/m_c)^2$ [30] which numerically are well below 10%.

As our new results are only a part of the complete NNLL contributions, we do not present a new prediction of the branching ratio in this paper. Instead, we only illustrate how the $\mathcal{O}(\alpha_s^2 n_f)$ corrections to the matrix elements of the operators O_1 , O_2 , O_7 and O_8 modify the NLL branching ratio for a given set of input parameters. For this purpose, we neglect power corrections and also electroweak terms.

In a NLL calculation the inclusive quark-level transition $b \rightarrow X_s \gamma$ involves the subprocesses $b \rightarrow s \gamma$ (including virtual corrections) and $b \rightarrow s \gamma g$, i.e., the gluon bremsstrahlung process. We write the amplitude for the first subprocess similar as in Ref. [14]:

$$\mathcal{A}^{\text{NLL}}(b \rightarrow s \gamma) = -\frac{4G_F}{\sqrt{2}} V_{ts}^* V_{tb} D^{\text{NLL}} \langle s \gamma | O_7 | b \rangle_{\text{tree}}, \tag{56}$$

where the reduced amplitude D^{NLL} reads

$$D^{\text{NLL}} = C_7^{\text{eff}}(\mu) + \frac{\alpha_s(\mu)}{4\pi} V^{(1)}(\mu). \tag{57}$$

The symbol $V^{(1)}(\mu)$, defined as

$$V^{(1)}(\mu) = \sum_{i=1}^8 C_i^{\text{eff}}(\mu) \left[\left(r_i^{(1)} - \frac{16}{3} \delta_{i7} \right) + (l_i^{(1)} + 8 \delta_{i7}) \ln \left(\frac{m_b}{\mu} \right) \right], \tag{58}$$

incorporates the NLL corrections, $r_i^{(1)}$ and $l_i^{(1)}$, to the matrix elements. In Eq. (57), the first term on the r.h.s. is understood to be the Wilson coefficient $C_7^{\text{eff}}(\mu)$ at NLL order, while the Wilson coefficients appearing in $V^{(1)}(\mu)$ are understood to be taken at LL order. As in Ref. [14], we convert the running mass factor $\overline{m}_b(\mu)$, which appears in the definition of the operator O_7 in Eq. (4), into the pole mass m_b . This conversion is absorbed into the function $V^{(1)}(\mu)$ and consequently the symbol $\langle s \gamma | O_7 | b \rangle_{\text{tree}}$ in Eq. (56) is the tree-level matrix element of the operator O_7 , where the running mass factor $\overline{m}_b(\mu)$ is understood

to be replaced by the pole mass m_b . The NLL virtual correction functions $r_i^{(1)}$ and $l_i^{(1)}$ in (58), taken from Ref. [20], are repeated for completeness in Appendix C. Note, that the quantity $r_7^{(1)}$ not only contains virtual corrections to the matrix element of O_7 , which would be infrared singular. $r_7^{(1)}$ is constructed in such a way, that the (O_7, O_7) interference term generates the sum of virtual and bremsstrahlung corrections when formally calculating the branching ratio from $\mathcal{A}^{\text{NLL}}(b \rightarrow s\gamma)$. For the details of this construction, we refer to Ref. [20]. Numerically, the square of this amplitude encodes the bulk of the decay width. The additional bremsstrahlung corrections, which are infrared finite for $E_{\text{gluon}} \rightarrow 0$, are relatively small. Therefore, when considering terms of order $\mathcal{O}(\alpha_s^2 n_f)$, we omit purely finite bremsstrahlung contributions.

When improving the amplitude for the subprocess $b \rightarrow s\gamma$ by including the terms of $\mathcal{O}(\alpha_s^2 n_f)$, the result can be written as

$$\mathcal{A}(b \rightarrow s\gamma) = -\frac{4G_F}{\sqrt{2}} V_{ts}^* V_{tb} D \langle s\gamma | O_7 | b \rangle_{\text{tree}}, \quad (59)$$

where the reduced amplitude D is

$$D = C_7^{\text{eff}}(\mu) + \frac{\alpha_s(\mu)}{4\pi} V^{(1)}(\mu) + \left(\frac{\alpha_s(\mu)}{4\pi}\right)^2 n_f V^{(2)}(\mu). \quad (60)$$

$V^{(2)}(\mu)$, defined as

$$V^{(2)}(\mu) = \sum_{i=1}^8 C_i^{\text{eff}}(\mu) \left[r_i^{(2)} + l_i^{(2)} \ln\left(\frac{m_b}{\mu}\right) + t_i^{(2)} \ln^2\left(\frac{m_b}{\mu}\right) \right], \quad (61)$$

incorporates the $\mathcal{O}(\alpha_s^2 n_f)$ corrections to the matrix elements calculated in the previous sections of this paper. The explicit $C_7^{\text{eff}}(\mu)$ term in Eq. (60) in principle stands for the NLL Wilson coefficient, supplemented by the n_f dependent NNLL contributions. As the latter are not known yet, we take this Wilson coefficient at NLL precision in the numerical evaluations. The Wilson coefficients entering $V^{(1)}(\mu)$ are in principle the LL coefficients, supplemented by the n_f dependent NLL contributions. In practice, we decide to replace these Wilson coefficients by the respective complete NLL version. Finally, the Wilson coefficients entering $V^{(2)}(\mu)$ are the LL versions. Note, that the gluon bremsstrahlung and the quark-antiquark emission processes associated with O_7 are effectively transferred into $r_7^{(2)}$, $l_7^{(2)}$ and $t_7^{(2)}$, as described in Section 3. As already mentioned above, the square of the so-defined amplitude incorporates the major part of the branching ratio. We therefore consider the additional finite bremsstrahlung corrections to the decay width only at the NLL level, i.e. we do not calculate the $\mathcal{O}(\alpha_s^2 n_f)$ corrections to these contributions.

As the square of the amplitude for $b \rightarrow s\gamma$ (in the sense defined above) encodes the dominant part of the decay width, it is reasonable to compare the NLL result D^{NLL} in Eq. (57) with the corresponding $\mathcal{O}(\alpha_s^2 n_f)$ -improved result D in Eq. (60). In Fig. 5.1, the function D is plotted as a function of the renormalization scale μ . We note, as already

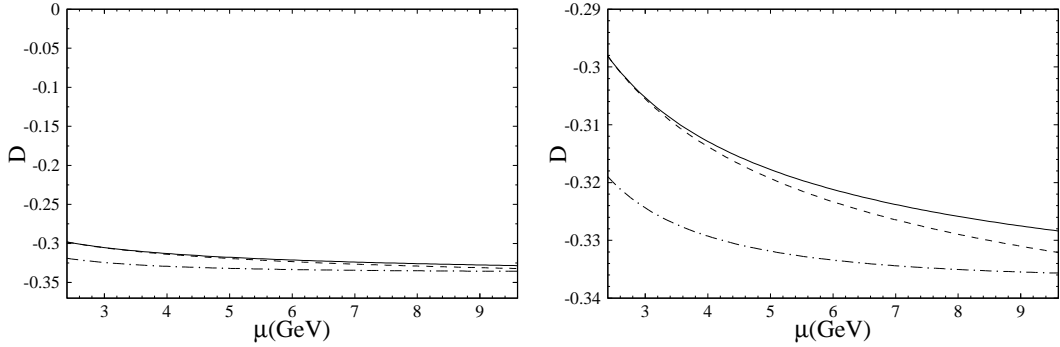


Figure 5.1: The reduced amplitude D as a function of the renormalization scale μ where the plot on the right is an enlargement of the one on the left. The dash-dotted curve represents the NLL approximation and the solid curve includes the corrections of $\mathcal{O}(\alpha_s^2 n_f)$. For comparison we also show the result where the Wilson coefficients in $V^{(1)}$ (cf. Eq. (58)) are inserted to LL precision only (dashed curve).

discussed in the Introduction, that we use in the numerical evaluations the hypothesis of naive non-abelianization, which amounts to replacing n_f by $-3\beta_0/2$. Nevertheless, in the following we still write $\mathcal{O}(\alpha_s^2 n_f)$. The dash-dotted line shows the NLL approximation as defined in Eq. (57), while the solid curve shows the result after including the $\mathcal{O}(\alpha_s^2 n_f)$ terms as discussed above. The dashed line shows the result with $\mathcal{O}(\alpha_s^2 n_f)$ improvements, in which, however, the Wilson coefficients in $V^{(1)}(\mu)$ are taken in LL approximation. The three curves illustrate that the changes between the $\mathcal{O}(\alpha_s^2 n_f)$ improved version (solid line) and the NLL prediction (dash-dotted line) are mainly due to the new $\mathcal{O}(\alpha_s^2 n_f)$ corrections of the matrix elements calculated in the previous sections.

From $\mathcal{A}(b \rightarrow s\gamma)$ in Eq. (59) the decay width $\Gamma(b \rightarrow s\gamma)$ is easily obtained to be

$$\Gamma(b \rightarrow s\gamma) = \frac{G_F^2}{32\pi^4} |V_{ts}^* V_{tb}|^2 \alpha_{\text{em}} m_b^5 |D|^2. \quad (62)$$

When giving numerical results for the NLL predictions, we only retain terms in $|D|^2$ up to order α_s , while for the improved version we retain terms up to $\mathcal{O}(\alpha_s^2 n_f)$ in $|D|^2$ and systematically dismiss higher order contributions. For completeness we should mention that $\alpha_s(\mu)$ is evaluated using two-loop accuracy in the β function. We checked that the contribution of the three-loop term β_2 is numerically small.

To obtain the inclusive decay rate for $b \rightarrow X_s \gamma$, we have to take into account those terms which have not yet been absorbed into the virtual corrections. At NLL precision, these contributions consist of those gluon bremsstrahlung corrections which are finite when the gluon energy goes to zero; they have been calculated in Refs. [31, 32]. As the (O_8, O_8) contribution to $\Gamma(b \rightarrow s\gamma g)$ becomes infrared singular for *soft photon energies*, we introduce a photon energy cutoff E_{cut} as in Ref. [12] and define the kinematical decay width

$$\Gamma(b \rightarrow X_s \gamma)_{E_\gamma \geq E_{\text{cut}}}. \quad (63)$$

At NLL the gluon bremsstrahlung contribution to this quantity can be written as

$$\Gamma(b \rightarrow s\gamma g)_{E_\gamma \geq E_{\text{cut}}} = \frac{G_F^2}{32\pi^4} |V_{ts}^* V_{tb}|^2 \alpha_{\text{em}} m_b^5 A, \quad (64)$$

where A is of the form [12]

$$A = \left(e^{-\alpha_s(\mu) \ln(\delta)(7+2\ln(\delta))/(3\pi)} - 1 \right) |C_7^{\text{eff}}(\mu)|^2 + \frac{\alpha_s(\mu)}{\pi} \sum_{i,j=1;i \leq j}^8 \text{Re} [C_i^{\text{eff}}(\mu) C_j^{\text{eff}}(\mu) f_{ij}(\delta)]. \quad (65)$$

The quantity δ is defined through

$$E_{\text{cut}} = \frac{m_b}{2}(1 - \delta) = E_{\text{max}}(1 - \delta). \quad (66)$$

In Eq. (65) we put $C_i^{\text{eff}} = 0$ for $i = 3, \dots, 6$, as in the virtual contributions. We list the explicit expressions for the quantities $f_{ij}(\delta)$ in Appendix C.

We should repeat that the $\mathcal{O}(\alpha_s^2 n_f)$ corrections are incorporated in the quantity D , defined in Eqs. (59) and (60). We stress that the absorbed gluon bremsstrahlung- and the quark-pair emission terms were obtained by integrating over the full range of the photon energy. Thus, since we decided to implement a photon energy cut as just described, the final expression for the kinematical decay width can be written as

$$\Gamma(b \rightarrow X_s \gamma)_{E_\gamma \geq E_{\text{cut}}} = \frac{G_F^2}{32\pi^4} |V_{ts}^* V_{tb}|^2 \alpha_{\text{em}} m_b^5 (|D|^2 + A) - \Gamma_{77}^{(2),n_f}(b \rightarrow X_s \gamma)_{E_\gamma \leq E_{\text{cut}}}, \quad (67)$$

where the expression for $\Gamma_{77}^{(2),n_f}(b \rightarrow X_s \gamma)_{E_\gamma \leq E_{\text{cut}}}$ is derived in Appendix E.

In a last step, the kinematical branching ratio is obtained as

$$\text{BR}(b \rightarrow X_s \gamma)_{E_\gamma \geq E_{\text{cut}}} = \frac{\Gamma(b \rightarrow X_s \gamma)_{E_\gamma \geq E_{\text{cut}}}}{\Gamma_{\text{SL}}} \text{BR}_{\text{SL}}, \quad (68)$$

where BR_{SL} is the measured semileptonic branching ratio and the semileptonic decay width Γ_{SL} (supplemented by the $\mathcal{O}(\alpha_s^2 n_f)$ terms [23]) is given by ($z = m_c^2/m_b^2$)

$$\Gamma_{\text{SL}} = \frac{G_F^2 |V_{cb}|^2 m_b^5}{192\pi^3} g(z) \left[1 - \frac{2\alpha_s(\mu)}{3\pi} \frac{h(z)}{g(z)} - \left(\frac{\alpha_s(\mu)}{\pi} \right)^2 \beta_0 \left(\chi_\beta \left(\frac{m_c}{m_b} \right) - \frac{1}{3} \frac{h(z)}{g(z)} \ln \left(\frac{m_b}{\mu} \right) \right) \right], \quad (69)$$

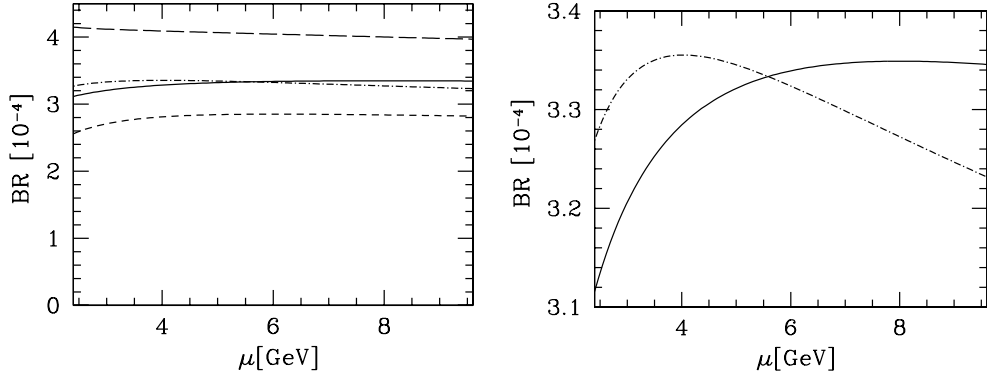


Figure 5.2: The branching ratio as a function of the renormalization scale μ where the plot on the right is an enlargement of the one on the left. The dash-dotted curve represents the NLL approximation and the solid curve includes the corrections of $\mathcal{O}(\alpha_s^2 n_f)$. For illustration in the left plot the latter are also shown for the case where $M_{1/2}^{(2)}$ ($M_7^{(2)}$) is set to zero which corresponds to short-dashed (long-dashed) curve. A photon energy cut of $E_{\text{cut}} = m_b/20$ is used, which corresponds to $\delta = 0.9$.

where the phase space function $g(z)$ and the $\mathcal{O}(\alpha_s)$ radiation function $h(z)$ [33] read

$$\begin{aligned}
 g(z) &= 1 - 8z + 8z^3 - z^4 - 12z^2 \ln(z), \\
 h(z) &= (z^2 - 1) \left(\frac{25}{4} - \frac{239}{3}z + \frac{25}{4}z^2 \right) + z \ln(z) \left(20 + 90z - \frac{4}{3}z^2 + \frac{17}{3}z^3 \right) \\
 &\quad + z^2 \ln^2(z) (36 + z^2) + (1 - z^2) \left(\frac{17}{3} - \frac{64}{3}z + \frac{17}{3}z^2 \right) \ln(1 - z) \\
 &\quad - 4(1 + 30z^2 + z^4) \ln(z) \ln(1 - z) - (1 + 16z^2 + z^4) (6 \text{Li}_2(z) - \pi^2) \\
 &\quad - 32z^{3/2}(1 + z) \left[\pi^2 - 4 \text{Li}_2(\sqrt{z}) + 4 \text{Li}_2(-\sqrt{z}) - 2 \ln(z) \ln \left(\frac{1 - \sqrt{z}}{1 + \sqrt{z}} \right) \right].
 \end{aligned}$$

The function $\chi_\beta(m_c/m_b)$, which encodes the $\mathcal{O}(\alpha_s^2 n_f)$ terms¹ is given in the form of a plot in Ref. [23]. For $m_c/m_b = 0.29$, which is the default value in our paper, one finds $\chi_\beta(0.29) \approx 1.68$.

In Fig. 5.2 the kinematical branching ratio is shown for the choice $E_{\text{cut}} = m_b/20$, or, equivalently, $\delta = 0.9$ [8] as a function of the renormalization scale μ . The input parameters were chosen to be: $m_b = 4.8$ GeV, $m_c/m_b = 0.29$, $m_t = 173.8$ GeV, $m_W = 80.41$ GeV, $m_Z = 91.187$ GeV, $\alpha_s(m_Z) = 0.119$, $\alpha_{\text{em}} = 1/137.036$, $|V_{ts}^* V_{tb}/V_{cb}|^2 = 0.95$ and $\text{BR}_{\text{SL}} = 10.49\%$. The dash-dotted line shows the branching ratio $\text{BR}(b \rightarrow X_s \gamma)$ in NLL precision. In this case the terms of $\mathcal{O}(\alpha_s^2 \beta_0)$ are consistently omitted in the expression for Γ_{SL} in Eq. (69). The solid line shows the branching ratio where the $\mathcal{O}(\alpha_s^2 n_f)$ (or the $\mathcal{O}(\alpha_s^2 \beta_0)$) improvements are included.

¹Note, that n_f is replaced by $-3\beta_0/2$.

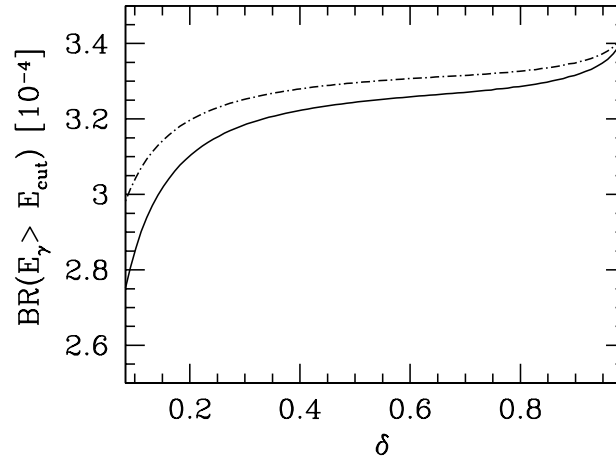


Figure 5.3: Dependence of the branching ratio on the photon energy cut, $E_{\text{cut}} = \frac{m_b}{2}(1 - \delta)$. The dash-dotted curve shows the NLL result, while the solid curve includes the $\mathcal{O}(\alpha_s^2 n_f)$ improvements. The renormalization scale is $\mu = 4.8$ GeV.

One observes that for $\mu \approx 5.5$ GeV the $\mathcal{O}(\alpha_s^2 n_f)$ corrections vanish and that they are negative (positive) for smaller (larger) values of μ . In this context it is instructive to look at the decomposition of the result. For this reason we show in the left plot of Fig. 5.2 the $\mathcal{O}(\alpha_s^2 n_f)$ corrections where either $M_1^{(2)}$ and $M_2^{(2)}$ or $M_7^{(2)}$ is artificially set to zero which corresponds to the short-dashed and long-dashed curve, respectively. This illustrates that there is a large cancellation between the negative contribution from O_7 and the one from O_1 and O_2 which is, of course, also present in the amplitude D . The effect of the $\alpha_s^2 n_f$ corrections from the operator O_8 is significantly smaller and at most of the order of 2% in the considered interval for μ .

Fig. 5.2 furthermore illustrates that the μ dependence of the $\mathcal{O}(\alpha_s^2 n_f)$ improved prediction for the branching ratio is somewhat flatter than in the NLL case if we restrict ourselves to $\mu \geq 4$ GeV. This is a welcome feature of our result, however, in general we cannot expect to reduce the μ dependence as the solid curve only represents a part of the $\mathcal{O}(\alpha_s^2)$ result. Indeed, we obtain a stronger μ -dependence in the region below 4 GeV. In Fig. 5.3 we show the dependence of the kinematical branching ratio on the photon energy cut. The dash-dotted line shows the NLL result, while the solid curve includes the order $\alpha_s^2 n_f$ improvements. We should mention at this point that we did not include any non-perturbative effects in the photon energy spectrum. The main purpose of this figure is to illustrate how the order $\alpha_s^2 n_f$ contributions modify the NLL result.

6 Conclusions

In this paper a first step towards a complete NNLL calculation is undertaken and radiative corrections to the matrix elements of the operators O_1 , O_2 , O_7 and O_8 are computed. More precisely, we consider the contributions of order $\alpha_s^2 n_f$ which are induced by a massless quark loop. It is expected that these corrections, after replacing n_f by $-3\beta_0/2$, may give an important contribution to the full order α_s^2 corrections. Furthermore, motivated by the NLL analysis, we expect that the $\mathcal{O}(\alpha_s^2 n_f)$ corrections to the matrix elements numerically dominate the ones of the same order to the Wilson coefficient functions and to the anomalous dimension matrix.

In practice our calculation requires the evaluation of two- and three-loop diagrams in the case of O_7 , O_8 and O_1 , O_2 , respectively. Furthermore, in order to obtain an infrared finite result in the case of O_7 , also the contributions from the gluon bremsstrahlung and from the quark-pair emission process are taken into account which requires the evaluation of three- and four-particle phase space integrals, respectively. All calculations are performed analytically where an expansion in m_c/m_b is applied to the three-loop diagrams. For practical purposes this expansion is equivalent to the exact result.

As far as the numerical impact of our result is concerned, we observe a striking cancelation among the individual contributions at order $\alpha_s^2 n_f$. When using a photon energy cut of $E_{\text{cut}} = m_b/20$, the $\mathcal{O}(\alpha_s^2 n_f)$ terms reduce (after replacing n_f by $-3\beta_0/2$) the branching ratio by -0.98% for $\mu = m_b = 4.8$ GeV and lead to corrections of -3.9% and $+3.4\%$ for $\mu = 3.0$ GeV and $\mu = 9.6$ GeV, respectively.

Acknowledgements

We would like to thank M. Misiak for making available to us his results for the renormalization constants of the operator mixing which provided important checks for our calculation. M.S. thanks T. Teubner for discussions on the quark-pair emission process. We thank A. Parkhomenko for carefully reading the manuscript. Our work is partially supported by the Swiss National Foundation and by RTN, BBW-Contract N0. 01.0357 and EC-Contract HPRN-CT-2002-00311 (EURIDICE).

A Building blocks

The three-loop diagrams involving O_1 and O_2 as well as the two-loop graphs involving O_7 and O_8 can be calculated by using one or more of the building blocks I_β , $J_{\alpha\beta}$ and $K_{\beta\beta'}^f$ to be discussed in this appendix. The corresponding diagrams are shown in Figs. [A.1](#) and [A.2](#) where the color indices are suppressed.

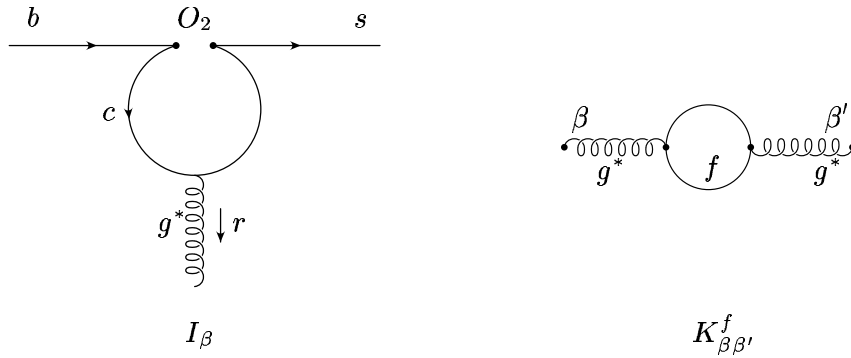


Figure A.1: The building blocks I_β and $K_{\beta\beta'}^f$ which are used in the calculation of the Feynman diagrams. The curly lines represent virtual gluons, whereas the letters b , c and s stand for the corresponding quark (f stands for a generic quark of mass m_f). Note that the external gluons are not amputated in the case of $K_{\beta\beta'}^f$.

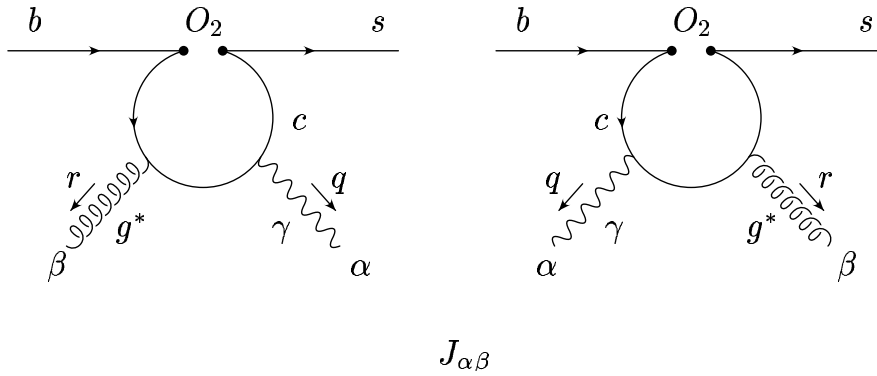


Figure A.2: The building block $J_{\alpha\beta}$ used in the calculation of the Feynman diagrams involving O_1 and O_2 . The curly and wavy lines represent off-shell gluons and on-shell photons, respectively.

The calculation of I_β is straightforward and yields

$$I_\beta = -\frac{g_s}{4\pi^2} \Gamma(\epsilon) \mu^{2\epsilon} e^{\gamma_E \epsilon} (1-\epsilon) e^{i\pi\epsilon} (r_\beta \not{\gamma} - r^2 \gamma_\beta) L \frac{\lambda}{2} \int_0^1 dx [x(1-x)]^{1-\epsilon} \left[r^2 - \frac{m_c^2}{x(1-x)} + i\delta \right]^{-\epsilon}, \quad (70)$$

where r is the momentum of the virtual gluon emitted from the c -quark loop. In the three-loop diagrams shown in Fig. 2.1 (cf. Section 2.1), the free index β will be contracted with the corresponding index of the dressed gluon propagator $K_{\beta\beta'}^f$.

It is also quite simple to obtain the building block $K_{\beta\beta'}^f$ (i.e., the dressed gluon propagator)

which can be cast into the form

$$K_{\beta\beta'}^f = -\frac{g_s^2}{2\pi^2} T \Gamma(\epsilon) e^{\gamma_E \epsilon} e^{i\pi\epsilon} \mu^{2\epsilon} \frac{1}{i} \frac{g_{\beta\beta'} - \frac{r_{\beta} r_{\beta'}}{r^2}}{r^2 + i\delta} \int_0^1 dx x(1-x) (x(1-x)r^2 - m_f^2 + i\delta)^{-\epsilon}, \quad (71)$$

where m_f denotes the mass of the quarks and $T = \frac{1}{2}$. Note that this expression is independent of the gauge parameter ξ which enters the free gluon propagators in the construction of $K_{\beta\beta'}^f$, when working in an arbitrary R_ξ gauge.

The building block $J_{\alpha\beta}$ is somewhat more involved. Adopting the notation of Ref. [34], it reads (for an on-shell photon) [20]

$$J_{\alpha\beta} = \frac{e g_s Q_u}{16 \pi^2} \left[E(\alpha, \beta, r) \Delta i_5 + E(\alpha, \beta, q) \Delta i_6 - E(\beta, r, q) \frac{r_\alpha}{q r} \Delta i_{23} - E(\alpha, r, q) \frac{r_\beta}{q r} \Delta i_{25} - E(\alpha, r, q) \frac{q_\beta}{q r} \Delta i_{26} \right] L \frac{\lambda}{2}, \quad (72)$$

where q and r denote the momenta of the on-shell photon and the off-shell gluon, respectively. When inserted into the full diagrams in Fig. 2.2, the indices α and β will be contracted with the polarization vector ε of the photon and with the dressed gluon propagator $K_{\beta\beta'}^f$, respectively. The matrix $E(\alpha, \beta, r)$ is defined as

$$E(\alpha, \beta, r) = \frac{1}{2} (\gamma_\alpha \gamma_\beta \not{r} - \not{r} \gamma_\beta \gamma_\alpha), \quad (73)$$

and the dimensionally regularized quantities Δi_k occurring in Eq. (72) read

$$\begin{aligned} \Delta i_5 &= 4 B^+ \int_S dx dy [4(qr)xy(1-x)\epsilon + r^2x(1-x)(1-2x)\epsilon \\ &\quad + (1-3x)C] C^{-1-\epsilon}, \\ \Delta i_6 &= 4 B^+ \int_S dx dy [-4(qr)xy(1-y)\epsilon - r^2x(2-2x+2xy-y)\epsilon \\ &\quad - (1-3y)C] C^{-1-\epsilon}, \\ \Delta i_{23} &= -\Delta i_{26} = 8 B^+(qr) \int_S dx dy xy \epsilon C^{-1-\epsilon}, \\ \Delta i_{25} &= -8 B^+(qr) \int_S dx dy x(1-x) \epsilon C^{-1-\epsilon}, \end{aligned} \quad (74)$$

where $B^+ = (1 + \epsilon)\Gamma(\epsilon) e^{\gamma_E \epsilon} \mu^{2\epsilon}$ and C is given by

$$C = m_c^2 - 2xy(qr) - r^2x(1-x) - i\delta.$$

The integration over the Feynman parameters x and y is restricted to the simplex S , i.e. $y \in [0, 1 - x]$, $x \in [0, 1]$. Due to Ward identities, the quantities Δi_k are not independent of one another. Namely,

$$q^\alpha J_{\alpha\beta} = 0 \quad \text{and} \quad r^\beta J_{\alpha\beta} = 0$$

imply that Δi_5 and Δi_6 can be expressed as

$$\Delta i_5 = \Delta i_{23}, \quad \Delta i_6 = \frac{r^2}{qr} \Delta i_{25} + \Delta i_{26}. \quad (75)$$

B Regularized three-loop results for $\langle s\gamma | \mathbf{O}_2 | b \rangle$

In Section 2.1 we explained in some detail the calculation of the virtual three-loop corrections to $\langle s\gamma | \mathbf{O}_2 | b \rangle$. Here we give the results for the four gauge-invariant sets of graphs depicted in Figs. 2.1 and 2.2. The results read, using $z = m_c^2/m_b^2$ and $L = \ln(z)$:

$$\begin{aligned} M_{2,\text{bare}}^{(2)}(1) &= \left\{ \frac{1}{\epsilon} \left[-\frac{1}{81\epsilon} - \frac{29}{243} + \frac{1}{6} (5 + 2L) z + \frac{1}{6} (5 - 2L + 2L^2 - 2\pi^2) z^2 \right. \right. \\ &\quad + \frac{1}{81} (17 + 30L - 18L^2 + 18\pi^2) z^3 - \frac{i\pi}{27} (1 - 9z + 9z^2 - 18Lz^2 \\ &\quad \left. \left. - 10z^3 + 12Lz^3) \right] \left(\frac{m_b}{\mu} \right)^{-6\epsilon} + \left[-\frac{1063}{1458} + \frac{19\pi^2}{324} \right. \right. \\ &\quad + \frac{1}{18} (61 + 4L - 9L^2 - 10\pi^2) z + \frac{1}{18} (79 - 22L + 28L^2 - 8L^3 - 9\pi^2 \\ &\quad \left. \left. - 14L\pi^2 - 12\zeta(3)) z^2 + \frac{1}{81} (63 - 27L - 36L^2 + 24L^3 - 59\pi^2 + 42L\pi^2 + \right. \right. \\ &\quad \left. \left. 36\zeta(3)) z^3 - \frac{i\pi}{162} (58 - 441z - 9(23 + 38L - 6L^2 - 12\pi^2) z^2 \right. \right. \\ &\quad \left. \left. - 12(4 + 3L + 3L^2 + 6\pi^2) z^3) \right] + \mathcal{O}(z^4) \right\} \left(\frac{\alpha_s}{\pi} \right)^2 C_F T n_f Q_d \langle s\gamma | \mathbf{O}_7 | b \rangle_{\text{tree}}, \\ M_{2,\text{bare}}^{(2)}(2) &= \left\{ \frac{1}{\epsilon} \left[\frac{7}{162\epsilon} + \frac{5}{486} + \frac{1}{18} (3 - \pi^2) z + \frac{2\pi^2}{9} z^{3/2} - \frac{1}{6} (6 - 6L + L^2) z^2 \right. \right. \\ &\quad \left. \left. + \frac{1}{324} (157 - 6L - 144L^2 - 60\pi^2) z^3 \right] \left(\frac{m_b}{\mu} \right)^{-6\epsilon} \right. \\ &\quad + \left[-\frac{1387}{1458} + \frac{11\pi^2}{72} + \frac{1}{54} (96 - 17\pi^2 - 126\zeta(3)) z \right. \\ &\quad \left. + \frac{\pi^2}{27} (40 - 18L - 72 \ln(2)) z^{3/2} \right. \\ &\quad \left. + \frac{1}{36} (213 + 102L - 40L^2 + 8L^3 + 34\pi^2 + 96\zeta(3)) z^2 - \frac{20\pi^2}{9} z^{5/2} \right. \end{aligned}$$

$$\begin{aligned}
 & \left. + \frac{1}{324} (2799 - 995L - 198L^2 + 192L^3 - 10\pi^2 - 60L\pi^2 - 936\zeta(3)) z^3 \right] \\
 & + \mathcal{O}(z^{7/2}) \left. \right\} \left(\frac{\alpha_s}{\pi} \right)^2 C_F T n_f Q_d \langle s\gamma|O_7|b\rangle_{\text{tree}}, \\
 M_{2,\text{bare}}^{(2)}(3) = & \left\{ \frac{1}{\epsilon} \left[\frac{1}{36\epsilon} + \frac{137}{432} - \frac{1}{36} (18 + 24L + 3L^2 + 2L^3 - 3\pi^2 - 6L\pi^2 - 24\zeta(3)) z \right. \right. \\
 & - \frac{1}{36} (15 + 6L - 6L^2 + 2L^3 + 6\pi^2 - 6L\pi^2 - 24\zeta(3)) z^2 \\
 & + \frac{1}{36} (17 - 12L) z^3 + \frac{i\pi}{36} (3 - 24z - 6Lz - 6L^2z + 2\pi^2z - 6z^2 + 12Lz^2 \\
 & \left. \left. - 6L^2z^2 + 2\pi^2z^2 - 12z^3) \right] \left(\frac{m_b}{\mu} \right)^{-6\epsilon} \right. \\
 & + \left[\frac{6029}{2592} - \frac{17\pi^2}{144} - \frac{1}{1080} (7200 + 6240L - 120L^2 + 220L^3 - 105L^4 \right. \\
 & - 2040\pi^2 - 1200L\pi^2 + 90L^2\pi^2 + 111\pi^4 - 4440\zeta(3) + 1440L\zeta(3)) z \\
 & - \frac{1}{2160} (15135 - 5790L - 1050L^2 + 980L^3 - 210L^4 - 30\pi^2 - 780L\pi^2 \\
 & + 180L^2\pi^2 + 222\pi^4 - 4560\zeta(3) + 2880L\zeta(3)) z^2 + \frac{1}{72} (3 - 2L + 72\pi^2) z^3 \\
 & + \frac{i\pi}{432} (411 - 4(786 + 192L + 93L^2 - 24L^3 - 49\pi^2 - 12L\pi^2 - 72\zeta(3))) z \\
 & \left. \left. + 2(309 + 102L - 186L^2 + 48L^3 - 10\pi^2 + 24L\pi^2 + 144\zeta(3)) z^2 \right. \right. \\
 & \left. \left. + 8(75 - 54L) z^3 \right] + \mathcal{O}(z^4) \right\} \left(\frac{\alpha_s}{\pi} \right)^2 C_F T n_f Q_u \langle s\gamma|O_7|b\rangle_{\text{tree}}, \\
 M_{2,\text{bare}}^{(2)}(4) = & \left\{ \frac{1}{\epsilon} \left[\frac{1}{18\epsilon} + \frac{127}{432} - \frac{1}{36} (12 + 6L - L^3 - \pi^2 - 3L\pi^2 - 12\zeta(3)) z \right. \right. \\
 & - \frac{1}{36} (6 - 6L + 3L^2 - L^3 + 2\pi^2 + 24\zeta(3)) z^2 - \frac{1}{324} (27 + 108L \\
 & \left. \left. - 81L^2 - 27\pi^2) z^3 \right] \left(\frac{m_b}{\mu} \right)^{-6\epsilon} \right. \\
 & + \left[\frac{2839}{2592} + \frac{13\pi^2}{144} - \frac{1}{2160} (9480 + 2040L + 180L^2 - 340L^3 + 105L^4 \right. \\
 & + 260\pi^2 - 720L\pi^2 + 30L^2\pi^2 - 439\pi^4 - 3360\zeta(3) - 8640L\zeta(3)) z \\
 & \left. \left. - \frac{8\pi^2}{3} z^{3/2} + \frac{1}{4320} (29895 - 6270L - 1410L^2 + 740L^3 - 210L^4 + 920\pi^2 \right. \right.
 \end{aligned}$$

$$\begin{aligned}
 & -480L\pi^2 + 120L^2\pi^2 - 52\pi^4 - 16320\zeta(3) + 4320L\zeta(3) \left. z^2 + \frac{40\pi^2}{27}z^{5/2} \right. \\
 & \left. - \frac{1}{216} (1358 - 477L - 99L^2 + 90L^3 + 63\pi^2 - 18L\pi^2 - 432\zeta(3)) z^3 \right] \\
 & + \mathcal{O}(z^{7/2}) \left. \right\} \left(\frac{\alpha_s}{\pi} \right)^2 C_F T n_f Q_u \langle s\gamma | O_7 | b \rangle_{\text{tree}}.
 \end{aligned}$$

In these expressions, ζ denotes the Riemann ζ function with the value $\zeta(3) \approx 1.2020569$. $Q_u = 2/3$ and $Q_d = -1/3$ are the electric charge factors of the up- and down-type quarks, respectively, while $C_F = 4/3$ and $T = 1/2$ are color factors.

C Correction functions needed for the NLL result

The renormalization scale independent parts of the virtual corrections in NLL order precision, encoded in the functions $r_i^{(1)}$, appearing in Eq. (58), read

$$\begin{aligned}
 r_1^{(1)} &= -\frac{1}{6}r_2^{(1)}, \\
 r_2^{(1)} &= \frac{2}{243} \left\{ -833 + 144\pi^2 z^{3/2} \right. \\
 & \quad + [1728 - 180\pi^2 - 1296\zeta(3) + (1296 - 324\pi^2)L + 108L^2 + 36L^3] z \\
 & \quad + [648 + 72\pi^2 + (432 - 216\pi^2)L + 36L^3] z^2 \\
 & \quad + [-54 - 84\pi^2 + 1092L - 756L^2] z^3 \left. \right\} \\
 & \quad + \frac{16\pi i}{81} \left\{ -5 + [45 - 3\pi^2 + 9L + 9L^2] z + [-3\pi^2 + 9L^2] z^2 \right. \\
 & \quad \left. + [28 - 12L] z^3 \right\} + \mathcal{O}(z^{7/2}), \\
 r_7^{(1)} &= \frac{32}{9} - \frac{8}{9}\pi^2, \\
 r_8^{(1)} &= -\frac{4}{27}(-33 + 2\pi^2 - 6i\pi), \tag{76}
 \end{aligned}$$

where z is defined as $z = m_c^2/m_b^2$ and the symbol L denotes $L = \ln(z)$. The quantities $l_i^{(1)}$, appearing in Eq. (58), read

$$l_1^{(1)} = -\frac{1}{6}l_2^{(1)}, \quad l_2^{(1)} = \frac{416}{81}, \quad l_7^{(1)} = \frac{8}{3}, \quad l_8^{(1)} = -\frac{32}{9}. \tag{77}$$

Notice that $r_3^{(1)}$, $r_4^{(1)}$, $r_5^{(1)}$ and $r_6^{(1)}$, as well as $l_3^{(1)}$, $l_4^{(1)}$, $l_5^{(1)}$ and $l_6^{(1)}$ are not needed in the approximation $C_i^{\text{eff}}(\mu) = 0$ ($i = 3, 4, 5, 6$).

The functions f_{ij} needed for Eq. (65) are taken from Ref. [12] and are listed here for completeness. Note that $f_{77}(\delta)$ differs from the one given in Ref. [12] in order to be

compatible with our r_7 given in Eq. (76)¹.

$$f_{11}(\delta) = \frac{1}{36}f_{22}(\delta), \quad f_{12}(\delta) = -\frac{1}{3}f_{22}(\delta), \quad f_{17}(\delta) = -\frac{1}{6}f_{27}(\delta), \quad f_{18}(\delta) = -\frac{1}{6}f_{28}(\delta),$$

$$\begin{aligned} f_{22}(\delta) &= \frac{16z}{27} \left[\delta \int_0^{(1-\delta)/z} dt (1-zt) \left| \frac{G(t)}{t} + \frac{1}{2} \right|^2 \right. \\ &\quad \left. + \int_{(1-\delta)/z}^{1/z} dt (1-zt)^2 \left| \frac{G(t)}{t} + \frac{1}{2} \right|^2 \right], \\ f_{27}(\delta) &= -\frac{8z^2}{9} \left[\delta \int_0^{(1-\delta)/z} dt \operatorname{Re} \left(G(t) + \frac{t}{2} \right) \right. \\ &\quad \left. + \int_{(1-\delta)/z}^{1/z} dt (1-zt) \operatorname{Re} \left(G(t) + \frac{t}{2} \right) \right], \\ f_{28}(\delta) &= -\frac{1}{3}f_{27}(\delta), \\ f_{77}(\delta) &= \frac{10}{3}\delta + \frac{1}{3}\delta^2 - \frac{2}{9}\delta^3 + \frac{1}{3}\delta(\delta-4)\ln(\delta) - \frac{31}{9}, \\ f_{78}(\delta) &= \frac{8}{9} \left[\operatorname{Li}_2(1-\delta) - \frac{\pi^2}{6} - \delta \ln(\delta) + \frac{9}{4}\delta - \frac{1}{4}\delta^2 + \frac{1}{12}\delta^3 \right], \\ f_{88}(\delta) &= \frac{1}{27} \left\{ -2 \ln \left(\frac{m_b}{m_s} \right) \left[\delta^2 + 2\delta + 4 \ln(1-\delta) \right] + 4 \operatorname{Li}_2(1-\delta) - \frac{2\pi^2}{3} \right. \\ &\quad \left. - \delta(2+\delta) \ln(\delta) + 8 \ln(1-\delta) + 7\delta + 3\delta^2 - \frac{2}{3}\delta^3 \right\}, \end{aligned} \tag{78}$$

where the function $G(t)$ is defined through

$$G(t) = \begin{cases} -2 \arctan^2 \left(\sqrt{\frac{t}{4-t}} \right) & \text{for } t < 4 \\ -\frac{\pi^2}{2} + 2 \ln^2 \left(\frac{1}{2}(\sqrt{t} + \sqrt{t-4}) \right) - 2i\pi \ln \left(\frac{1}{2}(\sqrt{t} + \sqrt{t-4}) \right) & \text{for } t \geq 4. \end{cases}$$

The functions f_{ij} associated with the operators $O_3 - O_6$ are not needed in our approximation.

Note that in the numerics we set m_s equal to zero in all terms except $f_{88}(\delta)$, where a value of $m_b/m_s = 50$ is chosen.

¹The additional, δ -independent addend appearing in our $f_{77}(\delta)$ is such that $f_{77}(1)$ vanishes: the contribution of $f_{77}(\delta)$ at $\delta = 1$ is already absorbed into our r_7 .

D $\mathcal{O}(\alpha_s^2 n_f)$ contributions to various Z factors

In this appendix we give the results for the $\mathcal{O}(\alpha_s^2 n_f)$ contributions for various Z factors entering the calculation of the counterterm $M_{7,ct_2}^{(2),(a)}$ in Eq. (45) in Section 3. For the meaning of the various terms, see the text after Eq. (45). The $\mathcal{O}(\alpha_s^2 n_f)$ contributions to the relevant Z factors read

$$\begin{aligned} \delta Z_{2,b}^{(2),n_f} &= \left(\frac{\alpha_s}{\pi}\right)^2 \frac{C_F T n_f}{288} \left(\frac{18}{\epsilon} \left(1 - 4 \ln(f) - 8 \ln\left(\frac{m_b}{\mu}\right) \right) + 443 \right. \\ &\quad \left. + 30\pi^2 + 96 \ln(f) + 72 \ln^2(f) - 264 \ln\left(\frac{m_b}{\mu}\right) \right. \\ &\quad \left. + 288 \ln(f) \ln\left(\frac{m_b}{\mu}\right) + 432 \ln^2\left(\frac{m_b}{\mu}\right) \right), \end{aligned} \quad (79)$$

$$\begin{aligned} \delta Z_{2,s}^{(2),n_f} &= \left(\frac{\alpha_s}{\pi}\right)^2 \frac{C_F T n_f}{96} \left(\frac{6}{\epsilon} \left(1 - 4 \ln(f) - 8 \ln\left(\frac{m_b}{\mu}\right) \right) - 5 + 2\pi^2 \right. \\ &\quad \left. - 44 \ln(f) + 12 \ln^2(f) + 24 \ln(f) \ln(r) - 88 \ln\left(\frac{m_b}{\mu}\right) \right. \\ &\quad \left. + 96 \ln(f) \ln\left(\frac{m_b}{\mu}\right) + 48 \ln(r) \ln\left(\frac{m_b}{\mu}\right) + 144 \ln^2\left(\frac{m_b}{\mu}\right) \right), \end{aligned} \quad (80)$$

$$\begin{aligned} \delta Z_{m_b}^{\text{on},(2),n_f} &= \left(\frac{\alpha_s}{\pi}\right)^2 \frac{C_F T n_f}{96} \left(71 + 8\pi^2 - 104 \ln\left(\frac{m_b}{\mu}\right) + 48 \ln^2\left(\frac{m_b}{\mu}\right) \right. \\ &\quad \left. + \frac{10}{\epsilon} - \frac{12}{\epsilon^2} \right), \end{aligned} \quad (81)$$

$$\delta Z_{77}^{(2),n_f} = \left(\frac{\alpha_s}{\pi}\right)^2 \frac{C_F n_f T}{36\epsilon} \left(\frac{6}{\epsilon} - 7 \right), \quad (82)$$

with $r = m_s^2/m_b^2$ and $f = m_f^2/m_b^2$.

E Implementing the photon energy cut-off in the $\mathcal{O}(\alpha_s n_f)$ terms

In this appendix we provide the formulas which are needed to calculate the $\mathcal{O}(\alpha_s^2 n_f)$ piece of the kinematical branching ratio $\text{BR}(b \rightarrow X_s \gamma)_{E_\gamma \geq E_{\text{cut}}}$, where E_{cut} represents a cut-off on the photon energy. As can be seen from the structure of Eq. (67), this amounts to calculate $\Gamma_{77}^{(2),n_f}(b \rightarrow X_s \gamma)_{E_\gamma \leq E_{\text{cut}}}$, which is contained in the quantity D of Eq. (67).

Note that only the gluon bremsstrahlung- and the quark-pair emission processes enter the calculation for $\Gamma_{77}^{(2),n_f}(b \rightarrow X_s \gamma)_{E_\gamma \leq E_{\text{cut}}}$ as the photon energy in the virtual contributions

is concentrated at $m_b/2$. The $\mathcal{O}(\alpha_s^2 n_f)$ contribution to $\Gamma_{77}^{(2),n_f}(b \rightarrow X_s \gamma)_{E_\gamma \leq E_{\text{cut}}}$ can be written in the form

$$\Gamma_{77}^{(2),n_f}(b \rightarrow X_s \gamma)_{E_\gamma \leq E_{\text{cut}}} = \Gamma_{77}^0 \left[\hat{\Gamma}_{77}^{(2),(b)}(E_\gamma \leq E_{\text{cut}}) + \hat{\Gamma}_{77}^{(2),(c)}(E_\gamma \leq E_{\text{cut}}) \right], \quad (83)$$

where (b) and (c) denote the gluon bremsstrahlung- and the quark-pair emission process, respectively, and Γ_{77}^0 is given in Eq. (32). Like in Section 3 we use a regulator mass m_f for the secondary quark-antiquark pair which means that Eq. (83) can be calculated in $d = 4$ dimensions and with $m_s = 0$.

The calculation for the gluon bremsstrahlung piece $\hat{\Gamma}_{77}^{(2),(b)}(E_\gamma \leq E_{\text{cut}})$ is straightforward. Adopting the notation

$$E_{\text{cut}} = \frac{m_b}{2}(1 - \delta) = E_{\text{max}}(1 - \delta), \quad (84)$$

the result reads

$$\begin{aligned} \hat{\Gamma}_{77}^{(2),(b)}(E_\gamma \leq E_{\text{cut}}) &= \left(\frac{\alpha_s}{4\pi} \right)^2 \frac{4C_F T n_f}{9} (31 - 30\delta - 3\delta^2 + 2\delta^3 + 21 \ln(\delta)) \\ &\quad + 12\delta \ln(\delta) - 3\delta^2 \ln(\delta) + 6 \ln^2(\delta) \left(\ln(f) + 2 \ln \left(\frac{m_b}{\mu} \right) \right), \end{aligned}$$

with $f = m_f^2/m_b^2$.

The calculation for $\hat{\Gamma}_{77}^{(2),(c)}(E_\gamma \leq E_{\text{cut}})$ is somewhat more involved but still can be performed analytically, yielding

$$\begin{aligned} \hat{\Gamma}_{77}^{(2),(c)}(E_\gamma \leq E_{\text{cut}}) &= \left(\frac{\alpha_s}{4\pi} \right)^2 \frac{2C_F T n_f}{9} \left(-147 - 9\pi^2 + 48\zeta(3) - 48\text{Li}_3(\delta) + 54\text{Li}_2(\delta) \right. \\ &\quad - \ln(\delta) (85 - 4\pi^2 - 54 \ln(1 - \delta) - 24\text{Li}_2(\delta)) + 13 \ln^2(\delta) + 12 \ln^3(\delta) \\ &\quad + \delta (160 + 4\pi^2 - 24\text{Li}_2(\delta) - 24 \ln(1 - \delta) \ln(\delta) - 94 \ln(\delta) + 36 \ln^2(\delta)) \\ &\quad + \delta^2 (1 - \pi^2 + 6\text{Li}_2(\delta) + 6 \ln(1 - \delta) \ln(\delta) + 19 \ln(\delta) - 9 \ln^2(\delta)) \\ &\quad - \delta^3 (14 - 4 \ln(\delta)) - 2 \ln(f) (31 - 30\delta - 3\delta^2 + 2\delta^3 + 21 \ln(\delta) \\ &\quad \left. + 12\delta \ln(\delta) - 3\delta^2 \ln(\delta) + 6 \ln^2(\delta)) \right). \quad (85) \end{aligned}$$

Note that the sum of $\hat{\Gamma}_{77}^{(2),(b)}(E_\gamma \leq E_{\text{cut}})$ and $\hat{\Gamma}_{77}^{(2),(c)}(E_\gamma \leq E_{\text{cut}})$ is finite in the limit $m_f \rightarrow 0$. This completes the calculation of $\Gamma_{77}^{(2),n_f}(b \rightarrow X_s \gamma)_{E_\gamma \leq E_{\text{cut}}}$, defined in Eq. (83).

We note that differentiating $\Gamma_{77}^{(2),n_f}(b \rightarrow X_s \gamma)_{E_\gamma \leq E_{\text{cut}}}$ with respect to the photon energy cut E_{cut} generates the corresponding term of order $\alpha_s^2 n_f$ to the photon energy spectrum. The result we obtain is in complete agreement with Eq. (9) of Ref. [25], where $\mathcal{O}(\alpha_s^2 n_f)$ corrections to the photon energy spectrum were calculated.

References

- [1] S. Chen *et al.* (CLEO Collaboration), *Phys. Rev. Lett.* **87** (2001) 251807, [hep-ex/0108032](#).
- [2] K. Abe *et al.* (Belle Collaboration), *Phys. Lett. B* **511** (2001) 151, [hep-ex/0103042](#).
- [3] R. Barate *et al.* (ALEPH Collaboration), *Phys. Lett. B* **429** (1998) 169.
- [4] B. Aubert *et al.* (BABAR Collaboration), [hep-ex/0207074](#).
- [5] B. Aubert *et al.* (BABAR Collaboration), [hep-ex/0207076](#).
- [6] C. Jessop, SLAC-PUB-9610.
- [7] A. Czarnecki and W. J. Marciano, *Phys. Rev. Lett.* **81** (1998) 277, [hep-ph/9804252](#).
- [8] A. L. Kagan and M. Neubert, *Eur. Phys. J. C* **7** (1999) 5, [hep-ph/9805303](#).
- [9] K. Baranowski and M. Misiak, *Phys. Lett. B* **483** (2000) 410, [hep-ph/9907427](#).
- [10] P. Gambino and U. Haisch, *J. High Energy Phys.* **0009** (2000) 001, [hep-ph/0007259](#).
P. Gambino and U. Haisch, *J. High Energy Phys.* **0110** (2001) 020, [hep-ph/0109058](#).
- [11] T. Hurth, *Rev. Mod. Phys.* **75** (2003) 1159, [hep-ph/0212304](#).
- [12] K.G. Chetyrkin, M. Misiak, and M. Münz, *Phys. Lett. B* **400** (1997) 206, E:*Phys. Lett. B* **425** (1998) 414, [hep-ph/9612313](#).
- [13] M. Ciuchini, G. Degrassi, P. Gambino, and G. F. Giudice, *Nucl. Phys. B* **527** (1998) 21, [hep-ph/9710335](#).
- [14] F. M. Borzumati and C. Greub, *Phys. Rev. D* **58** (1998) 074004; *Phys. Rev. D* **59** (1998) 057501.
- [15] A. J. Buras, A. Kwiatkowski, and N. Pott, *Nucl. Phys. B* **517** (1998) 353;
A. J. Buras, A. Kwiatkowski, and N. Pott, *Phys. Lett. B* **414** (1997) 157, E:*Phys. Lett. B* **434** (1998) 459, [hep-ph/9707482](#).
- [16] P. Gambino and M. Misiak, *Nucl. Phys. B* **611** (2001) 338, [hep-ph/0104034](#).
- [17] A. J. Buras, A. Czarnecki, M. Misiak, and J. Urban, *Nucl. Phys. B* **631** (2002) 219, [hep-ph/0203135](#).
- [18] A. Ali, E. Lunghi, C. Greub, and G. Hiller, *Phys. Rev. D* **66** (2002) 034002, [hep-ph/0112300](#).
- [19] A. J. Buras, M. Misiak, M. Münz, and S. Pokorski, *Nucl. Phys. B* **424** (1994) 374, [hep-ph/9311345](#).

-
- [20] C. Greub, T. Hurth, and D. Wyler, *Phys. Rev. D* **54** (1996) 3350.
- [21] M. Beneke and V. M. Braun, *Phys. Lett. B* **348** (1995) 513, [hep-ph/9411229](#).
- [22] S. J. Brodsky, G. P. Lepage, and P. B. Mackenzie, *Phys. Rev. D* **28** (1983) 228.
- [23] M. E. Luke, M. J. Savage, and M. B. Wise, *Phys. Lett. B* **345** (1995) 301, [hep-ph/9410387](#).
- [24] A. Czarnecki and K. Melnikov, *Phys. Rev. D* **59** (1999) 014036, [hep-ph/9804215](#).
- [25] Z. Ligeti, M. E. Luke, A. V. Manohar, and M. B. Wise, *Phys. Rev. D* **60** (1999) 034019, [hep-ph/9903305](#).
- [26] C. Greub and P. Liniger, *Phys. Lett. B* **494** (2000) 237.
- [27] H. H. Asatryan, H. M. Asatrian, C. Greub, and M. Walker. *Phys. Rev. D* **65** (2002) 074004.
- [28] M. Misiak, private communication.
- [29] A. Falk, M. Luke, and M. Savage, *Phys. Rev. D* **49** (1994) 3367;
I.I. Bigi, M. Shifman, N.G. Uraltsev, and A.I. Vainshtein, *Phys. Rev. Lett.* **71** (1993) 496;
A.V. Manohar and M.B. Wise, *Phys. Rev. D* **49** (1994) 1310;
A. Falk, M. Luke, and M. Savage, *Phys. Rev. D* **53** (1996) 2491.
- [30] M.B. Voloshin, *Phys. Lett. B* **397** (1997) 275;
Z. Ligeti, L. Randall, and M.B. Wise, *Phys. Lett. B* **402** (1997) 178;
A.K. Grant, A.G. Morgan, S. Nussinov, and R.D. Peccei, *Phys. Rev. D* **56** (1997) 3151; G. Buchalla, G. Isidori, and S.J. Rey, *Nucl. Phys. B* **511** (1998) 594.
- [31] A. Ali and C. Greub, *Z. Physik C* **49** (1991) 431; *Phys. Lett. B* **259** (1991) 182; *Phys. Lett. B* **361** (1995) 146.
- [32] N. Pott, *Phys. Rev. D* **54** (1996) 938.
- [33] Y. Nir, *Phys. Lett. B* **221** (1989) 184.
- [34] H. Simma and D. Wyler, *Nucl. Phys. B* **344** (1990) 283.

PART IV

Review on the inclusive rare decays

$$B \rightarrow X_s \gamma \text{ and } B \rightarrow X_d \gamma$$

in the Standard Model

Review on the inclusive rare decays $B \rightarrow X_s \gamma$ and $B \rightarrow X_d \gamma$ in the Standard Model ¹

K. Bieri and C. Greub

*Institut für Theoretische Physik, Universität Bern,
CH-3012 Bern, Switzerland.*

ABSTRACT

We review the NLL QCD calculations for the branching ratio of $B \rightarrow X_s \gamma$ in the SM. In particular, we emphasize the problem related to the definition of the charm quark mass which leads to a rather large uncertainty of the NLL predictions. The various steps needed for a NNLL calculation, in which the m_c issue can be settled, is also sketched. We briefly summarize the results of a calculation of the $\mathcal{O}(\alpha_s^2 n_f)$ corrections to $\text{BR}(B \rightarrow X_s \gamma)$, which was recently performed as a first step in the NNLL program. We then also briefly review the status of the photon energy spectrum and show the comparison with experimental data. Finally, we review the status of the CKM suppressed decay mode $B \rightarrow X_d \gamma$.

¹Work partially supported by Schweizerischer Nationalfonds, SCOPES and NFSAT (CRDF) programs.

1 Introduction

In the Standard model (SM), rare B decays like $B \rightarrow X_s \gamma$ or $B \rightarrow X_s \ell^+ \ell^-$ are induced by one-loop diagrams, where virtual W bosons and up-type quarks are exchanged. In many extensions of the SM, there are additional contributions, where the SM particles in the loop are replaced by nonstandard ones, like charged Higgs bosons, gluinos, charginos etc. If the masses of these new particles are not heavier by many orders of magnitude than the heaviest SM particles, the new physics contributions to rare B meson decays are expected to be generically large. The sensitivity for nonstandard effects implies the possibility for an indirect observation of new physics, or allows to put limits on the masses and coupling parameters of the new particles.

It is obvious that it is only possible to fully exploit the new physics potential of these decays when both, precise measurements and precise theoretical SM calculations exist.

In the following we mainly concentrate on the decays $B \rightarrow X_s \gamma$ and $B \rightarrow X_d \gamma$, while the rare semileptonic decay $B \rightarrow X_s \ell^+ \ell^-$ is reviewed at this conference by T. Hurth [1]. There are experimental analyses of the branching ratio $\text{BR}(B \rightarrow X_s \gamma)$ by CLEO [2, 3, 4], ALEPH [5], BELLE [6], and BABAR [7] as shown in Fig. 1.1,

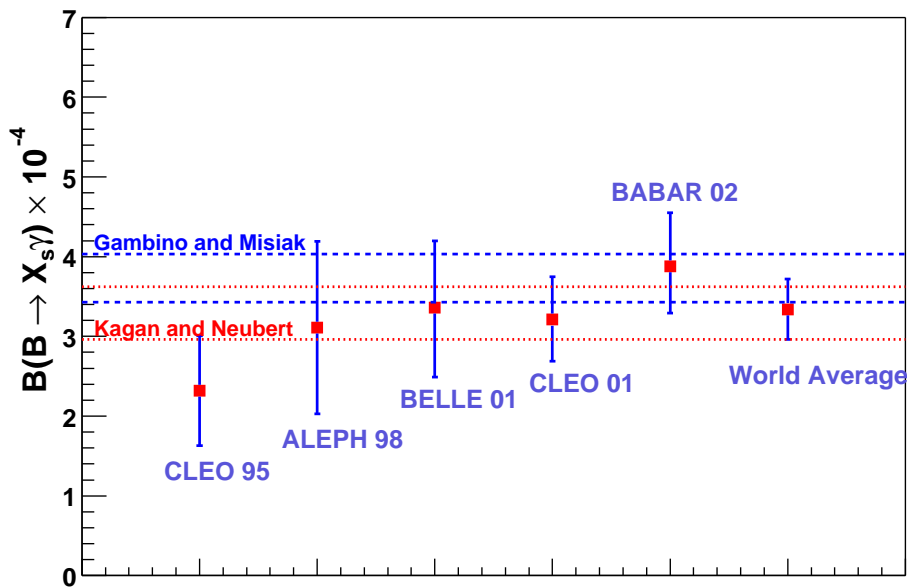


Figure 1.1: Branching ratio $\text{BR}(B \rightarrow X_s \gamma)$: The numbers attached to the various experiments reflect the year of publication of the corresponding result. The dashed (dotted) band shows the theoretical results based on the $\overline{\text{MS}}$ -bar (pole mass) interpretation of the charm quark mass; see eqs. (4) and (3). Figure taken from [7] and world average added from [8].

leading to the world average [8]

$$\text{BR}(B \rightarrow X_s \gamma)_{\text{exp}} = (3.34 \pm 0.38) \times 10^{-4}.$$

In contrast to the exclusive rare decay $B \rightarrow K^* \gamma$, the inclusive counterpart $B \rightarrow X_s \gamma$ is theoretically much cleaner as no specific model is needed to describe the hadronic final state. Indeed, nonperturbative effects in the inclusive decay mode are well under control due to the heavy quark expansion technique (HQE), which implies that the decay width $\Gamma(B \rightarrow X_s \gamma)$ is well approximated by the partonic decay rate $\Gamma(b \rightarrow X_s \gamma)$ which can be analyzed in renormalization group improved perturbation theory. The (nonperturbative) power corrections which scale like $1/m_b^2$ [9] and $1/m_c^2$ [10] were estimated to be well below 10%.

2 Theoretical framework

Short distance QCD effects enhance the partonic decay rate $\Gamma(b \rightarrow s \gamma)$ by more than a factor of two. Analytically, these QCD corrections contain large logarithms of the form $\alpha_s^n(m_b) \ln^m(m_b/M)$, where $M = m_t$ or $M = m_W$ and $m \leq n$ (with $n = 0, 1, 2, \dots$). In order to get a reasonable prediction for the decay rate, it turns out that one has to resum both, the leading-log (LL) terms ($m = n$) as well as the next-to-leading-log (NLL) terms ($m = n - 1$).

To achieve the necessary resummations, one usually constructs in a first step an effective low-energy theory and then resums the large logarithms by renormalization group techniques. The low energy theory is obtained by integrating out the heavy particles which in the SM are the top quark and the W -boson. The resulting effective Hamiltonian relevant for $b \rightarrow s \gamma$ in the SM and many of its extensions reads

$$H_{\text{eff}}(b \rightarrow s \gamma) = -\frac{4G_F}{\sqrt{2}} \lambda_t \sum_{i=1}^8 C_i(\mu) O_i(\mu), \quad (1)$$

where $O_i(\mu)$ are local operators consisting of light fields, $C_i(\mu)$ are the corresponding Wilson coefficients, which contain the complete top- and W - mass dependence, and $\lambda_t = V_{tb}V_{ts}^*$ with V_{ij} being the CKM matrix elements. The CKM dependence globally factorizes, because we work in the approximation $\lambda_u = 0$.

In the basis introduced by Misiak [11], the operators read

$$\begin{aligned} O_1 &= (\bar{s}_L \gamma^\mu T^a c_L) (\bar{c}_L \gamma_\mu T^a b_L), \\ O_2 &= (\bar{s}_L \gamma^\mu c_L) (\bar{c}_L \gamma_\mu b_L), \\ O_7 &= \frac{e}{16\pi^2} m_b(\mu) \bar{s} \sigma^{\mu\nu} R b F_{\mu\nu}, \\ O_8 &= \frac{g_s}{16\pi^2} m_b(\mu) \bar{s} \sigma^{\mu\nu} R T^a b G_{\mu\nu}^a. \end{aligned} \quad (2)$$

As the Wilson coefficients of the QCD penguin operators O_3, \dots, O_6 are small, we do not list them here.

A consistent calculation for $b \rightarrow s\gamma$ at NLL precision requires three steps:

- 1) a matching calculation of the full standard model theory with the effective theory at the scale $\mu = \mu_W$ to order α_s^1 for the Wilson coefficients, where μ_W denotes a scale of order M_W or m_t ;
- 2) a renormalization group evolution of the Wilson coefficients from the matching scale μ_W down to the low scale $\mu_b = \mathcal{O}(m_b)$, using the anomalous-dimension matrix to order α_s^2 ;
- 3) a calculation of the matrix elements of the operators at the scale $\mu = \mu_b$ to order α_s^1 .

As all three steps are rather involved, a common effort of several independent groups was needed in order to calculate the NLL prediction for $\text{BR}(B \rightarrow X_s\gamma)$ [12, 13, 14, 15, 11, 16, 17, 18]. For a detailed summary of the various steps and intermediate results, we refer to the recent review by T. Hurth [19]. However, we would like to point out that the most difficult part, viz. the calculation of three-loop anomalous dimensions performed by Chetyrkin, Misiak and Münz in 1996 [11], was only confirmed very recently by Gambino, Gorbahn and Haisch [20]. Their paper also contains the three-loop mixing of the four-Fermi operators into O_9 , which is important for the process $B \rightarrow X_s\ell^+\ell^-$.

During the completion of the NLL QCD corrections, also calculations of electroweak corrections were started [21, 22, 23]. At present, the corrections of order $\alpha_{\text{em}} \ln(\mu_b/M)$ [$\alpha_s \ln(\mu_b/M)$]ⁿ, as well as the subleading terms of order $\alpha_{\text{em}}[\alpha_s \ln(\mu_b/M)]^n$ [24] are systematically available.

3 NLL (and partial NNLL) results for $\text{BR}(B \rightarrow X_s\gamma)$

Combining NLL QCD corrections with the electroweak corrections just mentioned and also including the $1/m_b^2$ [9] and $1/m_c^2$ [10] power corrections, the branching ratio reads

$$\text{BR}(B \rightarrow X_s\gamma) = (3.32 \pm 0.14 \pm 0.26) \times 10^{-4}, \quad (3)$$

where the first error reflects the dependence on the renormalization scale μ_b varied in the interval $m_b/2 \leq \mu_b \leq 2m_b$, while the second error reflects the error due to the uncertainties in the input parameters.

Among the input parameters the charm quark mass m_c plays a crucial role. The charm quark mass dependence only enters the prediction for the decay width at the NLL level, more precisely through the $\mathcal{O}(\alpha_s)$ correction to the matrix elements $\langle s\gamma|O_{1,2}|b\rangle$. Until recently, all authors used the pole mass value m_c^{pole} for the charm quark mass in numerical evaluations, leading to a branching ratio as specified in eq. (3).

In 2001, however, Gambino and Misiak [25] pointed out that the $\overline{\text{MS}}$ -bar mass \overline{m}_c , normalized at $\mu \approx m_b/2$, could be the better choice, because the charm quark appears as an off-shell particle in the loop involved in the above mentioned matrix element with a typical virtuality of $m_b/2$. Using this interpretation, $\overline{m}_c/m_b = 0.22 \pm 0.04$ is substantially smaller than the value $m_c^{\text{pole}}/m_b = 0.29 \pm 0.02$ used in eq. (3), leading to a branching ratio of [25, 26]

$$\text{BR}(B \rightarrow X_s \gamma) = (3.70 \pm 0.30) \times 10^{-4}. \quad (4)$$

We would like to stress here that the above argument in favour of \overline{m}_c is an intuitive one. Formally, the difference between using m_c^{pole} or \overline{m}_c amounts to a NNLL effect at the level of the branching ratio. This means that a NNLL becomes necessary in order to unambiguously fix this issue.

Before sketching the NNLL program, we would like to stress that settling the m_c issue is also important when extracting bounds on new physics, based on NLL calculations [27, 28]. For example, in the type-II two-Higgs-doublet model, one obtains a bound from $b \rightarrow s \gamma$ on the charged Higgs boson mass of $m_H > 350$ GeV (99% C.L.) when using \overline{m}_c . When using on the other hand m_c^{pole} , the bound is $m_H > 280$ GeV (99% C.L.) [25].

Concerning the NNLL program, it is clear that in order to get a full NNLL QCD result for $\text{BR}(B \rightarrow X_s \gamma)$, all the three steps listed above have to be improved by one order in α_s . This means that three-loop matching calculations are needed, up to four-loop anomalous dimensions have to be worked out and up to three-loop calculations at the level of the matrix elements $\langle s \gamma | O_i(\mu_b) | b \rangle$ have to be performed. Several groups have been formed in order to attack this ambitious goal. Recently, a calculation of the $\mathcal{O}(\alpha_s^2 n_f)$ corrections to the matrix elements of the operators O_1 , O_2 , O_7 and O_8 was published [29]. Diagrammatically, these contributions are generated by inserting quark bubbles (n_f denotes the number of light quarks) into the gluon propagators in the diagrams which are involved in the calculations at NLL order. We note that these contributions are not related to the definition problem of m_c . However, in many other cases they are sources of large corrections. E.g., in the semileptonic decay width $\Gamma(B \rightarrow X_c \ell \nu_\ell)$ these $\mathcal{O}(\alpha_s^2 n_f)$ terms (after replacing $n_f \rightarrow -3\beta_0/2$, according to the procedure of naive non-abelianization) incorporate more than 80% of the complete $\mathcal{O}(\alpha_s^2)$ corrections [30]. The impact of the $\mathcal{O}(\alpha_s^2 n_f)$ corrections to $\text{BR}(B \rightarrow X_s \gamma)$ are shown in Fig. 3.1. The dash-dotted curve shows the NLL prediction, while the solid curve incorporates in addition the $\mathcal{O}(\alpha_s^2 n_f)$ terms (after the replacement $n_f \rightarrow -3\beta_0/2$, according to naive non-abelianization). As one sees from the figure, the $\mathcal{O}(\alpha_s^2 n_f)$ corrections seem to be small. Note, however, that this is a result of a relatively large accidental cancellation between corrections to O_2 and O_7 . This point is illustrated by the long-dashed and short-dashed curve, which are obtained by switching off the $\mathcal{O}(\alpha_s^2 n_f)$ corrections to O_7 and O_2 , respectively.

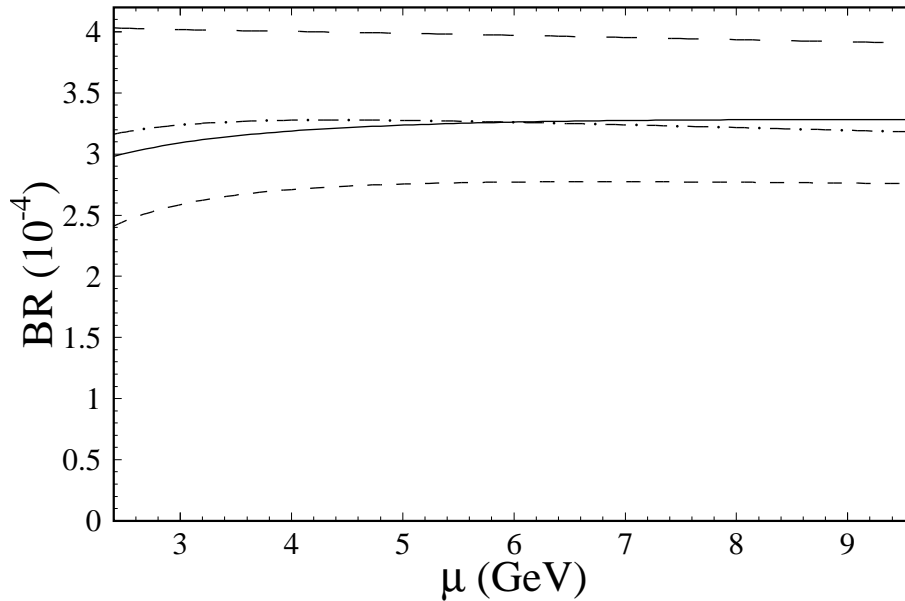


Figure 3.1: $\text{BR}(B \rightarrow X_s \gamma)$ as a function of the renormalization scale μ . The dash-dotted curve shows the NLL prediction; the solid curve contains in addition the $\mathcal{O}(\alpha_s^2 n_f)$ terms. The long-dashed (short-dashed) curve is obtained by switching off the $\mathcal{O}(\alpha_s^2 n_f)$ corrections to O_7 (O_2). Figure taken from ref. [29].

4 Partially integrated BR and photon energy spectrum

The photon energy spectrum of the partonic decay $b \rightarrow s\gamma$ is a delta function, concentrated at $\sim (m_b/2)$, when the b -quark decays at rest. This delta function gets smeared when considering the inclusive photon energy spectrum from a B meson decay. There is a perturbative contribution to this smearing, induced by the Bremsstrahlung process $b \rightarrow s\gamma g$ [16, 17], as well as a nonperturbative one, which is due to the Fermi motion of the decaying b quark in the B meson.

For small photon energies, the γ -spectrum from $B \rightarrow X_s \gamma$ is completely overshadowed by background processes, like $b \rightarrow c\bar{u}d\gamma$ and $b \rightarrow u\bar{u}d\gamma$. This background falls off very rapidly with increasing photon energy, and becomes small for $E_\gamma > 2$ GeV [31]. This implies that only the partial branching ratio

$$\text{BR}(B \rightarrow X_s \gamma)(E_\gamma^{\min}) = \int_{E_\gamma^{\min}}^{E_\gamma^{\max}} \frac{d\text{BR}}{dE_\gamma} dE_\gamma \quad (5)$$

can be directly measured, with $E_\gamma^{\min} = \mathcal{O}(2)$ GeV.

Putting the energy cut at $E_\gamma^{\min} = 2.0$ GeV, CLEO used two methods to analyze their data on the photon energy spectrum in their most recent analysis: First, the Ali-Greub

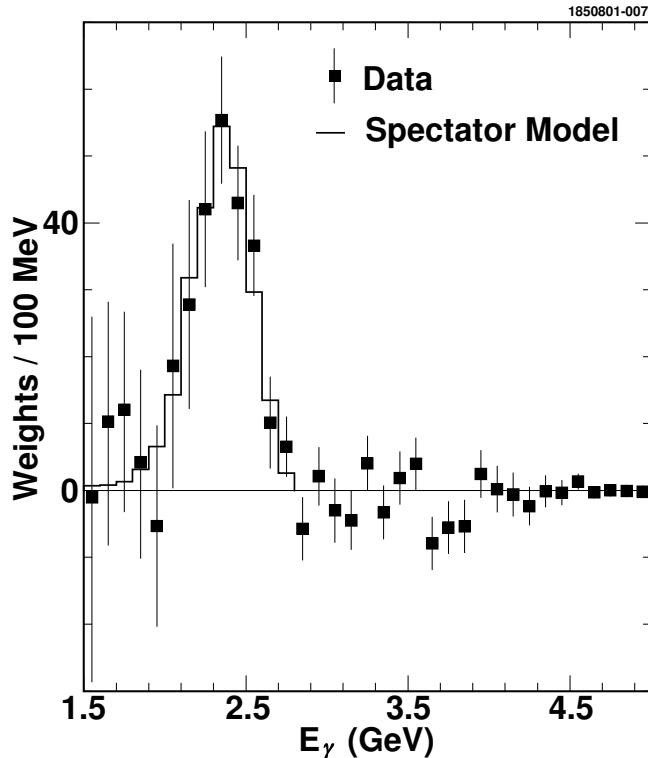


Figure 4.1: Photon energy spectrum: The data points represent the CLEO measurement [4]. The histogram shows the theory result based on the spectator model using $p_F = 410$ MeV and $\langle m_b \rangle = 4.69$ GeV. Fig. taken from ref. [4].

model [16, 32], based on the spectator model formulated in ref. [33] and second, methods based on HQET [22]. The spectator model contains two free parameters, viz. p_F , the average Fermi momentum of the b quark in the B meson and the mass of the spectator quark, m_{spec} . Equivalently $(p_F, \langle m_b \rangle)$ can be used as the free parameters, where $\langle m_b \rangle$ is the average b quark mass as defined in ref. [16, 32]. In Fig. 4.1 a comparison between theory and experiment is shown. Using $p_F = 410$ MeV and $\langle m_b \rangle = 4.69$ GeV the best fit is obtained. We would like to stress that similar values for these parameters are also obtained when fitting the lepton spectra in $B \rightarrow X_c \ell \nu$ and $B \rightarrow X_u \ell \nu$.

A modern way - based on first principles - implements the Fermi motion in the framework of the heavy-quark expansion. When probing the spectrum closer to the endpoint, the OPE breaks down, and the leading twist nonperturbative corrections must be resummed into the B meson structure function $f(k_+)$ [34], where k_+ is the light-cone momentum of the b quark in the B meson. The physical spectrum is then obtained by the convolution

$$\frac{d\Gamma}{dE_\gamma} = \int_{2E_\gamma - m_b}^{\bar{\Lambda}} dk_+ f(k_+) \frac{d\Gamma_{\text{part}}}{dE_\gamma}(m_b^*), \quad (6)$$

where $(d\Gamma_{\text{part}}/dE_\gamma)(m_b^*)$ is the partonic differential rate, written as a function of the “ef-

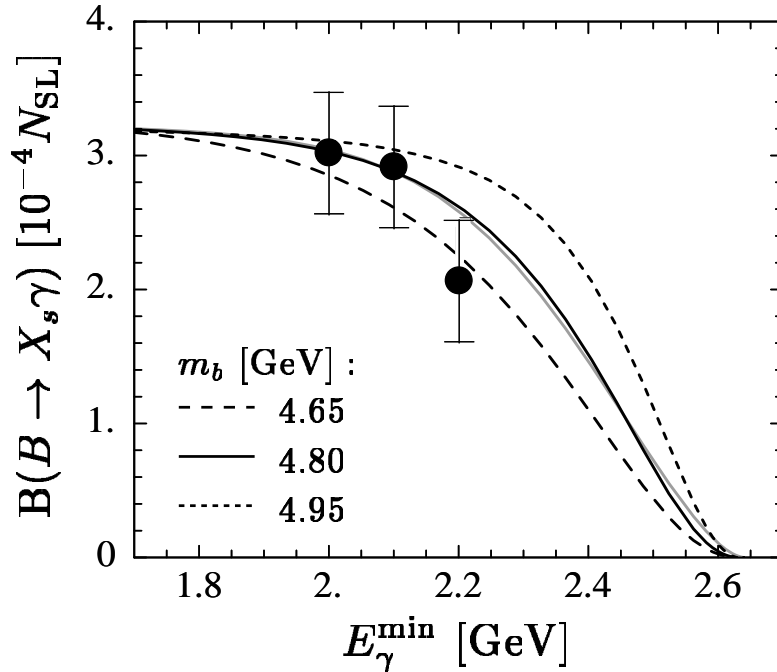


Figure 4.2: Partially integrated branching ratio as a function of the energy cutoff E_γ^{\min} ; Curves taken from Kagan and Neubert [22]. Data point represent CLEO measurements [2, 3, 4].

fective mass” $m_b^* = m_b + k_+$. The function $f(k_+)$ has support in the range $-\infty < k_+ < \bar{\Lambda}$, where $\bar{\Lambda} = m_B - m_b$ in the infinite mass limit. This implies that the addition of the structure function moves the partonic endpoint of the spectrum from $m_b/2$ to the physical endpoint $m_B/2$. While the shape of the function $f(k_+)$ is unknown, the first few moments $A_n = \int dk_+ k_+^n f(k_+)$ are known: $A_0 = 1$, $A_1 = 0$ and $A_2 = -\lambda_1/3$. As A_n ($n > 2$) are poorly known, several Ansätze were used for $f(k_+)$; e.g. Neubert and Kagan [22] used $f(k_+) = N(1-x)^a e^{(1+a)x}$, with $x = k_+/\bar{\Lambda}$. Taking into account the constraints from A_0 , A_1 and A_2 , the independent parameters in this Ansatz can be chosen to be m_b and λ_1 . As shown in [22], the uncertainty of m_b dominates the error of the partial branching ratio. In Figure 4.2 the partial branching ratio is shown for the relevant range of m_b as a function of E_γ^{\min} , keeping $\lambda_1/\bar{\Lambda}^2$ fixed. The data points show three CLEO measurements. In the oldest one the photon energy cut was put at $E_\gamma^{\min} = 2.2$ GeV, while in the most recent analysis this cut was lowered to 2.0 GeV, which is very important, because at 2.0 GeV the theoretical error on the partial branching ratio is considerably smaller, as seen from Fig. 4.2.

To determine from the measurement of the partial branching ratio the full BR, one needs from theory the fraction R of the $B \rightarrow X_s \gamma$ events with photon energies above E_γ^{\min} . Based on Kagan-Neubert [22], CLEO [4] obtained $R = (0.915_{-0.055}^{+0.027})$. A similar result is also obtained when using the spectator model.

It has been shown that up to corrections of $\mathcal{O}(\Lambda_{\text{QCD}}/m_b)$, the same shape function also describes $B \rightarrow X_u \ell \nu$ [35]. This implies that the photon energy spectrum can be used to predict the fraction of $B \rightarrow X_u \ell \nu$ events with $E_{\text{lept}} > 2.2$ GeV, where leptons coming from $B \rightarrow X_c \ell \nu$ are absent for kinematical reasons. Taking into account perturbative and Λ_{QCD}/m_b corrections [36, 37, 38], it is possible to extract V_{ub} from a measurement of the $B \rightarrow X_u \ell \nu$ decay rate in the region above 2.2 GeV. CLEO used this strategy in ref. [39] to extract the CKM matrix element $|V_{ub}|$, obtaining $|V_{ub}| = (4.08 \pm 0.56_{\text{exp}} \pm 0.29_{\text{th}}) \times 10^{-3}$.

5 $B \rightarrow X_d \gamma$ in the SM

The decay $B \rightarrow X_d \gamma$ can be treated in a similar way as $B \rightarrow X_s \gamma$ [40]. The only difference is that λ_u for $b \rightarrow d \gamma$ is not small relative to λ_t and λ_c ; therefore, also the current-current operators O_1^u and O_2^u , weighted by λ_u , contribute.

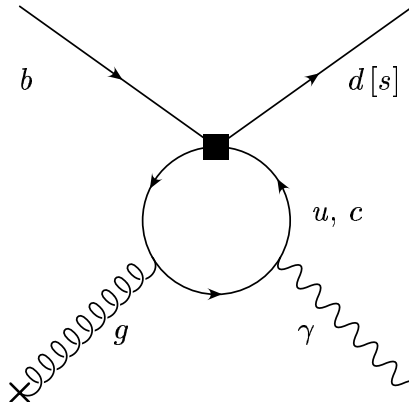


Figure 5.1: Interaction of the c - and u -quark loop with soft gluons surrounding the b quark in the B meson.

Unfortunately, these operators induce long-distance contributions to $B \rightarrow X_d \gamma$, which at present are not very well understood. To illustrate the problem, we first look at the corresponding charm quark loop, depicted in Fig. 5.1. In this case, one can expand the loop function

$$\sim \int_0^1 dx \int_0^{1-x} dy \frac{xy}{m_c^2 \left[1 - \frac{k_g^2}{m_c^2} x(1-x) - 2xy \frac{k_g k_\gamma}{m_c^2} \right]}$$

in powers of $t = k_g k_\gamma / m_c^2$, where k_g and k_γ denote the momentum of the gluon and the photon, respectively. This expansion generates the so-called Voloshin terms [10], which in $\text{BR}(B \rightarrow X_s \gamma)$ are a 3% effect. Obviously, there is no such OPE in the case of the u -quark loop. However, Buchalla, Isidori and Rey [41] argued that an expansion in $1/t$ can be done, leading to non-local operators. From naive dimensional counting, the leading contribution is expected to be of order Λ_{QCD}/m_b .

In reference [40], where NLL calculations for the process $B \rightarrow X_d\gamma$ were presented, the uncertainties due to the long-distance effects were absorbed into the theoretical error. Using $\mu_b = 2.5$ GeV and the central values of the input parameters, the analysis in reference [40] yields a difference between the LL and NLL predictions for $\text{BR}(B \rightarrow X_d\gamma)$ of $\sim 10\%$, increasing the branching ratio in the NLL case. For a fixed value of the CKM-Wolfenstein parameters ρ and η , the theoretical uncertainty of the average branching ratio $\langle \text{BR}(B \rightarrow X_d\gamma) \rangle$ of the decay $B \rightarrow X_d\gamma$ and its charge conjugate $\bar{B} \rightarrow \bar{X}_d\gamma$ is: $\Delta \langle \text{BR}(B \rightarrow X_d\gamma) \rangle / \langle \text{BR}(B \rightarrow X_d\gamma) \rangle = \pm(6 - 10)\%$. Of particular theoretical interest for constraining ρ and η is the ratio of the branching ratios, defined as

$$R(d\gamma/s\gamma) \equiv \frac{\langle \text{BR}(B \rightarrow X_d\gamma) \rangle}{\langle \text{BR}(B \rightarrow X_s\gamma) \rangle}, \quad (7)$$

in which a good part of the theoretical uncertainties cancels. Varying the CKM-Wolfenstein parameters ρ and η in the range $-0.1 \leq \rho \leq 0.4$ and $0.2 \leq \eta \leq 0.46$ and taking into account other parametric dependences, the results (without electroweak corrections) are

$$\begin{aligned} 6.0 \times 10^{-6} &\leq \text{BR}(B \rightarrow X_d\gamma) \leq 2.6 \times 10^{-5}, \\ 0.017 &\leq R(d\gamma/s\gamma) \leq 0.074. \end{aligned}$$

Another observable, which is also sensitive to the CKM parameters ρ and η , is the CP rate asymmetry a_{CP} , defined as

$$a_{\text{CP}} = \frac{\Gamma(B \rightarrow X_d\gamma) - \Gamma(\bar{B} \rightarrow \bar{X}_d\gamma)}{\Gamma(B \rightarrow X_d\gamma) + \Gamma(\bar{B} \rightarrow \bar{X}_d\gamma)}. \quad (8)$$

Varying ρ and η in the range specified above, one gets $7\% \leq a_{\text{CP}} \leq 35\%$ [40]. We would like to point out that a_{CP} is at the moment only available to LL precision and therefore suffers from a relatively large renormalization scale dependence.

In summary, this decay mode is very challenging, both in theory and experiment: On the theory side more work is needed concerning the nonperturbative contributions associated with the u -quark loop, while on the experimental side the observation of this decay needs high statistics and a very good discrimination between pions and kaons.

Acknowledgements

This work is partially supported by the Swiss National Foundation and by RTN, BBW-Contract N0. 01.0357 and EC-Contract HPRN-CT-2002-00311 (EURIDICE).

References

- [1] T. Hurth, these proceedings.
- [2] M.S. Alam et al. (CLEO Collab.), *Phys. Rev. Lett.* **74** (1995) 2885.
- [3] S. Ahmed et al. (CLEO Collab.) CLEO CONF 99-10, [hep-ex/9908022](#).
- [4] S. Chen et al. (CLEO Collab.), *Phys. Rev. Lett.* **87** (2001) 251807, [hep-ex/0108032](#).
- [5] R. Barate et al. (ALEPH Collab.), *Phys. Lett.* **B 429** (1998) 169.
- [6] K. Abe et al. (BELLE Collab.), *Phys. Lett.* **B 511** (2001) 151, [hep-ex/0103042](#).
- [7] B. Aubert et al. (BABAR Collab.), [hep-ex/0207074](#) and [hep-ex/0207076](#).
- [8] C. Jessop, SLAC-PUB-9610.
- [9] A. Falk, M. Luke, and M. Savage, *Phys. Rev.* **D 49** (1994) 3367;
I.I. Bigi, M. Shifman, N.G. Uraltsev, and A.I. Vainshtein, *Phys. Rev. Lett.* **71** (1993) 496;
A.V. Manohar and M.B. Wise, *Phys. Rev.* **D 49** (1994) 1310;
A. Falk, M. Luke, and M. Savage, *Phys. Rev.* **D 53** (1996) 2491.
- [10] M.B. Voloshin, *Phys. Lett.* **B 397** (1997) 275;
Z. Ligeti, L. Randall, and M.B. Wise, *Phys. Lett.* **B 402** (1997) 178 ;
A.K. Grant, A.G. Morgan, S. Nussinov, and R.D. Peccei, *Phys. Rev.* **D 56** (1997) 3151.
- [11] K. Chetyrkin, M. Misiak and M. Münz, *Phys. Lett.* **B 400** (1997) 206.
- [12] M. Ciuchini, E. Franco, G. Martinelli, L. Reina and L. Silvestrini, *Phys. Lett.* **B 316** (1993) 127; *Nucl. Phys.* **B 415** (1994) 403; G. Cella, G. Curci, G. Ricciardi and A. Vicere, *Phys. Lett.* **B 325** (1994) 227.
- [13] K. Adel and Y.-P. Yao, *Phys. Rev.* **D 49** (1994) 4945.
- [14] C. Greub and T. Hurth, *Phys. Rev.* **D 56** (1997) 2934.
- [15] A.J. Buras, A. Kwiatkowski and N. Pott, *Nucl. Phys.* **B 517** (1998) 353; *Phys. Lett.* **B 414** (1997) 157, E:*Phys. Lett.* **B 434** (1998) 459.
- [16] A. Ali and C. Greub, *Z. Physik* **C 49** (1991) 431; *Phys. Lett.* **B 259** (1991) 182.
- [17] N. Pott, *Phys. Rev.* **D 54** (1996) 938.
- [18] C. Greub, T. Hurth and D. Wyler, *Phys. Lett.* **B 380** (1996) 385; *Phys. Rev.* **D 54** (1996) 3350.

- [19] T. Hurth, *Rev. Mod. Phys.* **75** (2003) 1159, [hep-ph/0212304](#).
- [20] P. Gambino, M. Gorbahn and U. Haisch, *Nucl. Phys. B* **673** (2003) 238, [hep-ph/0306079](#).
- [21] A. Czarnecki and W. J. Marciano, *Phys. Rev. Lett.* **81** (1998) 277, [hep-ph/9804252](#).
- [22] A. L. Kagan and M. Neubert, *Eur. Phys. J. C* **7** (1999) 5, [hep-ph/9805303](#).
- [23] K. Baranowski and M. Misiak, *Phys. Lett. B* **483** (2000) 410, [hep-ph/9907427](#).
- [24] P. Gambino and U. Haisch, *J. High Energy Phys.* **0009** (2000) 001, [hep-ph/0007259](#).
P. Gambino and U. Haisch, *J. High Energy Phys.* **0110** (2001) 020, [hep-ph/0109058](#).
- [25] P. Gambino and M. Misiak, *Nucl. Phys. B* **611** (2001) 338, [hep-ph/0104034](#).
- [26] A. J. Buras, A. Czarnecki, M. Misiak, and J. Urban, *Nucl. Phys. B* **631** (2002) 219, [hep-ph/0203135](#).
- [27] M. Ciuchini, G. Degrossi, P. Gambino, and G. F. Giudice, *Nucl. Phys. B* **527** (1998) 21, [hep-ph/9710335](#).
- [28] F. M. Borzumati and C. Greub, *Phys. Rev. D* **58** (1998) 074004; *Phys. Rev. D* **59** (1998) 057501.
- [29] K. Bieri, C. Greub and M. Steinhauser, *Phys. Rev. D* **67** (2003) 114019, [hep-ph/0302051](#).
- [30] A. Czarnecki and K. Melnikov, *Phys. Rev. D* **59** (1999) 014036, [hep-ph/9804215](#).
- [31] A. Ali and C. Greub, *Phys. Lett. B* **293** (1992) 226.
- [32] A. Ali and C. Greub, *Z. Physik C* **49** (1991) 431; *Phys. Lett. B* **259** (1991) 182; *Phys. Lett. B* **361** (1995) 146.
- [33] G. Altarelli et al., *Nucl. Phys. B* **208** (1982) 365; A. Ali and E. Pietarinen, *Nucl. Phys. B* **154** (1979) 519.
- [34] M. Neubert, *Phys. Rev. D* **49** (1994) 3392, *Phys. Rev. D* **49** (1994) 4623; I.I. Bigi, M.A. Shifman, N.G. Uraltsev and A.I. Vainshtein, *Int. J. Mod. Phys. A* **9** (1994) 2467; R. D. Dikeman, M. Shifman and N.G. Uraltsev, *Int. J. Mod. Phys. A* **11** (1996) 571; T. Mannel and M. Neubert, *Phys. Rev. D* **50** (1994) 2037.
- [35] M. Neubert, *Phys. Rev. D* **49** (1994) 4623, [hep-ph/9312311](#).
- [36] A. K. Leibovich, I. Low and I. Z. Rothstein, *Phys. Rev. D* **61** (2000) 053006, [hep-ph/9909404](#).
- [37] C. W. Bauer, M. Luke and T. Mannel, *Phys. Lett. B* **543** (2002) 261, [hep-ph/0205150](#).

- [38] M. Neubert, *Phys. Lett. B* **543** (2002) 269, [hep-ph/0207002](#).
- [39] A. Bornheim *et al.* [CLEO Collaboration], *Phys. Rev. Lett.* **88** (2002) 231803, [hep-ex/0202019](#).
- [40] A. Ali, A. Asatrian and C. Greub, *Phys. Lett. B* **429** (1998) 87.
- [41] G. Buchalla, G. Isidori and S.J. Rey, *Nucl. Phys. B* **511** (1998) 594.

PART V

Virtual- and bremsstrahlung corrections to $b \rightarrow d \ell^+ \ell^-$ in the Standard Model

published in

Physical Review D 69 (2004) 074007

Virtual- and bremsstrahlung corrections to $b \rightarrow d \ell^+ \ell^-$ in the Standard Model ¹

H.M. Asatrian^a, K. Bieri^b, C. Greub^b and M. Walker^b

^a *Yerevan Physics Institute, 2 Alikhanyan Br., 375036 Yerevan, Armenia;*

^b *Institut für Theoretische Physik, Universität Bern,
CH-3012 Bern, Switzerland.*

ABSTRACT

We present the calculation of the virtual- and bremsstrahlung corrections of $\mathcal{O}(\alpha_s)$ to the matrix elements $\langle d \ell^+ \ell^- | O_i | b \rangle$. This is the missing piece in the full next-to-next-to-leading logarithmic (NNLL) results for various observables associated with the process $B \rightarrow X_d \ell^+ \ell^-$, like the branching ratio, the CP-rate asymmetry and the forward-backward asymmetry. This paper is an extension of analogous calculations done by some of us for the process $B \rightarrow X_s \ell^+ \ell^-$. As the contributions of the diagrams induced by the four-quark operators O_1^u and O_2^u with a u -quark running in the quark loop are strongly CKM suppressed, they were omitted in the analysis of $B \rightarrow X_s \ell^+ \ell^-$. This is no longer possible for $B \rightarrow X_d \ell^+ \ell^-$, as the corresponding contributions are not suppressed. The main new work therefore consists of calculating the $\mathcal{O}(\alpha_s)$ corrections to $\langle d \ell^+ \ell^- | O_{1,2}^u | b \rangle$. In this paper we restrict ourselves to the range $0.05 \leq s/m_b^2 \leq 0.25$ (s is the invariant mass of the lepton pair), which lies above the ρ - and ω -resonances and below the J/ψ -resonance. We present the analytic results for the mentioned observables related to the process $B \rightarrow X_d \ell^+ \ell^-$ as expansions in the small parameters $\hat{s} = s/m_b^2$, $z = m_c^2/m_b^2$ and $s/(4m_c^2)$. In the phenomenological analysis at the end of the paper we discuss the impact of the NNLL corrections on the observables mentioned above.

¹Work partially supported by Schweizerischer Nationalfonds, RTN, SCOPES, EURIDICE and NFSAT (CRDF) programs.

1 Introduction

It is well-known that various observables associated with inclusive rare B -decays like $B \rightarrow X_{s,d}\gamma$ and $B \rightarrow X_{s,d}\ell^+\ell^-$ sensitively depend on potential new physics contributions. But even in the absence of new physics these observables are important, because they provide checks on the one-loop structure of the Standard Model (SM) theory and can be used to gain information on the Cabibbo-Kobayashi-Maskawa (CKM) matrix elements V_{ts} and V_{td} , which are difficult to measure directly.

At present, a lot of data already exists on $\text{BR}(B \rightarrow X_s\gamma)$ [1, 2, 3, 4, 5, 6, 7] and on $\text{BR}(B \rightarrow X_s\ell^+\ell^-)$ [8, 9, 10] and it is expected that in the future also data on the CKM suppressed counterparts, i.e. on $\text{BR}(B \rightarrow X_d\gamma)$ and on $\text{BR}(B \rightarrow X_d\ell^+\ell^-)$ will become available. The same holds for experimental information on additional observables, like CP-rate asymmetries or forward-backward asymmetries in the decays $B \rightarrow X_{s,d}\ell^+\ell^-$.

In order to fully exploit and interpret the experimental data, it is obvious that precise calculations in the SM (or certain extensions thereof) are needed. The main problem in the theoretical description of the decay $B \rightarrow X_s\ell^+\ell^-$ is due to the long-distance contributions induced by $\bar{c}c$ resonant states and in principle also by $\bar{u}u$ resonant states. The latter are, however, strongly CKM suppressed. This suppression is not present in the case of $B \rightarrow X_d\ell^+\ell^-$, as the CKM factors involved in the contributions from $\bar{c}c$ and $\bar{u}u$ resonant states are of the same order. When the invariant mass \sqrt{s} of the lepton pair is close to the mass of a resonance, only model dependent predictions for such long distance contributions are available at present. It is therefore unclear whether the theoretical uncertainty can be reduced to less than $\pm 20\%$ when integrating over these domains [11].

However, restricting \sqrt{s} to a region below the $\bar{c}c$ resonances, the long distance effects in $B \rightarrow X_s\ell^+\ell^-$ are under control. The same is true for $B \rightarrow X_d\ell^+\ell^-$ when choosing a region of \sqrt{s} which is below the J/ψ - and above the ρ, ω -resonance regions. It turns out that in those ranges of \sqrt{s} the corrections to the pure perturbative picture can be analyzed within the heavy quark effective theory (HQET). In particular, all available studies indicate that for the region $0.05 < \hat{s} = s/m_b^2 < 0.25$ the non-perturbative effects are below 10% [12, 13, 14, 15, 16, 17]. Consequently, observables like differential decay rates, forward-backward asymmetries and CP-rate asymmetries for $B \rightarrow X_{s,d}\ell^+\ell^-$ can be precisely predicted in this region of \sqrt{s} using renormalization group improved perturbation theory. It was pointed out in the literature that the differential decay rate and the forward-backward asymmetry in $B \rightarrow X_s\ell^+\ell^-$ are particularly sensitive to new physics in this kinematical window [18, 19, 20].

In the context of the SM there exist computations of next-to-leading logarithmic (NLL) QCD corrections to the branching ratios for $B \rightarrow X_s\gamma$ [21, 22, 23, 24, 25, 26, 27, 28] and $B \rightarrow X_d\gamma$ and the corresponding CP-rate asymmetries [29, 30, 31]. Next-to-next-to-leading logarithmic (NNLL) QCD corrections to the branching ratio [32, 33, 34, 35, 36] and the forward-backward asymmetry in $B \rightarrow X_s\ell^+\ell^-$ are also available [37, 38, 39, 40]. For a recent review see e.g. [41].

The corresponding NNLL results for the process $B \rightarrow X_d \ell^+ \ell^-$ are missing, however. The aim of the present paper is to close this gap. The main difference between the calculations for $B \rightarrow X_s \ell^+ \ell^-$ and $B \rightarrow X_d \ell^+ \ell^-$ lies in the contributions of the current-current operators. In the existing NNLL calculations of $B \rightarrow X_s \ell^+ \ell^-$ only those associated with O_1^c and O_2^c were included at the two-loop level because those induced by O_1^u and O_2^u are strongly CKM suppressed (see Section 2 for the definition of the operators $O_{1,2}^{u,c}$). For $B \rightarrow X_d \ell^+ \ell^-$ the contributions generated by O_1^u and O_2^u are no longer CKM suppressed and have to be taken into account as well. At first sight, it seems that the two-loop matrix elements of O_1^u and O_2^u can be straightforwardly obtained from those of O_1^c and O_2^c by simply taking the limit $m_c \rightarrow 0$. This is, however, not possible for some of the diagrams in Fig. 3.1, because the two-loop matrix elements of O_1^c and O_2^c were derived by doing various expansions. In particular, one of the expansion parameters is $s/(4m_c^2)$, which is formally $\ll 1$ when restricting \sqrt{s} to the window discussed above. Obviously, the analogous quantity for the u -quark contribution, $s/(4m_u^2)$, cannot be used as an expansion parameter, which implies that genuinely new calculations for the u -quark contributions are needed. As discussed in Section 3, the calculations of certain diagrams associated with $O_{1,2}^u$ are even more involved than those associated with $O_{1,2}^c$. To derive the new results, we used dimension-shifting techniques in order to reduce certain tensor integrals to scalar ones and integration-by-parts techniques to further simplify the scalar integrals [42, 43].

As the main emphasis of this paper is the derivation of the matrix elements $\langle d \ell^+ \ell^- | O_{1,2}^u | b \rangle$ at order α_s , we keep the phenomenological analysis relatively short. In particular, we do not take into account power corrections, but merely illustrate how the NNLL contributions modify the scale dependences of the branching ratio, the forward-backward asymmetry and the CP-rate asymmetry. A more detailed phenomenology, including power corrections, will be presented elsewhere.

The paper is organized as follows: In Section 2 we present the effective Hamiltonian for the decay $b \rightarrow X_d \ell^+ \ell^-$. Section 3 is devoted to the virtual $\mathcal{O}(\alpha_s)$ corrections to the operators $O_1^{u,c}$ and $O_2^{u,c}$. Subsequently, Section 4 presents the corresponding contributions to the form factors of the operators O_7 , O_8 , O_9 and O_{10} . With these results at hand, we discuss in Section 5 the corrections to the decay width of $B \rightarrow X_d \ell^+ \ell^-$. In Section 6 we show some applications of our results. A summary of the paper is presented in Section 7. The appendices contain technical details about the performed calculation: Appendix A explains the dimension-shifting and integration-by-parts techniques. These techniques are then applied to the calculation of diagrams 3.1d), which is presented in Appendix B. Appendix C outlines a procedure on how to calculate the evolution matrix for the Wilson coefficients as a power series in α_s . Appendix D contains one-loop matrix elements needed in the calculation of the counterterms. Finally, in Appendix E we present the results for those bremsstrahlung contributions which are free of infrared and collinear divergences.

2 Effective Hamiltonian

The appropriate framework for studying QCD corrections to rare B -decays in a systematic way is the effective Hamiltonian technique. For the specific decay channels $B \rightarrow X_s \ell^+ \ell^-$ and $B \rightarrow X_d \ell^+ \ell^-$ ($\ell = \mu, e$), the effective Hamiltonian is derived by integrating out the t -quark, the W -boson and the Z^0 -boson. In the process $B \rightarrow X_s \ell^+ \ell^-$, the appearing CKM combinations are λ_u, λ_c and λ_t , where $\lambda_i = V_{ib} V_{is}^*$. Since $|\lambda_u|$ is much smaller than $|\lambda_c|$ and $|\lambda_t|$, it is a safe approximation to set λ_u equal to zero. Using then the unitarity properties of the CKM matrix, the CKM dependence of the Hamiltonian can be written as a global factor λ_t . In the case of $B \rightarrow X_d \ell^+ \ell^-$, all three quantities $\xi_i = V_{ib} V_{id}^*$ ($i = u, c, t$) are of the same order of magnitude. Therefore, as no approximation is possible, the CKM dependence does not globally factorize. The effective Hamiltonian reads

$$\mathcal{H}_{\text{eff}} = \frac{4 G_F}{\sqrt{2}} \left[\sum_{i=1}^2 C_i (\xi_c O_i^c + \xi_u O_i^u) - \xi_t \sum_{i=3}^{10} C_i O_i \right]. \quad (1)$$

We choose the operator basis according to [32]:

$$\begin{aligned} O_1^u &= (\bar{d}_L \gamma_\mu T^a u_L) (\bar{u}_L \gamma^\mu T^a b_L), & O_2^u &= (\bar{d}_L \gamma_\mu u_L) (\bar{u}_L \gamma^\mu b_L), \\ O_1^c &= (\bar{d}_L \gamma_\mu T^a c_L) (\bar{c}_L \gamma^\mu T^a b_L), & O_2^c &= (\bar{d}_L \gamma_\mu c_L) (\bar{c}_L \gamma^\mu b_L), \\ O_3 &= (\bar{d}_L \gamma_\mu b_L) \sum_q (\bar{q} \gamma^\mu q), & O_4 &= (\bar{d}_L \gamma_\mu T^a b_L) \sum_q (\bar{q} \gamma^\mu T^a q), \\ O_5 &= (\bar{d}_L \gamma_\mu \gamma_\nu \gamma_\rho b_L) \sum_q (\bar{q} \gamma^\mu \gamma^\nu \gamma^\rho q), & O_6 &= (\bar{d}_L \gamma_\mu \gamma_\nu \gamma_\rho T^a b_L) \sum_q (\bar{q} \gamma^\mu \gamma^\nu \gamma^\rho T^a q), \\ O_7 &= \frac{e}{g_s^2} m_b (\bar{d}_L \sigma^{\mu\nu} b_R) F_{\mu\nu}, & O_8 &= \frac{1}{g_s} m_b (\bar{d}_L \sigma^{\mu\nu} T^a b_R) G_{\mu\nu}^a, \\ O_9 &= \frac{e^2}{g_s^2} (\bar{d}_L \gamma_\mu b_L) \sum_\ell (\bar{\ell} \gamma^\mu \ell), & O_{10} &= \frac{e^2}{g_s^2} (\bar{d}_L \gamma_\mu b_L) \sum_\ell (\bar{\ell} \gamma^\mu \gamma_5 \ell), \end{aligned} \quad (2)$$

where the subscripts L and R refer to left- and right-handed components of the fermion fields, respectively.

The factors $1/g_s^2$ in the definition of the operators O_7, O_9 and O_{10} as well as the factor $1/g_s$ present in O_8 have been chosen by Misiak [44] in order to simplify the organization of the calculation. With these definitions, the one-loop anomalous dimensions [needed for a leading logarithmic (LL) calculation] of the operators O_i are all proportional to g_s^2 , while two-loop anomalous dimensions [needed for a next-to-leading logarithmic (NLL) calculation] are proportional to g_s^4 , etc.

After this important remark we now outline the principal steps which lead to a LL, NLL, and a NNLL prediction for the decay amplitude for $b \rightarrow d \ell^+ \ell^-$:

1. A matching calculation between the full SM theory and the effective theory has to be performed in order to determine the Wilson coefficients C_i at the high scale $\mu_W \sim m_W, m_t$. At this scale, the coefficients can be worked out in fixed order

perturbation theory, i.e. they can be expanded in g_s^2 :

$$C_i(\mu_W) = C_i^{(0)}(\mu_W) + \frac{g_s^2}{16\pi^2} C_i^{(1)}(\mu_W) + \frac{g_s^4}{(16\pi^2)^2} C_i^{(2)}(\mu_W) + \mathcal{O}(g_s^6). \quad (3)$$

At LL order, only $C_i^{(0)}$ are needed, at NLL order also $C_i^{(1)}$, etc. The coefficient $C_7^{(2)}$ was worked out in Refs. [23, 24, 25], while $C_9^{(2)}$ and $C_{10}^{(2)}$ were calculated in Ref. [32].

2. The renormalization group equation (RGE) has to be solved in order to get the Wilson coefficients at the low scale $\mu_b \sim m_b$. For this RGE step the anomalous dimension matrix $\gamma(\alpha_s)$, which can be expanded as

$$\gamma(\alpha_s) = \gamma^{(0)} \frac{\alpha_s}{4\pi} + \gamma^{(1)} \left(\frac{\alpha_s}{4\pi} \right)^2 + \gamma^{(2)} \left(\frac{\alpha_s}{4\pi} \right)^3 + \dots, \quad (4)$$

is required up to the term proportional to $\gamma^{(2)}$ when aiming at a NNLL calculation. After the matching step and the RGE evolution, the Wilson coefficients $C_i(\mu_b)$ can be decomposed into a LL, NLL and NNLL part according to

$$C_i(\mu_b) = C_i^{(0)}(\mu_b) + \frac{g_s^2(\mu_b)}{16\pi^2} C_i^{(1)}(\mu_b) + \frac{g_s^4(\mu_b)}{(16\pi^2)^2} C_i^{(2)}(\mu_b) + \mathcal{O}(g_s^6). \quad (5)$$

We stress at this point that the entries in $\gamma^{(2)}$ which describe the three-loop mixings of the four-quark operators $O_1 - O_6$ into the operator O_9 have been calculated only recently [33]. In order to include the impact of these new ingredients on the Wilson coefficient $C_9(\mu_b)$, we had to reanalyze the RGE step. In Appendix C, we derive a practical formula for the evolution matrix $U(\mu_b, \mu_W)$ at NNLL order, generalizing existing formulas at NLL order (see e.g. [45]).

3. In order to get the decay amplitude, the matrix elements $\langle d \ell^+ \ell^- | O_i(\mu_b) | b \rangle$ have to be calculated. At LL precision, only the operator O_9 contributes, as this operator is the only one which at the same time has a Wilson coefficient starting at lowest order and an explicit $1/g_s^2$ factor in the definition. Hence, at NLL precision, QCD corrections (virtual and bremsstrahlung) to the matrix element of O_9 are needed. They have been calculated in Refs. [44, 46]. At NLL precision, also the other operators start contributing, viz. $O_7(\mu_b)$ and $O_{10}(\mu_b)$ contribute at tree-level and the four-quark operators O_1, \dots, O_6 at one-loop level. Accordingly, QCD corrections to the latter matrix elements are needed for a NNLL prediction of the decay amplitude.

The formally leading term $\sim (1/g_s^2) C_9^{(0)}(\mu_b)$ to the amplitude for $b \rightarrow d \ell^+ \ell^-$ is smaller than the NLL term $\sim (1/g_s^2) [g_s^2/(16\pi^2)] C_9^{(1)}(\mu_b)$ [47]. We adapt our systematics to the numerical situation and treat the sum of these two terms as a NLL contribution. This is, admittedly some abuse of language, because the decay amplitude then starts out with a term which is called NLL.

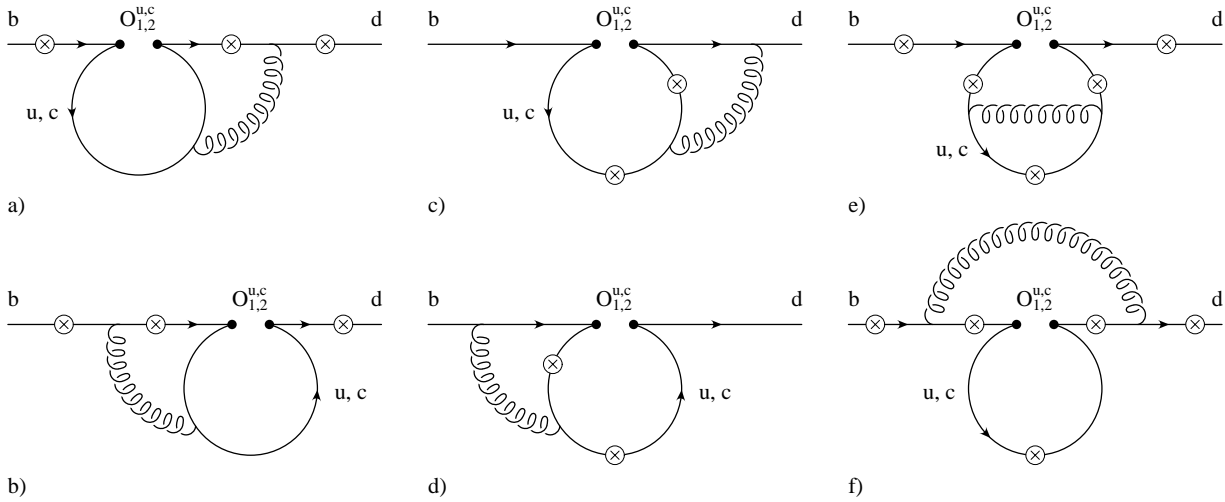


Figure 3.1: Complete list of two-loop Feynman diagrams for $b \rightarrow d \gamma^*$ associated with the operators $O_1^{u,c}$ and $O_2^{u,c}$. The fermions (b -, d -, u - and c -quarks) are represented by solid lines, whereas the curly lines represent gluons. The circle-crosses denote the possible locations where the virtual photon (which then splits into a lepton pair) is emitted.

As pointed out in step 3), $\mathcal{O}(\alpha_s)$ QCD corrections to the matrix elements $\langle d \ell^+ \ell^- | O_i(\mu_b) | b \rangle$ have to be calculated in order to obtain the NNLL prediction for the decay amplitude. In the present paper we systematically evaluate virtual corrections of order α_s to the matrix elements of O_1 , O_2 , O_7 , O_8 , O_9 and O_{10} . As the Wilson coefficients of the gluonic penguin operators O_3, \dots, O_6 are much smaller than those of O_1 and O_2 , we neglect QCD corrections to their matrix elements. We also systematically include gluon bremsstrahlung corrections to the matrix elements of the operators just mentioned. Some of these contributions contain infrared and collinear singularities, which are canceled when combined with the virtual corrections.

3 Virtual $\mathcal{O}(\alpha_s)$ corrections to the matrix elements $\langle d \ell^+ \ell^- | O_{1,2}^{u,c} | b \rangle$

In this section we present the calculation of the virtual $\mathcal{O}(\alpha_s)$ corrections to the matrix elements of the current-current operators $O_1^{u,c}$ and $O_2^{u,c}$. Using the naive dimensional regularization scheme (NDR) in $d = 4 - 2\epsilon$ dimensions, both ultraviolet and infrared singularities show up as $1/\epsilon^n$ poles ($n = 1, 2$). The ultraviolet singularities cancel after including the counterterms. Collinear singularities are regularized by retaining a finite down quark mass m_d . They are canceled together with the infrared singularities at the level of the decay width when taking the bremsstrahlung process $b \rightarrow d \ell^+ \ell^- g$ into account.

We use the $\overline{\text{MS}}$ renormalization scheme, i.e. we introduce the renormalization scale in the form $\bar{\mu}^2 = \mu^2 \exp(\gamma_E)/(4\pi)$ followed by minimal subtraction. The precise definition of the evanescent operators, which is necessary to fully specify the renormalization scheme, will be given later.

Gauge invariance implies that the QCD corrected matrix elements of the operators O_i^q can be written as

$$\langle d \ell^+ \ell^- | O_i^q | b \rangle = \hat{F}_{i,q}^{(9)} \langle O_9 \rangle_{\text{tree}} + \hat{F}_{i,q}^{(7)} \langle O_7 \rangle_{\text{tree}} \quad (i = 1, 2; q = u, c), \quad (6)$$

where $\langle O_9 \rangle_{\text{tree}}$ and $\langle O_7 \rangle_{\text{tree}}$ are the tree-level matrix elements of O_9 and O_7 , respectively. Equivalently, we may write

$$\langle d \ell^+ \ell^- | O_i^q | b \rangle = -\frac{\alpha_s}{4\pi} \left[F_{i,q}^{(9)} \langle \tilde{O}_9 \rangle_{\text{tree}} + F_{i,q}^{(7)} \langle \tilde{O}_7 \rangle_{\text{tree}} \right], \quad (7)$$

where the operators \tilde{O}_7 and \tilde{O}_9 are defined as

$$\tilde{O}_7 = \frac{\alpha_s}{4\pi} O_7, \quad \tilde{O}_9 = \frac{\alpha_s}{4\pi} O_9. \quad (8)$$

We present the final results for the QCD corrected matrix elements in the form of Eq. (7). The full set of the diagrams contributing at $\mathcal{O}(\alpha_s)$ to the matrix elements

$$M_i^q = \langle d \ell^+ \ell^- | O_i^q | b \rangle \quad (9)$$

is shown in Fig. 3.1. As indicated, the diagrams associated with $O_1^{u,c}$ and $O_2^{u,c}$ are topologically identical. They differ only in the color structure. While the matrix elements of the operator $O_2^{u,c}$ all involve the color structure

$$\sum_a T^a T^a = C_F \mathbf{1}, \quad C_F = \frac{N_c^2 - 1}{2N_c},$$

there are two possible color structures for the corresponding diagrams of $O_1^{u,c}$, viz

$$\tau_1 = \sum_{a,b} T^a T^b T^a T^b \quad \text{and} \quad \tau_2 = \sum_{a,b} T^a T^b T^b T^a.$$

The structure τ_1 appears in diagrams 3.1a)-d), and τ_2 enters diagrams 3.1e) and 3.1f). Using the relation

$$\sum_a T_{\alpha\beta}^a T_{\gamma\delta}^a = -\frac{1}{2N_c} \delta_{\alpha\beta} \delta_{\gamma\delta} + \frac{1}{2} \delta_{\alpha\delta} \delta_{\beta\gamma},$$

we find that $\tau_1 = C_{\tau_1} \mathbf{1}$ and $\tau_2 = C_{\tau_2} \mathbf{1}$, with

$$C_{\tau_1} = -\frac{N_c^2 - 1}{4N_c^2} \quad \text{and} \quad C_{\tau_2} = \frac{(N_c^2 - 1)^2}{4N_c^2}.$$

Inserting $N_c = 3$, the color factors are $C_F = \frac{4}{3}$, $C_{\tau_1} = -\frac{2}{9}$ and $C_{\tau_2} = \frac{16}{9}$. The contributions from $O_1^{u,c}$ are obtained by multiplying those from $O_2^{u,c}$ by the appropriate factors, i.e. by $C_{\tau_1}/C_F = -\frac{1}{6}$ and $C_{\tau_2}/C_F = \frac{4}{3}$, respectively. As the renormalized $\mathcal{O}(\alpha_s)$ contributions of the operators O_1^c and O_2^c are discussed in detail in Ref. [34], we only discuss the calculations of the contributions from O_1^u and O_2^u to the individual form factors.

The rest of this section is organized as follows: We discuss the calculations of the diagrams 3.1a)-e) for the operators $O_{1,2}^u$. Notice that all results are given as an expansion in the small quantity $\hat{s} = s/m_b^2$, where s is the invariant mass squared of the lepton pair, and that we keep only terms up to $\mathcal{O}(\hat{s}^3)$. After deriving the counterterms that cancel the divergences of the diagrams mentioned above, we present the renormalized contributions to the form factors. We postpone the discussion of diagrams 3.1f) as it turns out to be more convenient to take them into account when discussing the virtual corrections to O_9 .

3.1 Diagrams 3.1a) and b)

The calculation of the contributions to $F_{2,u}^{(7)}$ and $F_{2,u}^{(9)}$ from the diagrams in Figs. 3.1a) and 3.1b) opposes no difficulties, as it can be performed by using the Mellin-Barnes approach [48]. Alternatively, one may get the results directly from the corresponding form factors of the $b \rightarrow s \ell^+ \ell^-$ transition by taking the limit $m_c \rightarrow 0$. The form factors associated with the diagrams in Fig. 3.1a) are given by

$$\begin{aligned}
 F_{2,u}^{(9)}[a] = C_F \cdot & \left[-\frac{2}{27\epsilon^2} + \left(\frac{1}{\epsilon} + 4L_\mu\right) \left(-\frac{19}{81} + \frac{4}{27}L_s - \frac{4}{27}i\pi\right) - \frac{8}{27\epsilon}L_\mu \right. \\
 & - \frac{16}{27}L_\mu^2 + \left(-\frac{463}{486} - \frac{38i\pi}{81} + \frac{5\pi^2}{27}\right) - \frac{4}{27}\hat{s} + \left(-\frac{1}{27} - \frac{2}{27}L_s\right)\hat{s}^2 \\
 & \left. + \left(-\frac{4}{243} - \frac{8}{81}L_s\right)\hat{s}^3 + \frac{26}{81}L_s + \frac{8}{27}i\pi L_s - \frac{2}{27}L_s^2 \right], \quad (10)
 \end{aligned}$$

$$F_{2,u}^{(7)}[a] = C_F \cdot \left[\frac{1}{27} \left(\frac{1}{\epsilon} + 4L_\mu\right) + \frac{37}{162} + \frac{2}{27}i\pi + \frac{2}{27}\hat{s}(1 + \hat{s} + \hat{s}^2)L_s \right],$$

where

$$L_s = \ln(\hat{s}) \quad \text{and} \quad L_\mu = \ln\left(\frac{\mu}{m_b}\right).$$

For the sum of the diagrams in Fig. 3.1b) we find

$$\begin{aligned}
 F_{2,u}^{(9)}[b] = C_F \cdot & \left[-\frac{2}{27\epsilon^2} + \left(\frac{1}{\epsilon} + 4L_\mu\right) \left(\frac{1}{81} - \frac{4}{135}\hat{s} - \frac{1}{315}\hat{s}^2 - \frac{4}{8505}\hat{s}^3\right) - \frac{8}{27\epsilon}L_\mu \right. \\
 & - \frac{16}{27}L_\mu^2 + \left(\frac{917}{486} - \frac{19\pi^2}{81}\right) + \left(\frac{172}{225} - \frac{2\pi^2}{27}\right)\hat{s} \\
 & \left. + \left(-\frac{871057}{396900} + \frac{2\pi^2}{9}\right)\hat{s}^2 + \left(-\frac{83573783}{10716300} + \frac{64\pi^2}{81}\right)\hat{s}^3 \right], \quad (11)
 \end{aligned}$$

$$\begin{aligned}
 F_{2,u}^{(7)}[b] = C_F \cdot & \left[-\frac{5}{27\epsilon} - \frac{20}{27}L_\mu \right. \\
 & \left. + \frac{13}{162} + \left(\frac{25}{81} - \frac{\pi^2}{27}\right)\hat{s} + \left(\frac{118}{81} - \frac{4\pi^2}{27}\right)\hat{s}^2 + \left(\frac{10361}{2835} - \frac{10\pi^2}{27}\right)\hat{s}^3 \right].
 \end{aligned}$$

3.2 Diagrams 3.1d)

The computation of the diagrams in Fig. 3.1d) is by far the most complicated piece in our entire calculation of the $\mathcal{O}(\alpha_s)$ corrections to the matrix element for $b \rightarrow d \ell^+ \ell^-$. After various unsuccessful attempts, we managed to obtain the result by using the dimension-shifting method [42] (see Appendix A.1), combined with the method of partial integration (see Appendix A.2). Since we want to include the details of the actual calculation, we relegate them to Appendix B. Here, we merely present the final results, viz the contributions to the form factors, which read

$$\begin{aligned}
 F_{2,u}^{(9)}[d] = C_F \cdot & \left[\frac{2}{3\epsilon^2} + \frac{1}{\epsilon} \left(\frac{5}{3} - \frac{4L_s}{3} + \frac{8}{3}L_\mu + \frac{4i\pi}{3}\right) + \frac{16}{3}L_\mu^2 + \frac{7}{6} - 4L_s \right. \\
 & + \frac{2}{3}L_s^2 + 4i\pi - \frac{4i\pi}{3}L_s - \pi^2 + \left(\frac{20}{3} - \frac{16}{3}L_s + \frac{16i\pi}{3}\right)L_\mu \\
 & + \left(\frac{2}{3} + \frac{2}{3}L_s - \frac{2}{3}L_s^2 - \frac{2i\pi}{3} + \frac{4i\pi}{3}L_s\right)\hat{s} + \left(\frac{2}{3} + 2L_s - 2i\pi\right)\hat{s}^2 \\
 & \left. + \left(\frac{2}{3} + \frac{10}{3}L_s + \frac{4}{3}L_s^2 - \frac{10i\pi}{3} - \frac{8i\pi}{3}L_s\right)\hat{s}^3 \right], \quad (12)
 \end{aligned}$$

$$\begin{aligned}
 F_{2,u}^{(7)}[d] = C_F \cdot & \left[\frac{2}{3\epsilon} + \frac{7}{3} + \frac{8}{3}L_\mu - \left(\frac{1}{3} - \frac{1}{3}L_s - \frac{1}{3}L_s^2 + \frac{i\pi}{3} + \frac{2i\pi}{3}L_s\right)\hat{s} \right. \\
 & \left. - \left(\frac{1}{3} + \frac{1}{3}L_s - \frac{1}{3}L_s^2 - \frac{i\pi}{3} + \frac{2i\pi}{3}L_s\right)\hat{s}^2 - \left(\frac{1}{3} + L_s - i\pi\right)\hat{s}^3 \right]. \quad (13)
 \end{aligned}$$

3.3 Diagrams 3.1c)

The calculation of this diagram can be done in a very simple and efficient way. We add the two subdiagrams and integrate out the loop momentum of the virtual gluon. Next we integrate over the remaining loop momentum, being left with a four dimensional Feynman parameter integral. After introducing a single Mellin-Barnes representation of the occurring denominator, the parameter integrals can all be performed. At this level, the result contains Euler Beta-functions involving the Mellin-Barnes parameter. Finally, the Mellin-Barnes integral can be resolved applying the residue theorem, which naturally leads to an expansion in the parameter \hat{s} . The contribution of the diagrams in Fig. 3.1c) to the form factors reads

$$\begin{aligned}
 F_{2,u}^{(9)}[c] = C_F \cdot & \left[\frac{2}{3\epsilon^2} + \frac{1}{\epsilon} \left(\frac{5}{3} - \frac{4L_s}{3} + \frac{8}{3}L_\mu + \frac{4i\pi}{3} \right) + \frac{16}{3}L_\mu^2 \right. \\
 & + \frac{1}{2} - 6L_s + \frac{2}{3}L_s^2 + \frac{10i\pi}{3} - \frac{8i\pi}{3}L_s - \frac{5\pi^2}{3} \\
 & + \left(\frac{4}{3} - 4L_s + \frac{2}{3}L_s^2 + \frac{2\pi^2}{9} \right) \hat{s} + \left(-1 - 2L_s + \frac{2}{3}L_s^2 + \frac{2\pi^2}{9} \right) \hat{s}^2 \\
 & \left. + \left(-\frac{41}{27} - \frac{10}{9}L_s + \frac{2}{3}L_s^2 + \frac{2\pi^2}{9} \right) \hat{s}^3 + \left(\frac{20}{3} + \frac{16i\pi}{3} - \frac{16}{3}L_s \right) L_\mu \right], \quad (14)
 \end{aligned}$$

$$\begin{aligned}
 F_{2,u}^{(7)}[c] = C_F \cdot & \left[\frac{1}{3\epsilon} + \frac{5}{2} + \frac{2i\pi}{3} + \left(\frac{2L_s}{3} - \frac{L_s^2}{3} - \frac{\pi^2}{9} \right) \hat{s} + \left(\frac{2}{3} - \frac{L_s^2}{3} - \frac{\pi^2}{9} \right) \hat{s}^2 \right. \\
 & \left. + \left(\frac{5}{6} - \frac{L_s}{3} - \frac{L_s^2}{3} - \frac{\pi^2}{9} \right) \hat{s}^3 + \frac{4}{3}L_\mu \right]. \quad (15)
 \end{aligned}$$

We also performed the calculation of this diagram in two different, more complicated ways, namely by

- using the building block $J_{\alpha\beta}$ given in [34] and then introducing a double Mellin-Barnes representation,
- using the dimension-shifting and integration-by-parts techniques as explained when discussing the computation of the diagrams in Fig. 3.1d) (see also Appendices A.1 and A.2).

We found that all three calculations yield the same result and thus serve as an excellent check for the dimension-shifting approach and for the very complicated double Mellin-Barnes calculation.

3.4 Diagrams 3.1e)

The diagrams in Fig. 3.1e) may again be solved in two ways. The first way is to use the large external momentum expansion technique [48]. The second possibility is to apply the dimension-shifting and integration-by-parts procedure [42] also for this diagram. We do without presenting the calculation and merely give the results for the contributions to the form factors.

$$F_{2,u}^{(9)}[e] = C_F \cdot \left[-\frac{2}{3} \left(\frac{1}{\epsilon} + 4L_\mu \right) - \frac{49}{9} - \frac{4i\pi}{3} + \frac{4}{3}L_s + \frac{16}{3}\zeta(3) \right], \quad (16)$$

$$F_{2,u}^{(7)}[e] = 0.$$

3.5 $\mathcal{O}(\alpha_s)$ counterterms to $\langle d\ell^+\ell^-|O_{1,2}^{u,c}|b\rangle$

So far, we have calculated the two-loop matrix elements $\langle d\ell^+\ell^-|C_i O_i^q|b\rangle$ ($i = 1, 2$; $q = u, c$). As the operators mix under renormalization, there are additional contributions proportional to C_i . These counterterms arise from the matrix elements of the operators

$$\sum_{j=1}^2 \delta Z_{ij}(O_j^u + O_j^c) + \sum_{j=3}^{10} \delta Z_{ij}O_j + \sum_{j=11}^{12} \delta Z_{ij}(O_j^u + O_j^c), \quad i = 1, 2, \quad (17)$$

where the operators O_1 – O_{10} are given in Eq. (2). $O_{11}^{u,c}$ and $O_{12}^{u,c}$ are evanescent operators, i.e. operators which vanish in $d = 4$ dimensions. In principle, there is some freedom in the choice of the evanescent operators. However, as we want to combine our matrix elements with the Wilson coefficients calculated by Bobeth et al. [32], we have to use the same definitions:

$$\begin{aligned} O_{11}^u &= (\bar{d}_L \gamma_\mu \gamma_\nu \gamma_\sigma T^a u_L) (\bar{u}_L \gamma^\mu \gamma^\nu \gamma^\sigma T^a b_L) - 16 O_1^u, \\ O_{12}^u &= (\bar{d}_L \gamma_\mu \gamma_\nu \gamma_\sigma u_L) (\bar{u}_L \gamma^\mu \gamma^\nu \gamma^\sigma b_L) - 16 O_2^u, \\ O_{11}^c &= (\bar{d}_L \gamma_\mu \gamma_\nu \gamma_\sigma T^a c_L) (\bar{c}_L \gamma^\mu \gamma^\nu \gamma^\sigma T^a b_L) - 16 O_1^c, \\ O_{12}^c &= (\bar{d}_L \gamma_\mu \gamma_\nu \gamma_\sigma c_L) (\bar{c}_L \gamma^\mu \gamma^\nu \gamma^\sigma b_L) - 16 O_2^c. \end{aligned} \quad (18)$$

The operator renormalization constants $Z_{ij} = \delta_{ij} + \delta Z_{ij}$ are of the form

$$\delta Z_{ij} = \frac{\alpha_s}{4\pi} \left(a_{ij}^{01} + \frac{1}{\epsilon} a_{ij}^{11} \right) + \frac{\alpha_s^2}{(4\pi)^2} \left(a_{ij}^{02} + \frac{1}{\epsilon} a_{ij}^{12} + \frac{1}{\epsilon^2} a_{ij}^{22} \right) + \mathcal{O}(\alpha_s^3). \quad (19)$$

The coefficients a_{ij}^{lm} needed for our calculation we take from Refs. [34, 32] and list them for $i = 1, 2$ and $j = 1, \dots, 12$:

$$\hat{a}^{11} = \begin{pmatrix} -2 & \frac{4}{3} & 0 & -\frac{1}{9} & 0 & 0 & 0 & 0 & -\frac{16}{27} & 0 & \frac{5}{12} & \frac{2}{9} \\ 6 & 0 & 0 & \frac{2}{3} & 0 & 0 & 0 & 0 & -\frac{4}{9} & 0 & 1 & 0 \end{pmatrix}, \quad (20)$$

$$\begin{aligned} a_{17}^{12} &= -\frac{58}{243}, & a_{19}^{12} &= -\frac{64}{729}, & a_{19}^{22} &= \frac{1168}{243}, \\ a_{27}^{12} &= \frac{116}{81}, & a_{29}^{12} &= \frac{776}{243}, & a_{29}^{22} &= \frac{148}{81}. \end{aligned} \quad (21)$$

We denote the counterterm contributions to $b \rightarrow d\ell^+\ell^-$ which are due to the mixing of O_1^u or O_2^u into four-quark operators by $F_{i,u \rightarrow 4\text{quark}}^{\text{ct}(7)}$ and $F_{i,u \rightarrow 4\text{quark}}^{\text{ct}(9)}$. They can be extracted from the equation

$$\sum_j \left(\frac{\alpha_s}{4\pi} \right) \frac{1}{\epsilon} a_{ij}^{11} \langle d\ell^+\ell^- | O_j^u | b \rangle_{1\text{-loop}} = - \left(\frac{\alpha_s}{4\pi} \right) \left[F_{i,u \rightarrow 4\text{quark}}^{\text{ct}(7)} \langle \tilde{O}_7 \rangle_{\text{tree}} + F_{i,u \rightarrow 4\text{quark}}^{\text{ct}(9)} \langle \tilde{O}_9 \rangle_{\text{tree}} \right], \quad (22)$$

where j runs over the four-quark operators. The operators O_j^u are understood to be identified with O_j for $j = 3, 4, 5, 6$. As certain entries of \hat{a}^{11} are zero, only the one-loop matrix elements of $O_1^{u,c}$, $O_2^{u,c}$, $O_4^{u,c}$, $O_{11}^{u,c}$ and $O_{12}^{u,c}$ are needed. In order to keep the presentation transparent, we relegate their explicit form to Appendix D. We do not repeat the renormalization of the O_1^c and O_2^c contributions at this place and refer to [34].

There is a counterterm related to the two-loop mixing of O_i^u ($i = 1, 2$) into O_7 , followed by taking the tree-level matrix element $\langle d\ell^+\ell^- | O_7 | b \rangle$. Denoting the corresponding contribution to the counterterm form factors by $F_{i,u \rightarrow 7}^{\text{ct}(7)}$ and $F_{i,u \rightarrow 7}^{\text{ct}(9)}$, we obtain

$$F_{i,u \rightarrow 7}^{\text{ct}(7)} = -\frac{a_{i7}^{12}}{\epsilon}, \quad F_{i,u \rightarrow 7}^{\text{ct}(9)} = 0. \quad (23)$$

The counterterms which are related to the mixing of O_i^u ($i = 1, 2$) into O_9 can be split into two classes: The first class consists of the one-loop mixing $O_i^u \rightarrow O_9$, followed by taking the one-loop corrected matrix element of O_9 . It is obvious that this class contributes to the renormalization of diagram 3.1f), which we take into account when discussing the virtual corrections to O_9 . We proceed in the same way with the corresponding counterterm.

The second class of counterterm contributions due to $O_i^u \rightarrow O_9$ mixing is generated by two-loop mixing of O_2^u into O_9 as well as by one-loop mixing and one-loop renormalization of the g_s factor in the definition of the operator O_9 . We denote the corresponding contribution to the counterterm form factors by $F_{i,u \rightarrow 9}^{\text{ct}(7)}$ and $F_{i,u \rightarrow 9}^{\text{ct}(9)}$. We obtain

$$F_{i,u \rightarrow 9}^{\text{ct}(9)} = - \left(\frac{a_{i9}^{22}}{\epsilon^2} + \frac{a_{i9}^{12}}{\epsilon} \right) - \frac{a_{i9}^{11} \beta_0}{\epsilon^2}, \quad F_{i,u \rightarrow 9}^{\text{ct}(7)} = 0, \quad (24)$$

where we used the renormalization constant Z_{g_s} given by

$$Z_{g_s} = 1 - \frac{\alpha_s}{4\pi} \frac{\beta_0}{2} \frac{1}{\epsilon}, \quad \beta_0 = 11 - \frac{2}{3} N_f, \quad N_f = 5. \quad (25)$$

The total counterterms $F_{i,u}^{\text{ct}(j)}$ ($i = 1, 2; j = 7, 9$), which renormalize diagrams 3.1a)–3.1e), are given by

$$F_{i,u}^{\text{ct}(j)} = F_{i,u \rightarrow 4\text{quark}}^{\text{ct}(j)} + F_{i,u \rightarrow 7}^{\text{ct}(j)} + F_{i,u \rightarrow 9}^{\text{ct}(j)}. \quad (26)$$

Explicitly they read

$$\begin{aligned} F_{2,u}^{\text{ct}(9)} = & - F_{2,u,\text{div}}^{(9)} - \frac{8}{25515} [2870 - 6300 \pi^2 - 420 i\pi + 126 \hat{s} - \hat{s}^3] \\ & + \frac{8}{25515} [-420 - 21420 i\pi + 252 \hat{s} + 27 \hat{s}^2 + 4 \hat{s}^3] L_\mu \\ & - \frac{136}{81} L_s^2 + \left[\frac{16}{243} (-2 + 51 i\pi) + \frac{544}{81} L_\mu \right] L_s - \frac{512}{81} L_\mu^2, \end{aligned} \quad (27)$$

$$F_{2,u}^{\text{ct}(7)} = - F_{2,u,\text{div}}^{(7)} + \frac{2}{2835} (840 L_\mu + 70 \hat{s} + 7 \hat{s}^2 + \hat{s}^3),$$

$$\begin{aligned} F_{1,u}^{\text{ct}(9)} = & - F_{1,u,\text{div}}^{(9)} + \frac{4}{76545} [59570 - 6300 \pi^2 + 33600 i\pi + 126 \hat{s} - \hat{s}^3] \\ & + \frac{4}{76545} [68460 + 21420 i\pi - 252 \hat{s} - 27 \hat{s}^2 - 4 \hat{s}^3] L_\mu \\ & + \frac{68}{243} L_s^2 - \left[\frac{8}{729} (160 + 51 i\pi) + \frac{272}{243} L_\mu \right] L_s + \frac{256}{243} L_\mu^2, \end{aligned} \quad (28)$$

$$F_{1,u}^{\text{ct}(7)} = - F_{1,u,\text{div}}^{(7)} - \frac{1}{8505} (840 L_\mu + 70 \hat{s} + 7 \hat{s}^2 + \hat{s}^3).$$

The quantities $F_{i,u,\text{div}}^{(j)}$ ($i = 1, 2; j = 7, 9$) compensate the divergent parts of the form

factors associated with the virtual corrections to $O_{1,2}^u$. They are given by

$$\begin{aligned}
 F_{2,u,\text{div}}^{(9)} &= \frac{128}{81 \epsilon^2} + \frac{4}{25515 \epsilon} [20790 + 21420 i\pi - 252 \hat{s} - 27 \hat{s}^2 - 4 \hat{s}^3] \\
 &\quad + \frac{16}{81 \epsilon} (32 L_\mu - 17 L_s), \\
 F_{2,u,\text{div}}^{(7)} &= \frac{92}{81 \epsilon}, \\
 F_{1,u,\text{div}}^{(9)} &= -\frac{64}{243 \epsilon^2} - \frac{2}{76545 \epsilon} [71820 + 21420 i\pi - 252 \hat{s} - 27 \hat{s}^2 - 4 \hat{s}^3] \\
 &\quad - \frac{8}{243 \epsilon} (32 L_\mu - 17 L_s), \\
 F_{1,u,\text{div}}^{(7)} &= -\frac{46}{243 \epsilon}.
 \end{aligned}$$

As mentioned before, we will take diagram 3.1f) into account only in Section 4. The same holds for the counterterms associated with the b - and d -quark wave function renormalization and, as stated earlier in this subsection, the $\mathcal{O}(\alpha_s)$ correction to the matrix element of $\delta Z_{i9} O_9$. The sum of these contributions is

$$\delta \bar{Z}_\psi \langle O_i^u \rangle_{1\text{-loop}} + \frac{\alpha_s}{4\pi} \frac{a_{i9}^{11}}{\epsilon} [\delta \bar{Z}_\psi \langle O_9 \rangle_{\text{tree}} + \langle O_9 \rangle_{1\text{-loop}}], \quad \delta \bar{Z}_\psi = \sqrt{Z_\psi(m_b) Z_\psi(m_d)} - 1,$$

and provides the counterterm that renormalizes diagram 3.1f). We use on-shell renormalization for the external b - and d -quark. In this scheme the field strength renormalization constants are given by

$$Z_\psi(m) = 1 - \frac{\alpha_s}{4\pi} \frac{4}{3} \left(\frac{\mu}{m} \right)^{2\epsilon} \left(\frac{1}{\epsilon} + \frac{2}{\epsilon_{\text{IR}}} + 4 \right). \quad (29)$$

So far, we have discussed the counterterms which renormalize the $\mathcal{O}(\alpha_s)$ corrected matrix elements $\langle d \ell^+ \ell^- | O_i^u | b \rangle$ ($i = 1, 2$). The corresponding one-loop matrix elements [of $\mathcal{O}(\alpha_s^0)$] are renormalized by adding the counterterms

$$\frac{\alpha_s}{4\pi} \frac{a_{i9}^{11}}{\epsilon} \langle O_9 \rangle_{\text{tree}}.$$

3.6 Renormalized form factors of O_1^u and O_2^u

We now have all ingredients necessary to present the renormalized form factors associated with the operators O_1^u and O_2^u . We stress again that only the contributions of the diagrams 3.1a)-e) and the counterterms discussed in Subsection 3.5 are accounted for in the result below. Diagram 3.1f) and associated counterterms will be included in the discussion of the virtual corrections to O_9 . We decompose the renormalized matrix elements of O_i ($i = 1, 2$) as

$$\langle d \ell^+ \ell^- | O_i^u | b \rangle = -\frac{\alpha_s}{4\pi} \left[F_{i,u}^{(9)} \langle \tilde{O}_9 \rangle_{\text{tree}} + F_{i,u}^{(7)} \langle \tilde{O}_7 \rangle_{\text{tree}} \right], \quad (30)$$

where the operators \tilde{O}_7 and \tilde{O}_9 are defined in Eq. (8). The renormalized form factors read:

$$\begin{aligned}
 F_{1,u}^{(7)} = & -\frac{833}{729} - \frac{208}{243} L_\mu - \frac{40 i\pi}{243} + \left(-\frac{2}{729} - \frac{58}{243} L_s + \frac{2 i\pi}{27} + \frac{4 i\pi}{27} L_s + \frac{8 \pi^2}{243} \right) \hat{s} \\
 & + \left(-\frac{1453}{3645} + \frac{14}{243} L_s - \frac{2 i\pi}{27} + \frac{4 i\pi}{27} L_s + \frac{14 \pi^2}{243} \right) \hat{s}^2 \\
 & + \left(-\frac{4712}{5103} + \frac{68}{243} L_s + \frac{2}{27} L_s^2 - \frac{2 i\pi}{9} + \frac{26 \pi^2}{243} \right) \hat{s}^3,
 \end{aligned} \tag{31}$$

$$\begin{aligned}
 F_{1,u}^{(9)} = & -\frac{1736}{243} + \frac{224}{81} L_s - \frac{2864}{729} L_\mu + \frac{272}{243} L_s L_\mu - \frac{256}{243} L_\mu^2 \\
 & - \frac{520 i\pi}{243} + \frac{64 i\pi}{243} L_s - \frac{272 i\pi}{243} L_\mu + \frac{200 \pi^2}{729} + \frac{256}{27} \zeta(3) \\
 & + \left(-\frac{388}{675} + \frac{20}{27} L_s + \frac{16}{1215} L_\mu + \frac{4 i\pi}{27} - \frac{8 i\pi}{27} L_s - \frac{8 \pi^2}{243} \right) \hat{s} \\
 & + \left(\frac{1018057}{1786050} + \frac{4}{243} L_s - \frac{4}{27} L_s^2 + \frac{4}{2835} L_\mu + \frac{4 i\pi}{9} - \frac{8 \pi^2}{81} \right) \hat{s}^2 \\
 & + \left(\frac{92876363}{48223350} - \frac{344}{729} L_s - \frac{4}{9} L_s^2 + \frac{16}{76545} L_\mu + \frac{20 i\pi}{27} + \frac{16 i\pi}{27} L_s - \frac{164 \pi^2}{729} \right) \hat{s}^3,
 \end{aligned} \tag{32}$$

$$\begin{aligned}
 F_{2,u}^{(7)} = & \frac{1666}{243} + \frac{416}{81} L_\mu + \frac{80 i\pi}{81} + \left(\frac{4}{243} + \frac{116}{81} L_s - \frac{4 i\pi}{9} - \frac{8 i\pi}{9} L_s - \frac{16 \pi^2}{81} \right) \hat{s} \\
 & + \left(\frac{2906}{1215} - \frac{28}{81} L_s + \frac{4 i\pi}{9} - \frac{8 i\pi}{9} L_s - \frac{28 \pi^2}{81} \right) \hat{s}^2 \\
 & + \left(\frac{9424}{1701} - \frac{136}{81} L_s - \frac{4}{9} L_s^2 + \frac{4 i\pi}{3} - \frac{52 \pi^2}{81} \right) \hat{s}^3,
 \end{aligned} \tag{33}$$

$$\begin{aligned}
 F_{2,u}^{(9)} = & -\frac{380}{81} - \frac{304}{27} L_s + \frac{3136}{243} L_\mu - \frac{544}{81} L_s L_\mu + \frac{512}{81} L_\mu^2 \\
 & + \frac{608 i\pi}{81} - \frac{128 i\pi}{81} L_s + \frac{544 i\pi}{81} L_\mu - \frac{400 \pi^2}{243} + \frac{64}{9} \zeta(3) \\
 & + \left(\frac{776}{225} - \frac{40}{9} L_s - \frac{32}{405} L_\mu - \frac{8 i\pi}{9} + \frac{16 i\pi}{9} L_s + \frac{16 \pi^2}{81} \right) \hat{s} \\
 & + \left(-\frac{1018057}{297675} - \frac{8}{81} L_s + \frac{8}{9} L_s^2 - \frac{8}{945} L_\mu - \frac{8 i\pi}{3} + \frac{16 \pi^2}{27} \right) \hat{s}^2 \\
 & + \left(-\frac{92876363}{8037225} + \frac{688}{243} L_s + \frac{8}{3} L_s^2 - \frac{32}{25515} L_\mu - \frac{40 i\pi}{9} - \frac{32 i\pi}{9} L_s + \frac{328 \pi^2}{243} \right) \hat{s}^3,
 \end{aligned} \tag{34}$$

with

$$L_s = \ln(\hat{s}) \quad \text{and} \quad L_\mu = \ln\left(\frac{\mu}{m_b}\right).$$

As has been mentioned before, we only include terms up to $\mathcal{O}(\hat{s}^3)$ in the result. We checked, however, that the terms of order \hat{s}^4 are numerically negligible.

4 Virtual corrections to the matrix elements of the operators O_7 , O_8 , O_9 and O_{10}

The virtual corrections to the matrix elements of O_7 , O_8 , O_9 and O_{10} and their renormalization are discussed in detail in Refs. [34, 49]. For completeness we list the results of the renormalized matrix elements. They may all be decomposed according to

$$\langle d \ell^+ \ell^- | C_i O_i | b \rangle = \tilde{C}_i^{(0)} \left(-\frac{\alpha_s}{4\pi} \right) \left[F_i^{(9)} \langle \tilde{O}_9 \rangle_{\text{tree}} + F_i^{(7)} \langle \tilde{O}_7 \rangle_{\text{tree}} \right],$$

where

$$\begin{aligned} \tilde{O}_i &= \frac{\alpha_s}{4\pi} O_i, \\ \tilde{C}_7^{(0)} &= C_7^{(1)}, \quad \tilde{C}_8^{(0)} = C_8^{(1)}, \\ \tilde{C}_9^{(0)} &= \frac{4\pi}{\alpha_s} \left(C_9^{(0)} + \frac{\alpha_s}{4\pi} C_9^{(1)} \right) \quad \text{and} \quad \tilde{C}_{10}^{(0)} = C_{10}^{(1)}. \end{aligned}$$

4.1 Renormalized matrix element of O_7

The renormalized corrections to the form factors $F_7^{(9)}$ and $F_7^{(7)}$ are given by

$$F_7^{(9)} = -\frac{16}{3} \left(1 + \frac{1}{2} \hat{s} + \frac{1}{3} \hat{s}^2 + \frac{1}{4} \hat{s}^3 \right), \quad (35)$$

$$F_7^{(7)} = \frac{32}{3} L_\mu + \frac{32}{3} + 8 \hat{s} + 6 \hat{s}^2 + \frac{128}{27} \hat{s}^3 + f_{\text{inf}}. \quad (36)$$

The function f_{inf} collects the infrared- and collinear singular parts:

$$f_{\text{inf}} = \frac{\left[\frac{\mu}{m_b} \right]^{2\epsilon}}{\epsilon_{\text{IR}}} \frac{8}{3} \left(1 + \hat{s} + \frac{1}{2} \hat{s}^2 + \frac{1}{3} \hat{s}^3 \right) + \frac{\left[\frac{\mu}{m_b} \right]^{2\epsilon}}{\epsilon_{\text{IR}}} \frac{4}{3} \ln(r) + \frac{2}{3} \ln(r) - \frac{2}{3} \ln^2(r), \quad (37)$$

where ϵ_{IR} and $r = (m_d^2/m_b^2)$ regularize the infrared- and collinear singularities, respectively.

4.2 Renormalized matrix element of the operator O_8

The renormalized corrections to the form factors of the matrix element of O_8 are

$$\begin{aligned} F_8^{(9)} &= \frac{104}{9} - \frac{32}{27} \pi^2 + \left(\frac{1184}{27} - \frac{40}{9} \pi^2 \right) \hat{s} + \left(\frac{14212}{135} - \frac{32}{3} \pi^2 \right) \hat{s}^2 \\ &+ \left(\frac{193444}{945} - \frac{560}{27} \pi^2 \right) \hat{s}^3 + \frac{16}{9} L_s (1 + \hat{s} + \hat{s}^2 + \hat{s}^3), \end{aligned} \quad (38)$$

$$\begin{aligned}
 F_8^{(7)} = & -\frac{32}{9} L_\mu + \frac{8}{27} \pi^2 - \frac{44}{9} - \frac{8}{9} i\pi + \left(\frac{4}{3} \pi^2 - \frac{40}{3} \right) \hat{s} + \left(\frac{32}{9} \pi^2 - \frac{316}{9} \right) \hat{s}^2 \\
 & + \left(\frac{200}{27} \pi^2 - \frac{658}{9} \right) \hat{s}^3 - \frac{8}{9} L_s (\hat{s} + \hat{s}^2 + \hat{s}^3) .
 \end{aligned} \tag{39}$$

4.3 Renormalized matrix element of O_9 and O_{10}

The renormalized matrix elements of O_9 and O_{10} , finally, are described by the form factors

$$F_9^{(9)} = \frac{16}{3} + \frac{20}{3} \hat{s} + \frac{16}{3} \hat{s}^2 + \frac{116}{27} \hat{s}^3 + f_{\text{inf}} , \tag{40}$$

$$F_9^{(7)} = -\frac{2}{3} \hat{s} \left(1 + \frac{1}{2} \hat{s} + \frac{1}{3} \hat{s}^2 \right) , \tag{41}$$

$$F_{10}^{(9)} = F_9^{(9)} , \tag{42}$$

$$F_{10}^{(7)} = F_9^{(7)} , \tag{43}$$

where f_{inf} is defined in Eq. (37).

The contribution of the renormalized diagrams 3.1f), which have been omitted so far, is properly included by modifying $\tilde{C}_9^{(0)}$ as follows:

$$\tilde{C}_9^{(0)} \rightarrow \tilde{C}_9^{(0,\text{mod})} = \tilde{C}_9^{(0)} - \frac{1}{\xi_t} \left(C_2^{(0)} + \frac{4}{3} C_1^{(0)} \right) (\xi_u H_0(0) + \xi_c H_0(z)) .$$

For $\hat{s} < 4z$ ($z = m_c^2/m_b^2$) the loop function $H_0(z)$ can be expanded in terms of $\hat{s}/(4z)$. We give the expansion of $H_0(z)$ as well as the result for $H_0(0)$:

$$H_0(z) = \frac{1}{2835} \left[-1260 + 2520 \ln \left(\frac{\mu}{m_c} \right) + 1008 \left(\frac{\hat{s}}{4z} \right) + 432 \left(\frac{\hat{s}}{4z} \right)^2 + 256 \left(\frac{\hat{s}}{4z} \right)^3 \right] , \tag{44}$$

$$H_0(0) = \frac{8}{27} - \frac{4}{9} \ln(\hat{s}) + \frac{4i\pi}{9} + \frac{8}{9} L_\mu .$$

5 Corrections to the Decay Width $B \rightarrow X_d \ell^+ \ell^-$

The decay width differential in \hat{s} can be written as

$$\begin{aligned} \frac{d\Gamma(b \rightarrow X_d \ell^+ \ell^-)}{d\hat{s}} &= \left(\frac{\alpha_{\text{em}}}{4\pi}\right)^2 \frac{G_F^2 m_{b,\text{pole}}^5 |\xi_t|^2}{48\pi^3} (1-\hat{s})^2 \left\{ (1+2\hat{s}) \left(\left| \tilde{C}_9^{\text{eff}} \right|^2 + \left| \tilde{C}_{10}^{\text{eff}} \right|^2 \right) \right. \\ &\quad \left. + 4(1+2/\hat{s}) \left| \tilde{C}_7^{\text{eff}} \right|^2 + 12 \text{Re} \left(\tilde{C}_7^{\text{eff}} \tilde{C}_9^{\text{eff}*} \right) \right\} \\ &\quad + \frac{d\Gamma^{\text{Brems, A}}}{d\hat{s}} + \frac{d\Gamma^{\text{Brems, B}}}{d\hat{s}}. \end{aligned} \quad (45)$$

The last two terms in Eq. (45) correspond to certain finite bremsstrahlung contributions specified in Appendix E. Their result can also be found in this appendix. All other corrections have been absorbed into the effective Wilson coefficients \tilde{C}_7^{eff} , \tilde{C}_9^{eff} and $\tilde{C}_{10}^{\text{eff}}$. We follow [34, 49, 32] and write the effective Wilson coefficients as

$$\begin{aligned} \tilde{C}_9^{\text{eff}} &= \left(1 + \frac{\alpha_s(\mu)}{\pi} \omega_9(\hat{s}) \right) \left(A_9 - \frac{\xi_c}{\xi_t} T_{9a} h(z, \hat{s}) - \frac{\xi_u}{\xi_t} T_{9a} h(0, \hat{s}) + T_{9b} h(z, \hat{s}) \right. \\ &\quad \left. + U_9 h(1, \hat{s}) + W_9 h(0, \hat{s}) \right) \\ &\quad + \frac{\alpha_s(\mu)}{4\pi} \left(\frac{\xi_u}{\xi_t} \left(C_1^{(0)} F_{1,u}^{(9)} + C_2^{(0)} F_{2,u}^{(9)} \right) + \frac{\xi_c}{\xi_t} \left(C_1^{(0)} F_{1,c}^{(9)} + C_2^{(0)} F_{2,c}^{(9)} \right) - A_8^{(0)} F_8^{(9)} \right), \\ \tilde{C}_7^{\text{eff}} &= \left(1 + \frac{\alpha_s(\mu)}{\pi} \omega_7(\hat{s}) \right) A_7 \\ &\quad + \frac{\alpha_s(\mu)}{4\pi} \left(\frac{\xi_u}{\xi_t} \left(C_1^{(0)} F_{1,u}^{(7)} + C_2^{(0)} F_{2,u}^{(7)} \right) + \frac{\xi_c}{\xi_t} \left(C_1^{(0)} F_{1,c}^{(7)} + C_2^{(0)} F_{2,c}^{(7)} \right) - A_8^{(0)} F_8^{(7)} \right), \\ \tilde{C}_{10}^{\text{eff}} &= \left(1 + \frac{\alpha_s(\mu)}{\pi} \omega_9(\hat{s}) \right) A_{10}, \end{aligned} \quad (46)$$

where we have provided the necessary modification to account for the CKM structure of $b \rightarrow d \ell^+ \ell^-$. The renormalized form factors $F_{1,u}^{(7,9)}$ and $F_{2,u}^{(7,9)}$ and can be found in Section 3.6 while the renormalized form factors $F_{1,c}^{(7,9)}$, $F_{2,c}^{(7,9)}$ and $F_8^{(7,9)}$ are given in [34, 49]. The functions $\omega_7(\hat{s})$ and $\omega_9(\hat{s})$ encapsulate the interference between the tree-level and the one-loop matrix elements of O_7 and $O_{9,10}$ and the corresponding bremsstrahlung corrections, which cancel the infrared- and collinear divergences appearing in the virtual corrections. When calculating the decay width (45), we retain only terms linear in α_s (and thus in ω_7 , ω_9) in the expressions for $|\tilde{C}_7^{\text{eff}}|^2$, $|\tilde{C}_9^{\text{eff}}|^2$ and $|\tilde{C}_{10}^{\text{eff}}|^2$. Accordingly, we drop terms of $\mathcal{O}(\alpha_s^2)$ in the interference term $\text{Re} \left(\tilde{C}_7^{\text{eff}} \tilde{C}_9^{\text{eff}*} \right)$, too, where by construction one has to make the replacements $\omega_9 \rightarrow \omega_{79}$ and $\omega_7 \rightarrow \omega_{79}$ in this term. The function ω_9 has already

been calculated in [32], where also the exact expression for $h(\hat{s}, z)$ can be found. For the functions ω_7 and ω_{79} and more information on the cancellation of infrared- and collinear divergences we refer to [34].

The auxiliary quantities $A_7, A_9, A_{10}, T_{9a}, T_{9b}, U_9$ and W_9 are the following linear combinations of the Wilson coefficients $C_i(\mu)$:

$$\begin{aligned}
A_7 &= \frac{4\pi}{\alpha_s(\mu)} C_7(\mu) - \frac{1}{3} C_3(\mu) - \frac{4}{9} C_4(\mu) - \frac{20}{3} C_5(\mu) - \frac{80}{9} C_6(\mu), \\
A_8 &= \frac{4\pi}{\alpha_s(\mu)} C_8(\mu) + C_3(\mu) - \frac{1}{6} C_4(\mu) + 20 C_5(\mu) - \frac{10}{3} C_6(\mu), \\
A_9 &= \frac{4\pi}{\alpha_s(\mu)} C_9(\mu) + \frac{4}{3} C_3(\mu) + \frac{64}{9} C_5(\mu) + \frac{64}{27} C_6(\mu) \\
&\quad + \left[\frac{\xi_u + \xi_c}{-\xi_t} \left(C_1(\mu) \gamma_{19}^{(0)} + C_2(\mu) \gamma_{29}^{(0)} \right) + \sum_{i=3}^6 C_i(\mu) \gamma_{i9}^{(0)} \right] \ln \left(\frac{m_b}{\mu} \right), \\
A_{10} &= \frac{4\pi}{\alpha_s(\mu)} C_{10}(\mu), \\
T_{9a} &= \frac{4}{3} C_1(\mu) + C_2(\mu), \\
T_{9b} &= 6 C_3(\mu) + 60 C_5(\mu), \\
U_9 &= -\frac{7}{2} C_3(\mu) - \frac{2}{3} C_4(\mu) - 38 C_5(\mu) - \frac{32}{3} C_6(\mu), \\
W_9 &= -\frac{1}{2} C_3(\mu) - \frac{2}{3} C_4(\mu) - 8 C_5(\mu) - \frac{32}{3} C_6(\mu).
\end{aligned} \tag{47}$$

In these definitions we also include some diagrams induced by $O_{3,4,5,6}$ insertions, viz the $\mathcal{O}(\alpha_s^0)$ contributions, the diagrams of topology 3.1f) and those bremsstrahlung diagrams where the gluon is emitted from the b - or d -quark line (cf [35]).

For completeness, we give in Table 5.1 numerical values for $C_1, C_2, A_7, A_8, A_9, A_{10}, T_{9a}, T_{9b}, U_9$ and W_9 at three different values of the renormalization scale μ . We note that the recently calculated contributions [33] to the anomalous dimension matrix which correspond to the three-loop mixings of the four-quark operators into O_9 have been included by adopting the procedure described in Appendix C. As can be seen in Table 5.1, some of the entries have a very small amount of significant digits. In our numerical analysis presented in Section 6 we work with a much higher accuracy.

6 Phenomenological analysis

As the main point of this paper is the *calculation* of the NNLL corrections to the process $b \rightarrow X_d \ell^+ \ell^-$, we keep the phenomenological analysis rather short. In the following we investigate the impact of the NNLL corrections on three observables: the branching ratio,

	$\mu = 2.5 \text{ GeV}$	$\mu = 5 \text{ GeV}$	$\mu = 10 \text{ GeV}$
α_s	0.267	0.215	0.180
$(C_1^{(0)}, C_1^{(1)})$	(-0.696, 0.240)	(-0.486, 0.206)	(-0.326, 0.184)
$(C_2^{(0)}, C_2^{(1)})$	(1.046, -0.276)	(1.023, -0.017)	(1.011, -0.010)
$(A_7^{(0)}, A_7^{(1)})$	(-0.360, 0.032)	(-0.321, 0.018)	(-0.287, 0.009)
$(A_8^{(0)}, A_8^{(1)})$	(-0.169, -0.015)	(-0.153, -0.013)	(-0.140, -0.012)
$(A_9^{(0)}, A_9^{(1)})$	(4.241, -0.091)	(4.128, 0.066)	(4.131, 0.190)
$(T_{9a}^{(0)}, T_{9a}^{(1)})$	(0.118, 0.292)	(0.376, 0.258)	(0.577, 0.235)
$(T_{9b}^{(0)}, T_{9b}^{(1)})$	(-0.003, -0.013)	(-0.001, -0.007)	(0.000, -0.004)
$(U_9^{(0)}, U_9^{(1)})$	(0.045, 0.023)	(0.033, 0.015)	(0.022, 0.010)
$(W_9^{(0)}, W_9^{(1)})$	(0.044, 0.016)	(0.032, 0.012)	(0.022, 0.009)
$(A_{10}^{(0)}, A_{10}^{(1)})$	(-4.373, 0.135)	(-4.373, 0.135)	(-4.373, 0.135)

Table 5.1: Coefficients appearing in Eq. (47) for $\mu = 2.5 \text{ GeV}$, $\mu = 5 \text{ GeV}$ and $\mu = 10 \text{ GeV}$. For $\alpha_s(\mu)$ (in the $\overline{\text{MS}}$ scheme) we used the two-loop expression with 5 flavors and $\alpha_s(m_Z) = 0.119$. The entries correspond to the pole top quark mass $m_t = 174 \text{ GeV}$. The matching for the top and for the charm contribution was performed at a scale of 120 GeV and 80 GeV, respectively [32]. The superscript (0) refers to lowest order quantities, while the superscript (1) denotes the correction terms of order α_s , i.e. $X = X^{(0)} + X^{(1)}$ with $X = C, A, T, U, W$. Note that the contributions calculated recently in Ref. [33] are included. These contributions only affect the entries for $A_9^{(1)}$.

the CP asymmetry and the normalized forward-backward asymmetry. As our main point is to illustrate the differences between NLL and NNLL results, we do not include power corrections (and/or effects from resonances), postponing this to future studies.

Since the decay width given in Eq. (45) suffers from a large uncertainty due to the factor $m_{b,\text{pole}}^5$, we follow common practice and introduce the ratio

$$R_{\text{quark}}(\hat{s}) = \frac{1}{\Gamma(b \rightarrow X_c e \bar{\nu}_e)} \frac{\frac{d\Gamma(b \rightarrow X_d \ell^+ \ell^-)}{d\hat{s}} + \frac{d\Gamma(\bar{b} \rightarrow X_{\bar{d}} \ell^+ \ell^-)}{d\hat{s}}}{2}, \quad (48)$$

in which the factor $m_{b,\text{pole}}^5$ drops out. Note that we define $R_{\text{quark}}(\hat{s})$ as a charge-conjugate average as this is likely to be the first quantity measured. The expression for the semilep-

tonic decay width $\Gamma(b \rightarrow X_c e \bar{\nu}_e)$ is as follows:

$$\Gamma(b \rightarrow X_c e \bar{\nu}_e) = \frac{G_F^2 m_{b,\text{pole}}^5}{192\pi^3} |V_{cb}|^2 \cdot g \left(\frac{m_{c,\text{pole}}^2}{m_{b,\text{pole}}^2} \right) \cdot K \left(\frac{m_c^2}{m_b^2} \right), \quad (49)$$

where $g(z) = 1 - 8z + 8z^3 - z^4 - 12z^2 \ln(z)$ is the phase space factor, and

$$K(z) = 1 - \frac{2\alpha_s(m_b) f(z)}{3\pi g(z)} \quad (50)$$

incorporates the next-to-leading QCD correction to the semileptonic decay. The function $f(z)$ has been given analytically in Ref. [50]:

$$\begin{aligned} f(z) = & -(1 - z^2) \left(\frac{25}{4} - \frac{239}{3} z + \frac{25}{4} z^2 \right) + z \ln(z) \left(20 + 90z - \frac{4}{3} z^2 + \frac{17}{3} z^3 \right) \\ & + z^2 \ln^2(z) (36 + z^2) + (1 - z^2) \left(\frac{17}{3} - \frac{64}{3} z + \frac{17}{3} z^2 \right) \ln(1 - z) \\ & - 4(1 + 30z^2 + z^4) \ln(z) \ln(1 - z) - (1 + 16z^2 + z^4) (6\text{Li}(z) - \pi^2) \\ & - 32z^{3/2}(1 + z) \left[\pi^2 - 4\text{Li}(\sqrt{z}) + 4\text{Li}(-\sqrt{z}) - 2\ln(z) \ln \left(\frac{1 - \sqrt{z}}{1 + \sqrt{z}} \right) \right]. \end{aligned} \quad (51)$$

In the following analysis we write the CKM parameters appearing in $b \rightarrow X_d \ell^+ \ell^-$ as (neglecting terms of $\mathcal{O}(\lambda^7)$)

$$\xi_u = A \lambda^3 (\bar{\rho} - i\bar{\eta}), \quad \xi_t = A \lambda^3 (1 - \bar{\rho} + i\bar{\eta}), \quad \xi_c = -\xi_u - \xi_t,$$

with $\bar{\rho} = \rho(1 - \lambda^2/2)$ and $\bar{\eta} = \eta(1 - \lambda^2/2)$ [51]. For V_{cb} , appearing in the semileptonic decay width, we use $V_{cb} = A\lambda^2$. Numerically, we set $A = 0.81$, $\lambda = 0.22$, $\bar{\rho} = 0.22$ and $\bar{\eta} = 0.35$. For the other input parameters we use $\alpha_s(m_Z) = 0.119$, $m_t^{\text{pole}} = 174$ GeV, $\alpha_{\text{em}} = 1/133$, $m_b = 4.8$ GeV, $m_c/m_b = 0.29$, $m_W = 80.41$ GeV, $m_Z = 91.19$ GeV, and $\sin^2(\theta_W) = 0.231$.

In Fig. 6.1 we show the μ -dependence of $R_{\text{quark}}(\hat{s})$ for $0.05 \leq \hat{s} \leq 0.25$. The solid lines correspond to the NNLL results, whereas the dashed lines represent the NLL results. We see that, going from NLL to NNLL precision, $R_{\text{quark}}(\hat{s})$ is decreased throughout the entire region by about 20 – 30%. Although the absolute uncertainty due to the μ -dependence decreases as well, the relative error remains roughly the same.

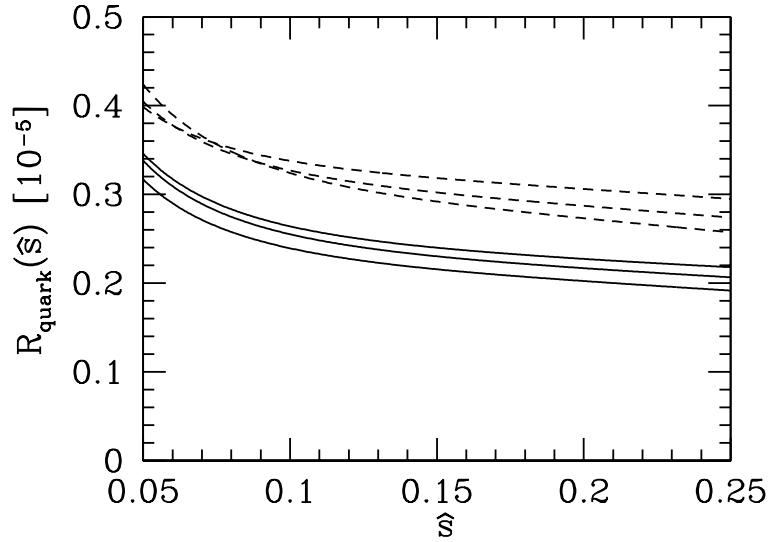


Figure 6.1: $R_{\text{quark}}(\hat{s})$ as defined in Eq. (48). The solid lines show the NNLL result for $\mu = 2.5, 5.0, 10.0$ GeV, whereas the dashed lines show the corresponding result in the NLL approximation. At $\hat{s} = 0.25$ the highest (lowest) curve correspond to $\mu = 10$ GeV ($\mu = 2.5$ GeV) both in the NLL and NNLL case.

As mentioned already in the introduction, the region $0.05 \leq \hat{s} \leq 0.25$ is free of resonances, as it lies below the J/Ψ threshold and above the ρ and ω resonances. The contribution of this region to the decay width (normalized by $\Gamma(b \rightarrow X_c e \bar{\nu}_e)$) is therefore well approximated by integrating $R_{\text{quark}}(\hat{s})$ over this interval. At NNLL precision, we get

$$R_{\text{quark}} = \int_{0.05}^{0.25} d\hat{s} R_{\text{quark}}(\hat{s}) = (4.75 \pm 0.25) \times 10^{-7}. \quad (52)$$

The error is obtained by varying the scale μ between 2.5 GeV and 10 GeV. The corresponding result in NLL precision is $R_{\text{quark}} = (6.29 \pm 0.21) \times 10^{-7}$. The renormalization scale dependence therefore increases from $\sim \pm 3.4\%$ to $\sim \pm 5.3\%$. The reason for this increase can be understood from Fig. 6.1: While for $0.13 < \hat{s} < 0.25$ the μ dependence of $R_{\text{quark}}(\hat{s})$ at NNLL and NLL precision is similar, the μ dependence almost cancels in the NLL case when integrating \hat{s} between 0.05 and 0.13 due to the crossing of the dashed lines in this interval. This cancellation does not happen in the NNLL case, leading to a slightly larger μ -dependence of R_{quark} at NNLL.

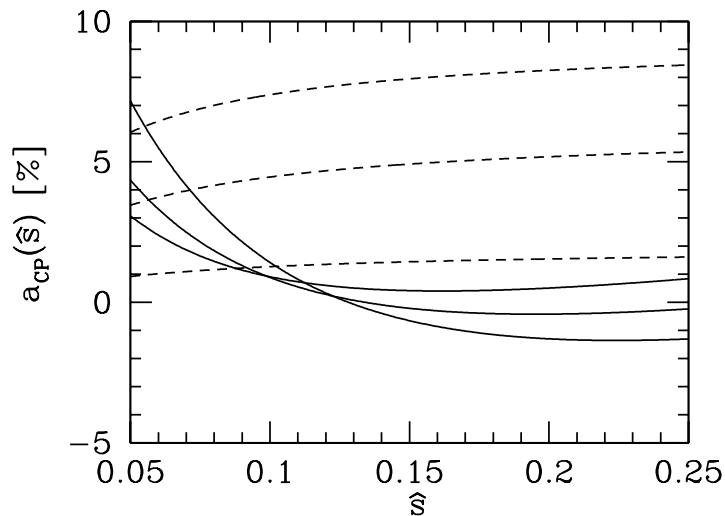


Figure 6.2: CP asymmetry: The solid lines show the NNLL result for $\mu = 2.5, 5.0, 10.0$ GeV, whereas the dashed lines show the corresponding result in the NLL approximation. At $\hat{s} = 0.25$ the highest (lowest) curve correspond to $\mu = 10$ GeV ($\mu = 2.5$ GeV) both in the NLL and NNLL case.

As pointed out already, in the process $b \rightarrow X_d \ell^+ \ell^-$ the contribution of the u -quark running in the fermion loop is, in contrast to $b \rightarrow X_s \ell^+ \ell^-$, not Cabibbo-suppressed. As a consequence, CP violation effects are much larger in $b \rightarrow X_d \ell^+ \ell^-$. The CP asymmetry $a_{\text{CP}}(\hat{s})$ is defined as

$$a_{\text{CP}}(\hat{s}) = \frac{\frac{d\Gamma(b \rightarrow X_d \ell^+ \ell^-)}{d\hat{s}} - \frac{d\Gamma(\bar{b} \rightarrow X_{\bar{d}} \ell^+ \ell^-)}{d\hat{s}}}{\frac{d\Gamma(b \rightarrow X_d \ell^+ \ell^-)}{d\hat{s}} + \frac{d\Gamma(\bar{b} \rightarrow X_{\bar{d}} \ell^+ \ell^-)}{d\hat{s}}}. \quad (53)$$

In Fig. 6.2 we show $a_{\text{CP}}(\hat{s})$ for $0.05 \leq \hat{s} \leq 0.25$. The solid and dashed lines correspond to the NNLL and NLL results, respectively. We find several differences between the two results: The solid lines are much closer together. Also they cross each other at $\hat{s} \approx 0.11$. Furthermore, the NLL result clearly shows a positive CP asymmetry throughout the entire \hat{s} region considered, while the NNLL lines indicate that $a_{\text{CP}}(\hat{s})$ can be both positive and negative, depending on the value of \hat{s} . Because of that, it does not make much sense to quantify the relative error due to the μ -dependence. The plot, however, clearly shows that the absolute uncertainty is much smaller in the NNLL result. For NLL results, see also Ref. [52].

We also give the averaged CP asymmetry a_{CP} in the region $0.05 \leq \hat{s} \leq 0.25$, defined as

$$a_{\text{CP}} = \frac{\int_{0.05}^{0.25} d\hat{s} \left(\frac{d\Gamma(b \rightarrow X_d \ell^+ \ell^-)}{d\hat{s}} - \frac{d\Gamma(\bar{b} \rightarrow X_{\bar{d}} \ell^+ \ell^-)}{d\hat{s}} \right)}{\int_{0.05}^{0.25} d\hat{s} \left(\frac{d\Gamma(b \rightarrow X_d \ell^+ \ell^-)}{d\hat{s}} + \frac{d\Gamma(\bar{b} \rightarrow X_{\bar{d}} \ell^+ \ell^-)}{d\hat{s}} \right)}. \quad (54)$$

Varying μ between 2.5 GeV and 10 GeV one obtains the ranges

$$1.4\% \leq a_{\text{CP}}^{\text{NLL}} \leq 7.7\%, \quad ; \quad 0.56\% \leq a_{\text{CP}}^{\text{NNLL}} \leq 0.93\%.$$

We now turn to the forward-backward asymmetry. As for $R_{\text{quark}}(\hat{s})$, we introduce a CP-averaged version of the normalized forward-backward asymmetry, defined as

$$\bar{A}_{\text{FB}}(\hat{s}) = \frac{\int_{-1}^1 d(\cos \theta) \text{sgn}(\cos \theta) \left(\frac{d^2\Gamma(b \rightarrow X_d \ell^+ \ell^-)}{d\hat{s} d(\cos \theta)} + \frac{d^2\Gamma(\bar{b} \rightarrow X_{\bar{d}} \ell^+ \ell^-)}{d\hat{s} d(\cos \theta)} \right)}{\frac{d\Gamma(b \rightarrow X_d \ell^+ \ell^-)}{d\hat{s}} + \frac{d\Gamma(\bar{b} \rightarrow X_{\bar{d}} \ell^+ \ell^-)}{d\hat{s}}}, \quad (55)$$

where θ is the angle between the three-momenta of the positively charged lepton ℓ^+ and the b -quark in the rest frame of the lepton pair. The result of the integrals in the numerator of Eq. (55) for the case $b \rightarrow X_s \ell^+ \ell^-$ can be found in [38]. The corresponding result for $b \rightarrow X_d \ell^+ \ell^-$ is, up to different CKM-structures, the same.

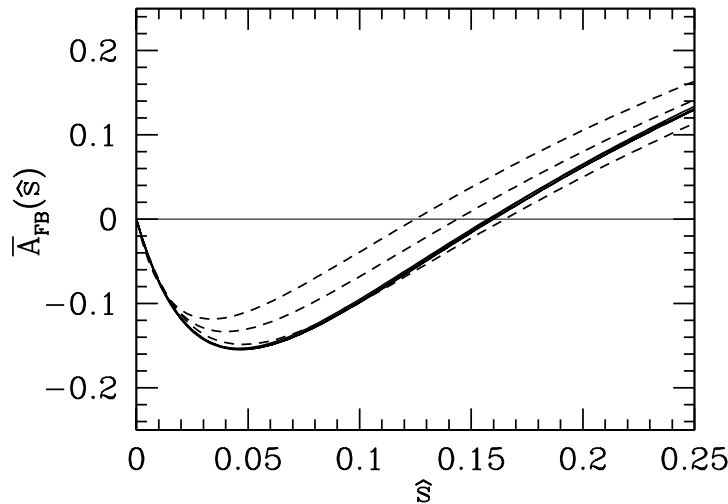


Figure 6.3: CP-averaged normalized forward-backward asymmetry. The solid lines show the NNLL result for $\mu = 2.5, 5.0, 10.0$ GeV, whereas the dashed lines represent the corresponding result in the NLL approximation.

In Fig. 6.3 we illustrate the μ -dependence of $\bar{A}_{\text{FB}}(\hat{s})$ in the region $0 \leq \hat{s} \leq 0.25$. Again, the solid and dashed lines represent the NNLL and the NLL results, respectively. The reduction of the μ -dependence going from NLL to NNLL precision is striking: one can clearly distinguish the three dashed lines, whereas the NNLL lines are on top of each other throughout the region. The position \hat{s}_0 at which the forward-backward asymmetries vanish, is essentially free of uncertainties due to the variation of μ : we find $\hat{s}_0^{\text{NNLL}} = 0.158 \pm 0.001$. To NLL precision we get $\hat{s}_0^{\text{NLL}} = 0.145 \pm 0.020$.

As a last illustration, we show in Fig. 6.4 the dependence of $R_{\text{quark}}(\hat{s})$ on the matching scales. In all the previous plots we used a matching scale of 120 GeV for the top contribution and a matching scale of 80 GeV for the charm contribution. In Fig. 6.4 the solid line corresponds to this scheme, while the dashed line is obtained by matching both contributions at a scale of 80 GeV. The difference between the two schemes is between 2% and 4%.

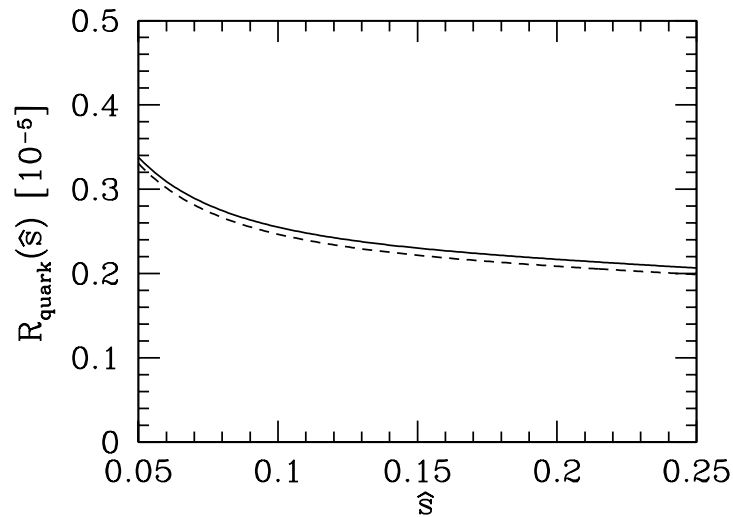


Figure 6.4: $R_{\text{quark}}(\hat{s})$ for $\mu = 5$ GeV. The solid line corresponds to matching top and charm contributions at 120 GeV and 80 GeV, respectively. The dashed curve is obtained by matching both contributions at a scale of 80 GeV.

7 Summary

In this paper we presented the calculation of virtual and bremsstrahlung corrections of $\mathcal{O}(\alpha_s)$ to the inclusive semileptonic decay $b \rightarrow X_d \ell^+ \ell^-$. Genuinely new calculations were necessary to attain the virtual contributions of the operators O_1^u and O_2^u . Some of the diagrams (in particular diagrams 3.1d) turned out to be more involved than the corresponding

diagrams for the c -quark contributions. We used dimension-shifting and integration-by-parts techniques to calculate them. The main result of this paper, namely the u -quark contributions to the renormalized form factors $F_{1,u}^{(7)}$, $F_{1,u}^{(9)}$, $F_{2,u}^{(7)}$, and $F_{2,u}^{(9)}$, is given in Section 3.6.

We shortly discussed the numerical impact of our results on various observables in the region $0.05 \leq \hat{s} \leq 0.25$, which is known to be free of resonances. As an example, we found the improvement on the forward-backward asymmetry $\bar{A}_{\text{FB}}(\hat{s})$ defined in Eq. (55) to be striking: the NNLL result is almost free of uncertainties due to the μ -dependence.

Acknowledgement

This work is partially supported by: the Swiss National Foundation; RTN, BBW-Contract No. 01.0357 and EC-Contract HPRN-CT-2002-00311 (EURIDICE); NFSAT-PH 095-02 (CRDF 12050); SCOPE 7AMPJ062165.

A Calculation techniques

A.1 Reducing tensor integrals with dimension-shifting techniques

We follow Ref. [42] and derive a method that allows to express tensor integrals in D dimensions in terms of scalar integrals of higher dimensions.

An arbitrary L loop tensor integral with N internal and E external lines can be written as a linear combination of integrals of the form (suppressing Lorentz indices of $G^{(D)}$)

$$G^{(D)}(\{s_u\}, \{m_v^2\}) = \int \left(\prod_{i=1}^L \frac{d^D k_i}{(2\pi)^D} \right) \prod_{j=1}^N P_{\bar{k}_j, m_j}^{\nu_j} \prod_{l=1}^{n_j} k_j^{\mu_{jl}}, \quad (56)$$

where

$$P_{k,m}^{\nu} = \frac{1}{(k^2 - m^2 + i\epsilon)^{\nu}} \quad \text{and} \quad \bar{k}_j = \sum_{n=1}^L \omega_{jn} k_n + \sum_{m=1}^E \eta_{jm} q_m.$$

k_i and q_j denote the loop and external momenta, respectively. The matrices of incidences of the diagram, ω and η , have matrix elements $\omega_{ij}, \eta_{ij} \in \{-1, 0, 1\}$. The quantities $\{s_u\}$ and $\{m_v^2\}$ denote a set of scalar invariants formed from the external momenta q_j and a set of squared masses of the internal particles, respectively. Generically, the exponents ν_i are equal to 1. However, often two or more internal lines are equipped with the same propagator. This may be taken into account by reducing N to $N^{\text{eff}} < N$, thus increasing some of the exponents ν_i .

Applying the integral representations

$$\frac{1}{(k^2 - m^2 + i\epsilon)^\nu} = \frac{(-i)^\nu}{\Gamma(\nu)} \int_0^\infty d\alpha \alpha^{\nu-1} \exp \left[i\alpha (k^2 - m^2 + i\epsilon) \right] \quad (57)$$

and

$$\prod_{l=1}^{n_j} k_j^{\mu_{jl}} = (-i)^{n_j} \prod_{l=1}^{n_j} \frac{\partial}{\partial (a_j)_{\mu_{jl}}} \exp \left[i(a_j k_j) \right] \Big|_{a_j=0} \quad (58)$$

allows us to easily perform the integration over the loop momenta by using the D dimensional Gaussian integration formula

$$\int d^D k \exp \left[i(A k^2 + 2(p k)) \right] = i \left(\frac{\pi}{iA} \right)^{\frac{D}{2}} \exp \left[-\frac{i p^2}{A} \right].$$

We find the following parametric representation:

$$G^{(D)} = i^L \left(\frac{1}{4i\pi} \right)^{\frac{DL}{2}} \prod_{j=1}^N \frac{(-i)^{n_j + \nu_j}}{\Gamma(\nu_j)} \times \prod_{l=1}^{n_j} \frac{\partial}{\partial (a_j)_{\mu_{jl}}} \times \int_0^\infty \dots \int_0^\infty \frac{d\alpha_j \alpha_j^{\nu_j-1}}{[D(\alpha)]^{\frac{D}{2}}} \exp \left[\frac{iQ(\{\bar{s}_i\}, \alpha)}{D(\alpha)} - i \sum_{r=1}^N \alpha_r (m_r^2 - i\epsilon) \right] \Big|_{a_j=0}. \quad (59)$$

The quantities \bar{s}_i are scalar invariants involving the external momenta q_i and the auxiliary momenta a_i . $D(\alpha)$ arises from the integral representations of the propagators: let \vec{k} be the L -dimensional vector that consists of all four-momentum loop vectors. The product of all $P_{\vec{k}_j, m_j}^{\nu_j}$ can then be written as

$$\prod_{j=1}^N P_{\vec{k}_j, m_j}^{\nu_j} = \int_0^\infty \left(\prod_{j=1}^N d\alpha_j \right) f(\alpha) \exp \left[i \left(\vec{k}^T B \vec{k} + (\vec{b} \vec{k}) + c \right) \right],$$

with k_i -independent quantities $f(\alpha)$, B , \vec{b} and c . $D(\alpha)$ denotes the determinant of the $L \times L$ matrix B .

The differentiation of $G^{(D)}$ in Eq. (59) with respect to a_j generates products of external momenta, metric tensors $g_{\mu\nu}$ and polynomials $R(\alpha)$ and provides an additional factor $D(\alpha)^{-1}$. Because of

$$R(\alpha) \exp \left[-i \sum_{r=1}^N \alpha_r m_r^2 \right] = R(i\partial) \exp \left[-i \sum_{r=1}^N \alpha_r m_r^2 \right], \quad \text{with} \quad \partial_j = \frac{\partial}{\partial m_j^2},$$

we may replace the polynomials $R(\alpha)$ with $R(i\partial)$. The additional factor of $1/D(\alpha)$ can be absorbed by a redefinition of D , i.e. by shifting D to $D + 2$ and multiplying with a factor $(4i\pi)^L$. The crucial point is that all factors generated by differentiation with respect to a_j may be written as operators which do not depend on the integral representations we have introduced in Eqs. (57), (58). Therefore, it is possible to write tensor integrals in momentum space in terms of scalar ones without direct appeal to the parametric representation (59):

$$\int \left(\prod_{i=1}^L \frac{d^D k_i}{(2\pi)^D} \right) \prod_{j=1}^N P_{\bar{k}_j, m_j}^{\nu_j} \prod_{l=1}^{n_j} k_j^{\mu_{jl}} = T(q, \partial, \mathbf{d}^+) \int \left(\prod_{i=1}^L \frac{d^D k_i}{(2\pi)^D} \right) \prod_{j=1}^N P_{\bar{k}_j, m_j}^{\nu_j}, \quad (60)$$

where the tensor operator T (suppressing its Lorentz indices) is given by

$$T(q, \partial, \mathbf{d}^+) = \exp \left[-i Q(\{\bar{s}_i\}, \alpha) (4i\pi)^L \mathbf{d}^+ \right] \times \prod_{j=1}^N \prod_{l=1}^{n_j} \frac{\partial}{\partial (a_j)_{\mu_{jl}}} \exp \left[i Q(\{\bar{s}_i\}, \alpha) (4i\pi)^L \mathbf{d}^+ \right] \Bigg|_{\substack{a_j=0 \\ \alpha_j=i\partial_j}}. \quad (61)$$

The operator \mathbf{d}^+ shifts the space-time dimension of the integral by two units:

$$\mathbf{d}^+ G^{(D)}(\{\bar{s}_i\}, \{m_j^2\}) = G^{(D+2)}(\{\bar{s}_i\}, \{m_j^2\}).$$

Notice that throughout the derivation of the tensor operator T the masses m_j must be kept as different parameters. They are set to their original values only in the very end.

A.2 Integration by parts

According to general rules of D dimensional integration, integrals of the form

$$\int d^D k_i \frac{\partial}{\partial k_i^\mu} \frac{k_i^\mu}{\prod_{j=1}^N (\bar{k}_j^2 - m_j^2 + i\epsilon)^{\nu_j}}$$

vanish. There may exist suitable linear combinations

$$\int d^D k_i \frac{\partial}{\partial k_i^\mu} \frac{\sum_l c_l k_l^\mu + \sum_e d_e q_e^\mu}{\prod_{j=1}^N (\bar{k}_j^2 - m_j^2 + i\epsilon)^{\nu_j}}$$

that lead to recurrence relations connecting the original integral to simpler ones. The task of finding such recurrence relations, however, is in general a nontrivial one. A criterion for irreducibility of multi-loop Feynman integrals is presented in [43]. In [42], the method of partial integration is combined directly with the technique of reducing tensor integrals by

means of shifting the space-time dimension.

The integral

$$\begin{aligned}
F_{\nu_1\nu_2\nu_3\nu_4\nu_5}^{(D)} &= \int d^D l d^D r I_{\nu_1\nu_2\nu_3\nu_4\nu_5} \\
&= \int d^D l d^D r \frac{1}{[l^2]^{\nu_1} [r^2]^{\nu_2} [(l+r)^2]^{\nu_3} [(l+q)^2]^{\nu_4} [(r+p)^2 - m_b^2]^{\nu_5}} \quad (62)
\end{aligned}$$

enters the calculation of diagrams 3.1d). At the same time it is a very good example to illustrate the integration by parts method. The operators $\mathbf{1}^\pm, \mathbf{2}^\pm, \dots$ are defined through

$$\mathbf{1}^\pm I_{\nu_1\nu_2\nu_3\nu_4\nu_5} = I_{\nu_1\pm 1\nu_2\nu_3\nu_4\nu_5}, \dots$$

The present case is especially simple because we only need to calculate one derivative. Using the shorthand notation $I_{\nu_1\nu_2\nu_3\nu_4\nu_5} = I_{\{\nu_i\}}$ we get (for $\nu_i > 0 \forall i$):

$$\frac{\partial}{\partial r^\mu} r^\mu I_{\{\nu_i\}} = \left[D - 2\nu_2 r^2 \mathbf{2}^+ - 2\nu_3 r(l+r) \mathbf{3}^+ - 2\nu_5 r(r+p) \mathbf{5}^+ \right] I_{\{\nu_i\}}.$$

Scalar products of the form (ab) we write as $[a^2 + b^2 - (a-b)^2]/2$ and find

$$\frac{\partial}{\partial r^\mu} r^\mu I_{\{\nu_i\}} = \left[D - 2\nu_2 - \nu_3 - \nu_5 - \nu_3(\mathbf{2}^- - \mathbf{1}^-) \mathbf{3}^+ - \nu_5 \mathbf{2}^- \mathbf{5}^+ \right] I_{\{\nu_i\}}.$$

At this stage we might also reduce some of the scalar products by shifting the dimension. The corresponding procedure is presented e.g. in [42]. In the present case, however, the pure integration by parts approach suffices. The identity

$$\int d^D r \frac{\partial}{\partial r_\mu} r^\mu I_{\{\nu_i\}} \equiv 0$$

yields directly the desired recurrence relation for the integral $F_{\nu_1\nu_2\nu_3\nu_4\nu_5}^{(D)}$:

$$F_{\nu_1\nu_2\nu_3\nu_4\nu_5}^{(D)} = \frac{\nu_3(\mathbf{2}^- - \mathbf{1}^-) \mathbf{3}^+ + \nu_5 \mathbf{2}^- \mathbf{5}^+}{D - 2\nu_2 - \nu_3 - \nu_5} F_{\nu_1\nu_2\nu_3\nu_4\nu_5}^{(D)}. \quad (63)$$

Subsequent application of this relation allows us to express any integral $F^{(D)}\{\nu_i\}$ with indices $\nu_i \in \mathbb{N}^+$ as a sum over integrals $F^{(D)}\{\nu_i\}$ with at least $\nu_1 = 0$ or $\nu_2 = 0$.

The general procedure is the following:

- One expresses suitable scalar products in the numerator of a given Feynman integrand in terms of inverse propagators $P_{\vec{k},m}$ and cancels them down. It is important to notice that it is not always the best strategy to try to cancel down as many scalar products as possible. The resulting set of integrals to calculate highly depends on which scalar products one cancels down. The best way is to try a couple of different cancellation schemes and compare the resulting integrals.

- One writes the integral as a sum over tensor integrals of the form (56) with products of k_i^μ . For each of those integrals the tensor operator T is determined in order to reduce the problem to scalar integrals with shifted space-time dimension.
- One applies appropriate recurrence relations to reduce the number of propagators in the integrals, hoping to be able to solve the remaining integrals.

B Calculation of the diagrams 3.1d)

The contribution of the sum of diagrams 3.1d) is given by a combination of integrals of the form

$$\int d^D l d^D r \frac{\prod_{i=1}^{n_l} l^{\mu_i} \prod_{j=1}^{n_r} r^{\rho_j}}{[l^2]^{\nu_1} [r^2]^{\nu_2} [(l+r)^2]^{\nu_3} [(l+q)^2]^{\nu_4} [(r+p)^2 - m_b^2]^{\nu_5}}. \quad (64)$$

In this section we show how to solve these integrals with the methods presented in Appendices A.1 and A.2. The function $D(\alpha)$, which is independent of n_l and n_r , is not needed in order to find the tensor operators T . Nevertheless, we give it as an illustration:

$$D(\alpha) = (\alpha_1 + \alpha_3 + \alpha_4)(\alpha_2 + \alpha_3 + \alpha_5) - \alpha_3^2.$$

The function $Q(\{\bar{s}_i\}, \alpha)$, however, must be calculated for each type of tensor integral. As an example we give $Q(\{\bar{s}_i\}, \alpha)$ for $n_l = 0$, $n_r = 1$:

$$Q(\{\bar{s}_i\}, \alpha) = -(\alpha_1 + \alpha_3 + \alpha_4)\alpha_5(a_1 p) - \alpha_3\alpha_4(a_1 q) - \frac{1}{4}(\alpha_1 + \alpha_3 + \alpha_4)a_1^2.$$

The corresponding tensor operator T reads:

$$T^{\rho_1}(q, p, \partial, \mathbf{d}^+) = 16\pi^2 \mathbf{d}^+ \left[q^{\rho_1} \partial_3 \partial_4 + p^{\rho_1} \partial_5 (\partial_1 + \partial_3 + \partial_4) \right].$$

The action of an operator ∂_i on the integral $F_{\{\nu\}}^{(D)}$ is

$$\partial_1^n F_{\nu_1 \nu_2 \nu_3 \nu_4 \nu_5}^{(D)} = \frac{\Gamma(\nu_1 + n)}{\Gamma(\nu_1)} F_{\nu_1 + n \nu_2 \nu_3 \nu_4 \nu_5}^{(D)}, \dots \quad (65)$$

The next step is to repeatedly apply the recurrence relation (63) on the integrals $F_{\nu_1 \nu_2 \nu_3 \nu_4 \nu_5}^{(D)}$ until ν_1 or ν_2 becomes zero. The problem is then reduced to the calculation of the two types of integrals

$$F_{0\nu_2\nu_3\nu_4\nu_5}^{(D)} \quad \text{and} \quad F_{\nu_1 0\nu_3\nu_4\nu_5}^{(D)}. \quad (66)$$

In the present calculation D may take the values

$$D = 4 - 2\epsilon, 6 - 2\epsilon, 8 - 2\epsilon \quad \text{or} \quad 10 - 2\epsilon. \quad (67)$$

It is important to note here that the denominator in Eq. (63) can become proportional to ϵ for certain values of D , ν_2 , ν_3 and ν_5 . Thus, some of the integrals in (66) need to be calculated up to $\mathcal{O}(\epsilon^1)$.

The first type of integrals ($F_{0\nu_2\nu_3\nu_4\nu_5}^{(D)}$) can easily be solved individually by using a single Mellin-Barnes approach. This method naturally results in an expansion in \hat{s} . Furthermore, the occasionally needed $\mathcal{O}(\epsilon^1)$ terms are easily obtained since the expansion in ϵ is done only in the very end. We now turn to the much more complicated calculation of the second set of integrals. Instead of calculating every single occurring integral individually, we derive a general formula for $F_{\nu_1 0\nu_3\nu_4\nu_5}^{(D)}$ where we are left with a three-dimensional Feynman parameter integral:

$$\begin{aligned}
 F_{\nu_1 0\nu_3\nu_4\nu_5}^{(D)} &= (-1)^{\nu_1+\nu_3\nu_4+\nu_5+D} \frac{\Gamma(\nu_1 + \nu_3 + \nu_4 + \nu_5)}{\Gamma(\nu_1) \Gamma(\nu_3) \Gamma(\nu_4) \Gamma(\nu_5)} \int_0^1 du dx dy u^{\nu_1+\nu_3+\nu_4-1-D/2} \\
 &\quad \times (1-u)^{D/2-\nu_3-1} x^{\nu_3-1} (1-x)^{\nu_3+\nu_5-1-D/2} y^{\nu_1-1} (1-y)^{D/2-1-\nu_1} \\
 &\quad \times \hat{\Delta}^{D-\nu_1-\nu_3-\nu_4-\nu_5} \\
 \hat{\Delta} &= m_b^2 (1-x)(1-uy) - sxyu - i\delta.
 \end{aligned} \tag{68}$$

We now replace all occurrences of $F_{\nu_1 0\nu_3\nu_4\nu_5}^{(D)}$ according to Eq. (68) and are left with a three-dimensional integral over a rather lengthy integrand. This integrand can be split up into three different parts:

- A part with no additional divergences arising from the integrations.
- A part with problematic x -integration.
- A part with problematic u -integration.

In the first part, the regulator ϵ is not needed at all and may be set equal to zero at the very beginning. The occurring integrals can then either be performed directly or with the use of a single Mellin-Barnes representation. The second part boils down to two different integrals, which can both be computed with subtraction methods. The last part is clearly the most difficult one. It can be reduced to three integrals which we calculate using a double Mellin-Barnes representation. Since this double Mellin-Barnes is very different from the one presented in Subsection 3.1.4 in [34], we give, as an example, the needed procedure to calculate one of the three integrals. Specifically, we have to deal with the integrals

$$I_j = \int_0^1 dx \int_0^1 dy \int_0^1 du \frac{u^\epsilon (1-y)^{2-\epsilon} x^j (1-x)^\epsilon}{(1-u)^{1+\epsilon} ((1-x)(1-uy) - \hat{s}xyu - i\delta)^{1+2\epsilon}}, \tag{69}$$

where j can take the values 0, 1 and 2. We focus on the case where $j = 0$. We introduce a first Mellin-Barnes integral in the complex t -plane with the identifications (for notation

see e.g. [34]):

$$K^2 \leftrightarrow (1-x)(1-uy), \quad M^2 \leftrightarrow \hat{s} x u y + i\delta, \quad \lambda = 1 + 2\epsilon,$$

and get

$$I_0 = \frac{e^{-i\pi(1+2\epsilon)}}{2i\pi\Gamma(1+2\epsilon)} \int_{\gamma} dt \int_0^1 dx \int_0^1 dy \int_0^1 du \Gamma(-t)\Gamma(1+2\epsilon+t) \\ \times \frac{u^{t+\epsilon} y^t (1-y)^{2-\epsilon} x^t}{(1-u)^{1+\epsilon} (1-x)^{1+\epsilon+t} (1-uy)^{1+2\epsilon+t}} \hat{s}^t. \quad (70)$$

The path γ lies in the left half-plane and can be chosen arbitrarily close to the imaginary t -axis. We introduce a second Mellin-Barnes representation in the complex t' -plane for the last factor in the denominator of Eq. (70). For this, we rewrite $1-uy$ as $1-u+u(1-y)$ and make the following identifications:

$$K^2 \leftrightarrow u(1-y), \quad M^2 \leftrightarrow -(1-u), \quad \lambda = 1 + 2\epsilon + t,$$

yielding

$$I_0 = \frac{e^{-i\pi(1+2\epsilon)}}{(2i\pi)^2 \Gamma(1+2\epsilon)} \int_{\gamma'} dt' \int_{\gamma} dt \int_0^1 dx \int_0^1 dy \int_0^1 du \Gamma(-t)\Gamma(-t') \\ \times \Gamma(1+2\epsilon+t+t') \frac{y^t (1-y)^{1-3\epsilon-t-t'} x^t}{u^{1+\epsilon+t'} (1-u)^{1+\epsilon-t'} (1-x)^{1+\epsilon+t}} \hat{s}^t. \quad (71)$$

The path γ' lies to the left of the imaginary t' -axis and can again be chosen arbitrarily close to that axis. The parameter integrals can now be performed and give products of Euler Beta-functions. We work out the remaining integrals over t and t' applying the residue theorem. For this, we close the t -integral in the right half-plane and focus on the enclosed poles. There are two different sequences of poles, namely poles that depend on t' (coupled poles) and poles that do not (uncoupled poles). The latter poles lie at the following positions:

- $t = 0, 1, 2, \dots, S, \dots,$
- $t = 0 - \epsilon, 1 - \epsilon, 2 - \epsilon, \dots, S - \epsilon, \dots,$

Note here that I_0 exists only for negative values of ϵ . The pole located at $t = -\epsilon$ therefore lies in the right half-plane and needs to be taken into account. Since we are interested in an expansion in \hat{s} , we can truncate the two pole sequences at a suitable S . After calculating the necessary residues, we close the t' -integral in the right half-plane as well and arrive at pole sequences situated at the following positions:

- $t' = 0, 1, 2, \dots,$
- $t' = 0 - \epsilon, 1 - \epsilon, 2 - \epsilon, \dots,$
- $t' = 2 - N - 3\epsilon, 3 - N - 3\epsilon, 4 - N - 3\epsilon, \dots$ for $t = N, \quad N \in \mathbb{N},$
 $t' = 2 - N - 2\epsilon, 3 - N - 2\epsilon, 4 - N - 2\epsilon, \dots$ for $t = N - \epsilon, \quad N \in \mathbb{N}.$

For $N \geq 3$, some of the poles above lie in the left t' -half-plane and must be omitted. Unlike the procedure given in Subsection 3.1.4 of [34], we need to sum up the residues of all poles in the enclosed area.

Calculating the contributions of the coupled poles in t , which lie at $t = 2 + n - 3\epsilon - t', n \in \mathbb{N}$, yields an expression that is proportional to $\hat{s}^{2+n-3\epsilon-t'}$. Two problems now arise if one closes the integration path of the t' -integral in the right half-plane: due to the $-t'$ in the exponent of \hat{s} , one gets an expansion in inverse powers of \hat{s} , forcing one to calculate the residues of all enclosed poles. The second problem is even worse: for any given value of n , there always exists an infinite pole series in t' which contributes to the desired result. Thus, one also has to consider the infinite pole series in t . In order to avoid these problems, we close the integration path in the left half-plane of t' . The poles are then located at

- $t' = -1 - \epsilon, -2 - \epsilon, -3 - \epsilon, \dots,$
- $t' = -1 - 2\epsilon, -2 - 2\epsilon, -3 - 2\epsilon, \dots,$
- $t' = -1 - 3\epsilon, -2 - 3\epsilon, -3 - 3\epsilon, \dots.$

After calculating the necessary residues we obtain the result for I_0 . The results for I_1 and I_2 are calculated in an analogous way.

C Solution of the renormalization group equation for the Wilson coefficients

The Wilson coefficients satisfy the renormalization group equation

$$\frac{d}{d \ln \mu} \vec{C}(\mu) = \gamma^T(\alpha_s) \vec{C}(\mu), \quad (72)$$

where $\gamma(\alpha_s)$ is the anomalous dimension matrix. This matrix can be written as a Taylor series in α_s :

$$\gamma(\alpha_s) = \gamma^{(0)} \frac{\alpha_s}{4\pi} + \gamma^{(1)} \left(\frac{\alpha_s}{4\pi} \right)^2 + \gamma^{(2)} \left(\frac{\alpha_s}{4\pi} \right)^3 + \dots$$

The general solution of Eq. (72) can be expressed with the evolution matrix $U(\mu, \mu_0)$:

$$\begin{aligned}\vec{C}(\mu) &= U(\mu, \mu_0) \vec{C}(\mu_0), \\ U(\mu_0, \mu_0) &= 1.\end{aligned}\tag{73}$$

The aim in this section is to find a handy expression for $U(\mu, \mu_0)$.

The matrix $\gamma^{(0)}$ can be diagonalized. We introduce new quantities in the following way:

$$\begin{aligned}\vec{C}(\mu) &= V \vec{\tilde{C}}(\mu), \\ \gamma^{(i)} &= V \tilde{\gamma}^{(i)} V^{-1}, \quad i = 0, 1, 2, \dots, \\ U(\mu, \mu_0) &= V \tilde{U}(\mu, \mu_0) V^{-1}.\end{aligned}\tag{74}$$

The matrix V is chosen such that $\tilde{\gamma}^{(0)}$ is diagonal. One can check that the new quantities satisfy equations similar to (72) and (73):

$$\begin{aligned}\frac{d}{d \ln \mu} \vec{\tilde{C}}(\mu) &= \tilde{\gamma}^T(\alpha_s) \vec{\tilde{C}}(\mu), \\ \vec{\tilde{C}}(\mu) &= \tilde{U}(\mu, \mu_0) \vec{\tilde{C}}(\mu_0), \\ \tilde{U}(\mu_0, \mu_0) &= 1.\end{aligned}\tag{75}$$

We will now construct a solution to Eq. (75). Once this solution is found, we can easily gain the solution of the initial problem for the nondiagonal $\gamma^{(0)}$. The evolution matrix $\tilde{U}(\mu, \mu_0)$ satisfies the same equation as $\vec{\tilde{C}}(\mu)$ itself:

$$\frac{d}{d \ln \mu} \tilde{U}(\mu, \mu_0) = \tilde{\gamma}^T(\alpha_s) \tilde{U}(\mu, \mu_0).\tag{76}$$

We make the following ansatz for $\tilde{U}(\mu, \mu_0)$:

$$\tilde{U}(\mu, \mu_0) = \left(1 + \sum_{i=1}^{\infty} \left(\frac{\alpha_s(\mu)}{4\pi} \right)^i \tilde{J}_i \right) \tilde{U}^{(0)}(\mu, \mu_0) \tilde{K},\tag{77}$$

where $\tilde{U}^{(0)}(\mu, \mu_0)$ solves Eq. (76) to leading logarithmic approximation and is given by

$$\tilde{U}^{(0)}(\mu, \mu_0) = \left(\left(\frac{\alpha_s(\mu_0)}{\alpha_s(\mu)} \right)^{\frac{\tilde{\gamma}^{(0)}}{2\beta_0}} \right)_D.$$

The vector $\tilde{\gamma}^{(0)}$ collects the diagonal elements of $\tilde{\gamma}^{(0)}$. The matrix \tilde{K} must be chosen such that the boundary condition given in Eq. (75) is met. The quantities β_i , $i = 0, 1, 2, \dots$ appear in the RGE for α_s :

$$\frac{d}{d \ln \mu} \alpha_s(\mu) = -2 \sum_{i=0}^{\infty} \frac{\alpha_s(\mu)^{i+2}}{(4\pi)^{i+1}} \beta_i.$$

Inserting the ansatz (77) into Eq. (76) and using the explicit expression for $\tilde{U}^{(0)}(\mu, \mu_0)$, the lhs and the rhs of this equation can be written as

$$\begin{aligned} \text{lhs} &= \sum_{j=1}^{\infty} \left(\frac{\alpha_s(\mu)}{4\pi} \right)^j L_j \tilde{U}^{(0)}(\mu, \mu_0) \tilde{K}, \\ \text{rhs} &= \sum_{j=1}^{\infty} \left(\frac{\alpha_s(\mu)}{4\pi} \right)^j R_j \tilde{U}^{(0)}(\mu, \mu_0) \tilde{K}. \end{aligned}$$

The unknown matrices \tilde{J}_i can now be constructed order by order in α_s through the relations $L_j = R_j$. We give the explicit solutions to \tilde{J}_1 and \tilde{J}_2 since we need them to find the Wilson coefficients $C_i(\mu)$ to NNLL precision:

$$\tilde{J}_{1,ij} = \delta_{ij} \tilde{\gamma}_i^{(0)} \frac{\beta_1}{2\beta_0^2} - \frac{\tilde{\gamma}_{ij}^{(1)\text{T}}}{2\beta_0 + \tilde{\gamma}_i^{(0)} - \tilde{\gamma}_j^{(0)}}, \quad (78)$$

$$\tilde{J}_{2,ij} = \delta_{ij} \tilde{\gamma}_i^{(0)} \frac{\beta_2}{4\beta_0^2} - \frac{\tilde{\gamma}_{ij}^{(2)\text{T}} + \left(2\beta_1 - \frac{\beta_1}{\beta_0} \tilde{\gamma}_j^{(0)} \right) \tilde{J}_{1,ij} + \left(\tilde{\gamma}^{(1)\text{T}} \tilde{J}_1 \right)_{ij}}{4\beta_0 + \tilde{\gamma}_i^{(0)} - \tilde{\gamma}_j^{(0)}}. \quad (79)$$

The result for \tilde{J}_1 agrees with the one given in Section III of [45]. After we did the calculation for \tilde{J}_2 , we found out that the result already exists in the literature [53]. The two results agree as well.

The matrix \tilde{K} is given through

$$\tilde{K} = 1 - \frac{\alpha_s(\mu_0)}{4\pi} \tilde{J}_1 - \left(\frac{\alpha_s(\mu_0)}{4\pi} \right)^2 \left(\tilde{J}_2 - \tilde{J}_1^2 \right) + \mathcal{O}(\alpha_s^3). \quad (80)$$

With these informations at hand, we can present the evolution matrix for the initial problem given in Eqs. (72) and (73):

$$U(\mu, \mu_0) = V \left(1 + \frac{\alpha_s(\mu)}{4\pi} \tilde{J}_1 + \left(\frac{\alpha_s(\mu)}{4\pi} \right)^2 \tilde{J}_2 \right) \tilde{U}^{(0)}(\mu, \mu_0) \tilde{K} V^{-1} + \mathcal{O}(\alpha_s^3). \quad (81)$$

D One-loop matrix elements of the four-quark operators

In order to fix the counterterms $F_{i,u \rightarrow 4\text{quark}}^{\text{ct}(7,9)}$ ($i = 1, 2$) in Eq. (22), we need the one-loop matrix elements $\langle d \ell^+ \ell^- | O_j | b \rangle_{1\text{-loop}}$ of the four-quark operators O_1^u , O_2^u , O_4 , O_{11}^u and O_{12}^u .

Due to the $1/\epsilon$ factor in Eq. (22) they are needed up to $\mathcal{O}(\epsilon^1)$. The explicit results read

$$\langle d\ell^+\ell^-|O_2^u|b\rangle_{1\text{-loop}} = \left(\frac{\mu}{m_b}\right)^{2\epsilon} \left\{ \frac{4}{9\epsilon} + \frac{4}{27} [2 + 3i\pi - 3L_s] + \frac{\epsilon}{81} [52 + 24i\pi - 21\pi^2 - (24 + 36i\pi)L_s + 18L_s^2] \right\} \langle \tilde{O}_9 \rangle_{\text{tree}},$$

$$\langle d\ell^+\ell^-|O_1^u|b\rangle_{1\text{-loop}} = \frac{4}{3} \langle d\ell^+\ell^-|O_2^u|b\rangle_{1\text{-loop}},$$

$$\begin{aligned} \langle d\ell^+\ell^-|O_4|b\rangle_{1\text{-loop}} = & - \left(\frac{\mu}{m_b}\right)^{2\epsilon} \left\{ \left[\frac{4}{9} + \frac{\epsilon}{945} (70\hat{s} + 7\hat{s}^2 + \hat{s}^3) \right] \langle \tilde{O}_7 \rangle_{\text{tree}} \right. \\ & + \left[\frac{16}{27\epsilon} + \frac{2}{8505} (-420 + 1260i\pi - 1260L_s + 252\hat{s} + 27\hat{s}^2 + 4\hat{s}^3) \right. \\ & + \frac{4\epsilon}{8505} (420i\pi + 910 - 630L_s i\pi - 420L_s - 315\pi^2 \\ & \left. \left. + 315L_s^2 - 126\hat{s} + \hat{s}^3) \right] \langle \tilde{O}_9 \rangle_{\text{tree}} \right\}, \end{aligned}$$

$$\langle d\ell^+\ell^-|O_{11}^u|b\rangle_{1\text{-loop}} = -\frac{64}{27} \left(\frac{\mu}{m_b}\right)^{2\epsilon} \left(1 + \frac{5}{3}\epsilon + i\pi\epsilon - L_s\epsilon \right) \langle \tilde{O}_9 \rangle_{\text{tree}},$$

$$\langle d\ell^+\ell^-|O_{12}^u|b\rangle_{1\text{-loop}} = \frac{3}{4} \langle d\ell^+\ell^-|O_{11}^u|b\rangle_{1\text{-loop}}.$$

E Finite bremsstrahlung corrections

In Section 5 those bremsstrahlung contributions were taken into account which generate infrared and collinear singularities. Combined with virtual contributions which also suffer from such singularities, a finite result was obtained. In this appendix we discuss the remaining finite bremsstrahlung corrections which are encoded in the last two terms of Eq. (45). Being finite, these terms can be directly calculated in $d = 4$ dimensions.

The sum of the bremsstrahlung contributions from $O_7 - O_8$ and $O_8 - O_9$ interference terms

and the $O_8 - O_8$ term can be written as

$$\frac{d\Gamma^{\text{Brems, A}}}{d\hat{s}} = \frac{d\Gamma_{78}^{\text{Brems}}}{d\hat{s}} + \frac{d\Gamma_{89}^{\text{Brems}}}{d\hat{s}} + \frac{d\Gamma_{88}^{\text{Brems}}}{d\hat{s}} = \left(\frac{\alpha_{\text{em}}}{4\pi}\right)^2 \left(\frac{\alpha_s}{4\pi}\right) \frac{m_{b,\text{pole}}^5 |\xi t|^2 G_F^2}{48\pi^3} \times (2 \text{Re} [c_{78} \tau_{78} + c_{89} \tau_{89}] + c_{88} \tau_{88}), \quad (82)$$

where

$$c_{78} = C_F \cdot \tilde{C}_7^{(0,\text{eff})} \tilde{C}_8^{(0,\text{eff})*}, \quad c_{89} = C_F \cdot \tilde{C}_8^{(0,\text{eff})} \tilde{C}_9^{(0,\text{eff})*}, \quad c_{88} = C_F \cdot \left| \tilde{C}_8^{(0,\text{eff})} \right|^2. \quad (83)$$

For the quantities τ_{78} , τ_{89} and τ_{88} we refer to [35].

The remaining bremsstrahlung contributions all involve the diagrams with an $O_{1,2}^u$ or $O_{1,2}^c$ insertion where the gluon is emitted from the u - or c -quark loop, respectively. The corresponding bremsstrahlung matrix elements depend on the functions $\bar{\Delta}i_{23}^{(u,c)}$, $\bar{\Delta}i_{27}^{(u,c)}$. In $d = 4$ dimensions we find

$$\begin{aligned} \bar{\Delta}i_{23}^{(u)} &= 8(qr) \int_0^1 dx dy \frac{xy(1-y)^2}{C^{(u)}}, & \bar{\Delta}i_{23}^{(c)} &= 8(qr) \int_0^1 dx dy \frac{xy(1-y)^2}{C^{(c)}}, \\ \bar{\Delta}i_{27}^{(u)} &= 8(qr) \int_0^1 dx dy \frac{y(1-y)^2}{C^{(u)}}, & \bar{\Delta}i_{27}^{(c)} &= 8(qr) \int_0^1 dx dy \frac{y(1-y)^2}{C^{(c)}}, \end{aligned}$$

where

$$\begin{aligned} C^{(u)} &= -2xy(1-y)(qr) - q^2y(1-y) - i\delta, \\ C^{(c)} &= m_c^2 - 2xy(1-y)(qr) - q^2y(1-y) - i\delta. \end{aligned}$$

The analytical expressions for $\bar{\Delta}i_{23}^{(c)}$ and $\bar{\Delta}i_{27}^{(c)}$ can be written in terms of functions $G_i(t)$:

$$\bar{\Delta}i_{23}^{(c)} = -2 + \frac{4}{w - \hat{s}} \left[z G_{-1}\left(\frac{\hat{s}}{z}\right) - z G_{-1}\left(\frac{w}{z}\right) - \frac{\hat{s}}{2} G_0\left(\frac{\hat{s}}{z}\right) + \frac{\hat{s}}{2} G_0\left(\frac{w}{z}\right) \right], \quad (84)$$

$$\bar{\Delta}i_{27}^{(c)} = 2 \left[G_0\left(\frac{\hat{s}}{z}\right) - G_0\left(\frac{w}{z}\right) \right], \quad (85)$$

where $z = m_c^2/m_b^2$. $G_k(t)$ ($k \geq -1$) is defined through the integral

$$G_k(t) = \int_0^1 dx x^k \ln[1 - tx(1-x) - i\delta], \quad G_1(t) = \frac{1}{2} G_0(t).$$

Explicitly, the functions $G_{-1}(t)$ and $G_0(t)$ read

$$G_{-1}(t) = \begin{cases} 2\pi \arctan\left(\sqrt{\frac{4-t}{t}}\right) - \frac{\pi^2}{2} - 2 \arctan^2\left(\sqrt{\frac{4-t}{t}}\right), & t < 4 \\ -2i\pi \ln\left(\frac{\sqrt{t+\sqrt{t-4}}}{2}\right) - \frac{\pi^2}{2} + 2 \ln^2\left(\frac{\sqrt{t+\sqrt{t-4}}}{2}\right), & t > 4 \end{cases}, \quad (86)$$

$$G_0(t) = \begin{cases} \pi \sqrt{\frac{4-t}{t}} - 2 - 2\sqrt{\frac{4-t}{t}} \arctan\left(\sqrt{\frac{4-t}{t}}\right), & t < 4 \\ -i\pi \sqrt{\frac{t-4}{t}} - 2 + 2\sqrt{\frac{t-4}{t}} \ln\left(\frac{\sqrt{t+\sqrt{t-4}}}{2}\right), & t > 4 \end{cases}. \quad (87)$$

The quantities $\bar{\Delta}i_j^{(u)}$ we obtain from $\bar{\Delta}i_j^{(c)}$ in the limit $z \rightarrow 0$:

$$\begin{aligned} \bar{\Delta}i_{23}^{(u)} &= -2 + \frac{2\hat{s}}{w-\hat{s}} [\ln(w) - \ln(\hat{s})], \\ \bar{\Delta}i_{27}^{(u)} &= -2 [\ln(w) - \ln(\hat{s})]. \end{aligned}$$

Following [35], we write

$$\frac{d\Gamma^{\text{Brems, B}}}{d\hat{s}} = \left(\frac{\alpha_{\text{em}}}{4\pi}\right)^2 \left(\frac{\alpha_s}{4\pi}\right) \frac{G_F^2 m_{b,\text{pole}}^5 |\xi_t|^2}{48\pi^3} \times \int_{\hat{s}}^1 dw \left\{ (c_{11} + c_{12} + c_{22}) \tau_{22} + 2 \text{Re} \left[(c_{17} + c_{27}) \tau_{27} + (c_{18} + c_{28}) \tau_{28} + (c_{19} + c_{29}) \tau_{29} \right] \right\}. \quad (88)$$

Expressed in terms of the quantities $\bar{\Delta}i_{23}^{\text{eff}}$ and $\bar{\Delta}i_{27}^{\text{eff}}$, defined by

$$\bar{\Delta}i_{23}^{\text{eff}} = -\frac{\xi_u}{\xi_t} \bar{\Delta}i_{23}^{(u)} - \frac{\xi_c}{\xi_t} \bar{\Delta}i_{23}^{(c)}, \quad (89)$$

$$\bar{\Delta}i_{27}^{\text{eff}} = -\frac{\xi_u}{\xi_t} \bar{\Delta}i_{27}^{(u)} - \frac{\xi_c}{\xi_t} \bar{\Delta}i_{27}^{(c)}, \quad (90)$$

the quantities τ_{ij} introduced in Eq. (88) read

$$\begin{aligned} \tau_{22} &= \frac{8}{27} \frac{(w-\hat{s})(1-w)^2}{\hat{s}w^3} \times \left\{ \left[3w^2 + 2\hat{s}^2(2+w) - \hat{s}w(5-2w) \right] |\bar{\Delta}i_{23}^{\text{eff}}|^2 + \right. \\ &\quad \left. \left[2\hat{s}^2(2+w) + \hat{s}w(1+2w) \right] |\bar{\Delta}i_{27}^{\text{eff}}|^2 + 4\hat{s} \left[w(1-w) - \hat{s}(2+w) \right] \cdot \text{Re} \left[\bar{\Delta}i_{23}^{\text{eff}} \bar{\Delta}i_{27}^{\text{eff}*} \right] \right\}, \quad (91) \end{aligned}$$

$$\tau_{27} = \frac{8}{3} \frac{1}{\hat{s} w} \times \left\{ \left[(1-w)(4\hat{s}^2 - \hat{s}w + w^2) + \hat{s}w(4 + \hat{s} - w) \ln(w) \right] \bar{\Delta}i_{23}^{\text{eff}} - \left[4\hat{s}^2(1-w) + \hat{s}w(4 + \hat{s} - w) \ln(w) \right] \bar{\Delta}i_{27}^{\text{eff}} \right\}, \quad (92)$$

$$\tau_{28} = \frac{8}{9} \frac{1}{\hat{s} w (w - \hat{s})} \times \left\{ \left[(w - \hat{s})^2 (2\hat{s} - w)(1-w) \right] \bar{\Delta}i_{23}^{\text{eff}} - \left[2\hat{s}(w - \hat{s})^2 (1-w) \right] \bar{\Delta}i_{27}^{\text{eff}} + \hat{s}w \left[(1 + 2\hat{s} - 2w) \bar{\Delta}i_{23}^{\text{eff}} - 2(1 + \hat{s} - w) \bar{\Delta}i_{27}^{\text{eff}} \right] \cdot \ln \left[\frac{\hat{s}}{(1 + \hat{s} - w)(w^2 + \hat{s}(1-w))} \right] \right\}, \quad (93)$$

$$\tau_{29} = \frac{4}{3} \frac{1}{w} \times \left\{ \left[2\hat{s}(1-w)(\hat{s} + w) + 4\hat{s}w \ln(w) \right] \bar{\Delta}i_{23}^{\text{eff}} - \left[2\hat{s}(1-w)(\hat{s} + w) + w(3\hat{s} + w) \ln(w) \right] \bar{\Delta}i_{27}^{\text{eff}} \right\}. \quad (94)$$

The coefficients c_{ij} include the dependence on the Wilson coefficients and the color factors.

$$\begin{aligned} c_{11} &= C_{\tau_1} \cdot \left| C_1^{(0)} \right|^2, & c_{17} &= C_{\tau_2} \cdot C_1^{(0)} \tilde{C}_7^{(0,\text{eff})*}, & c_{27} &= C_F \cdot C_2^{(0)} \tilde{C}_7^{(0,\text{eff})*}, \\ c_{12} &= C_{\tau_2} \cdot 2 \text{Re} \left[C_1^{(0)} C_2^{(0)*} \right], & c_{18} &= C_{\tau_2} \cdot C_1^{(0)} \tilde{C}_8^{(0,\text{eff})*}, & c_{28} &= C_F \cdot C_2^{(0)} \tilde{C}_8^{(0,\text{eff})*}, \\ c_{22} &= C_F \cdot \left| C_2^{(0)} \right|^2, & c_{19} &= C_{\tau_2} \cdot C_1^{(0)} \tilde{C}_9^{(0,\text{eff})*}, & c_{29} &= C_F \cdot C_2^{(0)} \tilde{C}_9^{(0,\text{eff})*}. \end{aligned} \quad (95)$$

The Wilson coefficients $C_{7,8,9,10}^{\text{eff}}$ are given in Eq. (46) and numerical values for the coefficients $C_i^{(0)}$ can be found in Table 5.1. The color factors C_F , C_{τ_1} and C_{τ_2} are presented in Section 2.

References

- [1] M.S. Alam *et al.* (CLEO Collab.), *Phys. Rev. Lett.* **74** (1995) 2885.
- [2] S. Ahmed *et al.* (CLEO Collab.) CLEO CONF 99-10, [hep-ex/9908022](#).
- [3] S. Chen *et al.* (CLEO Collab.), *Phys. Rev. Lett.* **87** (2001) 251807, [hep-ex/0108032](#).
- [4] R. Barate *et al.* (ALEPH Collab.), *Phys. Lett.* **B 429** (1998) 169.

- [5] K. Abe *et al.* (BELLE Collab.), *Phys. Lett. B* **511** (2001) 151, [hep-ex/0103042](#).
- [6] B. Aubert *et al.* (BABAR Collab.), [hep-ex/0207074](#) and [hep-ex/0207076](#).
- [7] C. Jessop, SLAC-PUB-9610.
- [8] J. Kaneko *et al.* [BELLE Collaboration], *Phys. Rev. Lett.* **90** (2003) 021801, [hep-ex/0208029](#).
- [9] K. Abe *et al.* [BELLE Collaboration], [hep-ex/0107072](#).
- [10] B. Aubert *et al.* [BABAR Collaboration], [hep-ex/0308016](#).
- [11] Z. Ligeti and M. B. Wise, *Phys. Rev. D* **53** (1996) 4937, [hep-ph/9512225](#).
- [12] A. F. Falk, M. Luke and M. J. Savage, *Phys. Rev. D* **49** (1994) 3367, [hep-ph/9308288](#).
- [13] A. Ali, G. Hiller, L. T. Handoko and T. Morozumi, *Phys. Rev. D* **55** (1997) 4105, [hep-ph/9609449](#).
- [14] J-W. Chen, G. Rupak and M. J. Savage, *Phys. Lett. B* **410** (1997) 285, [hep-ph/9705219](#).
- [15] G. Buchalla, G. Isidori and S. J. Rey, *Nucl. Phys. B* **511** (1998) 594, [hep-ph/9705253](#).
- [16] G. Buchalla and G. Isidori, *Nucl. Phys. B* **525** (1998) 333, [hep-ph/9801456](#).
- [17] F. Kruger and L. M. Sehgal, *Phys. Rev. D* **55** (1997) 2799, [hep-ph/9608361](#).
- [18] A. Ali, P. Ball, L.T. Handoko, G. Hiller, *Phys. Rev. D* **61** (2000) 074024, [hep-ph/9910221](#).
- [19] E. Lunghi and I. Scimemi, *Nucl. Phys. B* **574** (2000) 43, [hep-ph/9912430](#).
- [20] E. Lunghi, A. Masiero, I. Scimemi and L. Silvestrini, *Nucl. Phys. B* **568** (2000) 120, [hep-ph/9906286](#).
- [21] K. Chetyrkin, M. Misiak and M. Münz, *Phys. Lett. B* **400** (1997) 206, [hep-ph/9612313](#).
- [22] M. Ciuchini, E. Franco, G. Martinelli, L. Reina and L. Silvestrini, *Phys. Lett. B* **316** (1993) 127, [hep-ph/9307364](#); *Nucl. Phys. B* **415** (1994) 403, [hep-ph/9304257](#); G. Cella, G. Curci, G. Ricciardi and A. Vicere, *Phys. Lett. B* **325** (1994) 227, [hep-ph/9401254](#).
- [23] K. Adel and Y.-P. Yao, *Phys. Rev. D* **49** (1994) 4945, [hep-ph/9308349](#).
- [24] C. Greub and T. Hurth, *Phys. Rev. D* **56** (1997) 2934, [hep-ph/9703349](#).

-
- [25] A.J. Buras, A. Kwiatkowski and N. Pott, *Nucl. Phys. B* **517** (1998) 353, [hep-ph/9710336](#); *Phys. Lett. B* **414** (1997) 157, E:*Phys. Lett. B* **434** (1998) 459, [hep-ph/9707482](#).
- [26] A. Ali and C. Greub, *Z. Physik C* **49** (1991) 431; *Phys. Lett. B* **259** (1991) 182.
- [27] N. Pott, *Phys. Rev. D* **54** (1996) 938, [hep-ph/9512252](#).
- [28] C. Greub, T. Hurth and D. Wyler, *Phys. Lett. B* **380** (1996) 385, [hep-ph/9602281](#); *Phys. Rev. D* **54** (1996) 3350, [hep-ph/9603404](#).
- [29] A. Ali, H. Asatrian and C. Greub, *Phys. Lett. B* **429** (1998) 87, [hep-ph/9803314](#).
- [30] T. Hurth and T. Mannel, AIP Conf. Proc. **602** (2001) 212, [hep-ph/0109041](#).
- [31] T. Hurth and T. Mannel, *Phys. Lett. B* **511** (2001) 196, [hep-ph/0103331](#).
- [32] C. Bobeth, M. Misiak and J. Urban, *Nucl. Phys. B* **574** (2000) 291, [hep-ph/9910220](#).
- [33] P. Gambino, M. Gorbahn and U. Haisch, *Nucl. Phys. B* **673** (2003) 238, [hep-ph/0306079](#).
- [34] H. H. Asatryan, H. M. Asatrian, C. Greub and M. Walker, *Phys. Rev. D* **65** (2000) 074004, [hep-ph/0109140](#).
- [35] H. H. Asatryan, H. M. Asatrian, C. Greub and M. Walker, *Phys. Rev. D* **66** (2002) 034009, [hep-ph/0204341](#).
- [36] A. Ghinculov, T. Hurth, G. Isidori and Y. P. Yao, [hep-ph/0310187](#).
- [37] A. Ghinculov, T. Hurth, G. Isidori and Y. P. Yao, *Nucl. Phys. B* **648** (2003) 254, [hep-ph/0208088](#).
- [38] H. M. Asatrian, K. Bieri, C. Greub and A. Hovhannisyan, *Phys. Rev. D* **66** (2002) 094013, [hep-ph/0209006](#).
- [39] A. Ghinculov, T. Hurth, G. Isidori and Y. P. Yao, *Nucl. Phys.* **116** (*Proc. Suppl.*) (2003) 284, [hep-ph/0211197](#).
- [40] H. M. Asatrian, H. H. Asatryan, A. Hovhannisyan and V. Poghosyan, [hep-ph/0311187](#).
- [41] T. Hurth, *Rev. Mod. Phys.* **75** (2003) 1159, [hep-ph/0212304](#).
- [42] O. V. Tarasov, *Phys. Rev. D* **54** (1996) 6479, [hep-th/9606018](#).
- [43] P. A. Baikov, *Phys. Lett. B* **474** (2000) 385, [hep-ph/9912421](#).
- [44] M. Misiak, *Nucl. Phys. B* **393** (1993) 23, E:*Nucl. Phys. B* **439** (1995) 461.

- [45] G. Buchalla, A. J. Buras and M. E. Lautenbacher, *Rev. Mod. Phys.* **68** (1996) 1125, [hep-ph/9512380](#).
- [46] A. J. Buras and M. Munz, *Phys. Rev. D* **52** (1995) 186, [hep-ph/9501281](#).
- [47] B. Grinstein, M. J. Savage and M. B. Wise, *Nucl. Phys. B* **319** (1989) 271.
- [48] V. A. Smirnov, *Renormalization and Asymptotic Expansions* (Birkhäuser, Basel, 1991); *Applied Asymptotic Expansions in Momenta and Masses* (Springer-Verlag, Heidelberg, 2001); *Mod. Phys. Lett. A* **10** (1995) 1485, [hep-th/9412063](#).
- [49] H. H. Asatryan, H. M. Asatrian, C. Greub and M. Walker, *Phys. Lett. B* **507** (2001) 162, [hep-ph/0103087](#).
- [50] Y. Nir, *Phys. Lett. B* **221** (1989) 184.
- [51] A. J. Buras, M. E. Lautenbacher and G. Ostermaier, *Phys. Rev. D* **50** (1994) 3433, [hep-ph/9403384](#).
- [52] A. Ali and G. Hiller, *Eur. Phys. J. C* **8** (1999) 619, [hep-ph/9812267](#).
- [53] M. Beneke, T. Feldmann and D. Seidel, *Nucl. Phys. B* **612** (2001) 25, [hep-ph/0106067](#).

ACKNOWLEDGMENTS

First and foremost I would like to thank my supervisor Christoph Greub for his continuous support and competent advice throughout my work on this thesis. His knowledge, perceptiveness and never-ending patience have had an enormous positive influence both on this thesis as well as on my scientific work in general. Further I am indebted to professors H. M. Asatrian, Jürg Gasser and Peter Minkowski for providing an open ear whenever I sought their assistance. Also I would like to thank Prof. Daniel Wyler for being my co-supervisor.

Special thanks go to all the ITP members, especially Christoph Haefeli, Markus “Schnosi” Moser, Martin Schmid, Julia Schweizer and Peter Zemp. They have provided a surrounding which was both professional and enjoyable on all accounts. Furthermore they made sure that life didn’t get too demure and physics-centered.

Many thanks go to Patrick Liniger for sharing his knowledge about B physics and for providing his adjuvant Mathematica packages. Further my gratitude goes to Manuel Walker for countless discussions about physics and at least as many enthralling games of chess.

A special thanks belongs to Ottilia Hänni and Ruth Bestgen. It has always been a pleasure to chat with them about topics completely unrelated to physics. The institute will lose a lot of its charm and appeal once they leave.

Finally I want to express my gratitude to my family and to my friends. I’m especially thankful to Maria Gurtner for bearing with me and my sometimes unconventional working schedule.

Curriculum vitae

Personal Data

Name Bieri, Kay Axel
Date of birth June 22, 1976
Place of birth Bern, Switzerland
Nationality Swiss
Marital status Unmarried
Present address Institut für theoretische Physik
Universität Bern
Sidlerstrasse 5
CH-3012 Bern
E-mail: bierik@itp.unibe.ch

Schools

1983-1989 Schools in Bärswil, Höchstetten and Koppigen
1989-1996 Gymnasium Burgdorf
1996 Matura Typus C (University entrance exam)

University

1996-2001 University of Bern
Studies in physics, mathematics and astronomy
2001 University of Bern
M.Sc in theoretical physics
“NNLO calculations in $\gamma\gamma \rightarrow \pi\pi$ ”
(supervised by Prof. Dr. J. Gasser)
2001-2004 University of Bern
PhD in theoretical physics
“QCD Corrections in Inclusive Rare B Decays”
(supervised by PD Dr. Ch. Greub)

Other Activities

2001 29th Summer School Institute at SLAC in Stanford

